TECHNISCHE UNIVERSITÄT MÜNCHEN

Fakultät für Chemie

Surface Hydrosilylation: The Key to Silicon Nanocrystal Hybrid and Composite Materials

Julian Kehrle (M.Sc.)

Vollständiger Abdruck der von der Fakultät für Chemie der Technischen Universität München zur Erlangung des akademischen Grades eines

Doktors der Naturwissenschaften

genehmigten Dissertation.

Vorsitzender:		Prof. Dr. Tom Nilges
Prüfer der Dissertation:	1.	Prof. Dr. Dr. h.c. Bernhard Rieger
	2.	Prof. Dr. Johann Peter Plank

Die Dissertation wurde am 09.05.2018 bei der Technischen Universität München eingereicht und durch die Fakultät für Chemie am 11.10.2018 angenommen.

Zwei Dinge sind zu unserer Arbeit nötig: Unermüdliche Ausdauer und die Bereitschaft, etwas, in das man viel Zeit und Arbeit gesteckt hat, wieder wegzuwerfen.

Albert Einstein

Die vorliegende Arbeit wurde am WACKER-Lehrstuhl für Makromolekulare Chemie der Technischen Universität München in der Zeit von Dezember 2012 bis April 2018 angefertigt.

Ein besonderer Dank gilt meinem Doktorvater

Prof. Dr. Dr. h.c. Bernhard Rieger

für die freundliche Aufnahme in seine Arbeitsgruppe, die exzellenten und vielfältigen Forschungssmöglichkeiten, für die große Freiheit in der Forschung und die vielen tiefgründigen Gespräche und Diskussionen.

Darüber hinaus bedanke ich mich herzlichst bei meinem Mentor

Prof. Dr. Jonathan G.C. Veinot
von der University of Alberta in Edmonton, Kanada,

für die gute Zusammenarbeit, seine fachliche Hilfe bei der Forschung, seine interessanten Ideen und Denkanstöße und die Einladung Forschung im „*Centennial Center for Interdisziplinary Science*“ in Edmonton zu betreiben.

Des Weiteren danke ich **Dr. Carsten Troll,** der allzeit ein offenes Ohr hatte und sowohl bei wissenschaftlichen, wie auch technischen Fragestellungen zumeist die passende Lösung parat hatte. **Dr. Sergei Vagin** danke ich für die vielen fachlichen Diskussionen und seine Hilfe, wodurch er maßgeblich zu der Entwicklung dieser Arbeit beitragen konnte. Darüber hinaus konnten wir Zeit für einige freundschaftliche Stunden am See beim Angeln finden. **Katia Rodewald** danke ich für die vielen Hilfestellungen bei organisatorischen Dingen, sowie für die Einführung und unzählige Messstunden am REM. Bei **Frau Bauer** und **Frau Saul-Hubrich** bedanke mich für ihre Hilfe bei der Organisation von Terminen, und ihre allzeit freundliche Art.

Insbesondere möchte ich **Dr. Tobias Helbich,** meinem früheren Masteranden und Laborkollegen meinen herzlichen Dank für die gute Zusammenarbeit, das gegenseitige Vertrauen, die vielen spaßigen Momente, das eine oder andere ernste Wort, die vielen fachlichen Diskussionen und die aus der gemeinsamen Zeit entwickelte Freundschaft aussprechen. Wir hatten unglaublich viel Spaß zusammen und er schaffte es mich einmal etwas zu schocken, nämlich als er unser Labor während der Mittagspause etwas bromierte. Tobias war ein wesentlicher Faktor, der zum Gelingen meiner Arbeit beitrug, sei es durch seine unvergleichliche und ehrliche Art, seine tollen Einfälle oder seinen immer positiven Charakter! Vielen Dank dafür.

Ein weiterer sehr herzlicher Dank gilt **Dr. Ignaz Höhlein** und **Arzu Angı**, für die gute Zusammenarbeit, die vielen interessanten Diskussionen, die gemeinsame Lösung von diversen Fragestellungen, die ehrliche Art und die über die Zeit der Doktorarbeit hinausgehende Freundschaft. Darüber hinaus bedanke ich mich bei meinen weiteren Masteranden **Leopold Daum** und **Simon Kaiser**, die durch ihre jeweils unvergessliche Art und ihr großes Interesse an der Nanokristallforschung im Wesentlichen zum Gelingen dieser Doktorarbeit beitrugen. Ich freue mich sehr beide kennengelernt zu haben und mit ihnen zusammengearbeitet zu haben.

Dr. Stefan Weidle danke ich insbesondere für die Revision des Manuskriptes, aber auch für die vielen fachlichen Diskussionen und etlichen spaßigen Freizeitmomente.

Meinen Bacheloranden **Jacob Sag**, **Olivia Rindle**, **Tobias Stimpel** und **Petra Bestler**, meinen Praktikanten **Christoph Gallner**, **Katharine Kaiser**, **Annabelle Degg** und **Björn Klimas** danke ich für ihre ausdauernde Durchführung ihrer Forschungsarbeiten, ihre gute Laune im Labor und ihre positive Art. Hervorheben möchte ich noch die Hilfe der beiden Auszubildenden **Beat Thippeyajan** und **Markus Koll,** die beide ihre Aufgaben sehr gewissenhaft durchgeführt haben und mir hervorragend zugearbeitet haben. Die wohl spannendste Aufgabe erfuhr ich bei der wöchentlichen Betreuung des Schülerpraktikums von **Moritz Kleybolte**, der jede Woche mit sehr viel Elan an seinem Thema gearbeitet hat und sehr wissbegierig war. Vielen Dank für die gute gemeinsame Zeit und die hervorragende Zusammenarbeit.

Sehr wertvoll war auch die Zusammenarbeit mit meinen Kooperationspartnern **Dr. Tobias Kraus** und **Aljosha Rakim** vom Leibniz Institut für Neue Materialien, wofür ich mich hiermit bedanke. Darüber hinaus möchte ich **Prof. Dr. Christine Papadakis** und **Dr. Konstantinos Raftopoulos** vom Physik Department der TUM, sowie **Dr. Marianne Hanzlik** aus der

Abteilung für Elektronenmikroskopie der TUM meinen größten Dank für die sehr aussagekräftigen Messdaten und die Zusammenarbeit bei einer Publikation aussprechen.

Im Wesentlichen möchte ich einigen Lehrstuhlmitgliedern und Ehemaligen besonders danken, die durch ihre Hilfe, gute Gespräche, gemeinsame Freizeitunternehmungen, gemeinsamen Veröffentlichungen und viele weitere besondere Dinge und Momente der Zeit am Lehrstuhl die besondere „Würze“ verliehen haben:

Dr. Malte Winnacker, **Dr. Sven Heidsieck, Dr. Matthias Grübel, Dr. Simon Meister, Dr. Markus Hammann, Dr. Andrij Phlijkta, Dr. Dominik Lanzinger, Dr. Johannes Kainz, Dr. Victor Bretzler, Dr. Dominik Jantke, Dr. Konrad Hindelang, Dr. Andreas Eisele, Dr. Christian Anger, Dr. Stefan Salzinger, “Die Chipmunks”** (**Martin Machat, Daniel Wendel** und **Philipp Pahl**), **Marco Giuman**, **Theresa Ludwig**, **Dr. Maximilian Knaus**, **Sebastian Kraus**, **Dr. Kathrin Deller**, **Dr. Kathrin Bolz**, **Dr. Manuela Phillipp**, **Dr. Alexander Kronast**, **Michael Weger**, **Marco Decker**, **Kathrin Kratzl, Sebastian Weiß**, **Dr. Abdussalam Qaroush und Manuela Hollering.**

Bei allen weiteren Mitgliedern des WACKER Lehrstuhls bedanke ich mich für die gute Zusammenarbeit.

Sehr herzlich bedanke ich mich noch bei den Mitgliedern der „Veinot-Group“ an der University of Alberta. Insbesondere danke ich **Dr. Zhenyu „Kevin“ Yang**, **Dr. Mita Dasog**, **Dr. Muhammad Iqbal**, **Dr. Tapas Purkait**, **Dr. Christina Gonzalez**, **Dr. Lida Hadidi**, **Dr. Morteza Javadi**, **Regina Sinelnikov** und **Amirul Islam** für die sehr herzliche Aufnahme, die vielen gemeinsamen Abenteuer, die gute Zusammenarbeit (über den Atlantik) und die Freundschaft.

Ferner bedanke ich mich bei der **TUM Graduate School** für das reichhaltige Kursprogramm, das Angebot eines Lektoratsservices und die Finanzierungshilfe für den Auslandsaufenthalt.

Darüber hinaus bedanke ich mich bei allen Freunden, mir immer Rückhalt geben, mir helfen den Alltagsstress hinter mir zu lassen durch die vielen Unternehmungen, Telefonate und tollen Momente.

Zu guter Letzt möchte ich meine Familie hervorheben: Ohne meine Mutter **Jutta**, meinen Vater **Artur**, meinen Bruder **Patrick** und meine Frau **Vanessa** wäre ich wahrscheinlich nicht ermutigt gewesen meinen Lebensweg so einzuschlagen. Daher möchte ich mich für die großartige Unterstützung und Hilfe von ganzem Herzen danken. Ihr habt immer ein offenes Ohr für mich, habt Verständnis für lange Arbeitszeiten und gebt mir den Rückhalt im Leben, den ich brauche!

Abstract

Silicon Nanocrystals (SiNCs) are non-toxic and photoluminescent materials with possible benefits in a variety of applications. However, native SiNCs tend to aggregate and lose their photoluminescence (PL) properties. Functionalized surfaces improve the dispersibility of SiNCs in solvents, stabilize their photoluminescence or facilitate electronic effects. Hybrid materials with combined single material properties arouse high interest in this scientific field. Hence, the aim of this thesis was the design of novel SiNC-based hybrid materials and therewith the study of surface grafting procedures.

To prepare thermoresponsive and photoluminescent SiNC based hybrid materials, polymerization of dialkyl vinylphosphonates was conducted from an ethylene glycol dimethacrylate network with intercalated SiNCs. Group transfer polymerization reactions using bis(cyclopentadienyl)trimethylsilylmethylyttrium tetrahydrofurane ($Cp_2YCH_2TMS{\cdot}thf$) with a variety of molecules were studied. The investigations verified that the surface polymer concentration is controlled by the deployed catalyst amount. Surface polymerization of diethyl vinylphosphonate resulted in a water dispersible hybrid material, with stabilized PL and a lower critical solution temperature close to the physiological range.

The second part of the thesis focused on monitoring the radical initiated hydrosilylation process on SiNC surfaces. *In-situ* infrared spectroscopy (IR) studies of the azobisisobutyronitrile initiated surface grafting of vinylsilanes with tunable steric properties demonstrated that radical concentration dependent chain processes and bulkiness of the polymers play an important role during the grafting process. Furthermore, dissolved oligomer radicals were proven to be the dominant species for the initiation on the Si-H surface. Additionally, the data provided insight in the break-up mechanism of SiNC agglomerates during functionalization.

In another project, the intercalation of SiNCs into silica aerogels was studied. Triethoxy vinylsilane was grafted to the SiNC surfaces through radical hydrosilylation. Therefore, the SiNC surfaces readily reacted to free silanol groups by hydrolysis and condensation reactions. Two pathways of intercalation were studied: If SiNCs were added during the gelation process enhanced crosslinking of the final aerogels was obtained. In contrast, if SiNCs were washed in the alcogels after gelation, they settled into the pores. The alcogels gained their superhydrophobic properties by the reaction with trimethylsilylchloride and were subsequently dried by the supercritical approach (CO_2). The obtained aerogels exhibited the size dependent PL of the SiNCs and had a high surface (~1000 m^2/g). They could readily be used to accumulate and detect very low concentrations of 3-nitrotoluene (270µM) solved in water.

Although this thesis mainly focusses on SiNC grafting, the preparation of oxasilacycles, their reactivities towards photoacid generators and their uses in polymer chemistry were studied. The detailed project description can be found as *addendum*.

Zusammenfassung:

Die photolumineszierenden Silicium Nanokristalle (SiNK) haben gegenüber anderen Halbleiter-Quantenpunkten einige anwendungsspezifische Vorteile, wie zum Beispiel ihre physiologische Unbedenklichkeit. Jedoch kann durch eine erhöhte Aggregationsneigung ihr praktischer Nutzen durch unfunktionalisierte Oberflächen limitiert sein. Dagegen weisen oberflächenfunktionalisierte SiNKs eine verbesserte Dispergierbarkeit in organischen Lösemitteln und eine stabilisierte Photolumineszenz (PL) auf. Aufgrund eines Zusammenspiels einzelner Materialeigenschaften kann eine weitere Verbesserung durch Hybridisierung (z.B. mit Polymeren/Silica) erreicht werden. Daher sollten in dieser Arbeit neue Hybridmaterialien hergestellt werden und zugrundeliegende Funktionalisierungsprozesse studiert werden.

Zunächst wurde die Herstellung von thermoresponsiven und photolumineszenten SiNK basierten Hybridmaterialien untersucht. Dazu wurden die SiNK in ein Netzwerk aus Ethylenglycoldimethacrylat eingebunden, wovon Dialkylvinylphosphonate katalytisch anhand einer Gruppen-Transfer-Polymerisation mit Bis(cyclopentadienyl)trimethylsilylmethylyttrium tetrahydrofuran ($Cp_2YCH_2TMS{\cdot}thf$) polymerisiert wurden. Die Untersuchungen ergaben, dass der Gehalt an Oberflächenpolymer abhängig ist von der eingesetzten Katalysatormenge. Das anhand von Diethylvinylphosphonat hergestellte Material hatte eine untere kritische Lösungstemperatur in Wasser, wobei die Photolumineszenz der SiNK stabilisiert wurde.

Des Weiteren wurde die radikalischen Hydrosilylierungsreaktion auf Hydrid terminierten SiNK Oberflächen untersucht. Die anhand von *in-situ* Infrarotspektroskopie beobachteten Studien erfolgten mit Azobisisobutyronitril (AIBN) als Radikalinitiator und verschiedenen Vinylsilanen als Monomere. Die erhaltenen Messergebnisse zeigten zweifellos, dass SiNK-Aggregate während der Funktionalisierung aufgebrochen werden müssen. Des Weiteren laufen während der Funktionalisierung Kettenreaktionen ab, deren Geschwindigkeiten mit den Radikalkonzentrationen korrelieren. Weiterhin hat die Sterik der Monomere einen starken Einfluss auf die Funktionalisierungsgeschwindigkeit. Aufgrund dieser Erkenntnisse konnte gefolgert werden, dass Oligomerradikale in Lösung wesentlich an der Oberflächeninitiierung beteiligt sind.

In einem weiteren Teilprojekt wurde der Einbau von SiNK in Silica Aerogele untersucht. Triethoxyvinylsilan (TEVS) wurde als hydrolysierbare Oberflächengruppe eingesetzt um eine kovalente Anbindung der SiNK an die Aerogele zu ermöglichen. Die damit funktionalisierten SiNK wurden zum Gelierungsgemisch gegeben, wodurch die finalen Aerogele stark vernetzten, oder in das fertige Lyogel gewaschen, was zu einer Penetration der Poren führte. Die zuletzt erhaltenen superhydrophoben Aerogele zeigten SiNK-größenabhängige PL und hatten innere Oberflächen von ~1000 m^2/g. Somit konnte das Hybridmaterial zur Adsorption und Detektion niedriger Konzentrationen (270 µM) Nitrotoluol aus Wasser genutzt werden.

Darüber hinaus wurde in einem Nebenprojekt die Synthese von Oxasilacyclen, deren Reaktivität mit photoaktiven Brönstedtsäuren und deren Einsatz in der Polymerchemie untersucht. Eine Detaillierte Beschreibung und Zusammenfassung des Projektes kann im *Addendum* gefunden werden.

Abbreviations

2-VP	2-vinylpyridine
2,6-Br-4-DDB	2,6-bromo-4-decyl-diazobenzene tetrafluoroborate
2-NO-4-DDB	2-nitro-4-decyl-diazobenzene tetrafluoroborate
3-NT	3-nitrotoluene
4-bromo-DB	4-bromo diazobenzene tetrafluoroborate
4-DDB	4-decyl-diazobenzene tetrafluoroborate
AFM	atomic force microscopy
AIBN	azobisisobutyronitrile
ATR	attenuated total reflection
BCF	*tris*(pentafluorophenyl borane)
bipy	2,2′-bipyridine
BPO	dibenzoyl peroxide
C12	dodecyl functionalized
CB	conducting band
CIE	fr.: *Commission internationale de l'éclairage*
COOH	pentanoic acid functionalized
CNT	carbon nanotubes
CVD	chemical vapor deposition
D	dimension
D3/D4/D5	3, 4, 5 membered cyclic dialkylsiloxanes
DAVP	dialkyl vinylphosphonates
DEVP	diethyl vinylphosphonate
DHP	diphenyliodonium hexafluorophosphate
DIT	diphenyliodonium triflate
DMAA	dimethylacrylamide
DMVP	dimethyl vinylphosphonate
dppp,	1,3-bis(diphenylphosphino)propane
DPVP	di-n-propyl vinylphosphonates
E	energy
EGDM	ethylene glycol dimethacrylate
ET	electron transfer
FRET	fluorescence resonance energy transfer
FT	Fourier transfer
HeLa	Helena Lax
HMT	6-hydroxyhexyl 3-(methylthio)-2-phenyl-3-thioxopropanoate
HNDPB	N-hydroxy-5-norbornene-2,3-dicarboximide perfluoro-1-butanesulfonate
HOMO	highest occupied molecular orbital
IPOx	2-isopropenyl-2-oxazoline
IR	infrared spectroscopy
ITO	indium tin oxide

k	reciprocal space
KCTP	*Kumada* catalyst transfer polycondensation
LCST	lower critical solution temperature
LED	light emitting diode
LUMO	lowest unoccupied molecular orbital
MALDI	matrix assisted laser desorption/ionization
m-CPBA	*meta*-chloroperoxybenzoic acid
MMA	methyl methacrylate
M_n	number average molecular weight
M_w	weight average molecular weight
NBS	N-bromosuccinimide
OLED	organic light emitting diode
P3HT	poly-3-hexylthiophene
PAG	photoacid generator
Panc-1	human pancreas epithel cells
p_C	critical pressure
PDAVP	poly(dialkyl vinylphosphonate)
PDEVP	poly(diethyl vinylphosphonate)
PDMVP	poly(dimethyl vinylphosphonate)
PDPVP	poly(di-*n*-propyl vinylphosphonate)
PDMS-H	((15%−18% methylhydrosiloxane)−dimethylsiloxane copolymer)
PEDOT:PSS	poly(3,4-ethylenedioxythiophene) polystyrene sulfonate
PEG	polyethylene glycol
PEGDM	polyethylene glycol dimethacrylate
PETN	pentaerythritol tetranitrate
PL	photoluminescence
poly-TPD	poly[N,N'-bis(4-butylphenyl)-N,N'-bisphenylbenzidine]
PS	polystyrene
p-Si	porous silicon
QD	quantum dot
RAFT	reversible addition-fragmentation chain transfer polymerization
RDX	Research Department Explosive (cyclotrimethylene trinitramine)
REM-GTP	rare earth metal-mediated group transfer polymerization
ROP	ring opening polymerization
SAM	self-assembling monolayers
SAXS	small angle X-ray scattering
SEM	scanning electron microscopy
SI	surface-initiated
SiNC, Si-nc	silicon nanocrystal
SiNK	silicon nanocrystal (ger. *Silicium Nanokristall*)
SiNP	silicon nanoparticle
SiNR	silicon nanorod
SiNSs	silicon nanosheets
SiNT	silicon nanotube

SiNW	silicon nanowire/nanowhisper
STM/STS	scanning tunneling microscopy/spectroscopy
T_C	critical temperature
TEM	transmission electron microscopy
TEOS	tetraethyl orthosilicate
TEVS	triethoxyvinylsilane
THF	tetrahydrofurane
TMOS	tetramethyl orthosilicate
TMS	trimethylsilyl
TMSPM	3-(trimethoxsilyl)propyl methacrylate
TNT	trinitro toluene
TOF	turnover frequency/time of flight
TOPO	trioctylphosphine-oxide
TST	triphenylsulfonium triflate
UV	ultraviolet
VIS	visible
VLS	vapor-liquid-solid
VOC	volatile organic compound
VSS	vapor-solid-solid
XPS	X-ray photoelectron spectroscopy

Units

A	ampere
W	watt
ns	nanoseconds
µs	microseconds
%	per cent
mg	milligram
eV	electron volt
°C	degree Celsius
atm	atmospheres
d	days
m	meters
g	grams
h	hours
wt.%	weight per cent

Content

1. Introduction

Nanotechnology has matured into a widespread field of technologic and synthetic approaches for the production of smaller and smaller materials and devices. In 1959, when Richard P. Feynman held his famous talk "There is plenty of room at the bottom",[1] only a select few could imagine how nanoscience could impact today's processes. With his clear proposals, Feynman pioneered the field and almost all his suggestions have been realized. High resolution microscopy instruments such as transmission electron microscopes (TEM) and scanning tunneling microscopes (STM) became powerful tools for structure analyses with high magnifications and resolutions, and data storage devices have been prototyped using nanostructures in the sub-10 nm scale, just to name some examples.[2,3]

Since the 1970's, researchers have explored the nanoscience field and contributed to it by preparing materials in the sub-100 nm regime and elucidating general effects observed only in the nanoscale. Thus, several structures like mesoporous solids (e.g. mesoporous silica), cylindrical nanorods (e.g. carbon nanotubes), 2 dimensional (D) sheets (e.g. graphene) and particles with various shapes were realized by the usage of insulating, semiconductive, or conductive elements and chemical composites. Meanwhile nanoparticles have been widely tested and prototyped in various applications. For example, insulating silica nanoparticles can be used for drug delivery and release,[4] titanium nanoparticles exhibit photocatalytic surface activities[5], metallic platinum or gold nanoparticles are useful in catalysis,[6] and semiconductor nanoparticles of Ge or Si have been prototyped in photovoltaics.[7]

In the broad field of nanoparticle science, semiconductor nanoparticles (also known as quantum dots, QDs) consistent of group II-VI, IV-VI and III-V elements (e.g. CdAs, CdS or InGaAs) are of special interest, since they exhibit unique optoelectronic properties (e.g. photoluminescence, PL). Often, irradiation is responsible for the generation of excitons in several semiconductor materials. Thus, electron-hole pairs form if the energy of the incident light is greater than the band gap between the semiconductor's valence and conduction band. In quantum dots, energy levels within the band gaps become discrete levels and the band gap becomes size dependent, as the exciton mobility is strictly confined in the nanoscale by the Bohr radius of the electron-hole pair.[8] If smaller than the Bohr radius, particles exhibit photoluminescence in the visible region from recombination of the excitons. These properties make QDs suitable in a variety of applications: As promising alternatives to bulk materials, QDs have been tested in photon conversion devices such as solar cells or solar fuels, since tunneling effects allow electron transfer to matrix materials (e. g. conducting polymers).[9] Furthermore, due to their small sizes and PL, QDs can be useful for *in vivo* cancer targeting and imaging agents[10] and as efficient sensors for the detection of chemicals and biochemical molecules.[11] However, binary semiconductor QDs such as CdSe, CdS or CdAs exhibit acute cytotoxic behavior due to a low electrochemical stability and the consecutive release of toxic ions.[12]

Silicon Nanocrystals (SiNCs) have emerged as non-toxic and electrochemically stable alternatives.[13] Although bulk Si is an indirect semiconductor and the band gap optical transition is dipole forbidden,[14,15] exciton recombination in SiNCs below the Bohr radius (~5 nm) occurs through quantum confinement effects which results in PL in the visible region.[16] However, in an unmodified form, SiNC surfaces are prone to oxidation and aggregation, and PL quenching is likely to occur from external influences.[17,18] Hence, to adapt SiNCs to the requirements of their applications, surface functionalization is one of the major approaches to render them dispersible and to stabilize them. Modern approaches include the generation of SiNC hybrids and composite materials.

In this thesis, the recent developments in the generation of a thermoresponsive and photoluminescent diethylvinylphosphonate coated SiNC hybrid material, and the attachment of SiNCs to silica aerogels as optical sensors, as well as *in-situ* IR studies regarding the radical grafting of SiNCs with vinylsilanes are summarized and set in the context of today's SiNC field.

2. Background

2.1. Overview: Silicon-based Nanomaterials

For more than half a century silicon has been known as the dominant element for applications in photovoltaics, electronics and microelectronics.[19] The importance of this group IV element is demonstrated by its world production of about 8 million tons.[20] Silicon in its elemental form is prepared from reduction of SiO_2 with coal (Scheme 1). Due to several impurities, purification is performed by thermal oxidation with HCl and distillation of the $HSiCl_3$ previous to the reduction step with pure hydrogen. Further purification by Czochralski process or zone melting gives highly pure and crystalline silicon.[19]

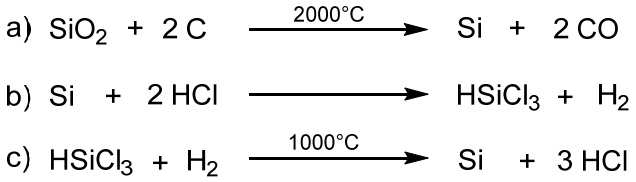

Scheme 1. General strategy for the preparation of pure silicon a) Technical reduction of SiO_2, b) Synthesis of trichlorosilane from HCl and subsequent distillation, c) Formation of pure silicon by hydrogen reduction of trichlorosilane.[19]

Although silicon wafers are incorporated in most of the electronic devices and solar cells, several drawbacks are attributed to its bulk form: Silicon surfaces are prone to native oxidation. Furthermore, due to the inherent indirect nature of silicon, exciton recombination and transfer is dipole forbidden and the introduction of selected impurities (also known as doping) is required to adjust the properties and allow exciton recombination through the dopant. In addition, a demand for smaller and smaller devices is hindered by technical top-down approaches (e.g. milling) and the selectivity to form uniform structures based on bulk silicon reaches its limits.[21]

To overcome oxidation, surface functionalization strategies including catalyzed (Karstedt's catalyst),[22] radically initiated,[23,24] electrochemical,[25] catalyst free (thermal, photochemical, Grignard- or organolithium compounds),[26,27] and halogenation methods[28,29] have been introduced.[21] The development of various silicon nanomaterials and nanostructured materials instigated a boom in the field with the aim to negotiate the limitations of the bulk material (Figure 1). For semiconductor nanomaterials quantum confinement effects emerge a modern pathway towards unprecedented optoelectronic properties.[16,21,30] Furthermore, silicon nanomaterials are proposed to enhance the construction of smaller and more defined devices due to their small sizes.[18] Nanostructured 3 dimensional (D) and 2, 1 or 0 D Si nanomaterials have been prototyped in sensing (e.g. chemical or biological sensing),[31–33,34] bioimaging,[35–41] catalysis,[42,43] solar and photovoltaic applications,[44,45] light emitting diodes or other optoelectronic devices,[46,47,48] (thin film) transistors,[49] as anode material in lithium-ion batteries[50,51–54] and in many more promising applications.[18,21,55,56]

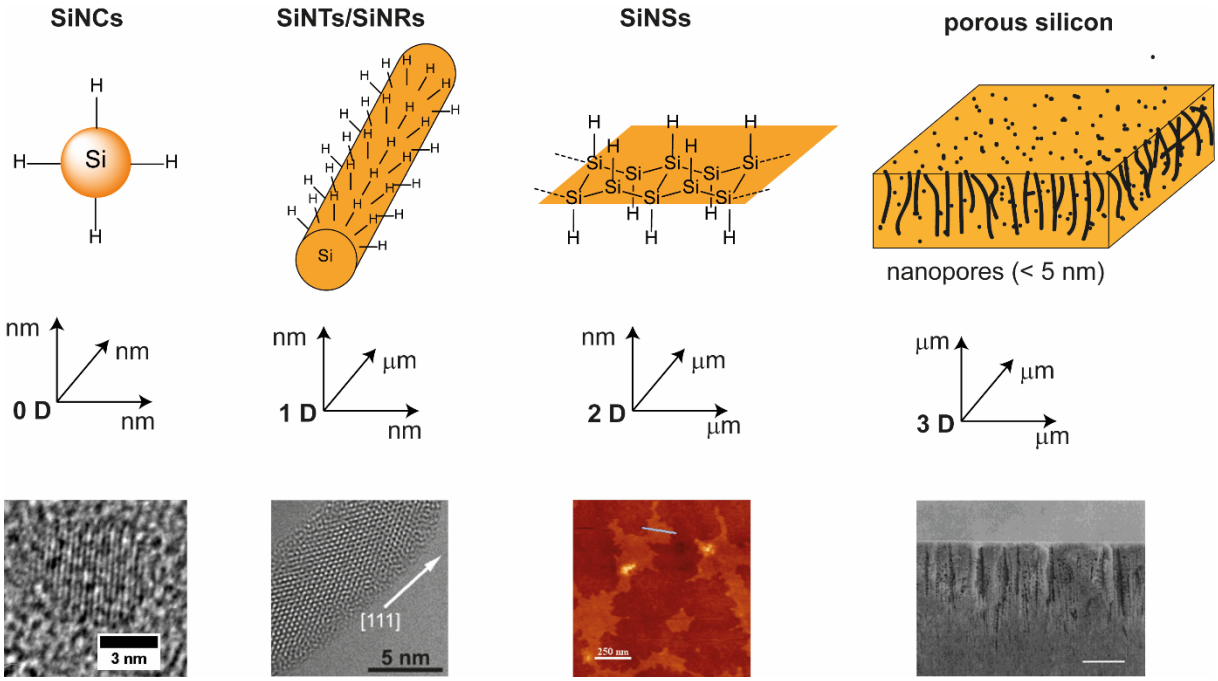

Figure 1. Overview of silicon nanostructures.[21,57,58] Reproduced and adapted with permission from references 21, 57, 58. Copyright 2002, 2015 American Chemical Society; 2016 WILEY-VCH Verlag GmbH & Co. KGaA, Weinheim.

Porous silicon (p-Si) is one of the earliest, and probably most examined example of a silicon nanostructure. It can easily be obtained by galvanostatic,[59] chemical[60] or photochemical etching[61] of Si (100) wafers, without changing the 3 D macroscopic morphology.[62,63] By discovering PL from p-Si, Canham kicked-off the investigation of the fascinating properties of Si nanomaterials.[64] This unprecedented feature was later reported for 1 D nanowires and 0 D nanocrystallites (2 nm in diameter), which also undergo quantum confinement effects.[21,62,65] In addition to PL, the discovery of chemiluminescence and electroluminescence of p-Si has widened the range of possible applications towards chemical or biological sensing, or light emitting diodes (LED).[66] However, to prevent quenching of the p-Si luminescence by oxidation and defects, surface functionalization is of higher importance, than for bulk Si.[21] Passivation of p-Si requires similar protocols as the functionalization of bulk Si. Though, a general tendency towards higher surface reactivity of p-Si has been observed.[21]

Magnesiothermic reduction has recently been presented as a very selective and efficient method for the transformation of various kinds of porous silica micro- and nanostructures to their 3 D silicon analogues. In 2007, Bao *et al.* succeeded in the preparation of silicon diatom frustules from their natural silica precursors.[67] In addition to the silica precursor, the reaction process requires magnesium as a reducing agent. During heating at 600 – 700°C, magnesium migrates to the vapor phase, penetrates the silica structure and reacts readily with the oxygen.[68] However, if Mg is added in high excess, Mg_2Si, (in the presence of carbon SiC) can form as side products; thus, the products require post-treatment with HCl (to remove Mg_2Si) and HF (removal of unreacted silica).[67,69] Besides diatom frustules, several other porous, mesoporous, bioinspired and naturally abundant silica structures could be transformed/reduced to silicon.[68,70,71] Also, some of the nanodomains emit PL in the visible region due to quantum confinement effects. Thus, the magnesiothermic reduction approach has high potential in the

generation of customized solutions, as already shown in drug delivery,[71] sensing,[72] or the preparation of battery anode materials.[54]

Going down the road of sizes, the two-dimensional silicon nanosheets (SiNSs) or layered polysilanes have emerged as interesting 2D materials (Figure 1). SiNSs can be obtained from different methods, such as magnesiothermic reduction from SiO_2,[73] growth on support by chemical vapor deposition (CVD),[74] or chemical exfoliation from $CaSi_2$ (Scheme 2).[75,76] Structurally, SiNSs have characteristic layers of Si atoms with thicknesses in the nano-scale and sheet sizes up to the micro scale.[77] They consist of 6 membered ring structures with hydride atoms standing out of the plane (Si_6H_6).[78] The layered characteristics make them promising for uses in field effect transistors,[79] photovoltaics[55] or as anode materials in Li-ion batteries.[80]

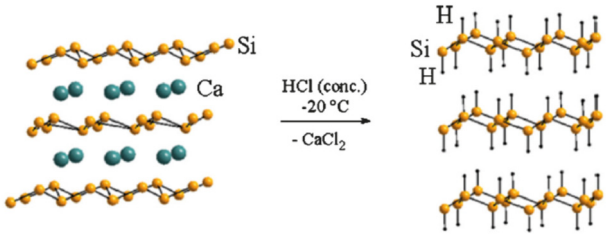

Scheme 2. Chemical exfoliation of hydride terminated SiNSs from calcium silicide.[58,76] Reproduced and adapted with permission from reference 58. Copyright 2016 WILEY-VCH Verlag GmbH & Co. KGaA, Weinheim.

Compared to other Si nanomaterials, SiNSs exhibit different optoelectronic properties, such as an absorption edge, which depends on the thickness of the SiNSs stacking,[81] or an enhanced direct band gap transition.[55,82] Theoretical studies remark that SiNSs' band gap is tunable by physical strain,[83] the degree of hydrogenation or functionalization with heteroatoms,[84] and surface passivation.[85] Although it is very important to prevent surface oxidation, enhance dispersibility in organic solvents and to break up the stacked structures,[58] only a few methods on surface functionalization of SiNSs have been presented so far. Attachment of n-alkylamines,[77,86] Pt catalyzed hydrosilylation[87] and surface reactions with phenylmagnesiumbromide[77] have been established to stabilize SiNSs. However, these methods lead to blue-shifting or quenching of the PL. Recently, Helbich *et al.* have shown that hydride terminated SiNSs react readily under thermal conditions (T = 130°C) or in the presence of a diazonium salt with alkenes and alkynes, with stabilization of the PL at about 500 nm.[58] SiNS were further surface grafted with polymers like polystyrene, poly(methyl methacrylate) and poly(acrylic acid), which protected them from decomposition by ultraviolet (UV) light or bases.[88]

1D structures have generated scientific interest as further promising Si nanomaterials (Figure 1). They have cylindrical structures with diameters of a few nanometers and lengths of up to several micrometers. In general 1D Si nanostructures are classified as silicon nanorods (SiNR), silicon nanowires or -whiskers (SiNWs) and silicon nanotubes (SiNTs) with remarkable structural differences.[55] SiNRs and SiNWs, which differ in the aspect ratios of diameter to length, have emerged as non-hollow structures with diameter of less than 100 nm, while SiNTs have emerged as carbon nanotube (CNT) analogous silicon material.[55,89,90]

Most challenging for the preparation of 1 D Si nanostructures is the directed growth along one axis.[91] Thus, several procedures follow templated or catalytic pathways with metal particles.[55,92] Vapor-liquid-solid (VLS)[93,94] and vapor-solid-solid (VSS)[95] syntheses have often been applied for the preparation of SiNWs. The procedure follows adsorption of a silicon precursor (e.g. SiH_4) to a surface of molten metal nanoparticles, diffusion of Si through the liquid alloy to a sink, crystallization at the liquid solid interface and finally lateral SiNW growth.[93,94] As further preparation methods, high temperature laser ablation,[96] oxide-assisted growth[97], molecular-beam epitaxy growth[98] and solution-based methods (e.g. supercritical-liquid-solid method)[93,99,100,101,102] have been discussed in literature. More convenient solution-based methods for SiNR preparation have recently been shown by Korgel *et al.*[57,90,103,104] Thereby, syntheses were conducted in squalane using silanes as substrates, Au or Sn nanocrystals as seeds and dodecylamine as ligand at 420 °C. Although gold seeds could be removed by aqua regia, SiNRs have been obtained with high amounts of surface oxide.[103] Sn particle based synthesis of SiNRs and removal of Sn particles and dodecylamine, and subsequent hydrosilylation of the Si-H surface with octadecene yielded photoluminescent 1 D nanomaterials.[57,104]

Emerging from their hollow structure, synthetic pathways for SiNTs follow complex protocols, especially since single wall SiNTs could not be obtained from roll up of the graphene analogue SiNSs yet.[55] Thus, a more precise definition of SiNTs would be hollow SiNWs.[91] SiNTs are attractive materials, as they are predicted to exhibit very intense PL in comparison to SiNWs.[105] Although theoretical calculations highlighting possible structures and properties for single wall SiNTs have been examined by several authors,[106] practical preparation approaches are very challenging compared to other silicon nanostructures.[55] Hence, closed-capped SiNTs have been obtained from self-organized, catalyst-free synthesis under high pressure and temperature conditions using silicon monoxide as precursor,[107] thin SiNTs were obtained from high purity Si-powder in gas phase under arc discharge conditions,[108] and templated or template replication methods resulted in SiNTs with various characteristics.[109] However, SiNTs did not find their way into practical approaches so far.

Silicon Nanocrystals (SiNCs), which are also referred to as Si quantum dots (QDs),[56] are most promising amongst the Silicon nanomaterials due to their size-dependent optoelectronic properties. Due to their small sizes, they are categorized as 0 D silicon with crystalline arrangement in diamond lattice (Figure 1). A variety of preparation[16] and surface functionalization methods have been presented in the literature with the aim to prevent oxidation, tune the PL properties and render them dispersible in various solvents.[18,56] SiNC preparation, surface chemistry as well as the preparation of hybrid and composite materials will be discussed in more detail in this thesis.

2.2. Properties of Silicon Quantum Dots

As mentioned in the previous section Silicon nanomaterials and in particular Silicon quantum dots exhibit unique optoelectronic properties, namely photo- and electroluminescence, making them promising materials in semiconductor industries, sensing or in biomedical applications.[16,18,56] SiNCs are well suitable for such uses due to their low toxicity,[110] good biocompatibility,[41] electrochemical stability[111] and a low rate of photobleaching.[35]

Silicon is generally known as indirect semiconductor - whereby the minimum of the conducting band and the maximum of the valence band are shifted along the *k*-axis - with a band gap energy difference of ~1.1 eV.[19,112] Band gap transition in an indirect band gap semiconductor is only possible by the contribution of a momentum change in the *k*-space induced by a phonon.[113] This momentum change cannot be achieved by a photon, since its momentum is negligible. Thus, for bulk silicon the direct band gap transition is only possible by crystal lattice defects emitting or absorbing a phonon. Such lattice defects in many cases can be created by doping of silicon by various elements (e.g. B, N, P, Li, Sb).[114] However, photoluminescence from radiative recombination of excitons is not likely to be induced and non-radiative recombination mechanisms have higher probabilities.[113]

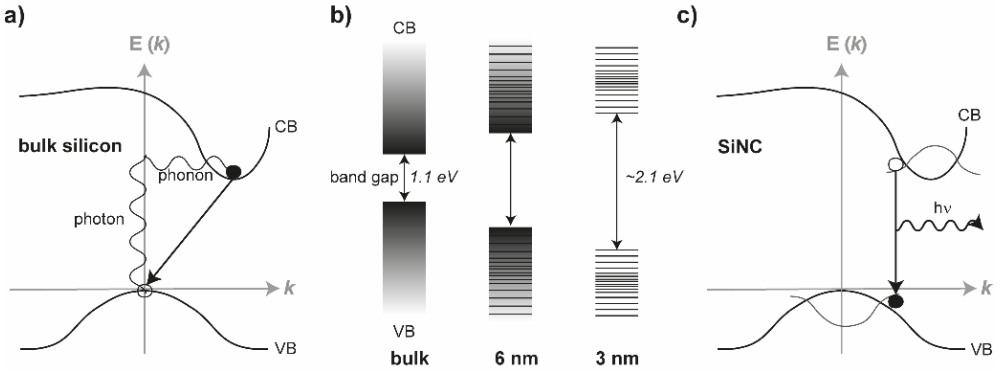

*Figure 2. Schematic illustration of the band structure of bulk silicon (**a**) and nanosilicon regarding quantum confinement effects (**c**). Development of the band gap and illustration of the change in the band structure towards pseudo concrete levels with decreasing size of the silicon structure (**b**). VB: valence band; CB: conducting band; k: reciprocal space; E(k): energy.*[112,115]

Although SiNCs are also indirect semiconductor materials, they exhibit PL without the presence/addition of dopants. Electron transfer from the valence band into the conduction band and recombination does not require the generation of a phonon in the *k*-vector (Figure 2 c). This is due to the confinement of the excitons in a nanoscale semiconductor with a diameter below the Bohr exciton radius (~ 4.3 nm).[8,116] Hence, the band energies get discrete energy levels and exciton recombination is allowed to take place by radiative recombination. Furthermore, due to the quantum confinement effect, band gap energies become size dependent, e.g. they increase with decreasing SiNC sizes (Figure 2 b).[16] This is evidenced by the size dependent reactivity and PL exhibited (Figure 3).[16,117–119]

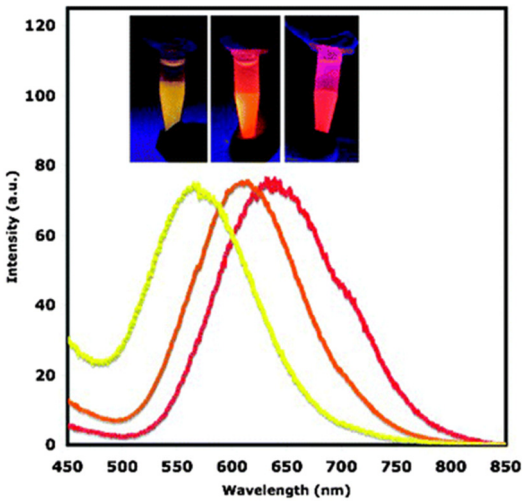

Figure 3. H-SiNC size dependent PL emission spectra (excitation wavelength is 350 nm).[16] Reproduced and adapted with permission from reference 16. Copyright 2006 The Royal Society of Chemistry.

Another important property is the high surface to volume ratio. Avramov *et al.* were recently able to calculate the amount of surface atoms of a 2 nm Si icosahedron, which consisted of 280 atoms with 120 surface atoms, a ratio of 43 %.[120] As generally known, surfaces and interfaces have higher free energy, than the materials' cores or bulks.[121] Thus, energies of nanoparticle surfaces are tremendously enhanced with an increasing ratio of surface to bulk atoms (and *vice versa*). Both, surface chemistry and size of the SiNCs can influence the final properties independently.[17,122] Hence, upon alkyl passivation band gap energies can slightly change or surface engineering with heteroatoms can greatly influence the final optoelectronic properties.[123,124] Therefore, an understanding of surface chemistry and physics is highly important and needs to be carefully evaluated for surface engineering.

2.3. Strategies for the Preparation of Silicon Nanocrystals

Silicon nanocrystals can be obtained by various methods, which are basically different than other Si nanomaterials. In principle properties like size, morphology control over crystallinity as well as surface functionalities play a major role for the choice of the appropriate synthesis route.[16,18] Two fundamental preparation strategies have been followed (Scheme 3): Bottom-up methods have most often been based on Si(IV) precursors, while top down approaches have emerged from the size reduction of macroscale Si(0) primary stages. The most common procedures can be classified in silicon halide or alkoxide reduction, metal silicide oxidation, silane decomposition and thermal disproportionation of silicon rich oxide.[18] Furthermore, several top-down approaches regarding the preparation of Si nanoparticles from p-Si by sonication or pulverization have been described.[125] However, by physical approaches, nano- and micrometer particles are often obtained in broad size distributions. In addition, such procedures allow low morphology-control and PL arises from 0D and 1D structures embedded in these porous Si nanoparticles,[16] which are not discussed in detail.

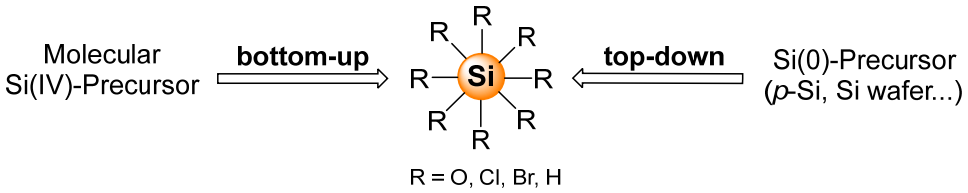

Scheme 3. General preparation strategies for SiNCs.

2.3.1. SiNC Preparation in Solution and Dispersion

Solution based protocols describe attractive methods for the preparation of SiNCs, with comparatively high yields and promising control over particle sizes and surface chemistry.[16] In 1992, Heath investigated a method for the reduction of a mixture of $SiCl_4$ and $RSiCl_3$ (R = H or n-octyl) by heterogeneously dispersed sodium (Scheme 4).[126] Reaction conditions required high temperatures (385 °C), high pressures (>100 atm) and long reaction times (5-7 d). This preparation procedure resulted in crystalline Si nanoparticles with broad size-distribution (3-9 nm) and mixed surfaces (Si-H, Si-O and Si-Cl). Using ultrasonication Dhas *et al.* simulated the high pressure conditions and could achieve a reduction of tetraethyl orthosilicate (TEOS) and $SiCl_4$ to Si(0) by colloidal Na-dispersion in toluene at -70 °C.[127] Subsequent annealing yielded agglomerated silicon nanoparticles with 2-5 nm sizes and diamond lattice. Furthermore, the co-reduction of a silicon precursor ($SiCl_4$) in the presence of PCl_3 by magnesium powder and surface functionalization *via* a Grignard reagent can be used to obtain 2-12 nm phosphorus doped and alkyl terminated Si nanoparticles.[128]

Besides the heterogeneous conditions, the use of $LiAlH_4$ resulted in a more monodisperse dispersions for the preparation of silicon nanoparticles (Scheme 4). Similar to the generation of

pyrophoric silanes by reduction of $SiCl_4$ with $LiAlH_4$,[129] Wilcoxon *et al.* yielded 2-10 nm crystalline Si nanoparticles in an inverse micellar emulsion; however, no evidence of surface functionality of the nanoparticles has been given.[130] Later, an adaption of the $LiAlH_4$ reduction allowed Tilley *et al.* to prepare small and monodispersed SiNCs, presumably equipped with hydride surface groups, as was evidenced by Si-H reactivities in the final products.[37,131–133]

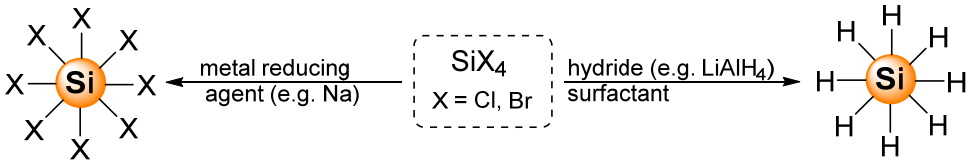

Scheme 4. Schematic illustration of the SiNC formation by metal or hydride reduction of silicon halide precursors.[16,18,56]

Sodium naphthalenide as reducing agent for $SiCl_4$ in glyme gave promising results with regard to varied sizes, surface chemistry and shape control of SiNCs.[134–136] By this pathway chloro-terminated SiNCs could be obtained, which were readily reacted with methanol[136] or octanol.[135] Thus extracted 4.51 nm (standard deviation, $\sigma = 1.1$) SiNCs had alkoxy surface groups and could undergo further surface functionalization.[136] Additionally, alkyl terminated tetrahedral SiNCs in the size range of 40–80 nm could be prepared by Na-naphthalenide reduction and post modification by n-butyllithium.[137]

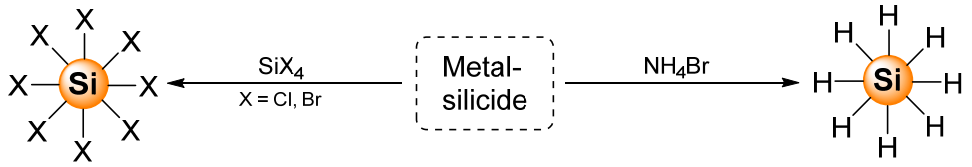

Scheme 5. Schematic illustration of the SiNC formation by metal silicide oxidation reaction.[16,18,56]

Yet another solution-based approach towards the generation of SiNCs is the application of Zintl salts of the form ASi (A = Na, K, Mg) obtained from high temperature reactions of metals with silicon (Scheme 5).[16] Zintl salts can either be used for the reduction of $SiCl_4$ or directly be converted into SiNCs. In 1996 Bley *et al.* reduced $SiCl_4$ by KSi in glyme to generate small amounts of freestanding SiNCs.[138] The powder obtained by this reaction consisted of amorphous material containing several silicon nanoparticles with diamond lattice properties. It was found that such SiNCs bear chloride surfaces, which could be reacted with methanol. Kauzlarich *et al.* further demonstrated that besides KSi, NaSi[139] as well as the less reactive Mg_2Si[140,141] are also suitable precursors for the preparation of SiNCs, although no size distribution data and limited information was given regarding their surface chemistry. Subsequently, Liu *et al.* proposed that Br_2 oxidation of Mg_2Si gave crystalline silicon particles,[141] which was later confirmed by Pettigrew *et al.*[142] Although isolation of particles could not be reported, transmission electron microscopy (TEM) analysis revealed SiNCs of about 4.8 nm in diameter with crystalline cores. A direct preparation of SiNCs from ultrasonication of NaSi was investigated by Lee *et al.*[143] SiNC particle sizes were at about 1-5 nm and blue or white light emission could be adjusted by the ultrasonication time. As further precursor method, reductive thermolysis of N, N′-di-tert-butyl-1,3-diaza-2,2-dichloro-2-silacyclopentane by elemental lithium in trioctylphosphine oxide (TOPO) gave TOPO-

capped SiNCs (5.2 nm ± 1.2 nm). By using this method, SiNC surfaces could not be liberated from the surface ligand and the surface could not be tailored further.[144]

2.3.2. Precursor Decomposition and Reassembly

Due to the good availability of precursors and the utility of the method, solution syntheses have promising prospects for the preparation of silicon nanoparticles (SiNPs) in mostly high yields.[16] However, arising from the harsh conditions or pyrophoric educts, syntheses are delimited to low SiNP concentrations and surface treatment procedures are scarce or require multiple preparation steps. Milder approaches conduct precursor decomposition and reassembly methods like synthesis in supercritical fluids, laser pyrolysis, or plasma synthesis.[56]

Thermal synthesis of SiNPs in supercritical fluids has already been shown in 2001 by Holmes *et al.*[145] The procedure ran *via* thermal degradation of diphenylsilane in a supercritical octanol/hexanes mixture with low yields. Due to size control arising from the variation of the octanol (or octanethiol) to silane ratio, the authors concluded, that the reaction is effectively quenched and surface functionalized by the ligand.[145,146] Hence, well passivated and high quantum yield SiNCs above 1.5 nm could be achieved with narrow size distributions, which became broader with increasing mean particle sizes. Furthermore, SiNCs were produced by thermolysis achieved by microwave heating of SiNWs in glutaric acid as precursor species.[99,101,102,147]

An extensively used procedure for the preparation of SiNCs has been the high temperature gas phase pyrolysis, with mainly SiH_4 aerosols used as precursor (Scheme 6).[16,56] This procedure has first been performed by Murthy *et al.* in 1976, who were able to synthesize crystalline and octahedral 30-80 nm Si particles.[148] In the early stage of SiNC sciences, this method has become a promising alternative preparation protocol being adapted by several research groups; particularly since it allowed for the size control of surface oxidized SiNCs.[14,15,149]

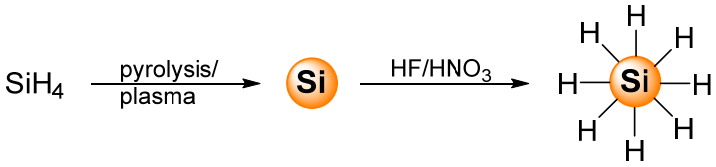

Scheme 6. Schematic illustration of the SiNC formation by pyrolysis or plasma induced silane decomposition.[16,18,56]

Further development in silane pyrolysis methods could be achieved by the use of a high power CO_2 laser, as was investigated by Cannon in 1982.[150,151] Due to high temperatures of up to 1000°C, SiNCs have formed in the area, where the laser beam was intersected with silane.[150,151] Although this method has been varied by several scientists,[152] only Huisken *et al.* could gain significant PL upon etching with HF.[153] Laser induced pyrolysis of SiH_4 aerosols have been used for the preparation of large quantities of silicon nanoclusters (~20-200 mg) up to 50 nm (Scheme 6).[13,119,154,155] Subsequently, freestanding SiNCs with tunable color and quantum yields of ~2-39 % could be obtained from size selective etching with HF and HNO_3.

Non-thermal plasma synthesis is a mild alternative for the formation of freestanding SiNCs compared to thermolysis procedures.[56,156] By dissociation of precursor molecules (e.g. SiH_4) by "hot" electrons, nucleation and subsequent growth of the particle cores from anion-molecule interactions is initiated. Particle growth can be stopped in plasm synthesis, since electrons can readily attach to the positively charged and unsaturated Si_nH_m clusters and confine them in the plasma.[156] Plasma synthesis has been used so far by several groups for the preparation of freestanding SiNCs from a few to several tens of nanometers with mainly Si-H surfaces, which are prone to oxidation.[157,158] The Jurbergs *et al*. approach yielded in freestanding SiNCs with quantum yields up to 60 %.[157] The plasma induced method has furthermore been modified, e.g. by using a microwave discharger operating at reduced pressure,[159] or under atmospheric conditions.[160]

2.3.3. Pyrolysis of Silicon Rich Oxides

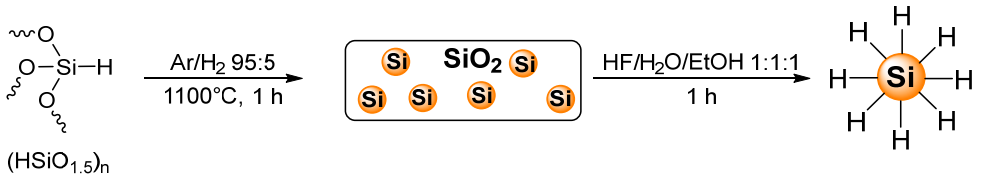

Scheme 7. General procedure for the generation of hydride terminated SiNCs, established by Veinot et al.: Thermal annealing and HF etching.[16,161,162]

Thermal annealing of silicon rich oxides (SiO_x; SRO)[163,164] and polymeric hydrogen silsesquioxanes (HSQ)[161] bearing the structure $(HSiO_{3/2})_n$ has been performed as probably the most promising and suitable method for the formation of SiNCs (Scheme 7). Preparation occurs under solvent free conditions and in a high temperature furnace (e.g. laser pyrolysis and plasma syntheses require complex apertures).

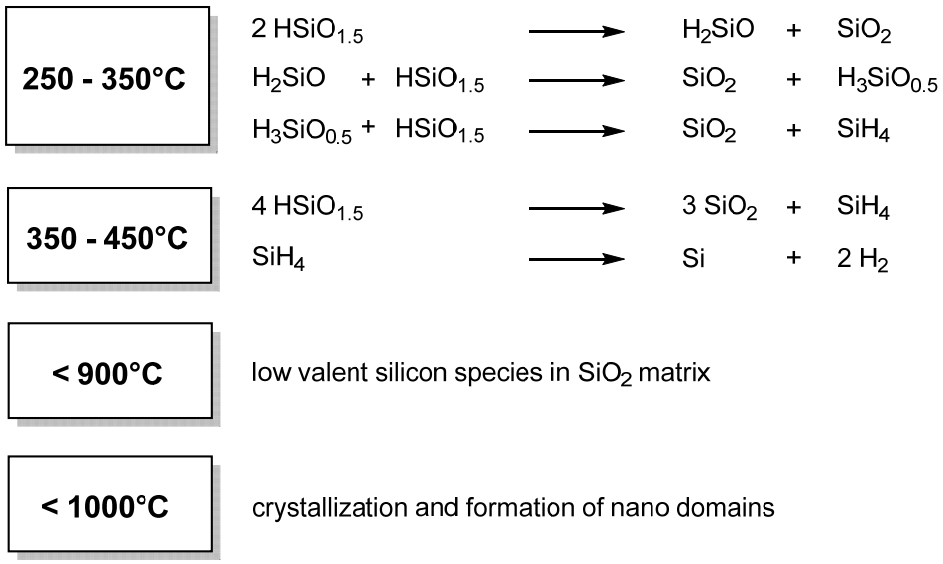

Scheme 8. Stages of thermal HSQ disproportionation and formation of SiNCs under reducing or inert atmosphere.[161,162,165]

The annealing procedure requires temperatures above 1000 °C and is mostly performed under reducing atmosphere (4% H_2/96% N_2).[161] During the heating phase, disproportionation of polymeric HSQ occurs at 250 – 450 °C, whereby elemental Si starts forming at 350 °C (Scheme 8), which arranges to low valent silicon species.[161,162] Crystallization of Si and the formation of Si(0) nanodomains runs above 1000 °C (Scheme 8).[162] Thus, SiNCs with a diameter of 3.3 nm could be obtained from annealing of HSQ at 1100 °C for 1 h. Particle sizes were controlled from changing temperatures (e.g. bigger nanocrystals were synthesized at elevated temperatures) or by the introduction of terminal methyl groups to the HSQ $(HSiO_{1.5})_n(CH_3SiO_{1.5})_m$ ($m<<n$, $m+n = 1$), which act as network modifiers.[162,165] In both cases diffusion rates of Si in the SiO_x matrix are enhanced. Longer reaction times gave a comparatively low influence on the growth rate of SiNCs; however, Yang *et al.* were able to obtain cubic SiNCs upon sintering of HSQ for 20 h at 1300°C.[166] The rearrangement of SiNC

morphologies from spheric to cubic has probably emerged from reduction of their surface energies.

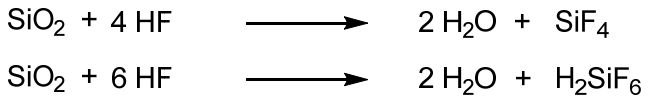

Scheme 9. Etching of the silicon dioxide matrix by hydrofluoric acid.[19]

HF etching of the silica matrix is performed to liberate the SiNCs from the silica matrix and to generate hydride surface groups (Scheme 9).[16,56] The SiO_2 etching mechanism proceeds through four sequential steps, in which water and HF are proposed to attack concertedly at the respective Si center.[167] Hence, water plays a catalytic role in the etching process of SiO_2 and enhances the rate of the nucleophilic attack. The formed SiF_4 reacts readily with an excess of HF to hexafluoro silicic acid or hydrolyses with water, and the SiNC surfaces eventually become fluorine terminated.[167] Further attack of HF on the surface Si atoms forms a hydride terminated surface and SiF_4 (Scheme 10).[19,168] The raised ionic character of the Si-F bond (arising from the high electronegativity of the fluoride) strongly polarizes the Si-Si bonds (Scheme 10).[169] Thus, the insertion of HF in the surface Si-Si bond leads to a fluorination of the surface silicon atom and a protonation of the second layer. For SiNCs, the pyrolysis and HF etching procedure renders an efficient pathway to the generation of hydride terminated SiNCs, which are then suitable for surface modification by hydrosilylation or other procedures.[18]

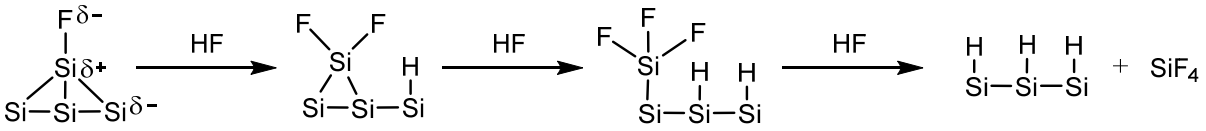

Scheme 10. Schematic illustration of the H passivation mechanism on Si surfaces.[168]

2.4. Surface Functionalization, Postmodification and Polymerization

The potential use of SiNCs in various applications like solar cells,[170,171,172] as sensors,[31,32] in biological imaging,[35,36,56] in battery anode materials,[18,52,173–175] and in light emitting diodes[47,48,176–178] engages the interest of many researchers. Devices have been prototyped with only limited success using SiNCs, bearing a native oxide layer.[16,18,56,171] Unfunctionalized SiNCs tend to aggregate, are hardly dispersible in any solvents and often do not exhibit PL upon UV excitation. HF etching of the oxide layer can help to overcome these issues;[161] however, fast oxidation still occurs *via* various pathways afterwards and thus SiNC properties change.[124,179] Oxidation could easily be followed by a blue shift of the PL.[149]

To obtain sustainable answers to this problem, surface grafting strategies have been developed in the last few years. Strategies for functionalizing SiNCs involve the formation of Si-C bonds (e.g. by hydrosilylation approaches), the modification of selectively oxidized SiNCs and the formation or application of heteroatoms.[16,18,56] Furthermore, post modification and the preparation of hybrid materials is discussed to entirely illuminate the field of SiNC surface chemistry.

2.4.1. Hydrosilylation: Various Approaches on SiNC Surfaces

Hydrosilylation is one of the most dominating methods for the formation of Si-C bonds, as it is well established in molecular and polymer chemistry.[180] In general it describes the reaction of a Si-H group with an alkene or an alkyne (Scheme 11). Mostly metal catalysts or radical initiators are used.[180] On silicon or porous silicon surfaces, hydrosilylation is well-studied, too.[21,23,181] Thus, several SiNC grafting approaches are based on these procedures, albeit with significant modifications.

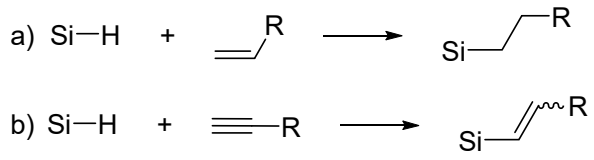

Scheme 11. Hydrosilylation reaction with a) alkenes and b) alkynes.

Platinum catalyzed hydrosilylation reactions on Si-H terminated surfaces are a powerful tool for a selective grafting of olefins at room temperature.[131–133,182] Reactions usually require H_2PtCl_6 and follow the generally accepted Chalk-Harrod mechanism with is characteristic steps (Scheme 12): Oxidative addition, alkene coordination and insertion, and eliminative reduction.[183,184]

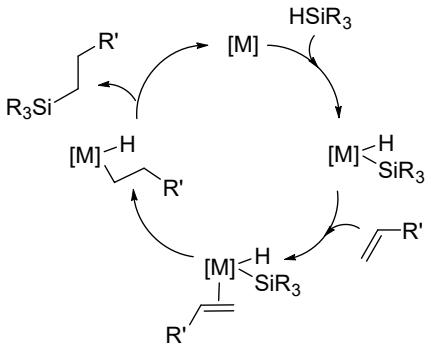

Scheme 12. Chalk-Harrod mechanism of hydrosilylation reactions with d^8 and d^{10} metal complexes.[183,184]

Arising from the mechanism, presumably monolayers are formed on the SiNC surfaces and a remarkable variety of substrates are tolerated (e.g. -NH_2, -COOH, alkyl, alkenyl).[39,131–133,185,186] However, the use of transition metals is limited by some issues; e.g. the removal of the catalyst is difficult and SiNC properties can change dramatically, which can result in a PL shift or quench.[187] Catalyst free methods are elegant hydrosilylation tools without influencing the SiNC properties. Yu *et al.* found a way of functionalizing hydride terminated SiNCs at room temperature with bifunctional alkenes bearing distal ethylester, methylester and carboxylic acid moieties.[188] The authors state, that the mechanism is similar to the functionalization in the presence of Lewis acids (e.g. Et_2AlCl), which catalyze the insertion of alkenes and alkynes into the Si-H bond by the formation of electropositive adducts.[189] Effectively, the nucleophilic ester carbonyl group coordinates to the Si surface, which increases the reactivity of the Si-H to the alkene end of another molecule (Scheme 13). The reactivity increased with decreasing SiNC sizes. Furthermore, higher yields were obtained if methyl or ethyl 10-undecenoate were used instead of 10-undecenoic acid. This effect emerged from stronger resonance of the esters due to the electron donating character of alkyl groups (Scheme 13 B).[188]

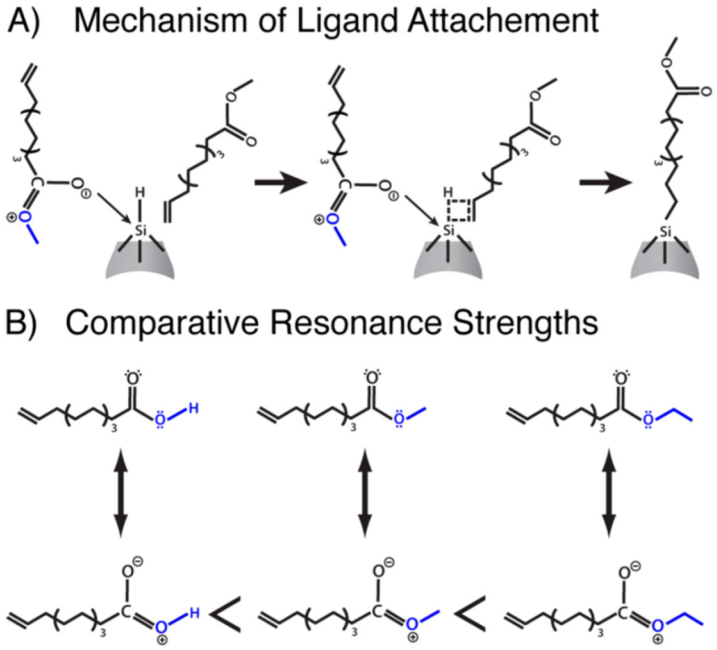

Scheme 13. Mechanism of room temperature hydrosilylation of 10-undecenoate (A) and resonance structures of 10-undecenoic acid, methyl 10-undecenoate and ethyl 10-undecenoate.[188] Reproduced and adapted with permission from reference 189. Copyright 2013 America Chemical Society.

Alternative catalyst free hydrosilylation methods on hydride terminated SiNCs surfaces require energy in form of heat or light.[18] Thermal grafting is a comparably fast process, which does not run size selectively but stabilizes the PL of SiNCs by passivation of the surface.[118,164,190] The reaction is presumably occurring through a homolytic cleavage of the Si-H bond and subsequent olefin addition to the free surface silyl radical, as has been shown on other Si morphologies before.[24,117,191] The mechanism has been proposed to proceed *via* propagation over the surface and thus monolayer formation. However, in 2014 Yang *et al.* used nano assisted laser desorption ionization (NALDI) to examine thermally functionalized SiNC. They found oligomers on the SiNC surface (Figure 4 a).[192] Furthermore, the degree of oligomer formation was strongly dependent on the amount of oxygen present, the applied reaction temperatures and the olefin concentration. Most of the thermal functionalization protocols require neat monomer, which causes the formation of long oligomer up to polymer chains. The results of Yang *et al.* were supported by Panthani *et al.*, who used TEM imaging to evidence a remarkable amorphous layer surrounding the crystalline SiNC cores (Figure 4 b).[3] The big oligomer cover reasonably adds to a raised stability, robustness and a good PL quantum yield, but can also lead to potential issues in the application in optoelectronic devices.[18,193]

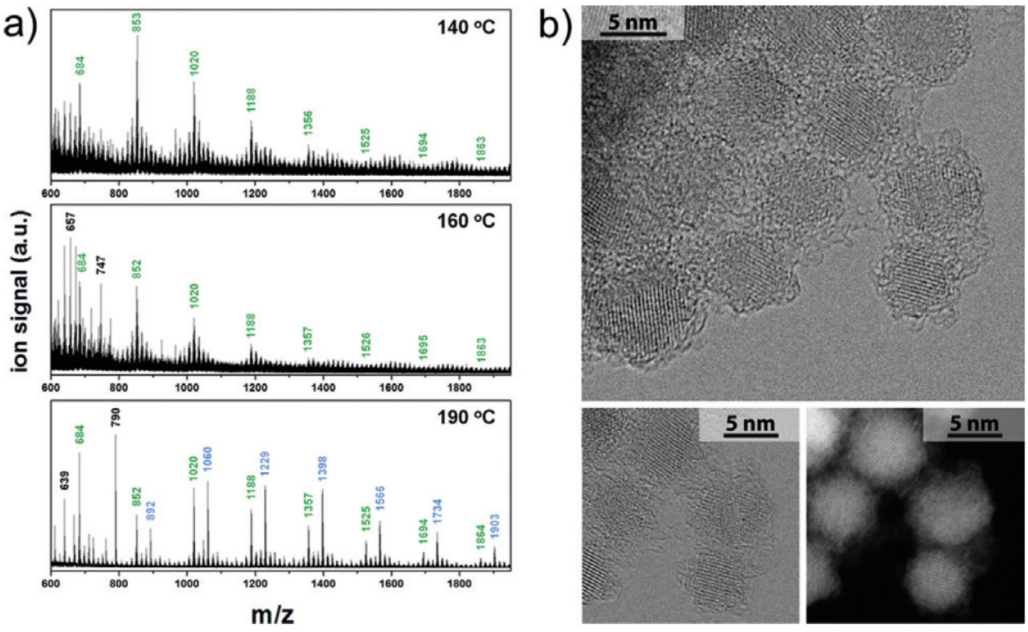

Figure 4. a) NALDI measurements of dodecyl oligomers attached to the SiNC surfaces. Functionalization has been achieved at the indicated temperatures. B) Bright field and dark field TEM measurements of alkyl terminated SiNCs after thermal grafting.[3,18,192] Reproduced and adapted with permission from references 3, 193. Copyrights 2012, 2013 America Chemical Society.

Thermal grafting procedures can be used with several variations. As one example, Quian *et al.* applied microwave synthesis at 170 °C in a closed vessel to decorate SiNC surfaces with fluoro substituted alkenes and promoted it as a "green" method for SiNC functionalization (Scheme 14).[194] The SiNC shell consists of fluorinated alkenes, which lead to an enhanced oxidation stability and a superhydrophobic surface. Furthermore, the authors state, that the enhanced electron withdrawing character shifts the PL to blue; elevated PL quantum yields have aroused from the lower-frequency carbon-fluorine stretching modes which disfavor non-radiative relaxation pathways. This has been reproduced by the introduction of C-S bonds to

the surface bonded alkyl or aryl groups (e.g. allylphenylsulfide); it has been specified, that lowering of the C-X (X = S, F) stretching vibration enhances the absolute photoluminescence quantum yields.[195]

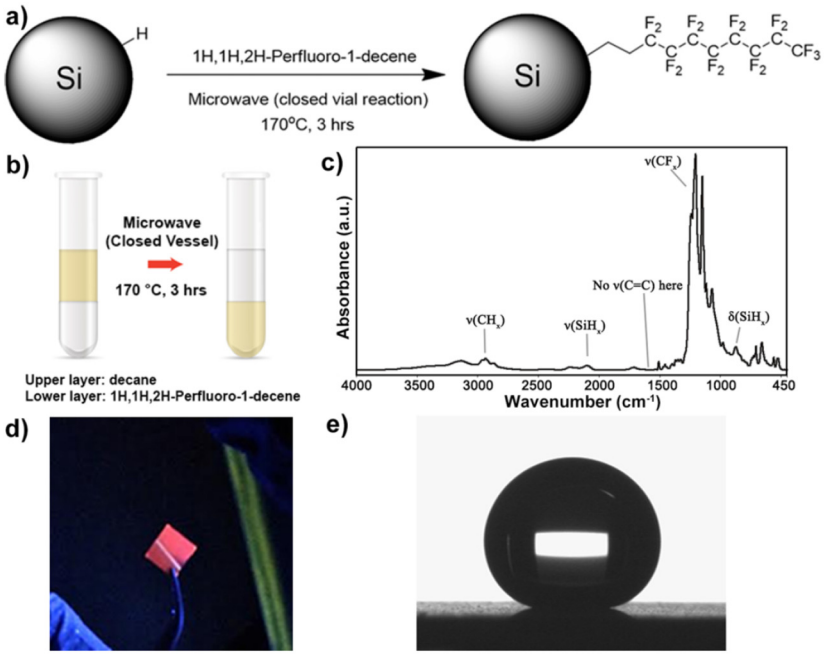

Scheme 14. a) Functionalization of hydride terminated SiNC surfaces with 1H,1H,2H perfluoro-1-decene b) schematic demonstration of the reaction by microwave synthesis; c) FT-IR spectrum of perfluorodecyl capped SiNCs; d) photoluminescence of spin coated SiNCs on a silicon wafer and e) water droplet on a film of perfluorodecyl capped SiNCs.[194] Reproduced and adapted with permission from reference 195. Copyrights 2014 America Chemical Society.

Thermografting is a well-established method for the functionalization of SiNCs. However, although a good stabilization of the SiNC properties can be achieved by surface oligomerization, small molecules are completely hindered from surface contact, which could lead to several drawbacks in the application of SiNCs (e.g., in sensing).[192] Furthermore, in most of the cases thermal grafting requires high boiling alkenes and alkynes. With a few exceptions,[196,197] thermal grafting has mostly been performed in the neat monomer. Thus, strategies were developed for a very selective decoration of SiNC surfaces.

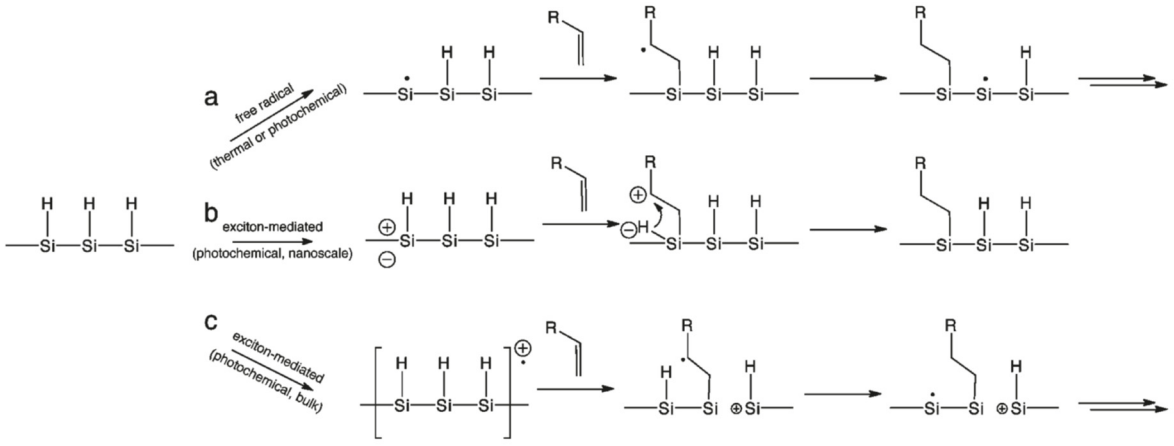

Scheme 15. a) Homolytic cleavage of a Si-H bond achieved under thermal and photochemical conditions; photochemical exciton-mediated hydrosilylation mechanism for b) nanoscale Si and c) bulk Si.[117] Reproduced and adapted with permission from reference 117. Copyrights 2011 America Chemical Society.

Photochemical grafting has developed as important alternative for the hydrosilylation of olefins. This method was presented to run *via* homolytic cleavage of the Si-H bond (3.5 eV) or by the generation of excitons on a bulk silicon surface (Scheme 15 a, c).[21,27,198,199] However, for nanomaterials it was proposed, that there is a second exciton based mechanism which runs *via* the adsorption of low energy "white" light (Scheme 15 b).[199,200] The exciton formation is followed by the addition of the double bond to the hole. Hydrosilylation is terminated by recombination of the hydride with the carbocation. Veinot *et al.* were able to demonstrate, that near UV hydrosilylation is size dependent due to quantum size effects.[117] This proposes that for near UV grafting of hydride terminated SiNCs, an exciton mediated mechanism is more likely to occur than homolytic cleavage. Furthermore, they used *in situ* photoluminescence spectroscopy to demonstrate the impact of the photografting of alkenes and alkynes on PL properties of the final products.[201] They could show that the PL of SiNCs with initial green/yellow emission shifts towards red upon reaction with model alkenes and those with initial red PL increase in intensity, but did not shift. With conjugated alkynes, a SiNC PL quench on a rate on the electron-donating ability could be observed. In a consecutive study, Yang *et al.* compared evolution of the PL of thermally and photografted SiNCs by following wavelengths and PL lifetime decays.[202] The authors observed, that thermally grafted SiNCs only exhibited size dependent microsecond (µs) lifetimes, while size independent nanosecond (ns) lifetimes were only measured if photografting was applied. The authors concluded, that particles with ns lifetimes were partially oxidized. Oxidation could be minimized by using longer reaction times. Although photografting is a very mild hydrosilylation method, because of its size dependent reactivity, the functional group intolerance and the long reaction times are significant limitations.

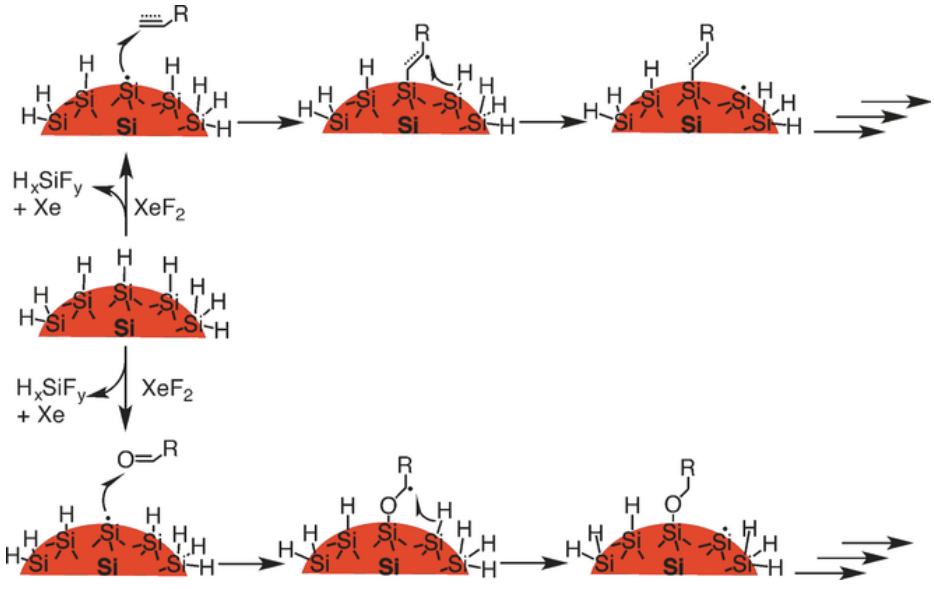

Scheme 16. Proposed Mechanism for XeF_2 grafting of SiNCs. [203] Reproduced and adapted with permission from reference 204. Copyrights 2017 Wiley-VCH Verlag GmbH &Co. KGaA, Weinheim.

Probably the fastest procedure of surface grafting has been presented by Mobarok *et al.*[203] Surface decoration with alkenes, alkynes and carbonyls was obtain within less than 60 s with XeF_2 as reactive platform. The authors stated, that the rate of the reaction arises from the formation of $F^{\bullet}$ radicals, which cleave surface Si-Si bonds (Scheme 16). Surface silyl radicals

are formed as a result of the removal of surface Si atoms as hydrofluorosilanes. The surface Si• radicals immediately react with unsaturated bonds of alkenes, alkynes and carbonyls. Furthermore, the authors state that radical propagation presumably occurs on the surface.

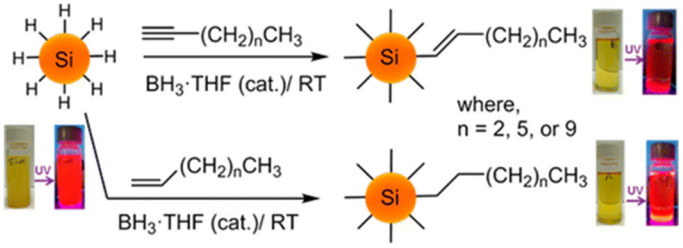

Scheme 17. Borane catalyzed hydrosilylation of H-SiNCs.[204] Reproduced and adapted with permission from reference 205. Copyrights 2014 America Chemical Society.

Although XeF_2 initiates a very fast grafting of alkenes, alkynes and carbonyls on H-SiNCs, its handling is very dangerous and the substance is expensive. As a good alternative, Purkait *et al.* presented borane catalyzed surface hydrosilylation at room temperature (Scheme 17).[204,205] Lewis acid catalyzed reactions have been demonstrated for molecular silanes, as well as H-terminated porous silicon surfaces before.[189,206,207] For H-SiNCs, bulky Lewis acids like $B(C_6F_5)_3$ could not be used under present conditions, but BH_3 exhibit good reactivity.[204] For BH_3, the authors proposed two possible reaction pathways (Scheme 18): In A, borane reacts with alkenes and alkynes by forming the intermediate A-II, which inserts into the Si-H bond. If the reaction follows pathway B, BH_3 is proposed to form an "activating complex" (B-I) from direct activation of the alkene or alkyne. H-migration from the surface to the complex B-I leads to the formation of B-II; the release of borane forms a defined mono layer on the surface. In contrast, to the use of metal catalysts, purification is easily possible and the PL properties of the SiNCs remain. However, the reaction is sensitive towards humidity, and is probably sensitive towards functional groups.

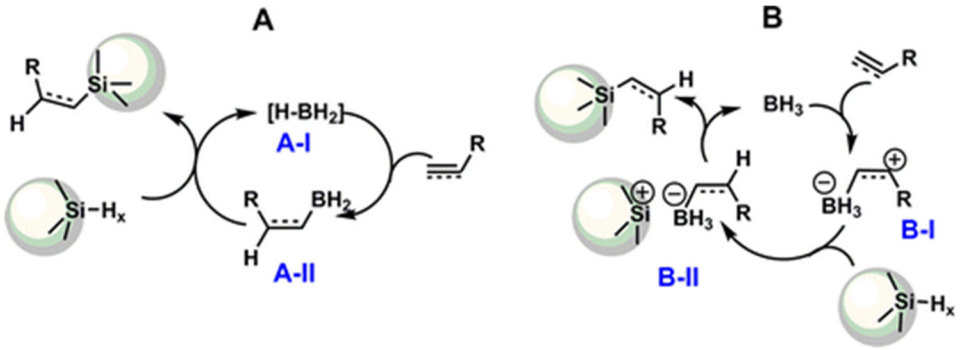

Scheme 18. Possible mechanisms of borane catalyzed hydrosilylation: A, "insertion" mechanism and B, "coordination" mechanism.[204] Reproduced and adapted with permission from reference 205. Copyrights 2014 America Chemical Society.

Like alkene and alkyne functionalization reactions, Purkait *et al.* decorated the Si-H surface with ketone carbonyls to form surface silyl ethers.[205] Aliphatic ketones required microwave conditions, while aromatic ketones readily react at room temperature. The formed alkoxy terminated SiNCs were stable towards air and moisture. After hydrosilylation of ketones, borane catalyzed ligand exchange at elevated temperatures was used to react alkenes with the surface. In all cases, the reaction is proposed to run *via* a hydroboration product (insertion into the alkene or alkyne; Scheme 18). Although not evidenced, a coordination of the boron atom to

the oxygen of the silylether is likely to occur, since the binding energy of the Si-O bond (452 kJ/mol) is weaker than the bond energy of the B-O bond (536 kJ/mol).

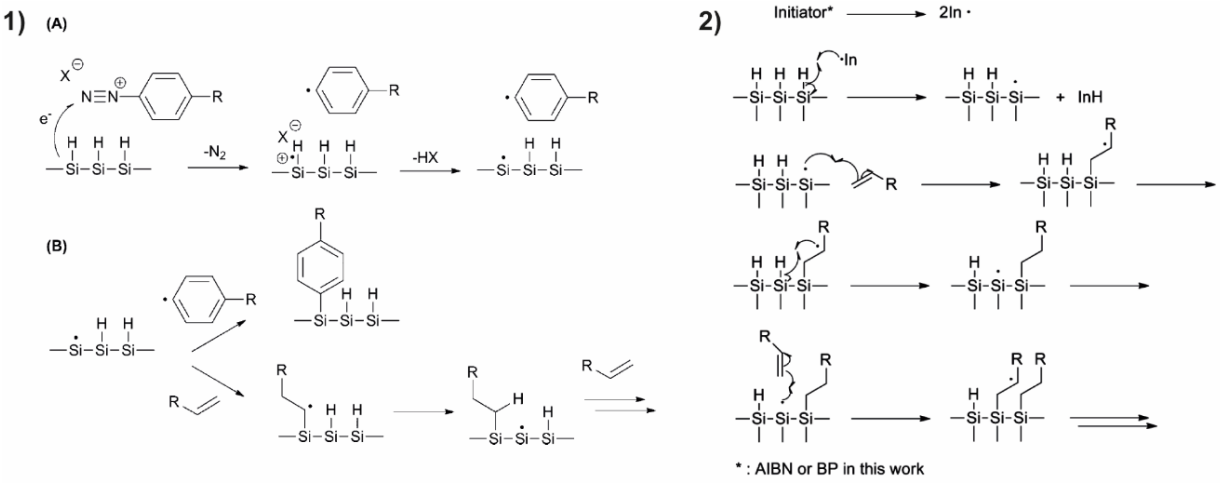

Scheme 19. Grafting of H-SiNCs using diazonium salts (1) and radical initiators (2, e.g. azobisisobutyronitrile – AIBN or dibenzoyl peroxide – BPO). A) Radical formation and B) proposed grafting mechanisms.[208,209] Reproduced and adapted with permission from references 209, 210. Copyrights 2014 Wiley-VCH Verlag GmbH & Co. KGaA, Weinheim; 2015 America Chemical Society.

Even if borane and XeF_2 catalyzed reactions are fast and selective methods for SiNC functionalization, they are limited by their functional group tolerance. Methods with radicals involved can overcome this issue. Surface radicals can either be generated by diazonium salts or by other radical initiators.[208,209] Diazonium salts presumably initiate the surface by electron transfer from the surface to the diazonium salt, and cleavage of a surface proton by the counter anion or homolytic Si-H cleavage by the aryl radical (Scheme 19, 1).[208] If radical initiators like azobisisobutyronitril (AIBN) or dibenzoyl peroxide (BPO) are used, surface radicals are generated from their thermal decomposition and homolytic Si-H cleavage (Scheme 19, 2).[209,210]. Surface propagation has been proposed to occur after olefin addition (Scheme 19). Both methods are very tolerant towards functional groups; Yang *et al.* and Höhlein *et al.* were able to functionalize SiNCs with alkynes and alkenes bearing ester, acid, silyl, alkyl and aryl moieties.[208,209,211,212]

Besides the functional group tolerance, both methods allow good control over the reaction speed, which has been monitored by the clearing of the dispersions in both cases. Diazonium salts were given dodecyl functionalities, which improve the solubility in nonpolar solvents (Figure 5, A, D). Furthermore, the reactivity of diazonium salts increases with the introduction of electron withdrawing groups, which was demonstrated by using 2-nitro- (2-NO-4-DDB) or 2,6-bromo-4-decyl-diazobenzene tetrafluoroborate (2,6-Br-4-DDB; Figure 5, B, C), which, with dodecene, lead to the hydrosilylation of the SiNC surface in less than one hour.[208]

When radical initiators were applied, reaction rates could be controlled by the decomposition rate at the respective temperatures and the structure (BPO vs. AIBN) of the initiator and the used solvents. Although functionalization has been shown as a slower process compared to diazonium salts and other methods, Yang *et al.* were able to demonstrate that radical initiated surface grafting provides monolayer surfaces.[209]

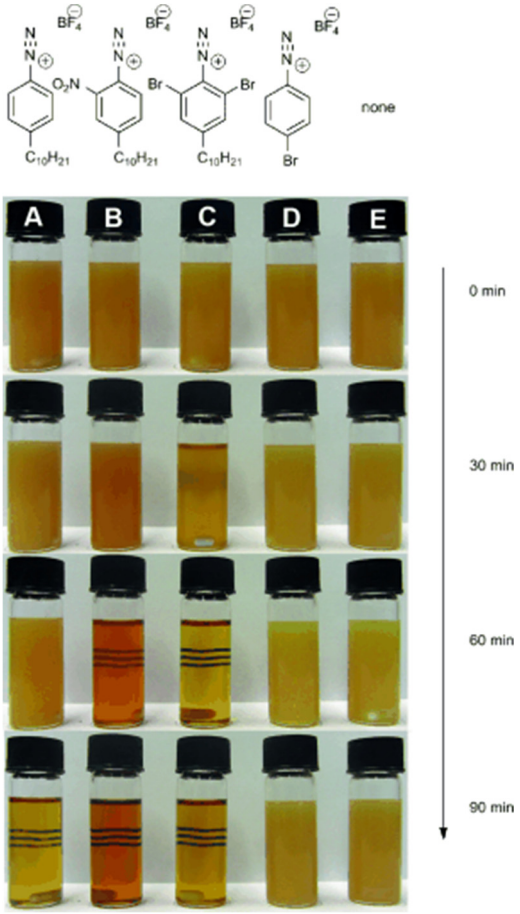

Figure 5. Comparison of the reactivity of diazonium salts in the hydrosilylation of H-SiNCs with dodecane; A) 4-decyl-diazobenzene tetrafluoroborate (4-DDB); B) 2-nitro-2-4-DDB; C) 2,6-bromo-4-DDB; D) 4-bromo-DB; and E) reference.[208] *Reproduced and adapted with permission from references 209. Copyrights 2014 Wiley-VCH Verlag GmbH & Co. KGaA, Weinheim.*

2.4.2. The Role of Heteroatoms in SiNC Functionalization

Although hydrosilylation is one of the dominating processes in SiNC science, heteroatom surfaces have aroused scientific interest as they have direct impact on the nanomaterials' properties.[16,18] Studies by Li *et al.* have shown, that selective HF/HNO_3 or "piranha acid" etching form hydroxyl terminated SiNCs (OH-SiNCs),[155] which could subsequently be grafted with octadecyltrimethoxysilane. The reaction presumably occurred from reesterification of ethoxy capped SiNCs with the octadecyltrimethoxysilane. Ethoxy terminated SiNCs resulted from the functionalization of SiNCs with alcohols like methanol, which has been described by Bley *et al.* earlier.[138] Generally, particles involving methoxy or ethoxy terminated SiNCs groups can be post modified by alkylsilanes, like alkyltrichlorosilanes, leading to the formation of crosslinked silane surfaces.[136] Surface oxidation leads to a PL shift, a change in PL lifetimes towards the ns regime and low passivation of the surface.[213]

As further reaction platform, halogen terminated SiNCs have been presented.[16,56] One of the earliest procedures for Si-Cl generation is the potassium silicide reduction of $SiCl_4$.[138] Wheeler *et al.* applied non-thermal plasma treatment of $SiCl_4$ in presence of H_2 for the generation of chloride terminated SiNCs.[214] Thus, generated chloride terminated SiNCs were stabilized by hypervalent interactions from hard donor molecules like n-alkanones and n-alkanenitrils. Hypervalent bonding shifted the attenuated total reflectance (ATR)-IR stretching modes of the respective carbonyl-, nitrile- and Si-Cl bonds. The authors concluded from their results, that the stability of the colloidal SiNC suspension depended on the donors strength and that the surface bonded groups were labile.[214]

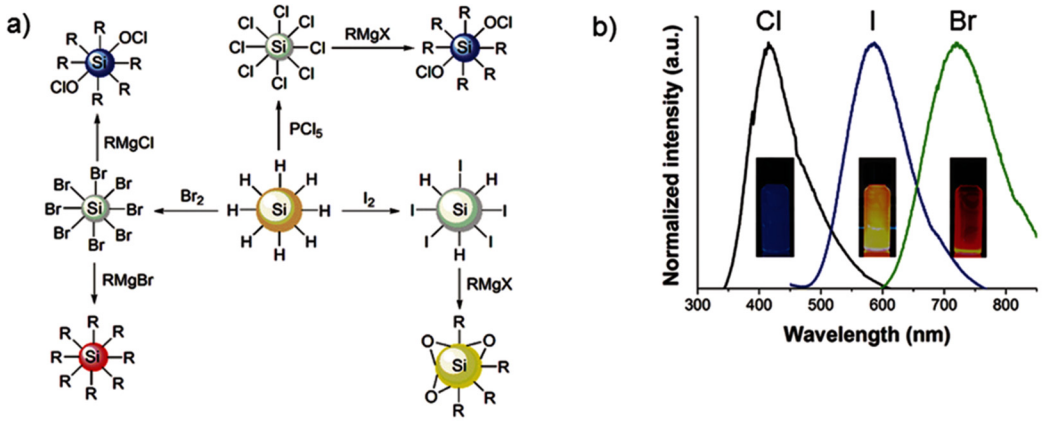

Scheme 20. Halogenation of hydride terminated SiNCs (a) and PL of alkylated surfaces derived from halogenated SiNC surfaces (b).[215] Reproduced and adapted with permission from references 216. Copyrights 2015, American Chemical Society.

A surface reaction approach for the preparation of Si-Cl surfaces has been presented on hydride terminated Si(111) and Si(100) surfaces earlier.[28] They were treated with PCl_5 and BPO for one hour at elevated temperatures. Post alkylation gave well-ordered passivated surfaces. As for silicon wafers, PCl_5 was used to form chlorinated SiNCs (Cl-SiNCs) from H-SiNCs.[216] The reactions occurred at room temperature without radical initiator present; however, complete dissolution of the particles occurred at elevated temperatures (Scheme 20).[215] Similarly,

H-SiNCs reacted with elemental bromine or iodine. Anisotropic etching happened for bromine-functionalization as well. Functionalization with iodine ran incompletely and hydride groups remained. After halogenation, post-modification was used to passivate the surfaces. Dasog *et al.* used alkyl Grignard reagents for halogen exchanges on the surfaces. Afterwards, the alkylated SiNCs had blue (chloride), red (bromide) and yellow (iodide) PL depending on the surface halogen (Scheme 20 b). Red PL raised from band gap transition with µs lifetime, while blue and yellow PL originated from surface defects as could be observed from ns photoluminescence lifetimes. Besides elemental bromine, N-bromosuccinimide (NBS) was used as brominating reagent.[217]

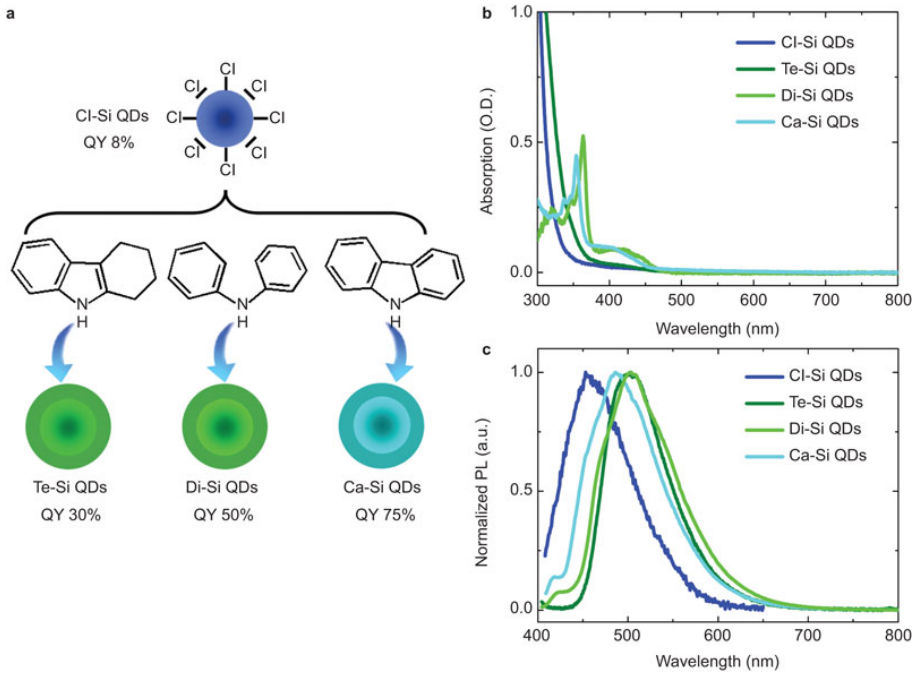

Figure 6. PL properties of SiNCs functionalized with different arylamines.[218] Reproduced and adapted with permission from references 219. Copyrights 2015 CIOMP.

Halogenated SiNCs have been useful precursors for further functionalization. They showed good reactivities towards amines.[124,216,218,219] Allylamine reacts with chloroterminated SiNCs over its free amino group and not through the alkene.[216] After reaction of allylamine with the surface, PL became SiNC size independent, which could be seen in the blue emission of 3, 6 and 9 nm SiNCs upon UV stimulation. Later, 1.5 and 6.5 ns photoluminescence lifetimes and 35 % PL yield for dodecylamine-SiNCs were obtained; these features probably resulted from charge-transfer effects.[124] Upon the application of diphenylamine the emission of the system shifted towards green.[124,218,219] Generally, a variation of the aromaticity of arylamines can change the optical properties, which emerged in a variable PL maximum (orange to blue) and PL quantum yields (Figure 6).[218] Similar to alkyl amines, PL lifetimes of aryl amine terminated SiNCs were short (~5 ns). Thus, PL seems to arise from charge-transfer states.[18,220]

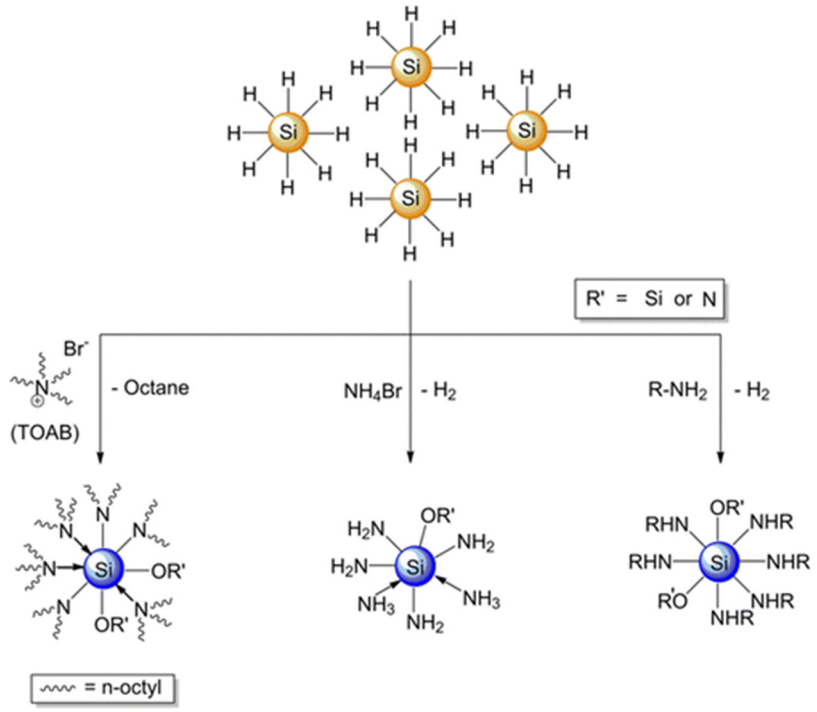

Scheme 21. Different approaches for the generation of blue emitting amino terminated SiNCs obtained from H-SiNCs. [179] *Reproduced and adapted with permission from references 179. Copyrights 2013, American Chemical Society.*

Although not as distinctive and selective, amines have a strong influences on H-SiNCs as well.[179] Like for chloride terminated SiNCs, they induced a blue shift of the PL with ns lifetime and solvatochroism (dependence of the PL emission maximum from the solvent polarity). The property change was independent from the amine structure (Scheme 21) and of the SiNCs sizes, but it increased with higher amine concentrations.[179] Dasog *et al.* could furthermore demonstrate that primary and secondary amines reacted to the surface but affected partial surface oxidation (Scheme 22).[179,221]

Not only surface reactions with amines elicited unprecedented PL properties (Scheme 22). Upon reaction of H-SiNCs at elevated pressures (10 bar) and temperatures (above 100 °C) with CO_2 an acetal surface could be formed.[124] Thus, grafted SiNCs emitted blue-green PL upon UV light excitation. However, photobleaching could be observed. *Dasog et al.* furthermore found, that if the reaction times were too long, surface acetals decomposed to formaldehyde and oxidized SiNCs.[124] In subsequent studies, Dasog *et al.* and Sun *et al.* were able to form CO and methanol from CO_2 reduction using silicon nanoparticles.[222,223]

Surface engineering using trioctylphosphine oxide (TOPO) under ambient conditions generated surface oxidized SiNCs with a corresponding ligand shell (Scheme 22).[124] Hence, the SiNCs were stabilized in organic solvents. Furthermore, phosphine-oxide stabilized SiNCs emitted bright yellow PL at 590 nm. The authors proposed, that the complex PL mechanism aroused from surface defect structures and band gap emission.[18,124] Although photobleaching occurred, the relative PL quantum yields of phosphine oxide-, amino- and acetal-terminated SiNCs were higher than the quantum yields of well passivated SiNCs, which emit PL from band gap transition.

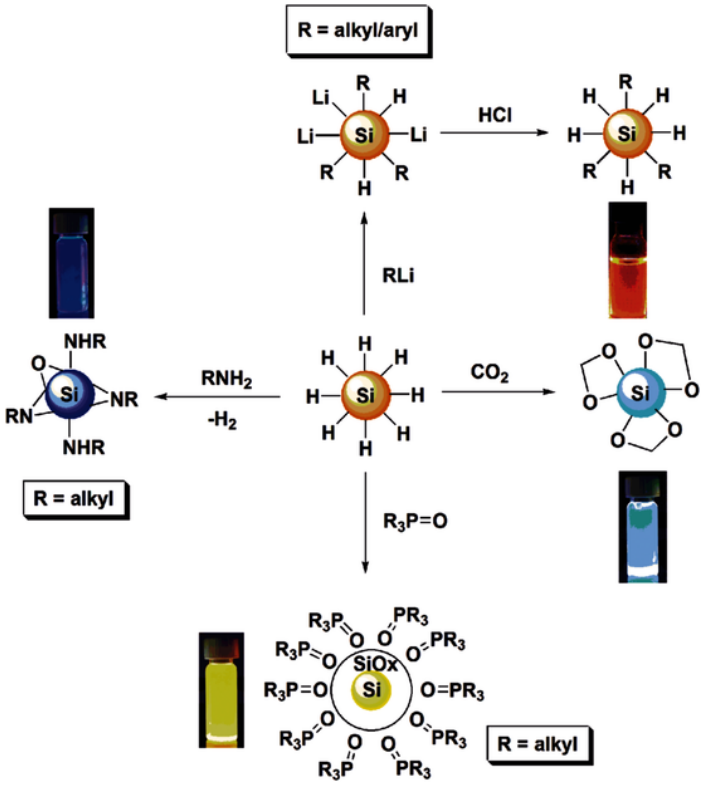

Scheme 22. Reaction of H-SiNCs with amines, alkylphosphine oxides, CO_2 and lithium organyls.[124,224] Reproduced and adapted with permission from references 18, 124, 225. Copyrights 2015, 2016, Wiley-VCH Verlag GmbH &Co. KGaA, Weinheim; 2014 American Chemical Society.

Höhlein *et al.* recently reacted hydride terminated SiNCs with an organolithium reagent.[224] Probably most interesting in this method is the fact, that a mixed surface could be synthesized. Particularly, phenyl lithium (PhLi) could be used to cleave Si-Si bonds and form a mixed Si-Ph and Si-Li surface, which could be reacted in a second step with the electrophiles hexyl bromide or propylene oxide (Scheme 23 a). By addressing the free Si-Li bonds with HCl, free Si-H groups were formed, which could subsequently be modified *via* hydrosilylation (Scheme 23 b).

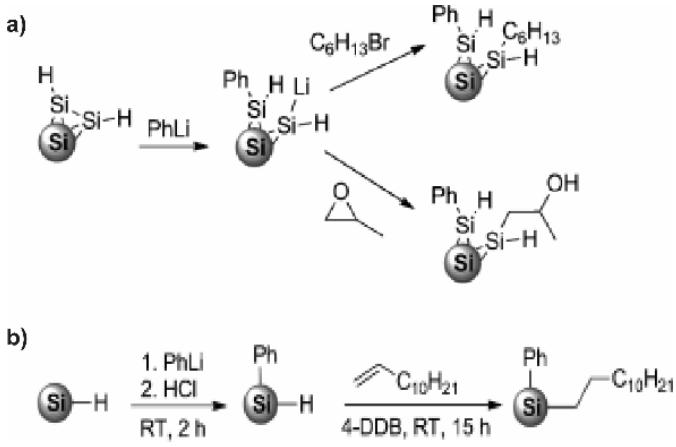

Scheme 23. a) Reaction of H-SiNCs with phenyl lithium and subsequent substitution of the Si-Li group and b) reaction of H-SiNCs, generation of hydride groups using HCl and subsequent hydrosilylation.[224] Reproduced and adapted with permission from references 225. Copyrights 2015, Wiley-VCH Verlag GmbH &Co. KGaA, Weinheim.

Angı et al. furthermore used organolithium reagents (hexyl lithium, phenyl lithium, lithium phenylacetylide) to engineer SiNCs PL properties (Figure 7).[115] While surface hexyl and

phenyl groups resulted in the same emission maximum, phenylacetylene groups shifted the maximum from 685 to 735 nm. This shift has been assigned to the appearance of an additional in-gap state close to the conducting band edge observed by scanning tunneling microscopy/spectroscopy (STM/STS).

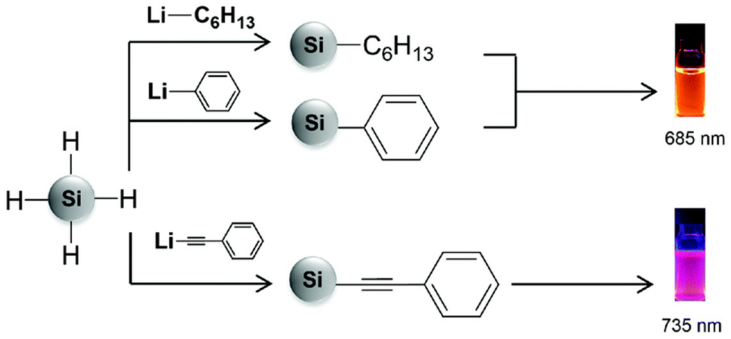

Figure 7. Impact of various surface groups (hexyl, phenyl and phenylacetylene) groups on the PL emission maximum of SiNCs.[115] Reproduced and adapted with permission from reference 115; DOI: 10.1039/C6NR01435F. Copyrights 2016, The Royal Society of Chemistry.

2.4.3. Post-Modification: The Route to SiNC Hybrid and Composite Materials

Physical blending of unfunctionalized SiNCs often affords aggregation in a polymer matrix.[44] To overcome the issue of aggregation, Erogbogbo *et al.* used a micellation approach to encapsulate photoluminescent SiNCs with different surface designs into phospholipid membranes.[13] Hessel *et al.* encapsulated alkyl terminated SiNCs in poly(maleic anhydride).[225] The formed amphiphilic micelles were luminescent, stable over a broad pH range and water dispersible; these features are required for biological imaging. However, in such micelles SiNCs are still available in agglomerated form. To improve the homogeneity of the SiNCs in the composite, Mitra *et al.* performed an atmospheric plasma technique to coat SiNCs with poly(3,4-ethylenedioxythiophene) polystyrene sulfonate.[226] The resulting hybrids were homogeneously coated, which improved their stability, solvent dispersibility and PL. Due to the physical adhesion, the long-time stabilities of noncovalent composite materials could not be guaranteed. Hence, multi-step processes for the preparation of "functional" surfaces, covalent composites, or the formation of SiNC/polymer hybrids are interesting options to address the properties of these seminal materials.

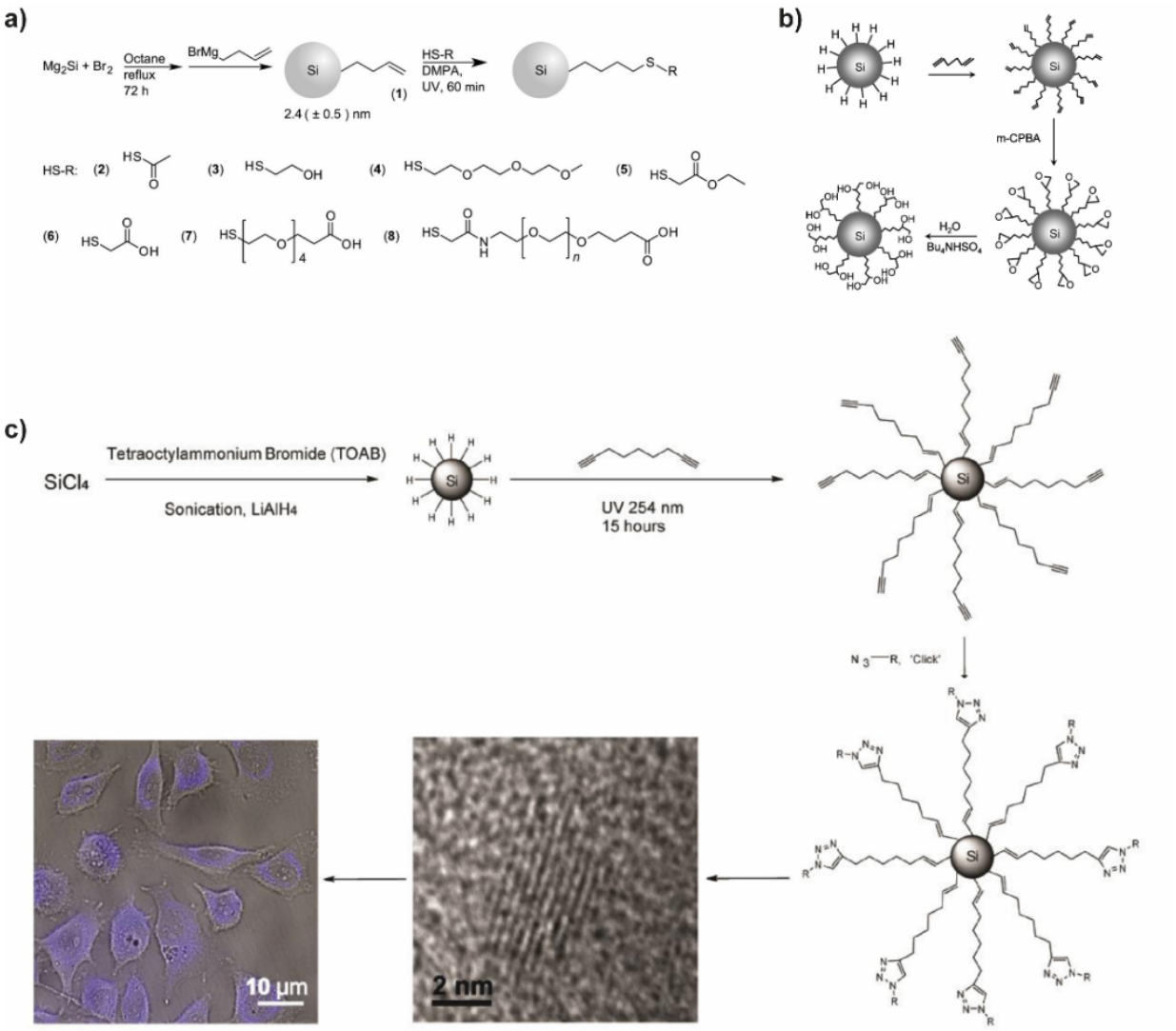

Scheme 24. Schematic illustration of multistep reactions performed on SiNC surfaces: a) Thiol-ene click, b) epoxidation, c) azide-alkyne cycloaddition ("click" chemistry).[38,185,227] Reproduced and adapted with permission from reference 28, 186, 228; Copyrights 2010, 2014, American Chemical Society; 2011 WILEY-VCH Verlag GmbH & Co. KGaA, Weinheim;

Surface chlorination, hydrosilylation or hydroxylation approaches have been used to prepare a precursor surface for multistep reactions.[38,56,136,185,211,215] Thus formed surface groups allowed the selective exploitation of well known (silicon-) organic reactions. As such, a thiol-ene click reaction has been conducted on SiNCs with free surface alkene moieties (Scheme 24 a).[185] Thiol-ene click reactions are usually very mild; hence a band width of thiols was coupled to the surface. The addition of a deoxyribonucleic acid fragment to the distal carboxylic acid group shows, that post synthetic approaches can give the SiNC surfaces direct functions, e.g., for biochemical uses. Distal dienes were hydrosilylated on SiNC surfaces by Shiohare *et al.* to obtain an alkene terminated surface. They used *meta*-chloroperoxybenzoic acid (*m*-CPBA) in a second step to epoxidize the double bonds (Scheme 24 b). The epoxy groups could subsequently be opened which resulted in a diol decoration of the surface groups. As a third example for the post functionalization of free multibonds, the "click" reactions of surface alkynes with molecules bearing terminal azide groups is given (Scheme 24 c).[227] Click chemistry is well known from organic chemistry and has widely been used for the connection

of biomolecules to other functional molecules. In this context, the aim of the study was the imaging of cancer cells.[227]

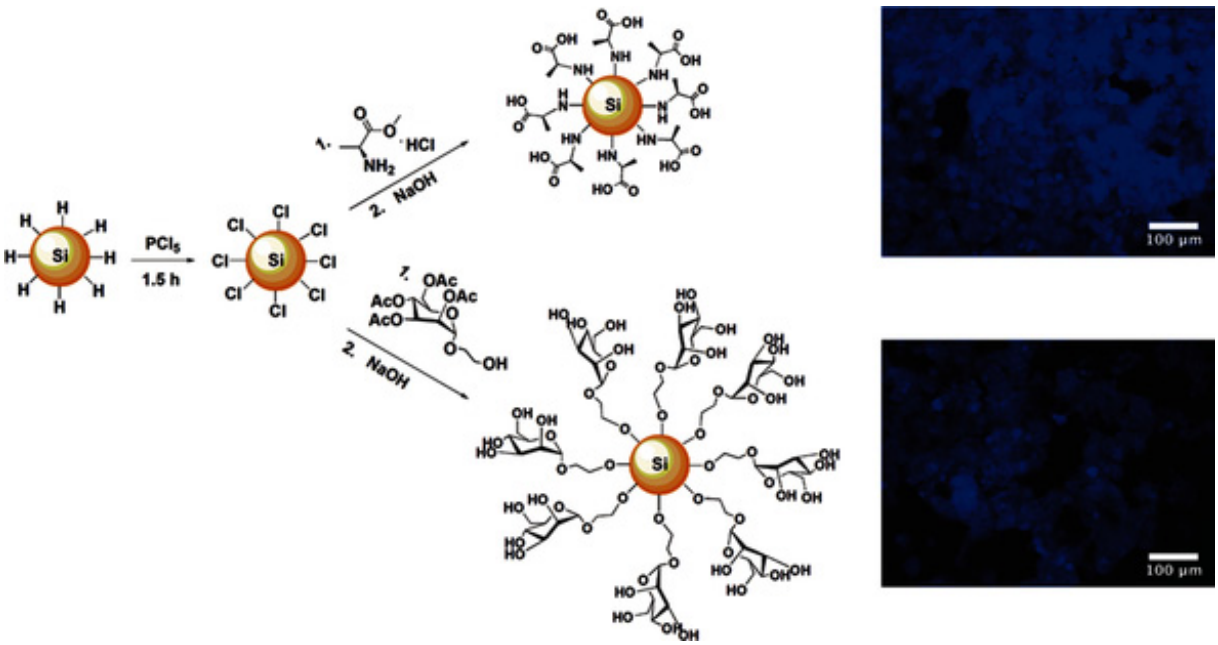

Scheme 25. Decoration of chloroterminated SiNCs with alanine and mannose for fluorescence imaging. [18,36] Reproduced and adapted with permission from references 18, 36. Copyrights 2016 Wiley-VCH Verlag GmbH &Co. KGaA, Weinheim; 2014 The Royal society of Chemistry.

Zhai et al. to reacted chlorinated surfaces with the biomolecules mannose and alanine (Scheme 22) to obtain SiNCs, which are ready for MCF-7 (Michigan Cancer Foundation – 7) breast cancer cell imaging.[36] In contrast SiNCs bearing pentenoic acid surface groups do not elicit this effect, which is a strong indicator that appropriate surface engineering is essential.

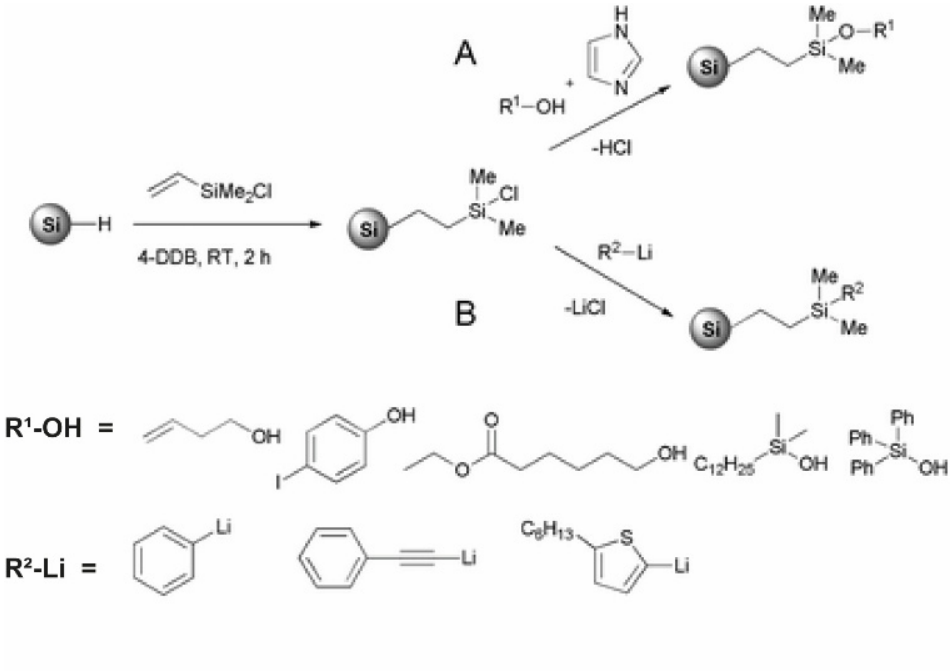

Scheme 26. Decoration of hydride terminated SiNCs with vinyldimethylchlorosilane as precursor for post functionalization with alcohols or silanols (A), or organolithium compounds (B). 4-DDB, 4-decyl-diazobenzene tetrafluoroborate.[211] Reproduced and adapted with permission from reference 212. Copyrights 2014 Royal Society of Chemistry.

The application of chloride SiNC surfaces as reaction platform for postmodification renders a straightforward process. However, the impacts on the PL properties and the blue shift from remaining chloride, oxychloride and oxide surface decoration should not be neglected.[215] Hence, Höhlein *et al.* investigated the diazonium salt based hydrosilylation approach with vinyldimethylchlorosilane (Scheme 26).[211] The formed chlorosilyl terminated SiNCs were immediately reacted with several alcohols, silanols or organolithium reagents. Photoluminescence maxima were stabilized at about 690 nm; however, lithium phenylacetylide shifted the maxima to about 745 nm. The effect emerged from a side reaction of the organolithium reagent with the surface, and the generation of an in-gap state (*vide supra*).[115,211]

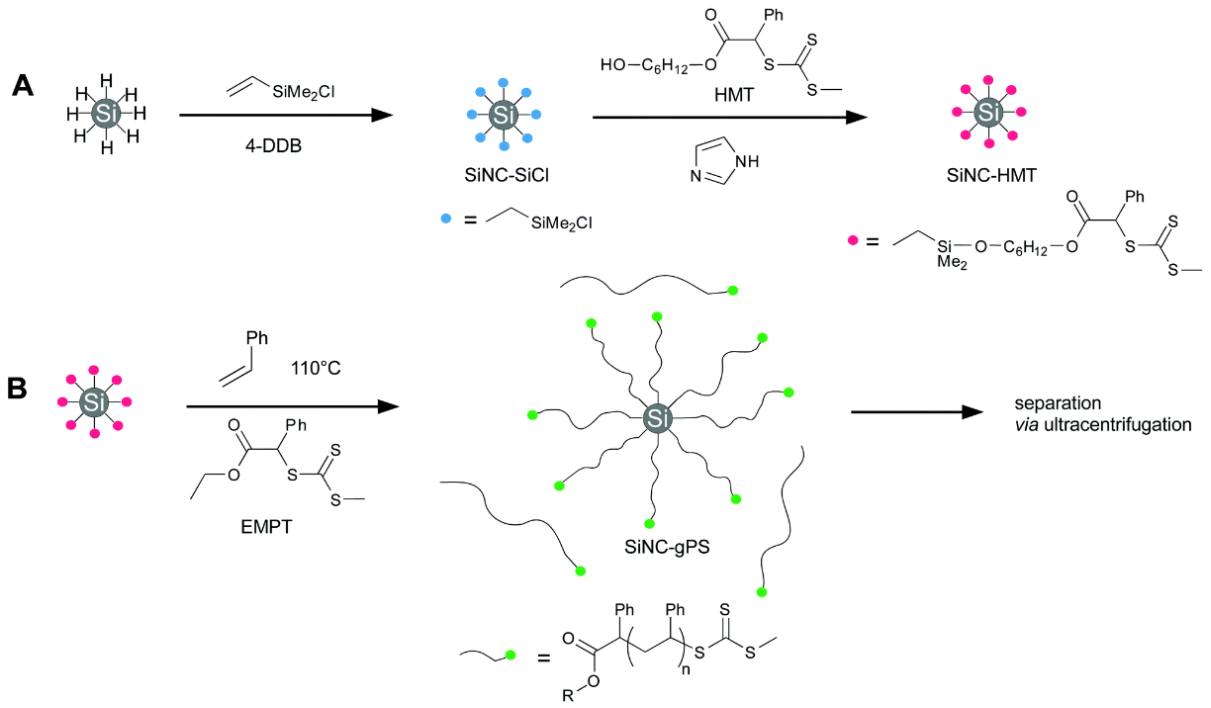

Scheme 27. A) Two stage formation of 6-hydroxyhexyl 3-(methylthio)-2-phenyl-3-thioxopropanoate (HMT)-functionalized SiNCs and B) RAFT polymerization on SiNC surfaces.[212] Reproduced and adapted with permission from reference 213. Copyrights 2015 Royal Society of Chemistry.

Höhlein *et al.* furthermore performed reversible addition-fragmentation chain transfer polymerization (RAFT) from SiNCs surfaces.[212] To do so, they reacted the RAFT reagent 6-hydroxyhexyl 3-(methylthio)-2-phenyl-3-thioxopropanoate (HMT) to the previously chlorodimethylvinylsilane functionalized SiNCs (Scheme 27 A). RAFT polymerization was performed with styrene and free RAFT reagent present. The authors demonstrated, that as well free polymer, as SiNC-surface polymers had narrow polydispersities. The RAFT reaction could furthermore be performed with methyl methacrylate, hexyl acrylate, N-isopropylacrylamide and 4-vinylbenzoylchloride under stabilization of the PL wavelength at ca. 700 nm; solely N-isopropylacrylamide affected a blue shift.[212]

The application of surface RAFT polymerization demonstrates the high potential, SiNC/polymer hybrid materials can exhibit. Yang *et al.* performed a study regarding the high potential of a simple SiNC/polystyrene (PS) hybrid obtained from thermal grafting of hydride terminated SiNCs in monomeric styrene.[228] As a side effect of surface grafting, solution polymerization occurred due to the auto initiation of polystyrene.[229] The SiNCs were well grafted with polystyrene, were distributed homogeneously in the polymer matrix, emitted red PL and were protected from chemicals (Figure 8). Furthermore, the SiNC/PS hybrid material could be processed in solution, which facilitated the manufacturing of photoluminescent thin films, microfibers and fiber bundles.[228] Dung *et al.* amended, that a similar material was stable up to 250 °C and was useful for charge-trapping in metal-insulating-semiconductor devices and thin-film field effect transistors.[230] Additionally, Choi *et al.* varied the SiNC concentration in the SiNC/polystyrene hybrid material; they observed an increase in the refractive index with rising SiNC content.[231]

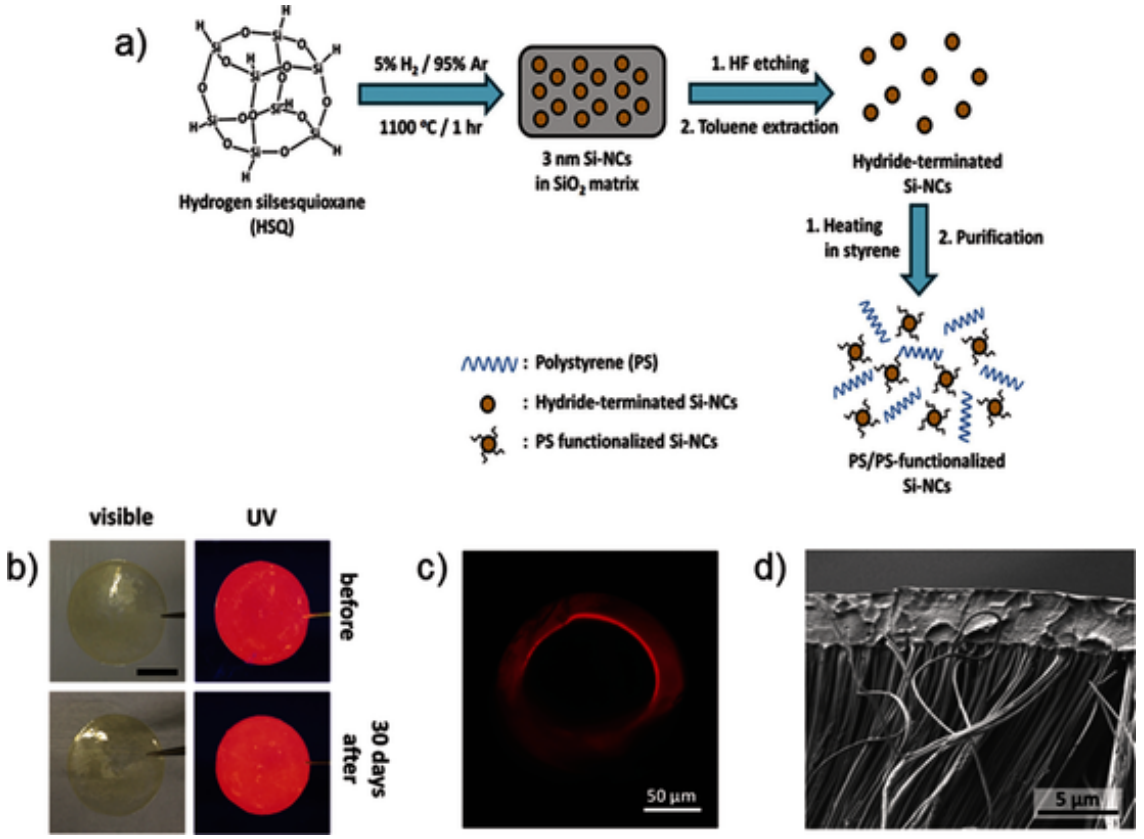

Figure 8. a) Preparation of a SiNC/polystyrene hybrid material; b) chemical stability of a SiNC/polystyrene film towards saturated NaOH; c) PL image of a directed fiber coated with the hybrid material and d) SEM image of a fiber bundle consistent of the hybrid material.[228] Reproduced and adapted with permission from references 18, 229. Copyright 2013, 2016 WILEY-VCH Verlag GmbH & Co. KGaA, Weinheim.

Sato *et al.* utilized the fascinating features of polysiloxanes to create an extendible, luminescent and transparent SiNC/silicone hybrid.[232] To obtain these promising materials, the polysiloxanes were directly linked to the SiNC surfaces *via* Si-O-Si bonds. The hybrid materials could be molded into different shapes and were stable in a variety of conditions; the SiNC photoluminescence properties remained size dependent (Figure 9).[232]

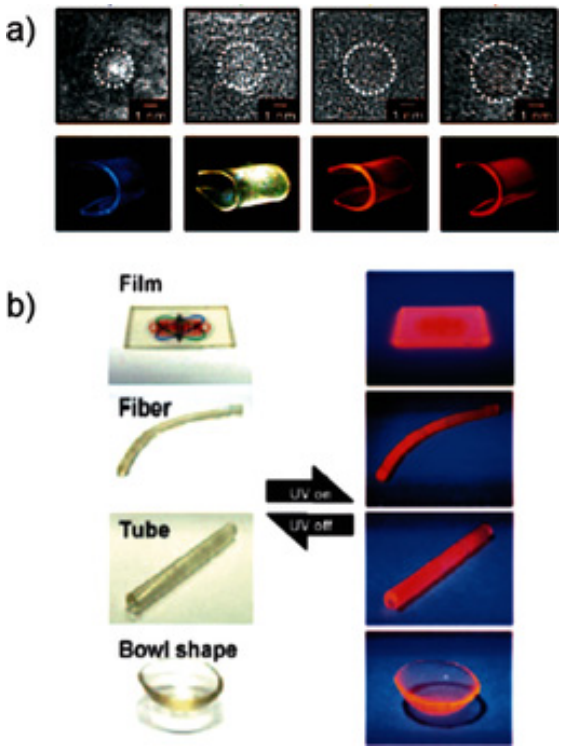

Figure 9. a) Size dependent photoluminescence of a SiNC/polysiloxane hybrid material; b) shapes obtained from molding of a SiNC/polysiloxanes hybrid material.[232] Reproduced and adapted with permission from reference 233. Copyrights 2010 Wiley-VCH Verlag GmbH & Co. KGaA, Weinheim.

While insulating materials are mainly used for molding and SiNC protection applications, the exploitation of conductible polymers introduced new features.[233] To do so, Islam *et al.* performed surface-initiated *Kumada* catalyst transfer polycondensation (SI-KCTP) which gave covalent poly-3-hexylthiophene (P3HT) SiNC bonds (Scheme 28 a). The properties of the SiNC/P3HT hybrid materials differ substantially from the physical blend; while the blend emitted PL in the orange region and the UV/VIS absorption was the sum of the single materials, the hybrid material emitted in the red region and had a unique absorption spectrum.[233] With the SiNC functionalization with Li-phenylacetylide, the reason for this effect was determined to arise due to an electronic in-gap state of the material's valence band (Scheme 28).[115,233]

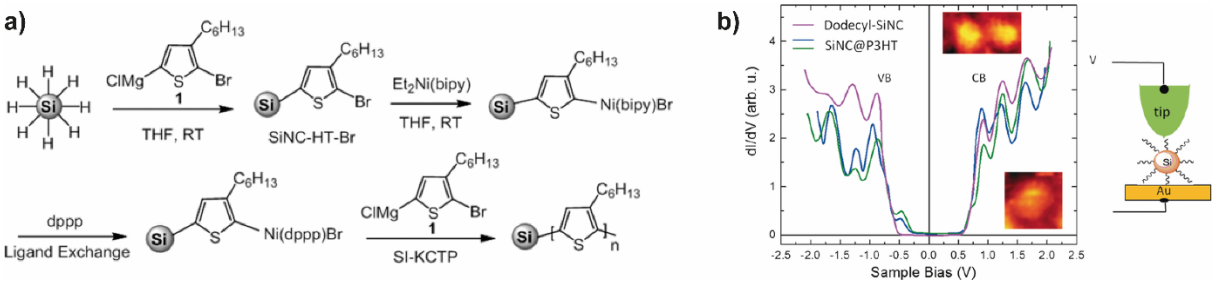

Scheme 28 a) Kumada catalyst transfer polycondensation (SI-KCTP) on hydride terminated SiNCs; b) STM/STS spectrum of a dodecyl-SiNC in comparison to a polythiophene-grafted SiNC.[233] bipy, 2,2'-bipyridine; dppp, 1,3-bis(diphenylphosphino)propane. Reproduced and adapted with permission from reference 234. Copyrights 2016 Wiley-VCH Verlag GmbH & Co. KGaA, Weinheim.

The generation of a SiNC silica composite has turned out to follow complex pathways; perhaps most problematic is, that sol-gel processes require harsh conditions, which can elicit negative impacts on the SiNC properties. Guan *et al.* executed grafting of triethoxyvinylsilane on

H-SiNCs in a first step.[197] The triethoxyvinylsilane (TEVS) functionalized SiNCs were subsequently assembled with tetraethyl orthosilicate; the polymer Pluronic P123, a triblock copolymer based on polyethylene glycol and polypropylene glycol was used as template for cylindrical micelles. After ageing and template removal, mesoporous SiNC/silica composite material with PL at 600 nm and a surface area of 256 m^2/g was obtained. However, the material was obtained in the form of a turbid powder.

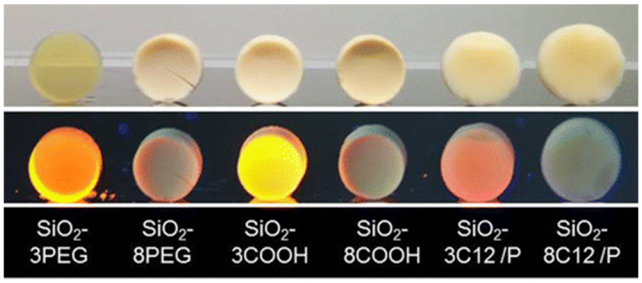

Figure 10. SiNC/silica aerogel composite materials obtained from sol-gel procedure of tetramethyl orthosilicate (TMOS) with surface engineered SiNCs present (3, 3 nm SiNCs; 8, 8 nm SiNCs; PEG, polyethylene glycol functionalized; COOH, pentanoic acid functionalized and C12, dodecyl functionalized).[234] Reproduced and adapted with permission from reference 235. Copyrights 2016 American Chemical Society.

Aghajamali *et al.* utilized SiNC surface engineering to study the impacts on SiNC/silica aerogel hybrid materials (Figure 10).[234] In the present study, base catalyzed sol-gel process with tetramethyl orthosilicate (TMOS) as precursor and supercritical CO_2 drying was performed (*vide infra*). From the present result, the authors concluded, that optical transparency could only be obtained, when 3 nm SiNCs decorated with polyethylene glycol (PEG) surface groups were used. Furthermore, the authors state that the PL response of the SiNCs could be retained; however, as is usual for functionalized SiNCs, PL quenching could be achieved with nitrobenzene.[31,234] As the inner surface of the composites significantly differs, dependent on the applied size and surface group, the study clearly shows, how material properties can be influenced by SiNC surface engineering.

2.5. Applications of SiNC Based Materials.

Silicon nanomaterials have gained much attention in the scientific community. SiNCs have aroused high interest, as they are semiconductor materials with big surfaces, good accessibility for changes and above all, they are based on a nontoxic element. Hence, several prototypes were developed with SiNCs as main or subordinate material. As the application of SiNCs has not been the main part of the present thesis, only an overview is given over battery anodes, solar cells, organic light emitting and photodiodes, catalysis, bioimaging and sensing.

Li-ion battery anode materials consistent of silicon are very promising due to the high theoretical charge capacity (4200 mAh g^{-1}) and the high working potential. However, during cycling (charging and discharging of the battery), volume changes of up to 400% can damage the silicon anode.[235] With a decreasing size of the silicon material, this issue can be minimized. Kim *et al.* synthesized 5, 10 and 20 nm silicon particles from $SiCl_4$ reduction and observed, that although smaller SiNCs exhibited higher charge capacities (~3000 mAh), their Coulombic efficiency decreased and after 40 cycles the capacity was quickly reduced.[173] The researchers concluded, that the critical SiNC size should not fall below 10 nm. Furthermore, good results were obtained when the silicon particles were hybridized with carbon composites.[174,236] The resulting materials were useful to overcome deficiencies like structural degradation, formation of unstable interfaces and electrical isolations.

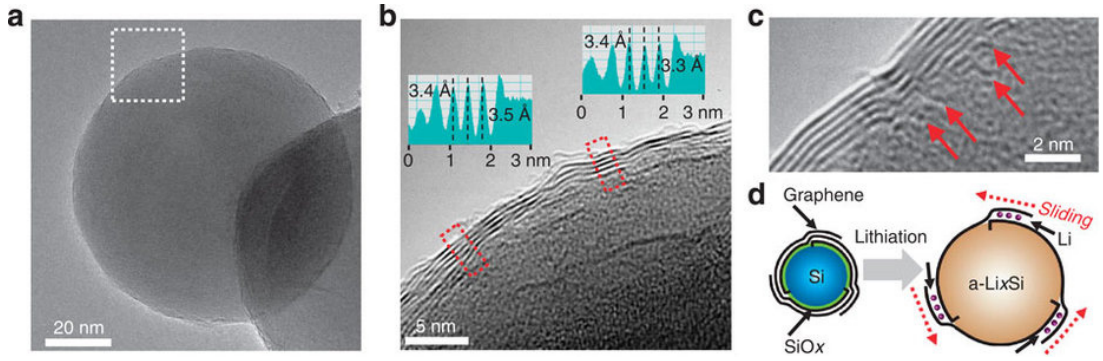

Figure 11. Low (a) and high magnification TEM images (b-c) of a surface grafted SiNC/graphene hybrid material with measurements of the distances of the graphene layers and the material interface (b inset). Furthermore the mechanism of Li uptake is demonstrated (d).[52] Reproduced and adapted with permission from reference 52. Copyrights 2015 Nature Publishing Group.

The most attractive method for the generation of the SiNC hybrid anode is encapsulation in graphene, as it is known to enhance carrier transport and reduces volume changes related to the Li ion uptake (Figure 11).[51,52,237] Furthermore, amorphous Si nanoparticles below 10 nm have been hybridized with graphene to obtain a capacity of 2858 mAh g^{-1} (92.5 % Coulomb efficiency) or SiNCs were grown on carbon nanotubes (CNT) by silane gas decomposition.[53,175] Based on the carbon approach, Liu *et al.* used a "yolk-shell" design, which gives some void space to the SiNCs for volume changes, but compensates the expansion (Figure 12).[238] The capacity of these hybrids was up to 2833 mAh g^{-1} at about 1000 cycles and 99.8 % Coulomb efficiency.

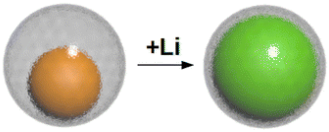

Figure 12. „Yolk shell" design of a SiNC/carbon hybrid material and schematic mechanism during Li uptake.[238] Reproduced and adapted with permission from reference 239. Copyrights 2012 American Chemical Society.

SiNCs have not only been tested as energy storage materials, but were successfully prototyped in energy conversion materials. As such, solar cells and photovoltaics have gained big interest. Some approaches of producing photovoltaics deal with SiNCs being homogeneously distributed in a semiconductor "host" material.[45] SiNCs preparation from SiO_2/SiO_x reduction is simple, control over size and crystallinity are easy and the product emit strong PL; however, as the SiO_x cover has isolating properties charge transport is poor. To improve this approach, SiNCs were grown from SiN_x/Si_3N_4 and Si_xC_{1-x}/SiC supperlattices. In both cases, the composites had weak PL and the quantum confinement features could not be measured. However, high conductivities and good light absorption were shown, which made the materials promising for photovoltaics.[45]

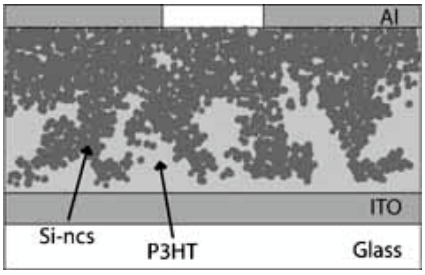

Figure 13. Schematic organization of a SiNC(Si-nc)/P3HT heterojunction solar cell.[239] ITO, indium tin oxide; P3HT, poly-3-hexylthiophene. Reproduced and adapted with permission from reference 240. Copyrights 2009 WILEY-VCH Verlag GmbH & Co. KGaA, Weinheim.

Stutzmann *et al.* blended SiNCs with P3HT for solar cell applications (Figure 13).[239] Such photovoltaics worked *via* silicon/organic semiconductor heterojunctions and had an open circuit voltage of 0.76 V. Dietmüller *et al.* later demonstrated, that charge transfer is the dominating mechanism for SiNCs in P3HT.[240] Furthermore, the authors observed, that the reduction or elimination of surface defects by vacuum annealing, HF etching, or SiNC passivation can improve the quality of a solar cell, e.g., by enhancing the photovoltaic conductivity by a factor of up to 400.[170,171,241] These results demonstrated, that efficient improvements can be achieved by means of surface grafting.

Light emitting diodes (LED) have become important for energy saving devices. SiNCs are useful materials due to their good tenability in light emission and a growing understanding for surface engineering and charge transfer processes. In this context, SiNCs are generally arranged between the hole and the electron transport layer, which is mainly consistent of conducting polymers (Figure 14).

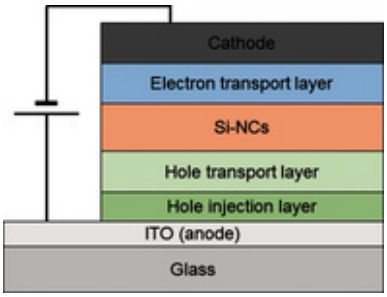

Figure 14. Schematic arrangement of SiNC based LEDs.[18] Reproduced and adapted with permission from reference 18. Copyrights 2016 WILEY-VCH Verlag GmbH & Co. KGaA, Weinheim.

Perhaps most important is, that surface engineering has a major influence on the LED properties and construction. Cheng *et al.* used dodecyl grafted SiNCs obtained from silane gas plasma decomposition to generate LEDs with electroluminescence in the infrared region (868 nm) and an external quantum efficiency of 0.6 %.[176] Furthermore, they observed, that the external quantum efficiency of the device strongly depends on the thickness of the SiNC layer. Later, external quantum efficiencies of 8.6 % were obtained of LEDs containing 3 and 5 nm SiNCs. The improvement of the efficiencies has been obtained from a better confinement of the charge carriers and excitons in the SiNC emission layer arising from an increase in the energy gap between the hole- and electron transport layer.[177] Maier-Flaig *et al.* observed red/orange electroluminescence from allylbenzene-grafted SiNCs used in a SiNC/organic light-emitting diode (OLED; Figure 15 a, b).[47] The devices had external quantum efficiencies of 1.1 %; however, inhomogeneous emission, defects and fast degradation of the OLED has occurred from the SiNC polydispersity. Hence, the research groups used size selective precipitation to prepare brighter and more homogeneous devices with longer lifetimes.[47] Ghosh *et al.* used a combination of materials with different emissions (e.g. red luminescence from octadecyl-SiNCs and blue-green emission from a luminescent polymer, e.g. poly-TPD) to generate LEDs with white light emission and external quantum efficiencies of 0.033-0.36 % (Figure 15 c, d).[48]

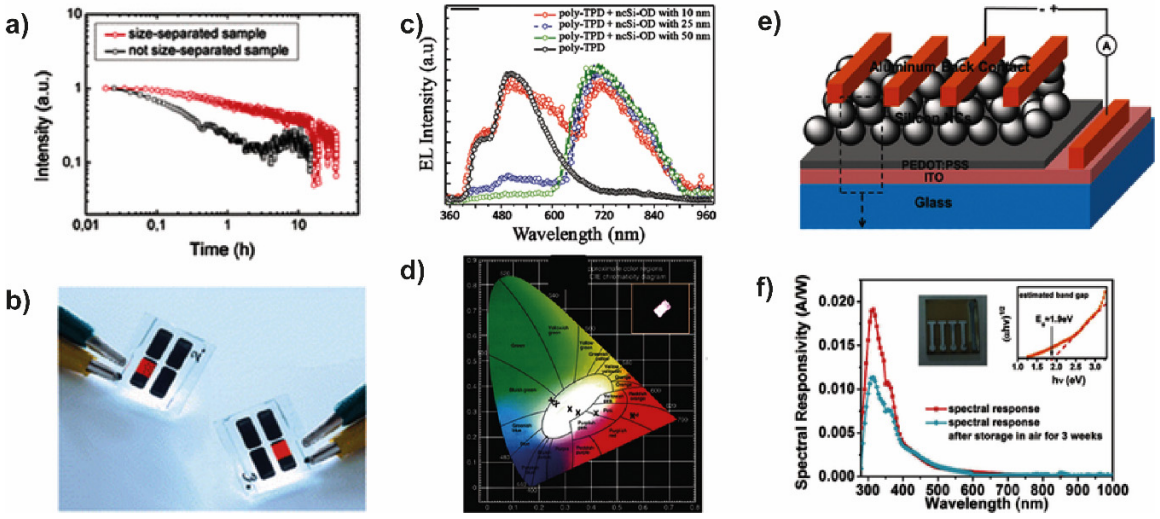

Figure 15. Electroluminescence of LEDs obtained from the application of polydispersity and size separated SiNCs at a constant currency of 1.6 mA cm^{-2} (a) and photographs of the corresponding LED devices (b).[47] Electroluminescence spectra of LED devices obtained from combination of poly-TPD and SiNCs of different sizes (c) with the corresponding CIE diagram (d; inlet photograph of white-light LED.[48] Architecture of a SiNC based photodiode (e) and its spectral response (f; inset photograph and band gap estimation using Tauc method).[178] Reproduced and adapted with permission from references 47, 48, 178. Copyrights 2013 American Chemical Society; 2014 WILEY-VCH Verlag GmbH & Co. KGaA, Weinheim.

Lin *et al.* recently produced a photodiode consistent of SiNCs (Figure 15 e).[178] They compared the application of allyl disulfide-grafted SiNCs with alkyl-SiNCs (Figure 15 f). Due to the lone pair electrons from the allyl disulfide moiety, enhanced conductivity could be obtained. The device was prepared using spin coating of a SiNC solution on the indium tin oxide (ITO) glass layer. PEDOT:PSS was used as electron blocking layer between ITO and SiNCs, to improve charge separation. In the present setup, the device showed UV responsivity with a photo response of 0.02 AW^{-1} (ampere/watt) peak.

Catalysis offers another suitable approach for SiNCs. As such, Erogbogbo *et al.* used Si nanoparticles to generate hydrogen from water without light, heat or electricity applied.[42] They observed, that 10 nm SiNCs formed H_2 1000 times faster than bulk silicon and 150 times faster than 100 nm silicon particles. Furthermore, silicon particles were six times faster than metals. El Demellawi *et al.* used H-SiNCs to convert secondary alcohols to ketones and hydrogen.[242] They reported, that the reactions ran at room temperature. Furthermore, they could demonstrate, that SiNCs can be sensitive towards the surrounding medium.

Peng *et al.* used the photo reactivity of H-SiNCs towards CO_2 to form formaldehyde.[243] Later, Dasog *et al.* followed the conversion of CO_2 to methanol by 155 nm SiNCs at elevated temperatures.[222] The Si-H consumption and the methanol formation were followed by *in-situ* IR spectroscopy (Figure16 A-C).

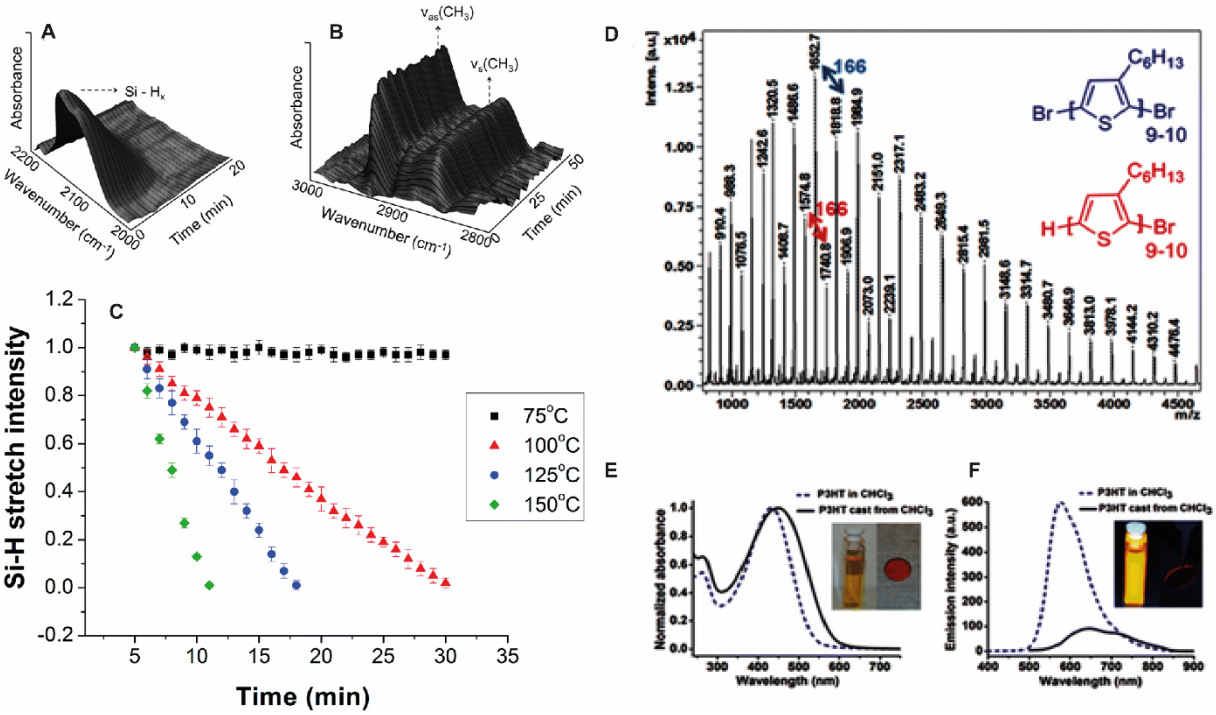

Figure 16. A) Si-H consumption, B) formation of methanol from CO_2 followed by in-situ IR spectroscopy. C) Temperature resolved study of the consumption of Si-H surface groups followed by in-situ IR.[222] D) Matrix assisted laser desorption-ionization (MALDI) of P3HT obtained from SiNC catalysis. E) UV-VIS absorption and F) PL emission spectra of P3HT (Inset: P3HT under ambient light (E) and und under UV light (F).[43] Reproduced and adapted with permission from references 43, 223. Copyrights 2014 American Chemical Society; 2017 The Royal Society of Chemistry.

Chloride terminated SiNCs obtained by PCl_5 reaction were used for the generation of polymeric P3HT (Figure 16 C).[43] The polymer was formed presumably from a room temperature Lewis-acid mediated polymerization of the Grignard reagent of 3-hexylthiophene. It had a light

absorption maximum at about 440 nm and emitted light at 580-700 nm. (Figure 16 E, F). Perhaps most important is the fact, that SiNCs accelerated the reaction faster than bulk silicon and molecular silanes.

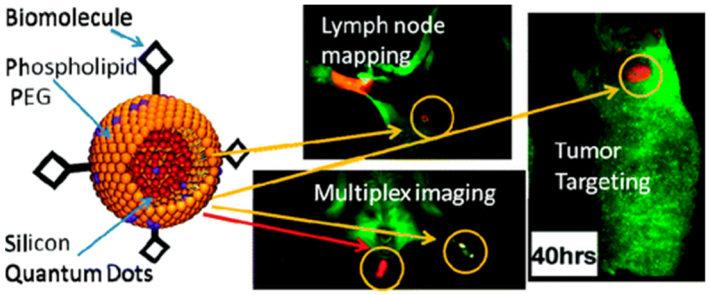

Figure 17. Biomolecule functionalized micelles containing a SiNC core and a phospholipid membrane and demonstration of possible applications.[35] Reproduced and adapted with permission from references 35. Copyrights 2011 American Chemical Society.

Bioimaging is a very promising application of SiNCs, as they are non-toxic.[13] Furthermore, the small sizes and the good adaptability of the SiNC surfaces makes them ideal platforms for medical diagnostics.[56] Erogbogbo *et al.* formed micelles with SiNC cores and biomolecules in the shell.[35] The authors observed, that the SiNC hybrids could be used for lymph node imaging, for Panc-1 tumor cell targeting and for multicolor imaging in living mice (Figure 17). The SiNCs emitted stable luminescence for more than 40 h. Although this *in vivo* study has a high impact on future research, most of the studies in bioimaging were conducted *in vitro*. As such, Erogbogbo *et al.* used similar PEGylated phospholipids to micellize SiNCs and render them water-dispersible with stabilized PL (2 % quantum yield).[41] The micelles were used for *in vitro* imaging of HeLa cells. The micellation approach made engineering of the phospholipid layer possible, e.g. with 1,4,7,10-tetraazacyclododecane-1,4,7,10-tetraacetic acid and the chelation of paramagnetic Gd^{3+}, which is a well-known contrast agent for magnetic resonance imaging.[244] Furthermore, a dye was added to the phospholipid cells, which effected an increase of the PL in the micelles from fluorescence resonance energy transfer.[245]

To emit PL, SiNCs require an excitation wavelength, which is in the near UV region (300-450 nm). As UV light is known to damage tissue, it is not useful in *in vivo* applications. Thus, Tu *et al.* invented the two photon technique which released two photons of half energy near IR region to excite the particles.[246] The authors used 4.3 nm Mn doped SiNCs with an external quantum yield of 8.1 % and emission at 441 nm; the SiNCs accumulated in macrophages. Another issue is the big size of SiNC micelles (>10 nm), which could possibly degrade slowly.[247,248] An improvement has been the development of self-assembling monolayers (SAM), which combine small radii with good biocompatibility and a bio active surface.[248,249] Zhong *et al.* used the SAM approach to prepare water dispersible 2.2 nm SiNCs with internal quantum yields of 20-25 %, which could be used for cell nuclei imaging for 60 min without photobleaching (Figure 18).[249] Further studies showed, that the conjugation of biomolecules like lysine, folate, antimesothelin, transferrin, arginine and mannose to SiNC surfaces are sufficient platforms to target various cancer cells; it is worth mentioning, that standard surface molecules like dodecane or pentanoic acid do not label the same cell types.[36,247]

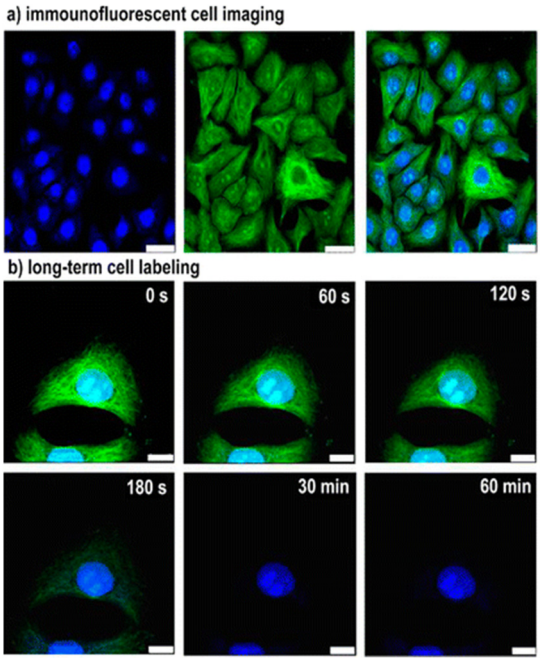

Figure 18. a) Immunofluorescent cell imaging obtained by laser confocal microscopy (scale bar = 5 µm; left: SiNC labeling of nuclei, middle labelling of microtubules by fluoresceinisothiocyanat, right: overlap of both images) and b) Time resolved stability of HeLa cells labelled by SiNCs and fluoresceinisothiocyanat.[249] Reproduced and adapted with permission from reference 250. Copyrights 2013 American Chemical Society.

The sensitivity of the SiNC surface towards various functional groups and a change in PL mechanisms makes them sufficient for sensing applications.[250] In general three quantum dot sensing mechanisms are known (Figure 19): Quenching of the SiNC PL can occur, once an analyte affects an electron transfer (ET) previous to the recombination of the exciton (Figure 19a).[251] If the lowest unoccupied molecule orbital of the analyte is lower than the band edge of the quantum dot's conducting band, an electron can be transferred to the analyte. In contrast, an electron can be transferred from the highest occupied molecular orbital (HOMO) into the hole located on the QD's valence band edge, if the HOMO has a higher energy. The ET mechanism is dependent on the QD'S redox properties.[252] Furthermore, surface traps and charges can have influences.

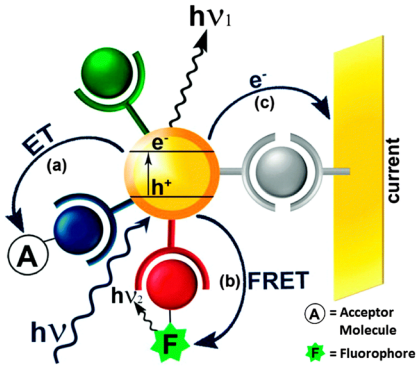

Figure 19. Schematic illustration of various mechanisms of SiQD sensing approaches: a) electron transfer (ET), b) fluorescence resonance energy transfer (FRET), and c) photocurrent generation as readout signals. [250,253] Reproduced and adapted with permission from references 254. Copyrights 2013 American Chemical Society.

If the sensing mechanism is fluorescence resonance energy transfer (FRET; Figure 19 b), nonradiative energy transfer induced from dipole-dipole interactions between an excited state donor to a ground state acceptor is involved.[250,253] FRET can run over larger distances than

ET; however, it's rate is dependent on the spectral overlap between the donor emission and the absorption of the acceptor, the donor's quantum yield, the distance between donor and acceptor and the orientation of the dipoles.[254]
Photochemical sensing can also gain interest.[11] Prototypes use the concept of immobilizing quantum dots on an electrode surface by covalent attachments, which induce a photocurrent from the conduction band to the electrode surface. The induced current depends on the concentration of analyte in the monitored solution.[250]

Based on the mentioned mechanisms, the design of cheap sensors could be achieved. Gonzalez *et al.* used papers coated with dodecyl-SiNCs to detect high energy materials.[31] The sensor stripes could be exploited for the detection of very low concentrations of trinitrotoluene (TNT), pentaerythritol tetranitrate (PETN) or cyclotrimethylene trinitramin (RDX; Figure 20 a). Furthermore, PL emission was quenched upon submission of the SiNC coated strip to nitrobenzene vapors (Figure 20 b). After the release of nitrobenzene, SiNC PL returned reversibly. The authors proposed, that consistent with previous investigations, an electron transfer is responsible for the quenching.[31,255] Ban *et al.* exploited 3-aminopropyl functionalized SiNC for the detection of trinitro toluene (TNT) in water.[32] The authors stated, that the detection limit was 1 nM. Mechanistically, FRET was suggested to occur.

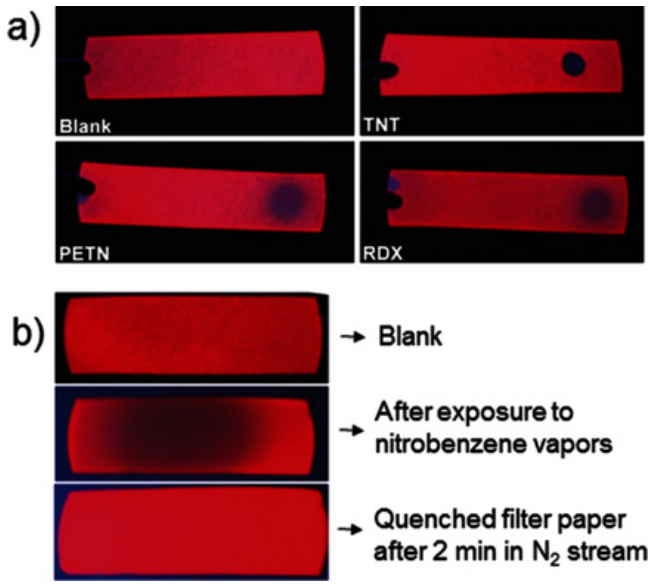

Figure 20. a) Detection of drops of solution of TNT, PETN and RDX; b) reversible detection of nitrobenzene vapor.[18,31] Reproduced and adapted with permission from references 18, 31. Copyrights 2014 Royal Society of Chemistry; 2016 Wiley-VCH Verlag GmbH &Co. KGaA, Weinheim.

Further work conducted by Nguyen *et al.* compared red emissive alkyl oligomer, alkyl monomer and blue emitting amine terminated SiNCs in the sensing of nitrobenzene vapors.[256] The authors observed, that an alkyl monomer surface is more sensitive than alkyl oligomer SiNCs and amino-SiNCs (Figure 21). Furthermore, they have proposed an electron transfer mechanism being responsible for the quenching. Amine terminated SiNCs have not been as sensitive since the functional groups were linked to the SiNC surface by the amino groups.[32,256]

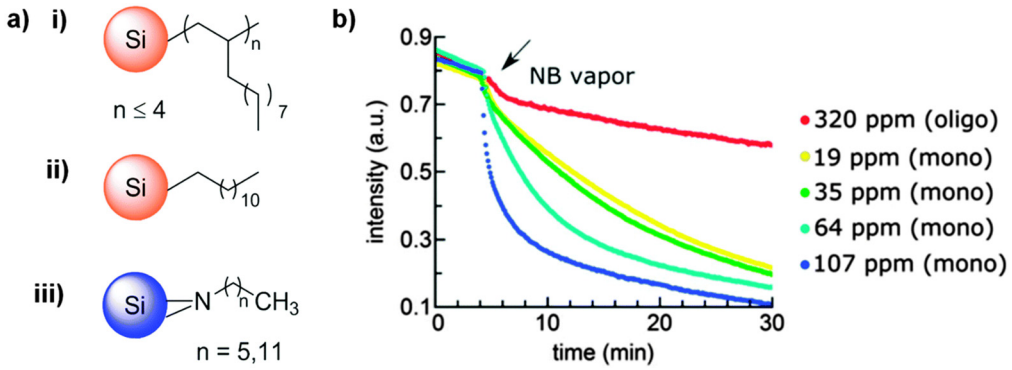

Figure 21. a) Alkyl oligomer (i), alkyl monomer (ii) and blue emitting amine terminated (iii) SiNCs used for the investigation of the PL response towards nitrobenzene.[250,256] Reproduced and adapted with permission from references 251. Copyrights 2016, Royal Society of Chemistry.

Many studies have been performed using SiNCs as highly sensitive platforms for the detection of metal ions,[257] biologic relevant molecules or biomolecules,[33,258] ethanol,[259] antibiotics,[260] and pesticides.[261] A summary of the studies on sensing evolving SiNCs has been given by Gonzalez and Veinot in 2016.[250]

2.6. Rare Earth Metal-Mediated Group Transfer Polymerization

Since the beginning the 20th century, polymers and plastics have played a more and more important role in people's lives.[262] Due to their light weights and the variabilities of properties, plastics are incorporated in nearly every item. Mostly, polymers with broad polydispersities are adequate for the requirements; however, precise control in certain areas, compared to chain length and end group functionalization, is key to tune the properties and tailor the polymers to the field of application.[263] Furthermore, some monomers (e.g. vinylphosphonates) are scarcely polymerizable or their polymerization is not controllable by standard polymerization procedures (e.g. radicals).[264] Rare earth metal-mediated group transfer polymerization (REM-GTP), also known as catalytic precision polymerization, of Michael type monomers is a young method, to prepare the highly precise tailored materials for a variety of applications (Figure 22).[263]

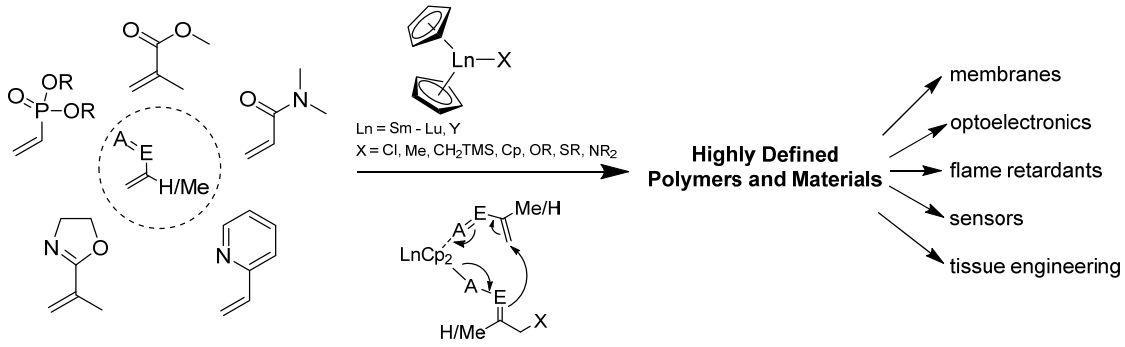

Figure 22. Overview of the catalytic precision polymerization process of various monomers (E = CR, PR_2; A = O, NR).[263]

The concept of the GTP goes back to 1992, when Yasuda *et al.* presented the neutral samarocene complex $[Cp^*_2SmH]^2$, and independently, Collins as well as Ward published a two-component Group 4 metallocene complex for the polymerization of acrylates.[265,266] In both cases the reactions occurred by multiple conjugate addition steps of the Michael type molecules (*vide infra*). Besides methyl methacrylate (MMA) nowadays a variety of O and N-coordinating monomers like dimethyl acrylamide (DMAA),[267] dialkyl vinylphosphonates (DAVP),[264,268] 2-vinylpyridine (2-VP)[269] and 2-isopropenyl-2-oxazoline (IPOx)[269] have been polymerized *via* REM-GTP with low PDIs.[263,270]

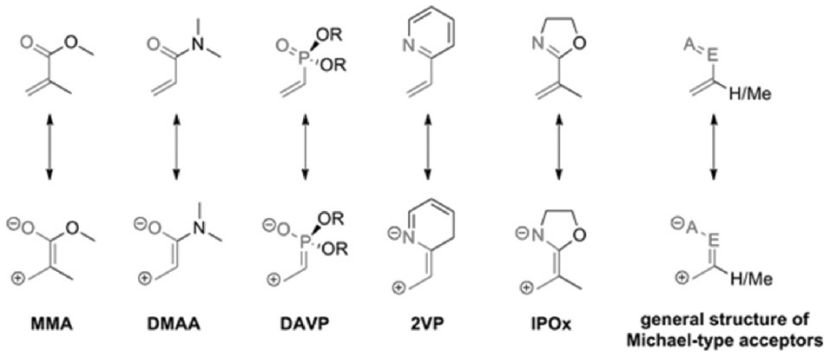

Figure 23. Overview over O and N-coordinating Michael Type acceptors.[263] Reproduced and adapted with permission from reference 264. 2014 WILEY-VCH Verlag GmbH & Co. KGaA, Weinheim.

DAVPs are of particular interest, as the polymers are non-toxic, biocompatible, contain phosphorus, conduct protons and have a lower critical solution temperature.[271] These properties make them useful as flame retardants, binders in dental or bone concrete, in membranes, in non-fouling coatings, in tissue engineering, in drug delivery or in cell proliferation surfaces. In 2010, Seemann *et al.* developed a trivalent ytterbocene Cp_2YbX (X = Cl, Me), which was sufficient for the polymerization of diethyl vinylphosphonate (DEVP) with molecular weights up to $M_W = 10^6$ g/mol.[272] Further work performed by Salzinger *et al.* focused on different REM-centered catalyst in the form of CP_3Ln with Ln = Lu, Yb, Tm, Er, Ho, Dy.[268] The authors observed that the initiator efficiency as well as the polymerization speed increased with the radii of the metal centers, but the molecular weights decreased. Poly(diethyl vinylphosphonate) (PDEVP) was prepared by Cp_3Lu in 30 min with an initiator efficiency of 89 %, an overall turnover frequency (TOF) of 17300 h^{-1} and a M_n of $1.28 \cdot 10^5$ g/mol. In contrast, Cp_3Ho afforded PDEVP polymerization in 5 h with 17 % initiator efficiency, a TOF of 500 h^{-1} and a M_n of $3.36 \cdot 10^5$ g/mol.[268]

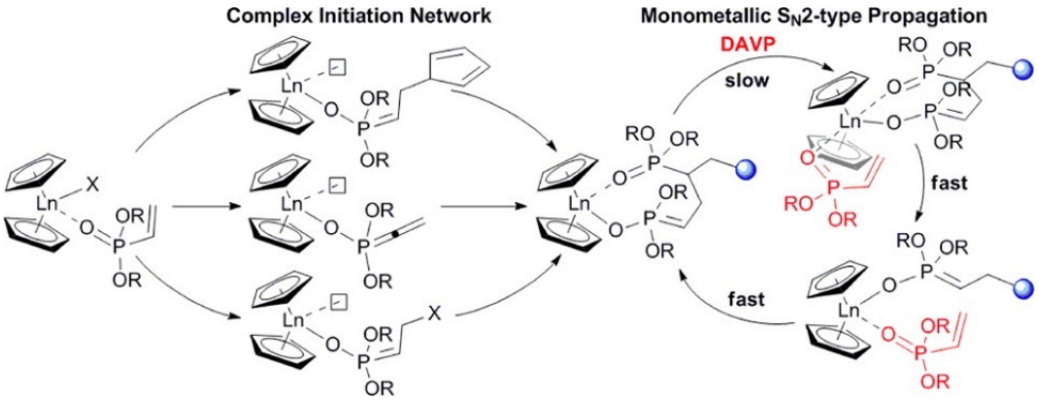

Scheme 29. Mechanism of initiation and propagation of DEVP by Cp_2LnX (X = CH_3; CH_2TMS, Cp, SR, Cl, OR) complexes.[273] Reproduced and adapted with permission from reference 274. Copyright 2013 American Chemical Society.

Salzinger *et al.* recently monitored the mechanisms of group transfer polymerization and initiation of diethyl vinylphosphonates (Scheme 29).[273] The studies were performed with catalysts in the form of CP_2LnX•thf or $[Cp_2LnX]_2$ with variation of the center metals (Tb, Y, Tm, Lu) and the functional group X. The most important finding is perhaps, that the pathway of initiation is strongly dependent on the nature of X (Scheme 30): CH_3 and CH_2TMS ligands induced an abstraction of the α-CH of the vinylphosphonate, Cp or SR ligands underwent a nucleophilic transfer to the coordinated monomer and Cl or -OR ligands affected a monomer induced ligand exchange reaction to form Cp_3Ln in equilibrium. Furthermore, it was possible that several pathways could occur simultaneously. This has been proven for X = $N(SiMe_2H)_2$.[273]

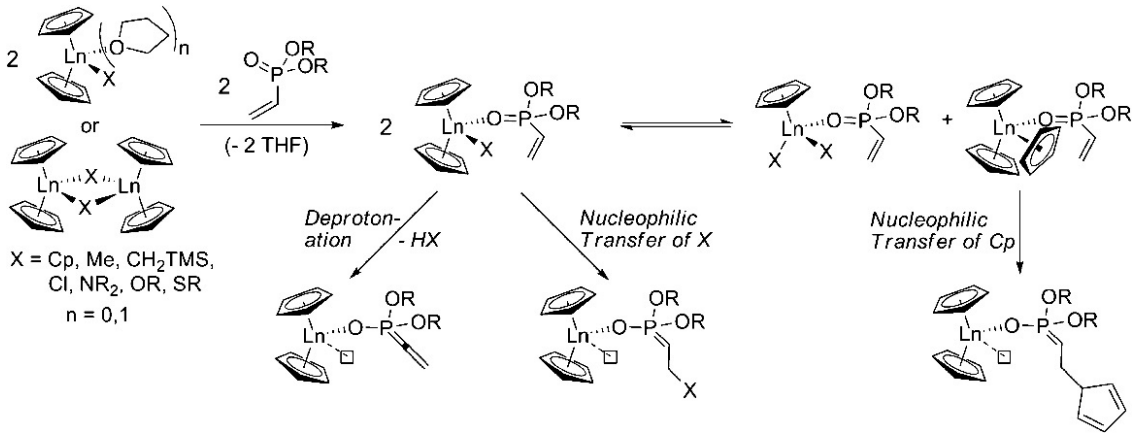

Scheme 30. Initiation pathways of REM-GTP using a catalyst of the design CP_2LnX•thf or $[Cp_2LnX]_2$.[273] Reproduced and adapted with permission from reference 274. Copyright 2013 American Chemical Society.

After initiation, a generally fast propagation occurs after the mechanism suggested by Yasuda *et al.* in 1992 for the MMA polymerization.[266] Coordination of DEVP to the free binding side started the propagation following a monometallic S_N2 type mechanism, with the displacement of polymer phosphonate ester being the rate determining step (Scheme 29).[273] Afterwards, the conjugate addition of the monomer occurred *via* a six-electron process (Scheme 31). The propagation process was strongly dependent on the activation entropy, which was shown to be influenced by the steric demand of the metal center and of the monomer.

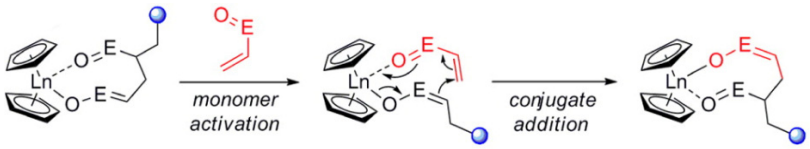

Scheme 31. Propagation step in group transfer polymerization mechanism.[273] Reproduced and adapted with permission from reference 274. Copyright 2013 American Chemical Society.

The study of Salzinger *et al.* was an important basis for understanding the transformations in the vinylphosphonates polymerization process. The formation of new metal complexes like bis(cyclopentadienyl)(4,6-dimethylpyridin-2-yl)methyl lanthanide (Y, Lu) has been one consequence.[274] These catalysts formed poly(dialkyl vinylphosphonate) (PDAVP) following a highly living character with unprecedented rates (TOF 59400 h^{-1}) and afforded end group functionalization *via* stable C-C bonds. Notably, the pre-initiated catalyst has been formed by C-H activation of Cp_2YCH_2TMS•thf with a methyl group of 2,4,6-trimethylpyridine *via* σ-bond metathesis (Scheme 32).

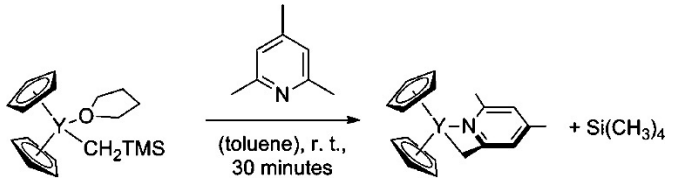

Scheme 32. Synthesis of $Cp_2Ln(CH_2(C_5H_2Me_2N))$.[274] Reproduced and adapted with permission from reference 275. Copyright 2015 American Chemical Society.

REM-GTP is the key to defined PDAVP architectures with unique properties. Perhaps most interesting is the lower critical solution temperature (LCST, an entropy driven effect)[275] of this

fascinating polymer class. The cloud point of a DEVP solution in water has been determined to be 40 – 46 °C.[268] To tune the LCST properties of the polymer, Zhang *et al.* applied random copolymerization of DEVP with dimethyl vinylphosphonate (DMVP) or di-n-propyl vinylphosphonates (DPVP; Figure 24 a).[276] LCST cloud points decreased as a result of an increasing poly(di-*n*-propyl vinylphosphonate) PDPVP content in the copolymer (PDEVP-co-PDPVP), as well they increased with poly(dimethyl vinylphosphonate) (PDMVP) being present in the copolymer (PDEVP-co-PDMVP; Figure 24 b). The changes in cloud points correlated directly proportional to the incorporated amount of DPVP or DMVP.[276] Furthermore the authors observed that the cloud point of the polymer could be reduced from 32-33°C ($DEVP_{0.89}$-co-$DPVP_{0.11}$) to 29-30°C by the addition of NaCl or buffer solutions.

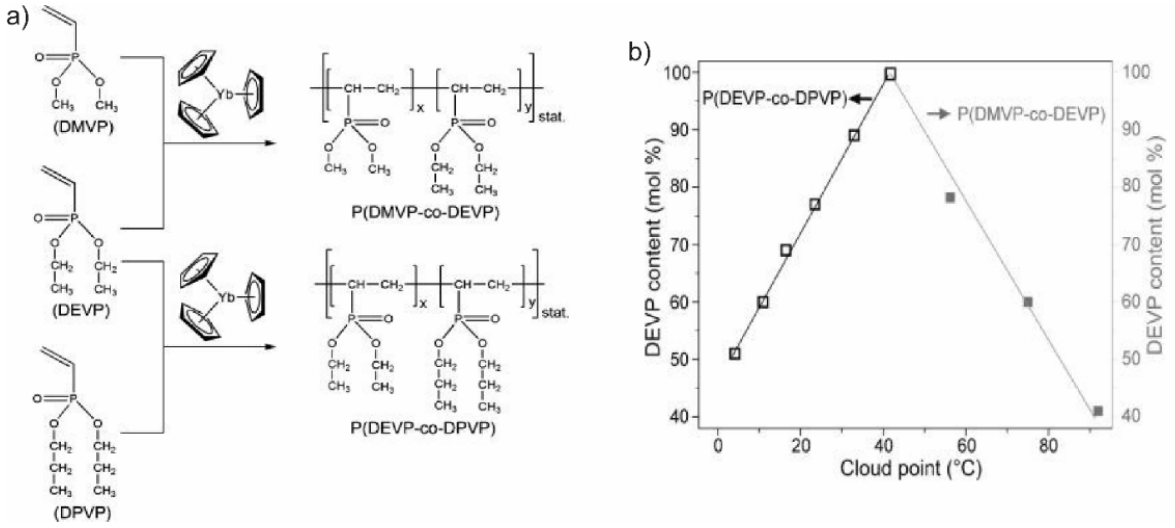

Figure 24. a) Schematic illustration of the copolymerization of DEVP with DMVP and DPVP, b) changes in cloud points by the variation of the DEVP concentration in the respective copolymers.[276] Reproduced and adapted with permission from reference 277. Copyright 2012 American Chemical Society.

Surface-initiated group transfer polymerization (SI-GTP) has been presented by Zhang *et al.* in 2012. It is another interesting example, of how GTP can be used to design materials with unprecedented properties.[277] In the first step, an oxidized Si surface was coated with 3-(trimethoxsilyl)propyl methacrylate (TMSPM; Scheme 33). Although the surface was homogeneously loaded with TMSPM, after catalyst impregnation and addition of monomer, mainly in plain polymerization occurred and the surface topography became inhomogeneous.

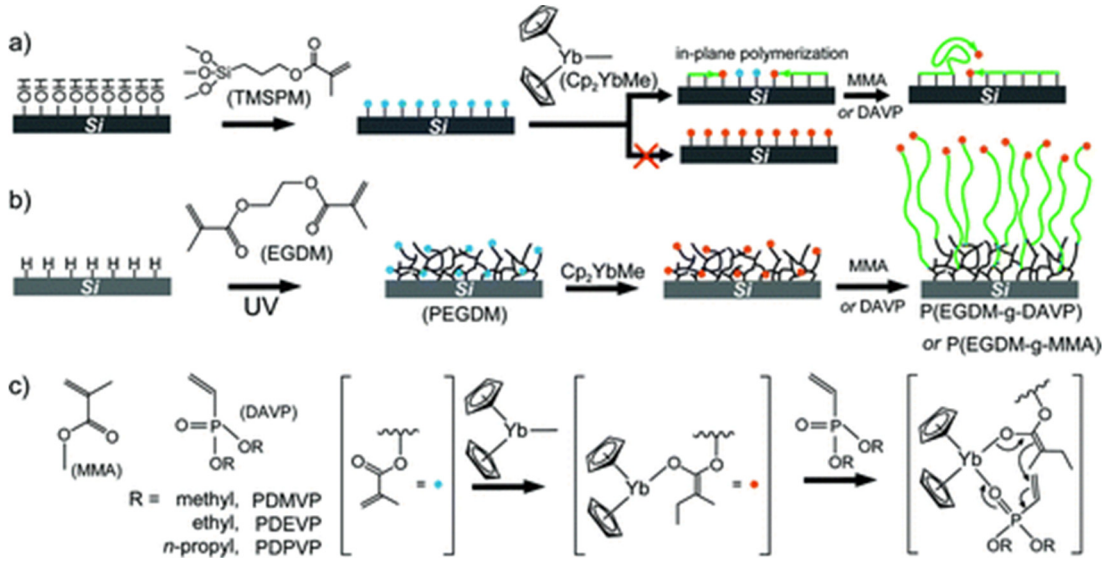

Scheme 33. Surface reaction, catalyst impregnation and SI-GTP using a) trimethoxysilylpropyl methacrylate, b) ethylene glycol dimethacrylate as initiator layer. c) SI-GTP mechanism for the surface polymerization.[277] Reproduced and adapted with permission from reference 278. Copyright 2012 American Chemical Society.

The authors conducted photografting of ethylene glycol dimethacrylate (EGDM) at 365 nm to form a "carpet" structure on the hydride terminated SiNC surface (Scheme 30 b).[277] As the acrylic moieties have not packed closely enough for in-plane polymerization, SI-GTP occurred, following the proposed mechanism (Scheme 30 c), that resulted of polymer chains (DAVP, MMA) grew from the surface. Zhang *et al.* monitored the growth by an atomic force microscopy (AFM) study of the covered surfaces (Figure 25). They demonstrated, by scratching, that the surface grew from ~29 nm (poly(ethylene glycol dimethacrylate); PEGDM) to ~146 nm (PDEVP) in 5 minutes; moreover, the polymer growth occurred highly linearly with time.

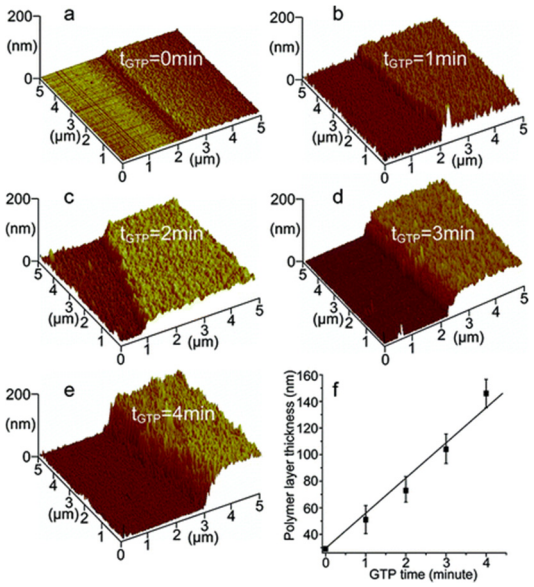

Figure 25. Investigation of the time resolved growth of PDEVP(a-f) from an EGDEM surface.[277] Reproduced and adapted with permission from reference 278. Copyright 2012 American Chemical Society.

SI-GTP was furthermore used to attach the vinylphosphonates to the surface, which resulted in a change of surface properties (Figure 26).[277] PDMVP, which was the most hydrophilic

molecule in the row had a contact angle of 17°, DEVP of 64° and DPVP, the most hydrophobic molecule of 76°. Even more fascinating is, that the LCST concept is applicable on the polymer brushes at the surface: The water-contact angle of DEVP changed distinctly from 46° at 25 °C to 66° at 50 °C (Figure 26 b, d). This feature made PDAVP surfaces promising materials for cell proliferation surfaces, on which cell breeding can occur directly on the surface and they can be released upon cooling below the LCST.[278]

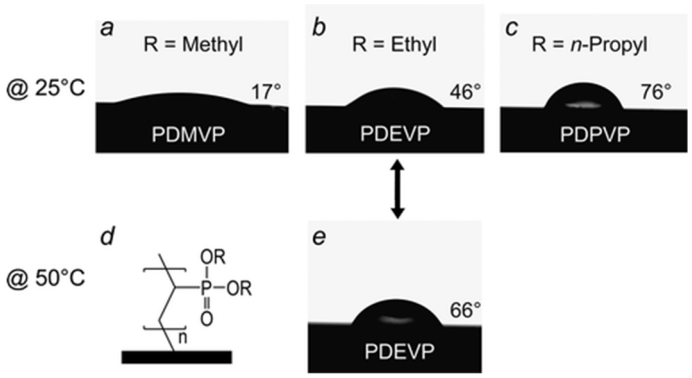

Figure 26. Static water contact angle measurements of a) PDMVP, b) PDEVP and c) PDPVP surfaces at 25 °C and of PDEVP at 50 °C; d) structures of the PDAVP on the surface.[277] Reproduced and adapted with permission from reference 278. Copyright 2012 American Chemical Society.

2.7. Silica Aerogels as High Impact Low Weight Materials

Since the first report of silica aerogels by Kistler in 1931, the interest in these fascinating materials grew more and more.[279] Nowadays aerogels are known as extremely porous, low weight, and high technology materials (Table 1) with a broad scope of applications (e.g. catalysis, superinsulation, optical fibers, ceramics, chemical absorbers).[280,281] Amongst others (e.g. graphene, metal oxides or polymers), silica has mainly been used as matrix material, due to its straightforward synthesis procedure, which goes *via* the sol-gel process of a silanol precursor.[281–285] Generally, the preparation of silica aerogels requires three engineering steps: Sol-gel procedure, solvent exchange, and supercritical drying.

Table 1. Properties of silica aerogels.[282]

Properties	Range	Typical Value
Bulk density [g cm^{-3}]	0.003-0.5	0.100
Porosity [%]	80 – 99.8 %	
Medium pore size [nm]	20 – 150	
Surface area [m^2 g^{-1}]	100 – 1600	600
Refractive Index	1.007 – 1.240	1.02
Heat Conductivity [W m^{-1} K^{-1}]	0.017 – 0.021	0.020

Tetraethyl orthosilicate (TEOS) or tetramethyl orthosilicate have been mainly used as silica sol-gel-precursors. Others like $SiCl_4$ or water glasses are also known precursors; however they lead to unselective gelation conditions and thus are of minor interest.[286] It is important to know, that either acids or bases are applied as catalysts (Scheme 34).[286–288] Acid catalyzed gelation (pH < 7) affords weakly branched gels with a polymer-like network structure and small pores.[285,286,289] In contrast basic hydrolysis and condensation generates silica sols (pH > 7, no salts) or gels with enhanced cross-linking, low micro porosity, a broader pore distribution, and a silica network consistent of particles. Addition of salts or pH changes during the sol gel procedure can lead to strong changes in gelation and offers a certain control too.[286]
An explanation for the mechanism of the sol-gel process can be found in the acidic and basic hydrolysis and condensation mechanisms. In the acid-catalyzed hydrolysis (Scheme 35 a), protonation at the alkoxy group occurs rapidly. As a result of enhanced electrophilic properties water is able to attack at the backside of the silicon center, whereby a transition state with significant S_N2 character has been proposed.[288,290] The acquired positive charge of the water molecule initiates the release of the alcohol molecule. Hence, hydrolysis occurs faster for less bulky alkoxides. Condensation under acidic condition begins with the protonation of a silanol group, which makes the silicon more electrophilic and facilitates the nucleophilic attack by other silanols. It is important to know, that the most basic silanols are located in monomers or weakly branched oligomers. Thus, they are prone for protonation and have a high tendency to react with neutral species afterwards.[288]

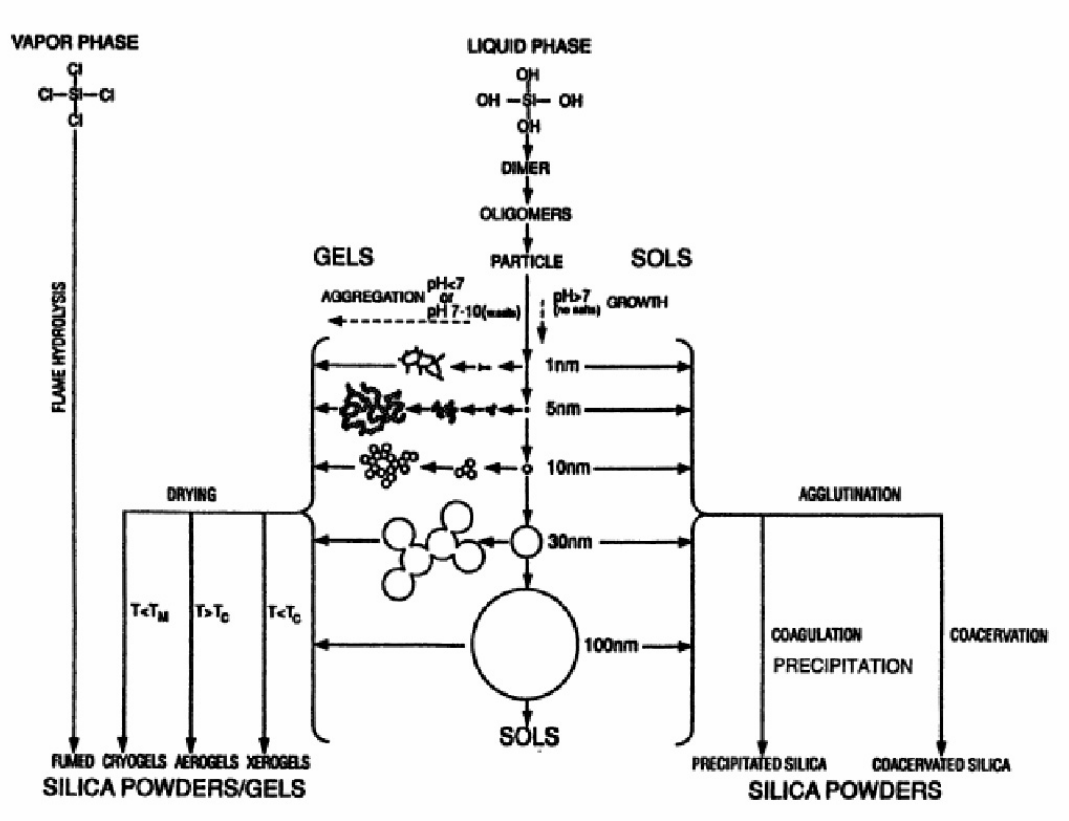

Scheme 34. Overview of the conditions of the sol gel process starting from $Si(OH)_4$.[286] Reproduced and adapted with permission from reference 287. Copyright 1994 American Chemical Society.

For hydrolysis under basic conditions, an OH^- ion attacks directly at the silicon center (Scheme 35 b).[288] At this point, a S_N2-Si mechanism may occur similar to the acidic mechanism with inversion of the tetrahedron, which is resulted from the backside attack of the silanol.[291] Another proposed mechanism is the S_N2*-Si or the S_N2**-Si pathway under consideration of a stable five bonded intermediate.[288,290] Decomposition of the intermediate affords alkoxide anions. As the mechanism runs *via* a negatively charged silicon center, external influences (e.g. salts) can change the reactivity significantly. Condensation reaction occurs *via* deprotonation of a silanol and nucleophilic attack of the deprotonated species at a neutral silicate.[288,291] In this reaction, the acidity of the required silanol group has major influence on the overall reactivity. The acidity depends on the other substituents around the Si core. Unlike alkoxy and OH groups, siloxy groups reduce the electron density of the center Si, which increases the acidity of the remaining silanols.[292] As a result of this mechanism, condensation is favored at larger and more branched species resulting in the formation of particles.

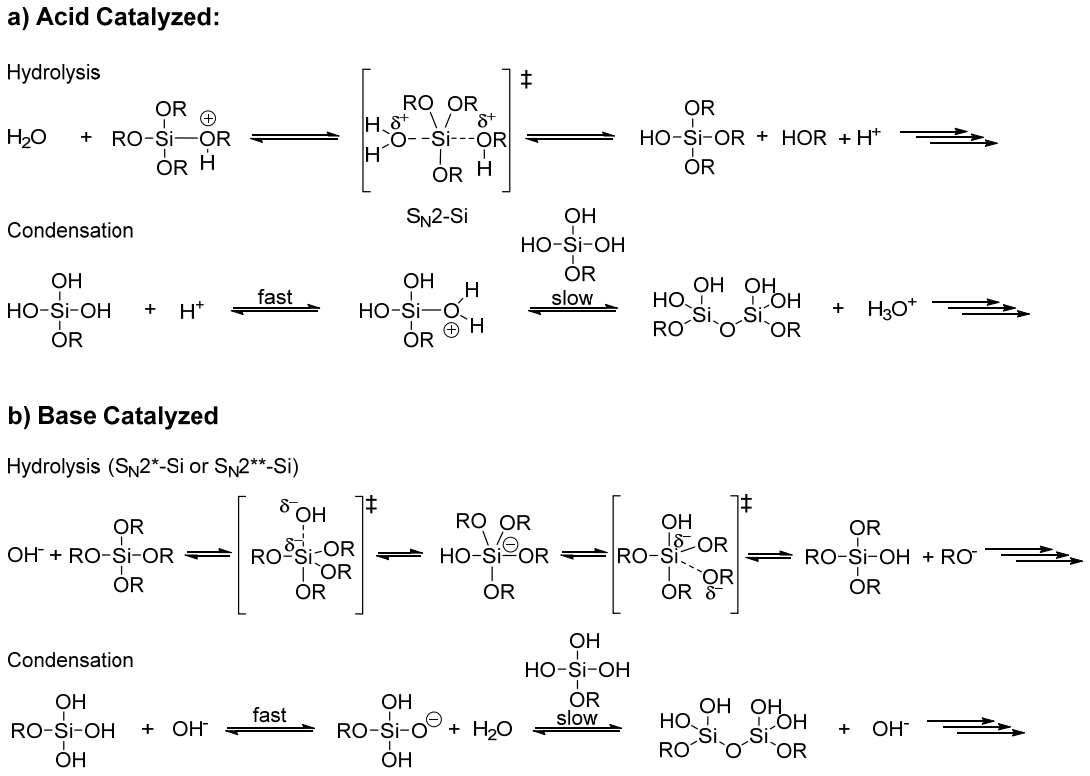

Scheme 35. Acid (a) and base catalyzed (b) hydrolysis and condensation mechanisms of tetraalkoxysilane precursors.[287,288,290]

Storage of the reaction mixtures at elevated temperatures for a period of time leads to the formation of hydro- or alcogels.[283] This procedure is also known as ageing or ripening. Drying of the alcogels under standard conditions in air affords the formation of a xerogel. Xerogels are densely packed gels with small pores and a tight network (Figure 27). The shrinkage and cracking of the gel is caused by high capillary forces that is evoked from a gradient by solvent evaporation.[293] The mechanism of this process is dependent on the structure of the alcogel.[283,285] The key to the formation of the highly porous and stable silica aerogels is the drying of the alcogel under supercritical conditions, *i.e.* heating and pressurizing of the liquid in the alcogel pores above its critical point to minimize capillary forces and eliminate liquid-vapor interfaces.[293] High temperature supercritical drying is known as the original procedure.[279] Thereby, the aerogel is placed in an autoclave with a respective fluid, which is slowly heated above its critical point. Subsequent slow pressure release affords a reduction of capillary forces and stabilizes the network structure.[285] Although, this method has many benefits (e.g. post-reaction and better stabilization of the silica network), several drawbacks like the required high pressure and temperature (e.g. methanol: T_c: 239.5 °C, p_c: 79.8 bar) and the flammability of the solvents are facing each other. The use of CO_2 as supercritical fluid, with a critical temperature of T_c = 31.1 °C and pressure p_c = 72.8 bar, offers the possibility of low temperature supercritical drying. To execute low temperature supercritical drying, the alcogel is placed in an autoclave with an excess of the solvent. Afterwards the autoclave is cooled and filled with liquid CO_2. During this process, the solvent is extracted from the autoclave. Solvent exchange shall be repeated after several hours. Afterwards, CO_2 is brought to supercritical conditions and the autoclave is slowly depressurized to obtain aerogels.[285,294] For supercritical drying, solvent exchange can have a big impact as it influences drying temperatures and pressures. The used solvents furthermore have divergent miscibility with liquid and

supercritical CO_2 (e.g. acetone is well miscible with CO_2 and thus it is often used for low temperature supercritical drying). Solvent exchange to unpolar solvents and surface silylation is often applied to obtain super hydrophobic silica aerogels.[281,285,286]

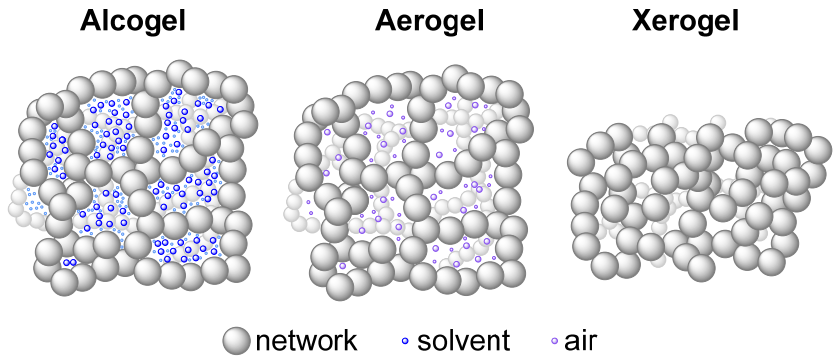

Figure 27. Comparison of the alcogel, aerogel and xerogel structures.

3. Motivation

SiNCs are suitable for a high number of applications (e.g. sensing, bioimaging, catalysis etc.) as they have promising optoelectronic properties and a low toxicity. Unmodified SiNCs often suffer from external influences such as surface defects, photobleaching and fast oxidation. Thus, their use in hybrid and composite materials is relatively limited, and the priority for the development of new strategies grew. The aim of this thesis is to investigate and analyze the surface functionalization strategies. Therefore, the preparation of novel stimuli-responsive hybrid and composite materials with unprecedented features is done. Three topics are highlighted in detail:

Preparation of Stimuli-Responsive Polymer Hybrid Silicon Nanoparticles by Surface-Initiated Group Transfer Polymerization: The interconnection of SiNCs with important materials, such as perfluorinated compounds, polysiloxanes[232] or polystyrene[228] results unprecedented hybrid materials with excellent stabilization of the SiNC surfaces and good processibilities. However, the thermal and microwave induced surface functionalization procedures used in these studies were unselective regarding to surface oligomerization.[192] Furthermore, the functions of the polymer materials were limited to their processability and SiNCs stabilizations. Poly(dialkyl vinylphosphonates) (DAVP) are well known water soluble materials with a lower critical solution temperature (LCST) close to the physiologic region.[272,276] The polymers are obtained in high molecular weights and narrow polydispersities by catalytic precision polymerization (group transfer polymerization; GTP) using rare earth metal catalysts.[263] The first strategy has demonstrated the suitability of this method on flat silicon surfaces *via* free acrylic groups. Therein the LCST effect of the surface by polarity changes was presented previously.[277] Thus, the goal of the thesis is to develop a SiNC-PDAVP hybrid materials with stable bright red PL, good dispersibility in water and a thermoresponsive behavior, which is going to be complied by precision polymerization (Scheme 36).

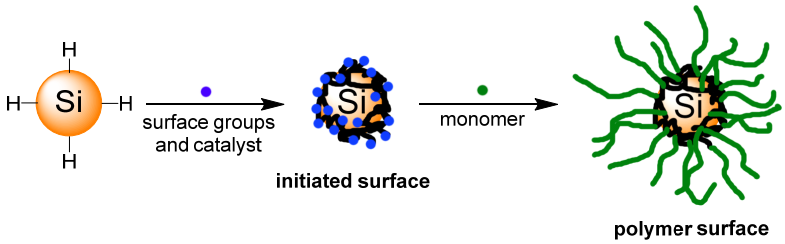

Scheme 36. Planned pathway for the preparation of SiNC-PDAVP hybrid materials.

In-Situ IR-Spectroscopy as Tool for Monitoring the Radical Hydrosilylation Process on Silicon Nanocrystal Surfaces: Surface hydrosilylation is the most important procedure to passivate and stabilize SiNCs.[16,18] Amongst a number of surface grafting procedures,[56,161,192,201,208,227] radical reactions stand out because they are comparably cheap, functional group tolerant and can be used to prepare monolayer surfaces.[209] Although a reaction mechanism has been proposed, no methodology has been developed to understand the detailed steps of surface

grafting so far. Therefore, time resolved *in-situ* infrared spectroscopy (IR) is exploited to study the consumption of surface Si-H groups during the grafting procedure (Scheme 37). The aim of this investigation is to draw conclusions regarding the variation of different factors like radical or monomer concentration and olefin sterics to postulate a sustainable grafting mechanism.

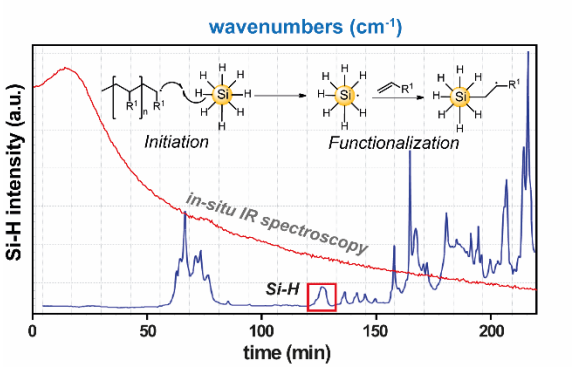

Scheme 37. Schematic illustration of the SiNC grafting mechanism combined with in-situ IR spectroscopy of the process.[295] *Reproduced and adapted with permission from reference 296. Copyright 2017 Royal Society of Chemistry.*

Superhydrophobic Silicon Nanocrystals - Silica Aerogel Hybrid Materials: Synthesis, Properties, and Sensing Application: Due to their unprecedented properties - low density, ultra-high porosity and defined inner surfaces silica aerogels and mesoporous silica materials have high potential in applications such as filtration, material adsorption or insulation.[282,283,286,291] They can easily be prepared by sol-gel chemistry and advanced drying procedures.[288] Guan *et al.* intercalated triethoxyvinylsilane grafted SiNCs into a customized mesoporous silica and gained a turbid material powder with ordered pores and PL at 600 nm.[197] Another example presented by Aghajamali *et al.* intercalated SiNCs with different surface polarities to gain a silica aerogel composite material.[234] Both examples demonstrated the great potential of composite materials. However, in the first example SiNCs were prepared by thermal protocols leading to surface oligomerization and no covalent linkages between the materials could be achieved in the second approach. The aim of the current study is to prepare a superhydrophobic and covalently linked silica aerogel-SiNC hybrid materials (Scheme 38), which combines the high porosity of the aerogel with the reversible PL quenching features of SiNCs towards nitroaromatics. Radical SiNC surface grafting of triethoxyvinylsilane is the reaction platform of choice to obtain good SiNC surface protection with reactive surface groups similar to the sol gel precursor.

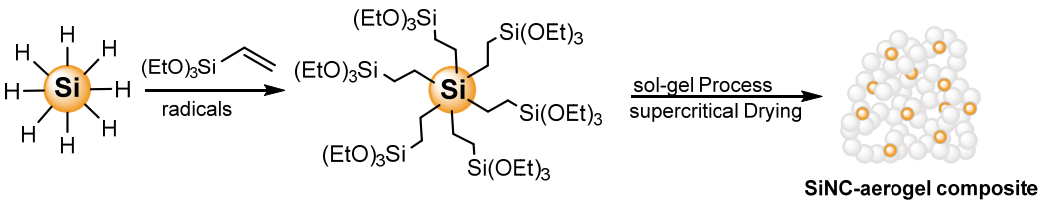

Scheme 38. Planned preparation strategy for SiNC-silica aerogel composite materials.

4. Silicon Nanocrystal Functionalization and Hybrid Materials

4.1. Preparation of Stimuli-Responsive Polymer Hybrid Silicon Nanoparticles by Surface-Initiated Group Transfer Polymerization

4.1.1. Thermoresponsive and Photoluminescent Hybrid Silicon Nanoparticles by Surface-Initiated Group Transfer Polymerization of Diethyl Vinylphosphonate

4.1.1.1. Summary

Group-transfer polymerization (GTP) is a very precise method to polymerize Michael-type molecules like methyl-methacrylate (MMA) or dialkyl vinylphosphonates (DAVP) with narrow PDIs and high molecular weights. Poly(dialkyl vinylphosphonates) (PDAVP) are polymers that exhibit a lower critical solution temperature (LCST) effect in water with sharp transitions from cloudy to clear. Combining these advantages, the development of a surface initiated group-transfer polymerization (SI-GTP) approach on silicon nanocrystals (SiNCs) using diethyl vinylphosphonate was applied to prepare water soluble and photoluminescent SiNC hybrid materials with LCST.

To establish functional surfaces, ethylene glycol dimethacrylate (EGDM) was reacted with the hydride terminated SiNCs using photografting at 365 nm. This resulted in a hybrid SiNC-poly(ethylene glycol dimethacrylate) (PEGDM) network structure with free methacrylic moieties. Addition of the GTP catalyst bis(cyclopentadienyl)trimethylsilylmethylyttrium tetrahydrofurane (Cp_2YCH_2TMS•thf) induced the impregnation of the surface by reaction with the free acrylic groups. Hence, intermediate enolate species were formed, which are well known as efficient initiators for GTP. Upon the addition of diethyl vinylphosphonate (DEVP), instantaneous polymerization to poly(diethyl vinylphosphonate) (PDEVP) was achieved. After purification, the particles had a hydrodynamic diameter of 441 ± 96 nm and contained of 15 % nanoparticles, 4 % EGDM and 81 % PDEVP. The SiNC-*g*-PEGDM-*g*-PDEVP hybrid material became water dispersible. Although a metal catalyst was applied, the bright red PL of the SINCs was sustained because of the good passivation of the nanoparticle surface. Furthermore, the hybrid materials exhibited the LCST effect of the polymer at temperatures above 34 °C, as determined by time resolved dynamic light scattering.

4.1.1.2. Bibliographic Data

Thermoresponsive and Photoluminescent Hybrid Silicon Nanoparticles by Surface-Initiated Group Transfer Polymerization of Diethyl Vinylphosphonate

Julian Kehrle, Ignaz M. D. Höhlein, Zhenyu Yang, Aljosha-Rakim Jochem, Tobias Helbich, Tobias Kraus, Jonathan G. C. Veinot, Bernhard Rieger

Angew. Chem. Int. Ed. **2014**, *53*, 12494.

Angew. Chem. **2014**, *126*, 12702.

M. Sc. J. Kehrle, M. Sc. I. M. D. Höhlein, M. Sc. T. Helbich, Prof. Dr. B. Rieger

WACKER-Lehrstuhl für Makromolekulare Chemie, Technische Universität München, Lichtenbergstraße 4, 85747 Garching bei München (Germany)

Dr. Z. Yang, Prof. Dr. J. G. C. Veinot

Department of Chemistry, University of Alberta, 11227 Saskatchewan Drive, Alberta T6G 2G2 (Canada)

M. Sc. A.-R. Jochem, Dr. T. Kraus

INM-Leibniz-Institut für neue Materialien, Campus D2 2, 66123 Saarbrücken (Germany)

Direct Link: DOI 10.1002/anie.201405946; 10.1002/ange.201405946

Supporting information:

http://onlinelibrary.wiley.com/store/10.1002/anie.201405946/asset/supinfo/anie_201405946_sm_miscellaneous_information.pdf?v=1&s=2e6a0ad136ebc29538342ca0f076e7f108e5c419

4.1.1.3. Reprint of the Original Manuscript

Angewandte Communications

Functional Nanoparticles

DOI: 10.1002/anie.201405946

Thermoresponsive and Photoluminescent Hybrid Silicon Nanoparticles by Surface-Initiated Group Transfer Polymerization of Diethyl Vinylphosphonate**

Julian Kehrle, Ignaz M. D. Höhlein, Zhenyu Yang, Aljosha-Rakim Jochem, Tobias Helbich, Tobias Kraus, Jonathan G. C. Veinot, and Bernhard Rieger**

Abstract: *We present a method to combine the functional features of poly(diethyl vinylphosphonate) (PDEVP) and photoluminescent silicon nanocrystals. The polymer–particle hybrids were synthesized in three steps through surface-initiated group transfer polymerization using Cp_2YCH_2TMS-(thf) as a catalyst. This pathway of particle modification renders the nanoparticle surface stable against oxidation. Although SiNC properties are known to be sensitive toward transition metals, the hybrid particles exhibit red photoluminescence in water. The temperature-dependent coiling of PDEVP results in a change of the hydrodynamic radius of the hybrid particles in water. To the best of our knowledge, this is the first example of controlled catalytic polymerization reactions on a silicon nanocrystal surface.*

In 1992, Yasuda et al. developed a new route of catalytic polymerization reactions, utilizing the rare earth metal catalyst [$Cp^*_2SmMe(THF)$] for the polymerization of methyl methacrylate to high molecular weight polymers.[1] The concept of this so-called rare earth metal-mediated group transfer polymerization (REM-GTP) was recently optimized and applied to a variety of monomers.[2] Especially dialkyl vinylphosphonates (DAVPs), which are structurally and electronically similar to acrylates, can easily be polymerized by REM catalysts yielding polymers with molecular weights in the region of 100 to 1000 kDa.[3–5] The obtained PDAVPs, for instance, poly(diethyl vinylphosphonate) (PDEVP), are water-soluble and exhibit thermoresponsivity close to the physiological range.[4] The temperature of this so-called "lower critical solution temperature (LCST) effect" is adjustable in the range of 5 °C to 92 °C by changing the comonomer composition of DEVP and di-*n*-propyl vinylphosphonate (DPVP), forming almost perfect alternating statistic copolymers.[6]

An additional important step was the development of covalently bound PDAVP brushes on flat surfaces for biomedical applications (cell growth and release surfaces). A REM catalyst, namely bis(cyclopentadienyl ytterbium methyl) [Cp_2YbMe] was immobilized on a modified silicon surface and the polymer growth occurred linearly within a few minutes. The polarity of the homogeneous surface layer can be tailored by temperature changes.[7]

The effects and strategies described before are useful for the modification of photoluminescent silicon nanocrystals (SiNCs). The application of such SiNCs requires non-agglomerating dispersions that are reasonably stable against oxidation. Such stability is readily achieved by a covalently bound organic layer that protects the particles against oxidation and renders them dispersible in various solvents.[8,9] In most cases, robust organic layers are formed through the hydrosilylation of unsaturated carbon compounds like dodecene or styrene with Si–H-terminated surfaces.[8,10,11] Instead of applying high temperatures, UV-light is often used as a mild hydrosilylation method.[11–13] Due to the size-dependent optical properties, the reactivity of SiNCs and bulk silicon surfaces often differ drastically and the mere adaption of existing protocols is likely to fail.[13] Routes to defined polymeric structures on SiNC surfaces are scarce in literature.[14,15] Hybrid particles bearing polymeric compounds on their surfaces offer the opportunity to combine the optoelectronic properties of the quantum dots with the polymer characteristics and are therefore of great interest.

Here we present a catalytic method to combine the material properties of PDEVP with the optoelectronic properties of SiNCs with a size of 3 nm. The PDEVP cover was grown using REM-GTP starting from methyl acrylic surface groups. Furthermore, we demonstrate the unique properties of both, SiNCs and PDEVP, united in one particular system.

[*] M. Sc. J. Kehrle, M. Sc. I. M. D. Höhlein, M. Sc. T. Helbich, Prof. Dr. B. Rieger
WACKER-Lehrstuhl für Makromolekulare Chemie
Technische Universität München
Lichtenbergstraße 4, 85747 Garching bei München (Germany)
E-mail: rieger@tum.de
Dr. Z. Yang, Prof. Dr. J. G. C. Veinot
Department of Chemistry, University of Alberta
11227 Saskatchewan Drive, Alberta T6G 2G2 (Canada)
E-mail: jveinot@ualberta.ca
M. Sc. A.-R. Jochem, Dr. T. Kraus
INM-Leibniz-Institut für neue Materialien
Campus D2 2, 66123 Saarbrücken (Germany)

[**] Z.Y. and J.G.C.V. acknowledge funding from the Natural Sciences and Engineering Research Council of Canada (NSERC), the Canada Foundation for Innovation (CFI), the Alberta Science and Research Investment Program (ASRIP), and the University of Alberta, Department of Chemistry. G. Popowich is thanked for assistance with TEM. The staff at the Alberta Centre for Surface Engineering and Sciences (ACSES) is thanked for XPS analysis. B. S. Soller, S. Weidle, Dr. C. Troll, Dr. Mita Dasog, and L. Daum are thanked for valuable discussions. I.M.D.H. is grateful for a generous scholarship from the Fonds der Chemischen Industrie.

Supporting information for this article is available on the WWW under http://dx.doi.org/10.1002/anie.201405946.

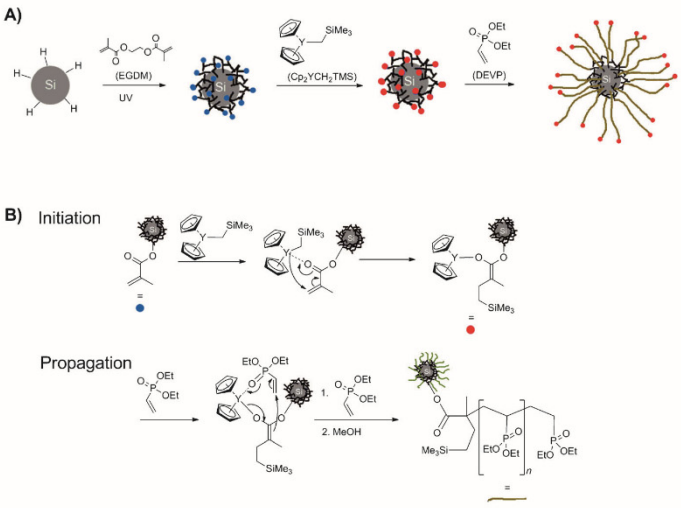

Scheme 1. A) Schematic description of the SI-GTP (grey: silicon nanocrystal, black: PEGDM network, blue: free methyl acrylate terminated binding sites, red: activated catalyst species, green: PDEVP chains). B) Insights into the mechanism of the SI-GTP achieved with methyl acrylic groups as initiating ligand and DEVP as the monomer.[16]

SiNCs with diameters of 3 nm were obtained in a silica matrix by the heating of hydrogen silsesquioxane (HSQ) for 1 h at 1100 °C under a slightly reducing atmosphere (5 % H_2/95 % Ar). SiNCs were liberated by HF etching, before the photografting of ethylene glycol dimethacrylate (EGDM).[16] UV irradiation (365 nm) of the SiNCs in an EGDM solution overnight leads to nanoparticles with free methyl acrylic surface groups (Scheme 1 A). Afterwards, the solution was diluted and centrifuged. Silicon nanocrystals-*graft*-poly(ethylene glycol dimethacrylate) (SiNCs-*g*-PEGDM) particles were sedimented by centrifugation, whereas the free homopolymer, which was formed in side reactions, was precipitated from the supernatant using pentane as an antisolvent. The particle fraction was redispersed in toluene and centrifuged to separate the residual monomer. The success of the EGDM grafting was seen in attenuated total reflectance infrared spectroscopy (ATR-IR) by a decrease of the Si–H stretch at 2109 cm^{-1} and the emergence of a C=O (1733 cm^{-1}) and C–O stretching band at 1170 cm^{-1} (Figure 1 A). Additionally, very weak C=C stretch vibrations were recorded at 1652 cm^{-1} (Figure 1 A).

The dried SiNCs-*g*-PEGDM particles were redispersed in dry toluene and impregnated with the GTP-catalyst Cp_2YCH_2TMS(thf) (15.9 µmol related to 100 mg silicon–silica composite material), which coordinated to the carbonyl functionality of the residual methyl acrylic groups. This effected a covalently bound catalyst–enolate species at the surface (Scheme 1 B).[17] An aliquot of the sample was isolated and centrifuged two times under inert gas atmosphere for purification. The initiation reaction of the catalyst on the surface was followed using ATR-IR spectroscopy. ATR-IR analysis showed a decrease of the carbonyl vibration at 1733 cm^{-1}, while other bands remained constant, which is in accordance with the formation of the catalyst–enolate species (Figure 1 B).

The impregnated particles were reacted without further purification. Due to the slow initiation rate in solution,[17] an excess of catalyst was used as water scavenger to protect the catalytic species at the surface during polymerization. GTP on the particle surfaces starts immediately after the addition of DEVP. The chain propagation proceeds comparably fast to the initiation reaction, according to an eight-electron process (Scheme 1 B).[3–5,17] The polymerization was terminated after one hour by the addition of methanol and yielded linearly grown PDEVP layers, which are covalently bound to the SiNCs (SiNCs-*g*-PEGDM-*g*-PDEVP; Scheme 1 A). The purification was achieved by redispersion and subsequent centrifugation processes in toluene and methanol (see above). The PDEVP-functionalized SiNCs exhibited vinylphosphonate bands (P=O stretch at 1220 cm^{-1} and the P–O stretch at 1015 cm^{-1}) of strong intensity compared to the bands of the methyl acrylic group (C=O at 1733 cm^{-1} and C–O at 1170 cm^{-1}), which indicates the formation of a PDEVP cover (Figure 1 A). Furthermore, the appearance of the CH_2 bending vibration at 1451 cm^{-1}, which could be assigned to the polymer backbone, demonstrates the existence of poly(diethyl vinylphosphonate).

The photografting of EGDM, catalyst impregnation, and the polymerization were proven by X-ray photoelectron spectroscopy (XPS; Figure S1–3) and electron-dispersive X-ray spectroscopy (EDX; Figure S4–6). We used X-ray diffraction measurements (XRD) to confirm the presence of the SiNCs in the hybrid systems (Figure S7). Asymmetric flow-field flow fractionation (AF4) measurements confirmed the purity of SiNCs-*g*-PEGDM-*g*-PDEVP. We could show that after three centrifugation steps, the polymer was quantitatively washed out and only polymer-modified particles were collected in the pellet (Figure S12). Homopolymer, which was found in the supernatant of the first centrifugation was mixed with some of the particles to confirm the separation by AF4 (Figure S13).

To evaluate the weight proportions of PEGDM, PDEVP, and SiNCs, TGA measurements were performed (Figure S9). In the SiNCs-*g*-PEGDM system, the amount of SiNCs is dominating compared to PEGDM (Table 1). After surface-initiated group transfer polymerization (SI-GTP), a distinct quantity of PDEVP was found, whereas the SiNCs as well as PEGDM are the minor species.

The bifunctional acrylic monomer EGDM generated aggregates of both, EGDM and covalently linked silicon nanocrystals. There were no single nanocrystals detected in

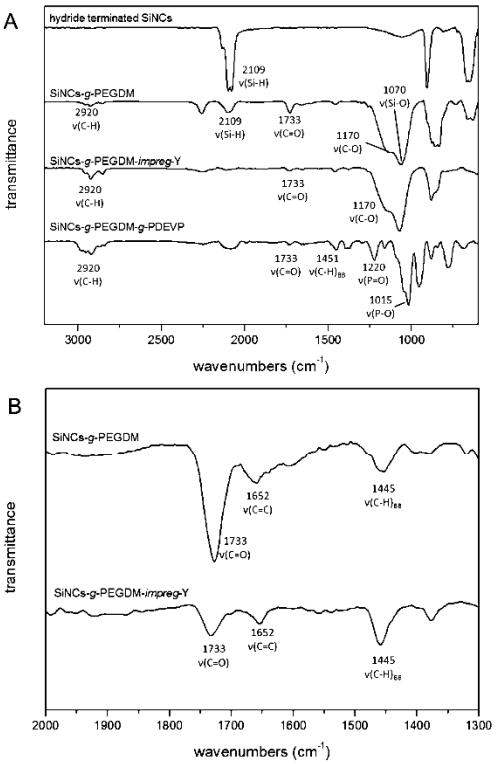

Figure 1. A) ATR-IR of hydride-terminated silicon nanocrystals, SiNCs-*g*-PEGDM, $Cp_2YCH_2TMS(thf)$-impregnated SiNCs-*g*-PEGDM (SiNCs-*g*-PEGDM-*impreg*-Y), and SiNCs-*g*-PEGDM-*g*-DEVP. B) Magnification of SiNCs-*g*-PEGDM and SiNCs-*g*-PEGDM-*impreg*-Y.

Table 1: Amounts of PEGDM, PDEVP, SiNCs, and the hydrodynamic radii (R_h) of the products.

	EGDM [wt%][a]	PDEVP [wt%][a]	SiNCs [wt%][a]	R_h [nm][b]
SiNCs-*g*-PEGDM	20	–	80	177 ± 81
SiNCs-*g*-PEGDM-*g*-PDEVP	4	81	15	441 ± 96

[a] Calculated from TGA measurements. [b] Obtained by DLS measurements using a regularization fit: SiNCs-*g*-PEGDM in ethylacetate; SiNCs-*g*-PEGDM-*g*-PDEVP in water.

transition electron microscopy (TEM) and dynamic light scattering (DLS) and the aggregates could not be redispersed by intense ultrasonication. We have shown earlier that dodecene, which is not known as a good monomer, tends to oligomerize during SiNC modification, and thus we conclude, hat EGDM tends to build up network structures.[18] We argue from the hydrodynamic radius (R_h) of 177 nm found by DLS (Table 1, Figure S10), which is much larger than the obtained radius from TEM images (Figure S8), that SiNCs-*g*-PEGDM underwent swelling while dispersed in ethyl acetate. Organic acrylates are known to be soluble in polar organic solvents like ethyl acetate, but not in water.[19] We believe that the EGDM layer collapses after SI-GTP, when a bulky PDEVP layer (Figure S11) coats the outer sphere of the SiNC-*g*-PEGDM aggregates. Particles coated with PDEVP were well dispersible in water at room temperature, whereas SiNCs-*g*-PEGDM could not be dispersed in water.

Some polymers show an LCST behavior that is caused by thermoresponsive coiling.[20] PDAVPs and their copolymers coil in a particularly narrow temperature interval and then precipitate from solution.[4,6] The temperature-dependent determination of the hydrodynamic radii of our particle–polymer combination by DLS indicated a thermoresponsive behavior of SiNCs-*g*-PEGDM-*g*-PDEVP. The hydrodynamic radius (R_h) decreased in a temperature range of 30 to 55 °C, probably due to coiling of surface polymers (Figure 2B). The smallest hydrodynamic radius, observed at temperatures above 55 °C, was 140 nm, smaller than the average radius of the swollen SiNCs-*g*-PEGDM determined in ethyl acetate. We believe that the PEGDM layer collapses in water and the PDEVP layer coils at above 55 °C. When the system was cooled to room temperature, R_h grew above the value found for freshly prepared particles. We assume that the increase in R_h after one temperature cycle is due to an elongation of the PDEVP chains on the surface to the maximum. The particles become too unpolar and slowly precipitate from water.

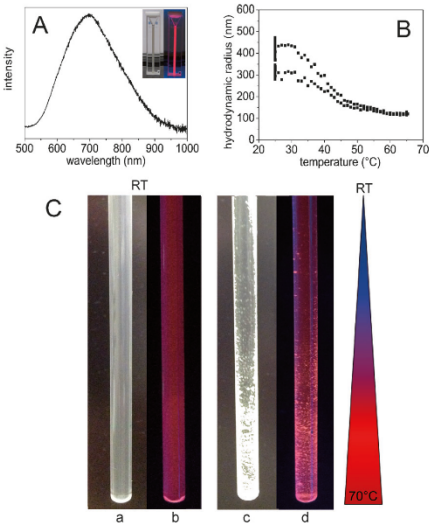

Figure 2. A) Red photoluminescence of SiNCs-*g*-PEGDM-*g*-PDEVP in water upon irradiation at 365 nm. B) LCST measurement (temperature gradient 1 °C min^{-1}, equilibration 1 min) of SiNCs-*g*-PEGDM-*g*-PDEVP in water. C) Turbid dispersion of SiNC-*g*-PEGDM-*g*-PDEVP in water at ambient conditions (a) and under UV-light (b). After heating the bottom part of the tube to 70 °C for several hours aggregates can be seen (c) and photoluminescence is focused to the aggregated part (d).

Grafting PDEVP from SiNC surfaces leads to water-dispersible particle systems with thermoresponsive behavior and red-light photoluminescence (PL, Figure 2A,B). To achieve a visible correlation of these effects, we heated the bottom part of a glass NMR tube containing a dispersion of SiNCs-*g*-PEGDM-*g*-PDEVP to 70 °C, while the upper part was kept at room temperature. After a few hours, we obtained a precipitate at the glass wall, which showed more focused PL then the residual dispersion (Figure 2C(c),(d)). This behavior and the absence of photobleaching might allow applications as conducting membranes or flocculating agents.[5] To adapt the nanohybrid sensors to their field of application, the temperature range and haziness of the demonstrated thermoresponsive behavior can be tuned by the copolymerization of different water-soluble PDAVPs, as shown previously.[6] Efforts towards the application of this method on freestanding 3 nm silicon nanocrystals might open chances in the biomedical field, for example, in bioimaging.[15]

In summary, we have shown an unprecedented method to decorate surfaces of photoluminescent SiNCs with a size of 3 nm with hydrophilic polymers. This was achieved in a three-step synthesis route. First PEGDM was photografted on the hydride-terminated silicon nanocrystal surface under near UV conditions, whereby the methyl acrylic groups remain intact. Further steps allow the attachment of bis(cyclopentadienyl)trimethylsilylmethylyttrium(thf), forming an enolate intermediate, which is known to be an efficient catalyst for group transfer polymerization reactions. Thus, we polymerized DEVP on the silicon nanoparticle surfaces using a catalytic pathway. Thermogravimetric analysis (TGA), DLS, and TEM measurements evidence the thick PDEVP covers on the SiNC surfaces. Although the SiNCs were in contact with a transition metal center, the obtained products exhibit photoluminescence in water. In combination with the LCST effect of the stimuli-responsive polymer, which was demonstrated by temperature-dependent DLS measurements, these particles are an interesting example for the combination of the properties of SiNCs and functional polymers. Further development with regard to the application of this catalytic method to the surface of freestanding silicon nanocrystals with a size of 3 nm are currently under way.

Experimental Section

All details about the synthesis of silicon nanocrystals, SiNCs-*g*-PEGDM, and SiNCs-*g*-PEGDM-*g*-PDEVP as well as analysis details are given in the Supporting Information.

Received: June 5, 2014
Revised: July 22, 2014
Published online: September 8, 2014

Keywords: group transfer polymerization · LCST · nanoparticles · silicon nanocrystals

[1] H. Yasuda, H. Yamamoto, K. Yokota, S. Miyake, A. Nakamura, *J. Am. Chem. Soc.* **1992**, *114*, 4908–4910.
[2] a) H. Yasuda, H. Tamai, *Prog. Polym. Sci.* **1993**, *18*, 1097–1139; b) E. Y.-X. Chen, *Chem. Rev.* **2009**, *109*, 5157–5214; c) N. Zhang, S. Salzinger, B. S. Soller, B. Rieger, *J. Am. Chem. Soc.* **2013**, *135*, 8810–8813.
[3] U. B. Seemann, J. E. Dengler, B. Rieger, *Angew. Chem. Int. Ed.* **2010**, *49*, 3489–3491; *Angew. Chem.* **2010**, *122*, 3567–3569.
[4] S. Salzinger, U. B. Seemann, A. Plikhta, B. Rieger, *Macromolecules* **2011**, *44*, 5920–5927.
[5] S. Salzinger, B. Rieger, *Macromol. Rapid Commun.* **2012**, *33*, 1327–1345.
[6] N. Zhang, S. Salzinger, B. Rieger, *Macromolecules* **2012**, *45*, 9751–9758.
[7] a) N. Zhang, S. Salzinger, F. Deubel, R. Jordan, B. Rieger, *J. Am. Chem. Soc.* **2012**, *134*, 7333–7336; b) N. Zhang, S. Salzinger, F. Deubel, B. Rieger, WO 2013/072309, **2012**;.
[8] J. G. C. Veinot, *Chem. Commun.* **2006**, 4160.
[9] M. Dasog, Z. Yang, S. Regli, T. M. Atkins, A. Faramus, M. P. Singh, E. Muthuswamy, S. M. Kauzlarich, R. D. Tilley, J. G. C. Veinot, *ACS Nano* **2013**, *7*, 2676–2685.
[10] a) Y. Yu, C. M. Hessel, T. D. Bogart, M. G. Panthani, M. R. Rasch, B. A. Korgel, *Langmuir* **2013**, *29*, 1533–1540; b) Z. Yang, M. Dasog, A. R. Dobbie, R. Lockwood, Y. Zhi, A. Meldrum, J. G. C. Veinot, *Adv. Funct. Mater.* **2014**, *24*, 1345; c) X. Cheng, S. B. Lowe, P. J. Reece, J. J. Gooding, *Chem. Soc. Rev.* **2014**, *43*, 2680.
[11] J. A. Kelly, J. G. C. Veinot, *ACS Nano* **2010**, *4*, 4645–4656.
[12] a) J. M. Buriak, *Chem. Rev.* **2002**, *102*, 1271–1308; b) R. L. Cicero, C. E. D. Chidsey, G. P. Lopinski, D. D. M. Wayner, R. A. Wolkow, *Langmuir* **2002**, *18*, 305–307; c) P. Stewart, J. M. Buriak, *Angew. Chem. Int. Ed.* **1998**, *37*, 3257–3260; *Angew. Chem.* **1998**, *110*, 3447–3450.
[13] J. A. Kelly, A. M. Shukaliak, M. D. Fleischauer, J. G. C. Veinot, *J. Am. Chem. Soc.* **2011**, *133*, 9564–9571.
[14] a) R. J. Clark, M. K. M. Dang, J. G. C. Veinot, *Langmuir* **2010**, *26*, 15657–15664; b) C. M. Hessel, M. R. Rasch, J. L. Hueso, B. W. Goodfellow, V. A. Akhavan, P. Puvanakrishnan, J. W. Tunnel, B. A. Korgel, *Small* **2010**, *6*, 2026–2034; c) F. Erogbogbo, K.-T. Yong, I. Roy, G. Xu, P. N. Prasad, M. T. Swihart, *ACS Nano* **2008**, *2*, 873–878; d) Y. He, Z.-H. Kang, Q.-S. Li, C. H. A. Tsang, C.-H. Fan, S.-T. Lee, *Angew. Chem. Int. Ed.* **2009**, *48*, 128–132; *Angew. Chem.* **2009**, *121*, 134–138.
[15] Z. F. Li, E. Ruckenstein, *Nano Lett.* **2004**, *4*, 1463–1467.
[16] C. M. Hessel, E. J. Henderson, J. G. C. Veinot, *Chem. Mater.* **2006**, *18*, 6139–6146.
[17] S. Salzinger, B. S. Soller, A. Plikhta, U. B. Seemann, E. Herdtweck, B. Rieger, *J. Am. Chem. Soc.* **2013**, *135*, 13030–13040.
[18] Z. Yang, M. Iqbal, A. R. Dobbie, J. G. C. Veinot, *J. Am. Chem. Soc.* **2013**, *135*, 17595–17601.
[19] M. D. Bhabhe, P. S. Galvankar, V. M. Desai, V. D. Athawale, *J. Appl. Polym. Sci.* **1995**, *56*, 485–494.
[20] C. de las Heras Alarcón, S. Pennadam, C. Alexander, *Chem. Soc. Rev.* **2005**, *34*, 276.

4.1.1.4. Reprint Permission

JOHN WILEY AND SONS LICENSE TERMS AND CONDITIONS

Jun 18, 2017

This Agreement between Julian Kehrle ("You") and John Wiley and Sons ("John Wiley and Sons") consists of your license details and the terms and conditions provided by John Wiley and Sons and Copyright Clearance Center.

License Number	4132001224380
License date	Jun 18, 2017
Licensed Content Publisher	John Wiley and Sons
Licensed Content Publication	Angewandte Chemie International Edition
Licensed Content Title	Thermoresponsive and Photoluminescent Hybrid Silicon Nanoparticles by Surface-Initiated Group Transfer Polymerization of Diethyl Vinylphosphonate
Licensed Content Author	Julian Kehrle,Ignaz M. D. Höhlein,Zhenyu Yang,Aljosha-Rakim Jochem,Tobias Helbich,Tobias Kraus,Jonathan G. C. Veinot,Bernhard Rieger
Licensed Content Date	Sep 8, 2014
Licensed Content Pages	4
Type of use	Dissertation/Thesis
Requestor type	Author of this Wiley article
Format	Print and electronic
Portion	Full article
Will you be translating?	No
Title of your thesis / dissertation	Surface Hydrosilylation: The Key to Silicon Nanocrystal Hybrid and Composite Materials
Expected completion date	Aug 2017
Expected size (number of pages)	190
Requestor Location	Julian Kehrle Lichtenbergstraße 4 Garching, 85748 Germany Attn: Julian Kehrle
Publisher Tax ID	EU826007151
Billing Type	Invoice
Billing Address	Julian Kehrle Lichtenbergstraße 4 Garching, Germany 85748 Attn: Julian Kehrle
Total	0.00 EUR
Terms and Conditions	

4.1.2. Surface-Initiated Group-Transfer Polymerization – A Catalytic Approach to Stimuli-Responsive Silicon Nanocrystal Hybrid Materials

4.1.2.1. Summary

SiNCs can be paired with PDEVP using the GTP approach, which emerges hybrid materials with both, bright red PL of the nanoparticles and the LCST effect of the polymer.[296] Copolymerization of DEVP with other DAVPs has an impact on the LCST cloud point of the resulting polymer.[276] Thus, the scope of this study was to find the appropriate conditions, in which SI-GTP could be executed and which Michael type monomers could be applied.

To generate an appropriate reaction platform, EGDM grafting was performed using hydrosilylation in near UV light resulting in a PEGDM-*g*-SiNC network with free acrylic groups, which were readily impregnated with Cp_2YCH_2TMS•thf. The catalyst amount, the DEVP-monomer concentration and the monomer types were then varied. The surface polymer concentration was strongly dependent on the catalyst concentration, whereby a minimum amount of catalyst was required to obtain a significant surface polymer. Hence, the application of 5.3 µmol, 10.6 µmol and 21.2 µmol Cp_2YCH_2TMS•thf resulted in 9 %, 57 % and 81 % PDEVP on 72 %, 34 % and 15 % SiNCs containing 19 %, 9 % and 4 % PEGDM, respectively. However, no significant changes in surface polymer concentrations were monitored, when the catalyst concentration was kept constant, but the monomer concentration was varied. Thus, the surface coverage with PDEVP is mainly dependent on the catalyst concentration, but not on the quantity of monomer. Based on these results, methyl methacrylate (MMA), dimethyl vinylphosphonate and diisopropyl vinylphosphonate could be successfully grafted on SiNC surfaces, which was confirmed by ATR-IR and XPS spectra.

4.1.2.2. Bibliographic Data

Surface-Initiated Group-Transfer Polymerization – A Catalytic Approach to Stimuli-Responsive Silicon Nanocrystal Hybrid Materials

Julian Kehrle,[1] Tobias Helbich,[1] Muhammad Iqbal,[2] Lida Hadidi,[2] Jonathan G.C. Veinot[2] and Bernhard Rieger[1]

MRS Proc. ***2015****, 1770,* 13.

[1]WACKER-Chair of Macromolecular Chemistry, Technical University Munich, Lichtenbergstraße 4, 85747 Garching, Germany

Department of Chemistry, University of Alberta, 11227 Saskatchewan Drive, Edmonton, Alberta T6G 2G2, Canada

Direct Link: DOI 10.1557//opl.2015.550

4.1.2.3. Reprint of the Original Manuscript

Mater. Res. Soc. Symp. Proc. Vol. 1770 © 2015 Materials Research Society
DOI: 10.1557/opl.2015.550

Surface-Initiated Group-Transfer Polymerization – A Catalytic Approach to Stimuli-Responsive Silicon Nanocrystal Hybrid Materials

Julian Kehrle[1], Tobias Helbich[1], Muhammad Iqbal ,[2] Lida Hadidi,[2] Jonathan G.C. Veinot[2] and Bernhard Rieger[1]

[1]WACKER-Chair of Macromolecular Chemistry, Technical University Munich, Lichtenbergstraße 4, 85757 Garching, Germany
[2]Department of Chemistry, University of Alberta, 11227 Saskatchewan Drive, Edmonton, Alberta, T6G 2G2, Canada

ABSTRACT

Silicon nanocrystals are photoluminescent materials with a tremendous scope in various niche applications especially the generation of hybrid materials. Our approach for the preparation of stimuli responsive SiNC hybrid materials is based on the application of surface-initiated group-transfer polymerization. As a first step we used photografting of ethyleneglycol di(methacrylate). Then we impregnated remaining methyl acrylic surface groups with the catalyst $Cp_2YCH_2TMS(thf)$. We performed polymerization studies regarding catalyst and diethyl vinylphosphonate (DEVP) concentrations, highlighting that surface grafting is dependent upon catalyst concentration and independent from added monomer amount. Furthermore, we successfully polymerized methyl methacrylate, dimethyl vinylphosphonate and di*iso*propyl vinylphosphonate from the SiNC surface.

INTRODUCTION

Photoluminescent silicon nanocrystals (SiNCs) are non-toxic and electrochemically stable alternatives to well-established group II-VI and III-V elements based semiconductor quantum dots.[1,2] They exhibit photoluminescence (PL) in the visible range (420–790 nm) below 5 nm often attributed to the quantum confinement effects.[3,4]
To preserve PL, render SiNCs dispersible in a variety of solvents, and protect their surfaces against oxidation, functionalization and thus, mainly the formation of Si-C groups is an important area of research in the SiNCs research community.[2,5–8] There is scarcity of literature on comprehensive investigations on SiNCs hybrid materials which are typical composed of polymers and SiNCs.[9]

Rare earth metal-mediated group-transfer polymerization (REM-GTP) offers a catalytic pathway to obtain polymers. Using a catalyst bearing a rear-earth metal in the center and organic ligands, a variety of polymers like poly (dialkyl vinylphosphonates) (PDAVPs), methyl methacrylate (MMA) or 2-vinylpyridine (2-VP) can be obtained with narrow polydispersities (PDIs) and high molecular weights.[10–14] PDAVPs like poly (diethyl vinylphosphonate) (PDEVP) are of high interest due to their water solubility and thermoresponsive behavior near physiological regime.[10,11] Upon copolymerization with different homologues (e.g. dimethyl vinylphosphonate or di*iso*propyl vinylphosphonate) the thermoresponsive coiling temperature of the polymers can be tuned based upon the required properties.[15]

We performed surface-initiated group transfer polymerization (SI-GTP) from SiNC surfaces to obtain stimuli responsive hybrid materials based on the SiNCs photoluminescence and the thermoresponsive behavior of PDEVP.[16] Using this method, we could demonstrate a catalytic process to obtain hybrid materials which could be useful for drug delivery, proton conducting membranes or flocculating agents after further developments. Thus, we performed studies to understand catalyst and monomer concentrations influence of PDEVP polymerization from SiNC surfaces and the findings are presented below for various polymer-hybrids obtained through SI-GTP on SiNCs.[16]

EXPERIMENTAL DETAILS

All chemicals were purchased from Sigma Aldrich and used without further purification if not stated otherwise. Ethylene glycol dimethacrylate (EGDM) was dried over calcium hydride and subsequently distilled. All reactions were performed under an inert gas atmosphere. General methods and synthetic procedures were adapted from elsewhere.[16] All catalyst and monomer concentrations are based on 100 mg Si/SiO_2 composite material before HF etching.

Group Transfer Polymerization on SiNCs-*g*-PEGDM surfaces

2 mL of a previously prepared SiNCs-*g*-PEGDM dispersion in ethyl acetate (100 mg Si/SiO_2) was dried in vacuum and afterwards dispersed in dried and degassed toluene. Afterwards various amounts of catalyst were added to 5 mL of toluene. The SiNCs-*g*-PEGDM dispersion is then added to the catalyst solution and was allowed to stir for 1 h. Then the monomer is added and polymerization was allowed to proceed for 1 h at room temperature. The reaction is quenched using 0.1 mL of methanol. The viscous dispersion so obtained is centrifuged for 20 min at 9000 rpm. Purification was achieved by three times repeating the centrifugation steps using different solvents (depending upon the monomer used). Catalyst- and monomer concentration as well as the solvent for purification can be found in Table I.

Table I: Reaction details referred to 100 mg Si/SiO_2 composite material. SiNCs-*g*-PEGDM are named as entry 1.

Entry	Monomer	Monomer amount		Catalyst amount		purification solvent
2	DEVP	0.2 mL	1.1 mmol	2.0 mg	5.3 µmol	methanol
3	DEVP	0.4 mL	2.3 mmol	4.0 mg	10.6 µmol	methanol
4	DEVP	0.8 mL	4.6 mmol	8.0 mg	21.2 µmol	methanol
5	DEVP	0.2 mL	1.1 mmol	8.0 mg	21.2 µmol	methanol
6	DEVP	0.4 mL	2.3 mmol	8.0 mg	21.2 µmol	methanol
7	DEVP	0.8 mL	4.6 mmol	8.0 mg	21.2 µmol	methanol
8	MMA	0.8 mL	8.0 mmol	8.0 mg	21.2 µmol	methylene chloride
9	DMVP	0.8 mL	5.0 mmol	8.0 mg	21.2 µmol	methanol
10	DIVP	0.8 mL	4.2 mmol	8.0 mg	21.2 µmol	methylene chloride

DISCUSSION

Photoreaction of SiNCs with EGDM leads to SiNCs embedded in a poly ethylene glycol (dimethacrylate) (SiNCs-*g*-PEGDM) network with free methacrylic groups (Scheme 1).[16] These moieties are impregnated with the catalyst bis(cyclopentadienyl)trimethylsilylmethyl-yttrium(*thf*) [Cp_2YCH_2TMS*thf*]. After the polymerization process, SiNCs-*g*-PEGDM-*g*-PDEVP are obtained with a hydrodynamic radius of 441 ± 96 nm (Scheme 1).[16]

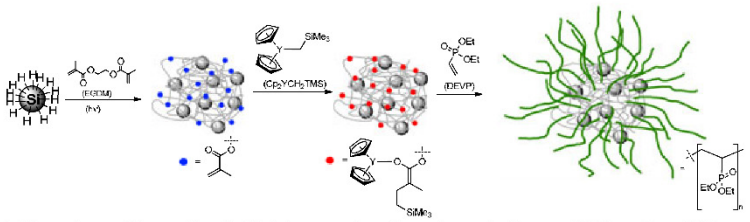

Scheme 1: Procedure of the surface-initiated group-transfer polymerization on SiNC surfaces.[16]

The Effect of Catalyst and Monomer loading

Earlier, we demonstrated the process of DEVP polymerization using high concentrations of catalyst and monomer (Table I, entry 1). We now turn our attention to the variation of the catalyst and monomer loading to optimize the concentrations for obtaining maximal yields. Therefore, we performed two series of experiments; first we varied both, catalyst and monomer amounts at a constant rate (Table I, entries 2-4). Secondly, we performed reactions at constant catalyst loading while varying the amount of monomer added (Table I, entries 5-7).

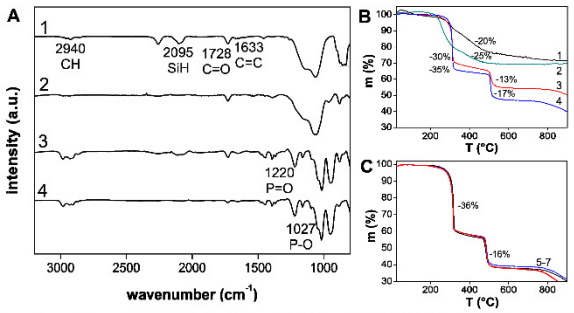

Figure 1: ATR-IR spectra (A) and TGA data (B) of SiNCs-*g*-PEGDM (1), SiNCs-*g*-PEGDM-*g*-PDEVP with 5.3 µmol catalyst and 1.1 mmol DEVP (2), 10.6 µmol catalyst and 2.3 mmol catalyst (3) and 21.2 µmol catalyst with 4.6 mmol DEVP (4); TGA data of SiNCs-*g*-PEGDM-*g*-DEVP with 21.2 µmol catalyst and various concentrations of monomer (5-7; C).

After the photoreaction of SiNCs, thermogravimetric analysis (TGA, Figure 2, B-1, Table II, entry 1) revealed a surface coverage of 21 wt.% assigned to the PEGMD cover, while a SiNCs residue of 79 wt.% remained, which agrees with previous results. EGDM grafting was

furthermore verified by attenuated total reflectance infrared spectroscopy (ATR-IR) measurements (Figure 2 A-1).[16] Thus, characteristic C=O stretches (1728 cm^{-1}) and residual C=C stretches (1633 cm^{-1}) were observed and the SiH stretch (2095 cm^{-1}) has significantly decreased compared to freshly etched SiNCs (Figure 1, A-1).[16]
SI-GTP of DEVP using a low amount of $Cp_2YCH_2TMS(thf)$ leads to a minimal coverage of PDEVP onto the SiNCs-*g*-PEGDM. This was further verified from the TGA measurement, whereof only 9 wt.% was determined for a partial PDEVP surface coverage which is significantly lower than full coverage. (Table II, entry 2). It is also worth mentioning that a small amount of catalyst is required to scavenge the trace water present in the reaction. Thus, at low catalyst amounts, polymerization does not occur due to catalyst decomposition. Upon increasing the amount of catalyst and monomer (at a constant ratio), the polymer surface coverage increased, as evidenced by the TGA measurements. (Figure 2 B-3, 4; Table II). Furthermore dynamic light scattering (DLS) also confirmed an increase in the hydrodynamic radii upon increasing the polymer coverage. (Table II). In ATR-IR P=O (1220 cm^{-1}) and P-O (1027 cm^{-1}) bonds are assigned to the the SiNCs surfaces, describing a good functionalization with DEVP (Figure 1 A-3,4). Based on these results we assume quantitative conversion of catalyst in respect to the surface groups and as consequence, the surface is densely grafted with PDEVP.[16]

Table II: Calculated amounts of EGDM, PDEVP and particles and hydrodynamic radii (R^h) obtained by DLS-measurements of modified nanoparticles. Entry 1-4 are according to Table I.

	EGDM (wt.%)	PDEVP(wt.%)	Particles (wt.%)	R^h [nm]
1	21	0	79	177 ± 81
2	19	9	72	
3	9	57	34	428 ± 91
4	4	81	15	441 ± 96

Upon varying of the monomer concentration at a constant catalyst concentration (Table I, entry 5-7) we found, that the polymer coverage is consistent with the concentrations used in entry 4 (Table I) as the TGA depicts similar weight losses as observed previously. (Figure 2, C).[10] Hydrodynamic radii for all these samples are around 275 nm. The polymerization seems to be dependent upon that catalyst concentrations as the polymer surface coverage increases with an increase in amount of $Cp_2YCH_2TMS(thf)$. Although the SI-GTP is known as fast living polymerization,[13] we assume that chain growth is interrupted during the reaction. We are currently investigating the termination behavior of the catalyst from SiNCs-*g*-PEGDM surfaces.

The Monomers Investigated

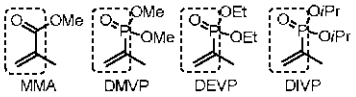

Figure 2: Monomers used for SI-GTP.

Once the reaction conditions were optimized, different monomers were used for SI-GTP to probe the properties of the various hybrid materials obtained (Figure 2). Especially, the

polymerization of vinylphosphonate homologues is of high interest as it can provide a handle to tune the thermoresponsive behavior on the obtained hybrid.[15] For these polymerization reactions, SiNCs-*g*-PEGDM were prepared and catalyst impregnation was performed as described elsewhere (Scheme 1).[16]

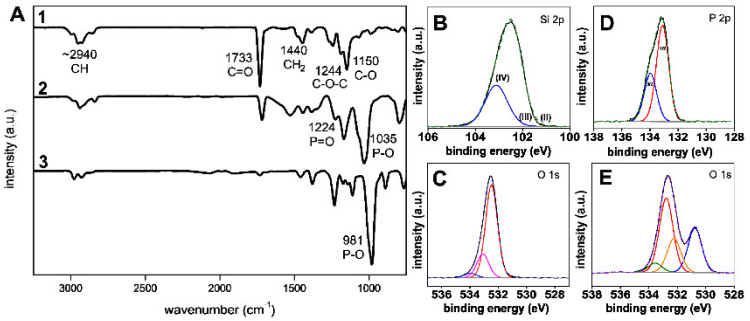

Figure 3: A) IR spectra of SiNCs-*g*-PEGDM-*g*-PMMA (1), SiNCs-*g*-PEGDM-*g*-PDMVP (2) and SiNCs-*g*-PEGDM-*g*-PDIVP (3); XPS spectra: B) Si 2p, SiNCs-*g*-PEGDM-*g*-PMMA; C) O 1s, SiNCs-*g*-PEGDM-*g*-PMMA; D) P 2p, SiNCs-*g*-PEGDM-*g*-DMVP; E) O 1s, SiNCs-*g*-PEGDM-*g*-DMVP.

In ATR-IR we assigned specific bands of the monomer besides the general available C-H stretching at around 2940 cm^{-1} and CH_2 bending at 1440 cm^{-1} (Figure 3 A 1-3). Thus, C=O (1733 cm^{-1}) and C-O stretching (1244 cm^{-1}, 1150 cm^{-1}) modes were observed for PMMA, while vinylphosphonates exhibit P=O (1224 cm^{-1}) and P-O stretches (1035 cm^{-1} for PDMVP; 1027 cm^{-1} for PDEVP and 981 cm^{-1} for PDIVP). High resolution XPS measurements further confirm these results. It is also worth noting that detection of Si(0) is very challenging as compared to Si(oxide) species due to low penetration depth of XPS in the present scenario due to thick polymer surface coverage. (Figure 3 B).[9] Using SiNCs-*g*-PEGDM-*g*-PMMA three oxygen species (Figure 3 C) were detected which can be assigned to Si-O (533.9 eV), C-O (532 eV) and C=O (533 eV). After grafting of vinylphosphonates, characteristic binding energies of phosphorus (133 eV; Figure 3 D) and oxygen could be obtained (Figure 3 E). The signal at 530.5 eV could be assigned to P=O bonds from dialkyl vinylphosphonates. XPS spectra of both, SiNCs-*g*-PEGDM-*g*-PDEVP and SiNCs-*g*-PEGDM-*g*-PDMVP are similar. Furthermore TGA and PL measurements confirmed successful the polymerization success from SiNCs surfaces and agrees with previously reported results thus not presented here.[10,16]

CONCLUSIONS

The aim of our work was to optimize reaction conditions regarding the surface-initiated group-transfer polymerization of poly(dialkyl vinylphosphonates) on silicon nanocrystal surfaces, to obtain various materials for applications like in drug delivery or thermosensitive membranes. Silicon nanocrystals were grafted with ethyleneglycol di(methacrylate) to obtain characteristic acrylic surface groups for a surface-initiated group transfer polymerization. Such modified SiNCs were impregnated with the rare earth metal catalyst *bis*(cyclopenta-dienyl)trimethylsilyl-methylyttrium(thf) and diethyl vinylphosphonate was polymerized from the

surfaces. We found by varying the catalyst and monomer concentration that a minimum amount of catalyst is necessary for the effective polymerization and the grafting density is dependent upon catalyst concentration. No change in polymer grafting density was observed, when catalyst concentrations were kept constant while varying the monomer concentrations. This indicates that termination reactions can occur during the polymerization reaction. Furthermore we demonstrated, that the method is applicable to variety of monomers like methyl methacrylate, dimethyl vinylphosphonate and di*iso*propyl vinylphosphonates thus showing the versatility of the approach. Investigations are underway to understand the mechanism of the SI-GTP from the SiNCs surface and we plan to apply copolymerizations of different dialkyl vinylphosphonates to tune the thermoresponsive behavior of hybrid SiNCs.

ACKNOWLEDGMENTS

M.I., L.H. and J.G.C.V. acknowledge funding from the Natural Sciences and Engineering Research Council of Canada (NSERC), Helmholtz Alberta Initiative (HAI), Canada Foundation for Innovation (CFI), Alberta Science and Research Investment Program (ASRIP), and University of Alberta, Department of Chemistry. The staff at the Alberta Centre for Surface Engineering and Sciences (ACSES) are thanked for XPS analysis. I.M.D.H. is grateful for a generous scholarship from the Fonds der Chemischen Industrie. T.H. is thankful Studienstiftung des deutschen Volkes for a generous scholarship.

REFERENCES

[1] J. Liu, F. Erogbogbo, K.-T. Yong, L. Ye, J. Liu, R. Hu, H. Chen, Y. Hu, Y. Yang, J. Yang, I. Roy, N.A. Karker, M.T. Swihart, P.N. Prasad, ACS Nano 7 (2013) 7303–7310.
[2] J.G.C. Veinot, Chem. Commun. (2006) 4160.
[3] Y. Wang, N. Herron, J. Phys. Chem. 95 (1991) 525–532.
[4] H. Weller, Angew. Chem. Int. Ed. Engl. 32 (1993) 41–53.
[5] X. Cheng, S.B. Lowe, P.J. Reece, J.J. Gooding, Chem. Soc. Rev. 43 (2014) 2680.
[6] I.M.D. Höhlein, J. Kehrle, T. Helbich, Z. Yang, J.G.C. Veinot, B. Rieger, Chem. Eur. J. 20 (2014) 4212–4216.
[7] I.M.D. Höhlein, A. Angı, R. Sinelnikov, J.G.C. Veinot, B. Rieger, Chem. Eur. J. 21 (2015) 2755–2758.
[8] I.M.D. Höhlein, J. Kehrle, T.K. Purkait, J.G.C. Veinot, B. Rieger, Nanoscale 7 (2015) 914–918.
[9] Z. Yang, M. Dasog, A.R. Dobbie, R. Lockwood, Y. Zhi, A. Meldrum, J.G.C. Veinot, Adv. Funct. Mater. 24 (2014) 1345.
[10] U.B. Seemann, J.E. Dengler, B. Rieger, Angew. Chem. Int. Ed. 49 (2010) 3489–3491.
[11] S. Salzinger, U.B. Seemann, A. Plikhta, B. Rieger, Macromolecules 44 (2011) 5920–5927.
[12] S. Salzinger, B.S. Soller, A. Plikhta, U.B. Seemann, E. Herdtweck, B. Rieger, J. Am. Chem. Soc. 135 (2013) 13030–13040.
[13] S. Salzinger, B. Rieger, Macromol. Rapid Commun. 33 (2012) 1327–1345.
[14] N. Zhang, S. Salzinger, B.S. Soller, B. Rieger, J. Am. Chem. Soc. 135 (2013) 8810–8813.
[15] N. Zhang, S. Salzinger, B. Rieger, Macromolecules 45 (2012) 9751–9758.
[16] J. Kehrle, I.M.D. Höhlein, Z. Yang, A.-R. Jochem, T. Helbich, T. Kraus, J.G.C. Veinot, B. Rieger, Angew. Chem. Int. Ed. 53 (2014) 12494–12497.

4.1.2.4. Reprint Permissions

4.2. In-Situ IR-Spectroscopy as Tool for Monitoring the Radical Hydrosilylation Process on Silicon Nanocrystal Surfaces

4.2.1. Summary

Radical grafting on SiNCs is a very promising tool due to its straightforward nature and its high tendency to form monolayer surfaces. Although efforts were made to propose a mechanism, several reactivities remained unclear. Furthermore, albeit often used as quantitative reaction indicator, not much has been known about the "clarification" of SiNC dispersions during hydrosilylations. The aim of the present study was the use of *in-situ* IR spectroscopy regarding Si-H surfaces as a tool for monitoring the SiNC surface hydrosilylation rates under a variety of conditions.

A combination of visible light (VIS) transmittance (800 nm) and *in-situ* IR spectroscopy measurements was used to demonstrate the clearing of the SiNC-agglomerates during the grafting process with 1-hexene, trimethylvinylsilane and triphenylvinylsilane. In all cases, the dispersion turned clear before the surface reactions were completed. The effect became more obvious for bulkier olefins, which generally exhibited slower reactivities. The radical concentration determining the grafting speed of olefins on SiNC surfaces is probably one of the most important factors for successful surface grafting. In the present study, vinylsilanes (e.g. trimethylvinylsilane-TMVS) were used as reaction platforms due to their variability at the silyl group. Although the SiNC grafting reactions were accelerated with increasing radical concentrations, the rate converged to a maximum. At a very low radical concentration, the radical efficiency for surface grafting increased above one – a clear indicator for the presence of chain processes. In any case, the grafting speed was strictly dependent on the radical concentration. Size exclusion chromatography experiments demonstrated, that solution oligomerization presumably ran as the favored process over surface grafting. Furthermore, we observed that the steric demand of the applied olefin or vinylsilane had a major impact on the grafting rates. Bulkier vinylsilanes reacted slower than less crowded ones, demonstrating that oligomer radicals and not free butyronitrile radicals are responsible for the generation of surface silyl radicals. Variation of the monomer concentrations did not have an influence on the SiNC grafting rates.

4.2.2. Bibliographic Data

In-situ IR-spectroscopy as a tool for monitoring the radical hydrosilylation process on silicon nanocrystal surfaces

Nanoscale, **2017***,9*, 8489-8495.

Julian Kehrle,[a] Simon Kaiser,[a] Tapas K. Purkait,[b] Malte Winnacker,[a] Tobias Helbich,[a] Sergei Vagin,[a] Jonathan G. C. Veinot[c] and Bernhard Rieger[a]

[a] Catalysis Research Center/WACKER-Lehrstuhl für Makromolekulare Chemie, Technische Universität München, Lichtenbergstraße 4, 85747 Garching bei München, Germany.

[b]Department of Chemistry, Johns Hopkins University, Baltimore, MD 21218, USA

[c]Department of Chemistry, University of Alberta, 11227 Saskatchewan Drive, Edmonton, Alberta T6G 2G2, Canada

Direct Link: DOI 10.1039/c7nr02265d

Supporting Information:

http://www.rsc.org/suppdata/c7/nr/c7nr02265d/c7nr02265d1.pdf

4.2.3. Reprint of the Original Manuscript

Nanoscale

PAPER

View Article Online
View Journal | View Issue

Cite this: *Nanoscale*, 2017, **9**, 8489

In situ IR-spectroscopy as a tool for monitoring the radical hydrosilylation process on silicon nanocrystal surfaces†

Julian Kehrle,‡[a] Simon Kaiser,‡[a] Tapas K. Purkait,[b] Malte Winnacker,[a] Tobias Helbich,[a] Sergei Vagin,[a] Jonathan G. C. Veinot*[c] and Bernhard Rieger*[a]

Received 30th March 2017,
Accepted 19th May 2017

DOI: 10.1039/c7nr02265d

rsc.li/nanoscale

Among a variety of SiNC functionalization methods, radical initiated grafting is very promising due to its straightforward nature and low propensity to form surface oligomers. In the present study, we employed *in situ* IR spectroscopy in combination with visible light transmittance measurements to investigate the radical induced grafting process on the well-defined SiNCs. Our findings support the proposed model: unfunctionalized hydride-terminated SiNCs form agglomerates in organic solvents, which break up during the grafting process. However, clearing of the dispersion is not a valid indicator for complete surface functionalization. Furthermore, radical-initiated grafting reactions in which azobisisobutyronitrile (AIBN) is the initiator are strongly influenced by external factors including initiator concentration, grafting temperature, as well as substrate steric demand. The monomer concentration was proven to have a low impact on the grafting process. Based on these new insights an underlying mechanism could be discussed, offering an unprecedented view on the functionalization of SiNC surfaces *via* radical initiated hydrosilylation.

Introduction

Silicon nanocrystals (SiNCs) have emerged as a class of non-toxic, electrochemically stable quantum dots.[1,2] It is well-established that the optical and electronic properties of these promising materials may be tuned by varying the particle size and surface chemistry.[3–6] As a result of their exquisitely tunable optoelectronic response, a variety of prototype applications have been demonstrated including sensors,[7,8] bioimaging,[9–11] and light-emitting diodes (LEDs).[12–14]

The most widely investigated methods for functionalizing SiNCs are based upon variations (*e.g.*, metal catalyzed,[15] thermally-[16–19] and photochemically-induced,[20,21] radical initiated,[22,23] *etc.*) of the general hydrosilylation reaction that involves hydrogen-terminated SiNCs (H-SiNCs); each procedural variant has its own advantages and challenges.[6,24] For example, residual metal catalyst impurities can compromise SiNC optical response.[25] Thermal and photoinitiated hydrosilylations apparently evade this issue. Thermal grafting of olefins and alkynes is most often performed on a neat substrate and, while it leads to surface modification, surface oligomerization and solution phase homopolymerization have been identified as potential limitations.[16,19] Oligomerization is minimized (if not eliminated) by applying photoinduced protocols, however, limited surface coverage often results and the NC surfaces remain susceptible to deleterious reactivity (*e.g.*, oxidation) that can lead to altered and unpredictable properties.[20,26] Furthermore, the general photochemical procedure is not effective for SiNCs of all sizes and substrates.[21] Of late there has been increased interest in metal-free catalysts or radical initiators that offer efficient surface coverage and short reaction times, however, even those can lead to unexpected consequences related to optical response.[20,27]

Despite the impressive advances, questions remain regarding the efficacy of SiNC surface modification; perhaps the chief among them is: how do SiNC surface reactions generally proceed? Typically, the reaction progress is evaluated qualitatively by monitoring the optical transparency of the reaction mixture.[22,23] The basis for this analysis is the assumption that the formation of sterically stabilized SiNC colloids will induce a "clearing" of the formerly turbid dispersion of H-SiNCs. SiNC grafting mechanisms have mostly been derived from flat silicon surfaces[22,23,28–31] or focused on thermal[32] and photoinitiated reactions.[20,21] To date, no quantitative evaluation of the reaction progress has been presented to support these findings for radical initiated SiNC surface grafting. To address

[a]*Catalysis Research Center/WACKER-Lehrstuhl für Makromolekulare Chemie, Technische Universität München, Lichtenbergstraße 4, 85747 Garching bei München, Germany. E-mail: rieger@tum.de*
[b]*Department of Chemistry, Johns Hopkins University, Baltimore, MD 21218, USA*
[c]*Department of Chemistry, University of Alberta, Edmonton, Alberta T6G 2G2, Canada. E-mail: jveinot@ualberta.ca*

†Electronic supplementary information (ESI) available: Further synthetic procedure and analysis (*e.g.* UV-VIS, PL, TEM, HR-TEM, DLS, ATR-IR, XPS, NALDI, TGA and elemental analysis). See DOI: 10.1039/c7nr02265d

‡J. K. and S. K. contributed equally.

this concern, we describe a detailed IR study of hydrosilylation reactions of a wide range of vinylsilanes on the surfaces of well-defined H-SiNCs ($d \sim 3$ nm) initiated using azobisisobutyronitrile (AIBN).

Experimental

Material characterization and instrumentation

Materials. All chemicals were purchased from Sigma Aldrich and ABCR and used without purification if not stated otherwise. Solvents were dried using a solvent purification system LABmaster 130 from MBraun. Triphenylvinylsilane,[33,34] 1,1,1,3,3-pentamethyl-3-vinyldisiloxane[35] and 1,1,1,5,5,5-hexamethyl-3-(trimethylsiloxy)-3-vinyltrisiloxane[36] were synthesized according to the known literature procedures (ESI section 1†). Vinylsilanes were dried over molecular sieves and distilled or recrystallized. AIBN was recrystallized from methanol prior to use. Functionalization reactions were performed under an inert gas using dry solvents. Centrifugations were performed using ETFE centrifuge tubes purchased from Roth, to prevent solvatization of oligoolefins from conventional centrifugation tubes. Schlenk tubes for *in situ* ATR-IR measurements were produced from the glassblower of the TUM, department of chemistry.

Attenuated total reflectance infrared (ATR-IR) spectra were measured by drop coating of the sample on the probe using a nitrogen cooled VERTEX 70 FTIR spectrometer from Bruker and a Platinum ATR unit (s – strong, m – medium and w – weak). *In situ* IR spectroscopy was performed on a liquid nitrogen cooled Mettler Toledo ReactIR 45 m with a silicon ATR probe into a SiNC-toluene dispersion. Measurements were performed every 30 seconds applying 125 scans.

UV/Vis spectra were recorded on a Cary 50 from Varian. Transmittance measurements were performed in the absorbance mode using a wavelength of 800 nm.

Gel permeation chromatography (GPC) was obtained from a Varian PL-GPS 50 Plus equipped with two PLgel MIXED-C columns using tetrahydrofuran with a flow rate of 1 mL min^{-1}. Calibration was performed using polystyrene standards.

Functionalization of SiNCs

600 mg of the SiNC composite are liberated by the HF etching procedure, redispersed in 6 mL of toluene and transferred into three *in situ* IR Schlenk tubes (ESI Table S2†). Afterwards, vinylsilane and toluene are added to provide a substrate concentration of 1.26 mmol mL^{-1} and a SiNC concentration of 1 ± 0.1 mg mL^{-1} at a fixed volume of 3.6 mL. The reaction mixture is then degassed using three freeze–pump–thaw cycles and ultrasonicated for 1 h. Subsequently the *in situ* IR probe is dipped into the dispersion under an Ar flow. The system is heated to the desired temperature (mainly 70 °C) and stirred at 400 min^{-1} to equilibrate. After 10 min, a solution of AIBN of the desired concentration (mainly 24.4 μmol dissolved in 0.20 mL dry, degassed toluene) is added *via* a syringe. The addition of AIBN defines $t = 0$ min. The characteristic Si–H band between 2158 and 2040 cm^{-1} is monitored. A two-point baseline has been used to integrate the signal.

Results and discussion

Reactivity of Si–H nanocrystal agglomerates

To quantitatively evaluate the progression of radical initiated hydrosilylation reactions on SiNCs it is preferable to monitor the cases involving a molecular reagent that readily attaches to the NC surfaces and exhibits a low propensity for solution-phase polymerization; it is also important to employ a radical initiator with well-understood reactivity. Vinylsilanes are an ideal substrate for the present study, because it is established that the pendant vinyl group affords effective functionalization of SiNCs[37] with low solution polymerization.[38] Similarly, the decomposition dynamics of the radical initiator azobisisobutyronitrile (AIBN) are intensely studied.[39]

In our study we used SiNCs prepared *via* thermal disproportionation of hydrogen silsesquioxane followed by etching with alcoholic HF.[18] After extraction, the resulting H-SiNCs are isolated by centrifugation and dispersed in dry toluene; subsequently, known quantities of vinylsilane precursors (*e.g.*, trimethylvinylsilane, TMVS) or other alkenes (ESI Part 1.2.1, Table S2†), and AIBN were added to the turbid reaction mixture. Finally, the reaction progress was monitored by *in situ* ATR-IR spectroscopy (ESI Fig. S1†).

Fundamental changes are observed in the IR spectrum of SiNCs upon functionalization with various substrates (Fig. 1) and monitoring key features such as the Si–H absorption band using *in situ* IR spectroscopy offers a unique opportunity to track the reaction progress (ESI Fig. S1†). In this regard, time resolved *in situ* IR analysis was performed on a known volume of a dispersion of H-SiNCs ($d \sim 3$ nm; 1 mg mL^{-1})[18] with a total Si–H concentration of 18.8 μmol mL^{-1} (ESI section 2.2†)

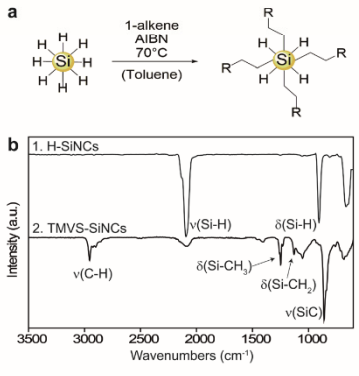

Fig. 1 (a) Schematic illustration of the radical SiNC functionalization process using trimethylvinylsilane as the substrate. (b) Attenuated total reflectance infrared (ATR-IR) spectrum of H-SiNCs (1) and TMVS-SiNCs (2).

and varying concentrations of vinylsilanes or alkenes, and AIBN (ESI Table S1†).

To correlate functionalization with optical clarity of the reaction mixture simultaneous time resolved visible light (800 nm) transmittance and *in situ* IR spectroscopy measurements were performed using 1-hexene (Fig. 2a, I), trimethylvinylsilane (TMVS, II), and triphenylvinylsilane (TPVS, III). With a decreasing size of SiNC agglomerates, particle dispersions appear transparent due to a weaker Rayleigh scattering; this observation has previously been used as a qualitative indicator for effective functionalization of SiNCs and was assumed to result from a nearly complete surface reaction.[22,23]

The performed kinetic studies clearly demonstrate the difference between the "clearing period" of the dispersion and the time required for complete functionalization. This effect depends on the steric bulk of the substrate, presumably because surface reactions involving bulkier olefins are slower. For instance, for the bulky TPVS (Fig. 2a, III) the dispersion becomes already clear after ~110 min, while the disappearance of the Si–H signal needs additional 231 min. For the sterically less bulky TMVS(II) the clarification time reduces to ~100 min, but complete Si–H consumption is reached after another 97 min. The influence of the steric bulk of the substrate becomes more obvious when using 1-hexene(I), which becomes transparent after ~55 min (plus 54 min for Si–H conversion). Fig. 2b shows the proposed underlying reaction sequence of the following procedure: the Si–H groups of the "outer surface" of the agglomerates react first. This induces a breaking up of these large particles and generates continuously "fresh" Si–H groups. Once the agglomerates reach a critical size, the dispersions become clear while the conversion of Si–H groups proceeds on the individual nanocrystals.

Radical formation and their reactions

To gain further insight into the general nature of radical initiated hydrosilylation grafting processes on H-SiNC surfaces, several parameters were varied and the reactions were again monitored using *in situ* IR spectroscopy. The influence of the present radical concentrations on the SiNC functionalization was determined by varying the AIBN concentrations (at constant temperatures) and reaction temperatures (at a constant AIBN concentration; ESI Table S2,† entries 1 and 2).[39] Fig. 3a shows that an increasing AIBN concentration affords higher functionalization rates. However, the rapidity of the functionalization converges and reaches a maximum at high AIBN concentrations (see Fig. 3a, I, II). Therefore, we propose that at very high AIBN concentrations, cleavage of SiNC agglomerates becomes the rate determining step.

As is the case with some literature proposals,[22,23] at lower AIBN concentrations surface hydrosilylation reactions proceed *via* a chain reaction mechanism, and radical efficiencies of the present SiNC surface reactions exceed unity as a consequence of reduced termination reactions (Fig. 3b, ESI Tables S9 and S10†).[40,41] The same proposal holds true, when the influence of the temperature on AIBN decomposition is considered (Fig. 3c). At 100 °C complete functionalization of H-SiNCs occurs within 10 minutes, although with a lower radical efficiency; at 50 °C the reactions require approximately 23 h.

In addition to SiNC surface reactions, the radical initiators formed by AIBN decomposition can also induce radical chain reactions in solution. Size exclusion chromatography (SEC) was used to investigate the possibility of solution phase substrate oligomerization (Fig. 3e and f). Samples evaluated included: (1) a reaction mixture prepared using AIBN and the substrate (*i.e.*, no SiNCs); (2) a reaction mixture using AIBN, the substrate and SiNCs; and (3) a purified functionalized SiNC fraction. TMVS forms small amounts of oligomers in solution, independent of the presence of SiNCs (Fig. 3e). The as-synthesized SiNCs in a mixture with solution oligomer (2) show lower molecular weights than the purified SiNCs (3), where small SiNCs were washed away during purification. Similar observations, but higher molecular weight fractions of polymers and oligomers were noted for triethoxyvinylsilane (TEVS; Fig. 3f).[38]

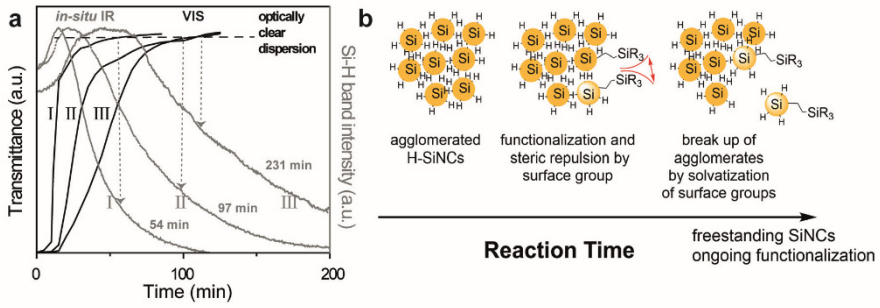

Fig. 2 (a) Comparison of the VIS-transmittance measurements using λ = 800 nm (black) and *in situ* IR evolutions of the Si–H band at 2100 cm^{-1} (grey) for 1-hexene (I), TMVS (II) and TPVS (III) measured during the functionalization reaction of hydride terminated SiNCs. (b) Schematic illustration of the agglomerate break-up process leading to clear reaction mixtures.

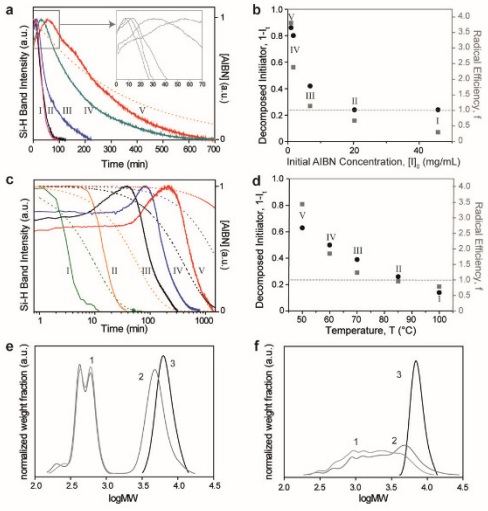

Fig. 3 (a) Evolution of the SiH band (2100 cm^{-1}) intensity during functionalization of hydride-terminated SiNCs with TMVS at 70 °C with AIBN concentrations of 45.7 μmol mL^{-1} (I), 20.3 μmol mL^{-1} (II), 6.8 μmol mL^{-1} (III), 1.7 μmol mL^{-1} (IV) and 1.0 μmol mL^{-1} (V) (inset: magnification of the starting evolutions). (b) Relative concentrations of the decomposed initiator 1-It at complete Si–H conversion and corresponding radical efficiencies f based upon 1-It (ESI Table S9†). (c) Evolution of the SiH band (2100 cm^{-1}) intensity during functionalization of hydride terminated SiNCs with a constant AIBN concentration of 6.8 μmol mL^{-1} at reaction temperatures of 100 °C (I), 85 °C (II), 70 °C (III), 60 °C (IV) and 50 °C (V); dashed lines show the respective AIBN decomposition rate calculated from the rate constants. (d) 1-It after complete Si–H conversion and corresponding f (ESI Table S10†). Size exclusion chromatogram (THF, relative to polystyrene standards) of the AIBN initiated reaction of (e) TMVS and (f) TEVS in toluene at 70 °C in the absence of SiNCs (1) and with SiNCs present (2 – workup in vacuum; 3 – workup *via* precipitation–centrifugation).

Sterics: the key to reaction rates

Stefanac *et al.* showed that under radical conditions vinyl oligomerization of diphenylvinylsilane is favored over its intermolecular hydrosilylation reaction.[38] Thus, in the SiNC surface reaction one would expect that after initiation, solution oligomerization of vinylsilanes dominates over surface grafting, consistent with the present SEC experiments.

Additionally, the surface hydrosilylation rates should correlate with the accessibility of the Si–H groups and the steric demand of the activating radical.[42] As a result of the surface hydrogen atom abstraction being a heterogeneous process (due to the necessity for the breakup of H-SiNC agglomerates), the steric demand of the activating radical was expected to play a crucial role for the reaction rates.[42] Hence, we propose that the available oligomer radicals would induce the formation of silyl radicals from H-SiNCs. To verify this proposal, a series of substrates with varying steric properties were investigated using *in situ* IR.

At first, the rates of 1-hexene and 1-dodecene, well-known substrates for SiNC surface functionalization, were compared to the TMVS reactivity (Fig. 4a).[22] All surface reactions run faster with 1-hexene (~110 min) and with slower rates for 1-dodecene (~160 min) and TMVS (~200 min). As a result of steric shielding of the surface from the solution formed oligomer radicals, the rates slow down. Steric surface shielding arises from conformational flexibilities of surface bonded dodecyl groups or dodecyl oligomer moieties.

Because of the observed influence of the nature of the olefin substrate and stability of bulky radicals on the surface functionalization rate, several vinylsilanes with different steric demands were investigated. The substrate bulkiness was increased upon changing the substitution around the central silicon of the substrate (ESI section 1.2; Table S2,† entry 3). Fig. 4b–d show conclusively that bulky substituents decrease the reaction rates compared to TMVS (~200 min). For example, dimethylphenylvinylsilane (DMPVS) needs 270 min and its bigger homologue triphenylvinylsilane (TPVS) needs 330 min. Upon ethoxy substitution, the gap between the single substituted dimethylethoxyvinylsilane (DMEVS) enhances from 220 min to 380 min for the triethoxyvinylsilane (TEVS). Most significant changes were observed, when trimethylsiloxy substituents were employed: pentamethylvinyldisiloxane (PMVDS) reacted in 280 min while the trisubstituted tris(trimethylsiloxy) vinylsilane (TTMSVS) needed ~31 h. This trend is further emphasized by decreasing surface coverages, decreasing the degrees of substitution (relative number of substituted Si–H groups by ligand molecules), as well as reduced radical efficiencies for bulkier substituents within the homologue series (as shown in Fig. 4e and f and ESI Tables S7 and S8†). In this regard, TTMSVS, which has a shielded vinyl group, exhibits the lowest reaction rate, degree of substitution (10%) and initiator efficiency (0.13) of all samples.

The behavior of bulky vinylic substrates toward the SiNC functionalization is similar to the findings for molecular silanes, where the silyl radical formation is highly dependent on the sterics of the incoming radical.[42] Furthermore, H-SiNCs only react with 2,2,6,6-tetramethylpiperidinyloxyl (TEMPO) if a radical initiator is available, but no reactivity was observed when olefins were added.[22] Hence, a capturing of solved radical species by TEMPO is dominant over surface reactions. This underlines the hypothesis that homolytic Si–H cleavage on SiNC surfaces occurs from oligomers or alkyl based radicals rather than from free butyronitrile radicals. Thus, we suggest that the Si–H cleavage by oligomer radicals is the rate-determining step in the radical SiNC functionalization mechanism under most of the conditions applied.

Does the monomer concentration matter?

A high reactivity of silyl radicals with vinylic compounds is known for molecular silanes and polymers.[40,41] We suggest that once the surface silyl radical has formed addition of the surface silyl radical to an alkene proceeds rapidly. If the substrate addition to the surface silyl radicals would determine the reaction rate, an increase of the SiNC functionalization rates should

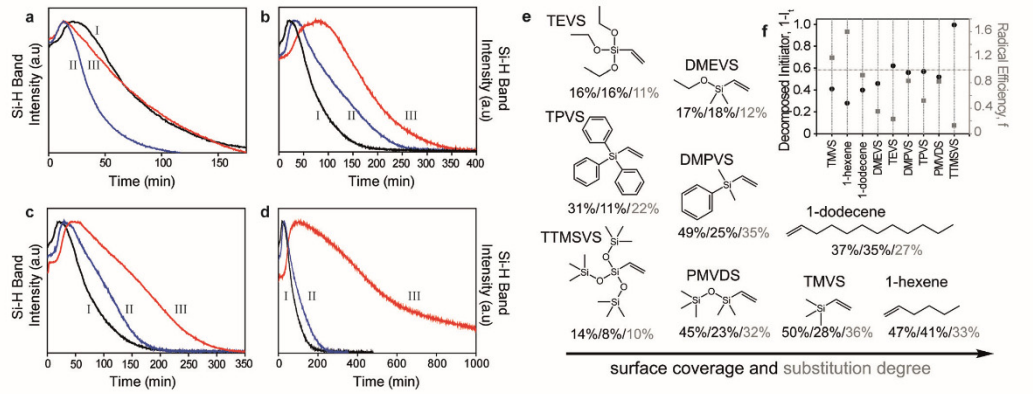

Fig. 4 Evolution of the SiH band intensity (2100 cm^{-1}) of SiNC functionalization at 70 °C with 6.8 μmol mL^{-1} AIBN in toluene (total volume: 3.6 mL). All figures show TMVS grafting (I) in comparison with functionalization using (a) 1-olefins: hexene (II) and dodecene (III); (b) phenylvinylsilanes: DMPVS (II), TPVS (III); (c) ethoxyvinylsilanes: DMEVS (II), TEVS (III); (d) siloxyvinylsilanes: PMVDS (II) and TTMSVS (III). (e) Surface coverage obtained from elemental analysis/TGA/molar Si–H substitution degree (grey). (f) Calculated relative amounts of decomposed initiators and radical efficiencies (ESI Table S11†) for applied substrates.

be observed in the *in situ* IR traces at higher monomer concentrations. This is not the case: the overall reaction rate does slow down with increasing monomer concentration (ESI Table S2,† entry 4). The major disparities, however, are observed in the regime where the agglomerates are large (Fig. 5a), which probably arise from poorer dispersibility in the neat substrates. Once the agglomerates are broken up, the decrease of the Si–H IR-signal (*e.g.*, Fig. 5a, trace IV) with increasing reaction time shows a similar slope to the traces I–III. Thus, the monomer addition to the Si˙ surface radicals cannot be the rate determining step, and the progress should be strictly driven by the radical concentrations and alkene structure.

To further investigate the dependence of the reaction on the presence of radicals, the SiNC functionalization with TMVS was interrupted by abrupt cooling of the reaction mixture from 70 °C to room temperature (r.t., Fig. 5b). At r.t., the Si–H signal intensity and, accordingly, the concentration of surface Si–H bonds remains constant. The reaction proceeds when reheated to 70 °C due to the fast generation of new radicals. The same reactivity has also been found when benzene was used as solvent, which is known as a weak radical transfer agent (ESI Fig. S1d†), indicating that the H-abstraction from the present substrate molecules is favored over the abstraction from solvent molecules. Both cases show that the reaction kinetics strictly depend on the presence of radicals in solution.

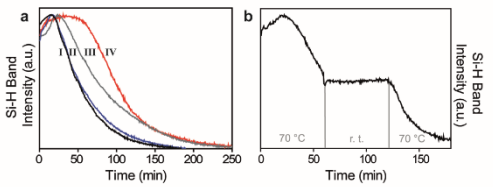

Fig. 5 (a) Time resolved *in situ* IR measurement of the Si–H band using 6.8 μmol mL^{-1} AIBN in toluene at TMVS concentrations of 1.26 mmol mL^{-1} (I), 0.63 mmol mL^{-1} (II), 2.52 mmol mL^{-1} (III) or neat (IV) TMVS. (b) Time resolved evolution of the Si–H bond of SiNCs using AIBN and TMVS in toluene. At 60 min, the temperature was decreased to room temperature using a water bath and reheated to 70 °C for 120 min.

Conclusions

In situ IR spectroscopy was used to follow the radical grafting process of hydride terminated SiNCs with unsaturated substrates. SiNC dispersions become clear during the functionalization with such olefins due to a break up of agglomerates, which has mostly been accepted as the end of the functionalization reaction. Here, we demonstrated that after clearing of the reaction solution, the surface functionalization of the individual SiNCs is far from being complete. The time difference between clearing of the dispersion and the finalization of the reaction arises with the bulkiness of the substrates. Furthermore, we observed that the hydrosilylation on SiNC surfaces is strongly dependent on the radical initiator concentration, the reaction temperature and the sterics of the alkenes applied; it is not related to the monomer concentration. Generally, radical efficiencies of the SiNC functionalization can exceed unity.

Acknowledgements

IRTG 2022 "ATUMS" (DFG) and NSERC are thanked gratefully for research funding. J. K. thanks TUM Graduate School for financial support. T. H. thanks the Studienstiftung des

deutschen Volkes and IGGSE for financial support. Dr Carsten Troll is thanked for support with the technical equipment. We thank our groups for helpful discussions.

Notes and references

1 Z. Ding, B. M. Quinn, S. K. Haram, L. E. Pell, B. A. Korgel and A. J. Bard, Electrochemistry and Electrogenerated Chemiluminescence from Silicon Nanocrystal Quantum Dots, *Science*, 2002, **296**, 1293–1297, DOI: 10.1126/science.1069336.

2 J. Liu, F. Erogbogbo, K.-T. Yong, L. Ye, J. Liu, R. Hu, H. Chen, Y. Hu, Y. Yang, J. Yang, I. Roy, N. A. Karker, M. T. Swihart and P. N. Prasad, Assessing clinical prospects of silicon quantum dots: studies in mice and monkeys, *ACS Nano*, 2013, 7, 7303–7310, DOI: 10.1021/nn4029234.

3 S. Regli, J. A. Kelly, A. M. Shukaliak and J. G. C. Veinot, Photothermal Response of Photoluminescent Silicon Nanocrystals, *J. Phys. Chem. Lett.*, 2012, **3**, 1793–1797, DOI: 10.1021/jz3004766.

4 M. Dasog, K. Bader and J. G. C. Veinot, Influence of Halides on the Optical Properties of Silicon Quantum Dots, *Chem. Mater.*, 2015, **27**, 1153–1156, DOI: 10.1021/acs.chemmater.5b00115.

5 A. Angı, R. Sinelnikov, A. Meldrum, J. G. C. Veinot, I. Balberg, D. Azulay, O. Millo and B. Rieger, Photoluminescence through in-gap states in phenylacetylene functionalized silicon nanocrystals, *Nanoscale*, 2016, **8**, 7849–7853.

6 M. Dasog, J. Kehrle, B. Rieger and J. G. C. Veinot, Silicon Nanocrystals and Silicon-Polymer Hybrids: Synthesis, Surface Engineering, and Applications, *Angew. Chem., Int. Ed.*, 2016, **55**, 2322–2339, DOI: 10.1002/anie.201506065.

7 R. Ban, F. Zheng and J. Zhang, A highly sensitive fluorescence assay for 2,4,6-trinitrotoluene using amine-capped silicon quantum dots as a probe, *Anal. Methods*, 2015, 7, 1732–1737, DOI: 10.1039/C4AY02729A.

8 C. M. Gonzalez, M. Iqbal, M. Dasog, D. G. Piercey, R. Lockwood, T. M. Klapotke and J. G. C. Veinot, Detection of high-energy compounds using photoluminescent silicon nanocrystal paper based sensors, *Nanoscale*, 2014, **6**, 2608–2612, DOI: 10.1039/C3NR06271F.

9 X. Cheng, S. B. Lowe, S. Ciampi, A. Magenau, K. Gaus, P. J. Reece and J. J. Gooding, Versatile "click chemistry" approach to functionalizing silicon quantum dots: applications toward fluorescent cellular imaging, *Langmuir*, 2014, **30**, 5209–5216, DOI: 10.1021/la500945f.

10 Y. Zhai, M. Dasog, R. B. Snitynsky, T. K. Purkait, M. Aghajamali, A. H. Hahn, C. B. Sturdy, T. L. Lowary and J. G. C. Veinot, Water-soluble photoluminescent d-mannose and l -alanine functionalized silicon nanocrystals and their application to cancer cell imaging, *J. Mater. Chem. B*, 2014, **2**, 8427–8433, DOI: 10.1039/C4TB01161A.

11 F. Erogbogbo, K.-T. Yong, I. Roy, R. Hu, W.-C. Law, W. Zhao, H. Ding, F. Wu, R. Kumar, M. T. Swihart and P. N. Prasad, In Vivo Targeted Cancer Imaging, Sentinel Lymph Node Mapping and Multi-Channel Imaging with Biocompatible Silicon Nanocrystals, *ACS Nano*, 2010, **5**, 413–423, DOI: 10.1021/nn1018945.

12 B. Ghosh, Y. Masuda, Y. Wakayama, Y. Imanaka, J. Inoue, K. Hashi, K. Deguchi, H. Yamada, Y. Sakka and S. Ohki, Hybrid white light emitting diode based on silicon nanocrystals, *Adv. Funct. Mater.*, 2014, **24**, 7151–7160.

13 F. Maier-Flaig, J. Rinck, M. Stephan, T. Bocksrocker, M. Bruns, C. Kübel, A. K. Powell, G. A. Ozin and U. Lemmer, Multicolor silicon light-emitting diodes (SiLEDs), *Nano Lett.*, 2013, **13**, 475–480, DOI: 10.1021/nl3038689.

14 T. Lin, X. Liu, B. Zhou, Z. Zhan, A. N. Cartwright and M. T. Swihart, A Solution-Processed UV-Sensitive Photodiode Produced Using a New Silicon Nanocrystal Ink, *Adv. Funct. Mater.*, 2014, **24**, 6016–6022, DOI: 10.1002/adfm.201400600.

15 A. Shiohara, S. Hanada, S. Prabakar, K. Fujioka, T. H. Lim, K. Yamamoto, P. T. Northcote and R. D. Tilley, Chemical reactions on surface molecules attached to silicon quantum dots, *J. Am. Chem. Soc.*, 2010, **132**, 248–253, DOI: 10.1021/ja906501v.

16 M. G. Panthani, C. M. Hessel, D. Reid, G. Casillas, M. José-Yacamán and B. A. Korgel, Graphene-Supported High-Resolution TEM and STEM Imaging of Silicon Nanocrystals and their Capping Ligands, *J. Phys. Chem. C*, 2012, **116**, 22463–22468, DOI: 10.1021/jp308545q.

17 M. Guan, W. Wang, E. J. Henderson, O. Dag, C. Kübel, V. S. K. Chakravadhanula, J. Rinck, I. L. Moudrakovski, J. Thomson, J. McDowell, A. K. Powell, H. Zhang and G. A. Ozin, Assembling photoluminescent silicon nanocrystals into periodic mesoporous organosilica, *J. Am. Chem. Soc.*, 2012, **134**, 8439–8446, DOI: 10.1021/ja209532e.

18 C. M. Hessel, E. J. Henderson and J. G. C. Veinot, Hydrogen Silsesquioxane: A Molecular Precursor for Nanocrystalline Si–SiO 2 Composites and Freestanding Hydride-Surface-Terminated Silicon Nanoparticles, *Chem. Mater.*, 2006, **18**, 6139–6146, DOI: 10.1021/cm0602803.

19 Z. Yang, M. Iqbal, A. R. Dobbie and J. G. C. Veinot, Surface-Induced Alkene Oligomerization: Does Thermal Hydrosilylation Really Lead to Monolayer Protected Silicon Nanocrystals?, *J. Am. Chem. Soc.*, 2013, **135**, 17595–17601, DOI: 10.1021/ja409657y.

20 J. A. Kelly and J. G. C. Veinot, An Investigation into Near-UV Hydrosilylation of Freestanding Silicon Nanocrystals, *ACS Nano*, 2010, **4**, 4645–4656, DOI: 10.1021/nn101022b.

21 J. A. Kelly, A. M. Shukaliak, M. D. Fleischauer and J. G. C. Veinot, Size-Dependent Reactivity in Hydrosilylation of Silicon Nanocrystals, *J. Am. Chem. Soc.*, 2011, **133**, 9564–9571, DOI: 10.1021/ja2025189.

22 Z. Yang, C. M. Gonzalez, T. K. Purkait, M. Iqbal, A. Meldrum and J. G. C. Veinot, Radical Initiated Hydrosilylation on Silicon Nanocrystal Surfaces: An Evaluation of Functional Group Tolerance and Mechanistic Study, *Langmuir*, 2015, **31**, 10540–10548, DOI: 10.1021/acs.langmuir.5b02307.

23 I. M. D. Höhlein, J. Kehrle, T. Helbich, Z. Yang, J. G. C. Veinot and B. Rieger, Diazonium Salts as Grafting Agents and Efficient Radical-Hydrosilylation Initiators for Freestanding Photoluminescent Silicon Nanocrystals, *Chem. – Eur. J.*, 2014, **20**, 4212–4216, DOI: 10.1002/chem.201400114.

24 X. Cheng, S. B. Lowe, P. J. Reece and J. J. Gooding, Colloidal silicon quantum dots: from preparation to the modification of self-assembled monolayers (SAMs) for bio-applications, *Chem. Soc. Rev.*, 2014, **43**, 2680, DOI: 10.1039/c3cs60353a.

25 Y. Wang, H. Wang, J. Guo, J. Wu, L. J. Gao, Y. H. Sun, J. Zhao and G. F. Zou, Water-Soluble Silicon Quantum Dots with Quasi-Blue Emission, *Nanoscale Res. Lett.*, 2015, **10**, 1012, DOI: 10.1186/s11671-015-1012-2.

26 J. Kehrle, I. M. D. Höhlein, Z. Yang, A.-R. Jochem, T. Helbich, T. Kraus, J. G. C. Veinot and B. Rieger, Thermoresponsive and photoluminescent hybrid silicon nanoparticles by surface-initiated group transfer polymerization of diethyl vinylphosphonate, *Angew. Chem., Int. Ed.*, 2014, **53**, 12494–12497, DOI: 10.1002/anie.201405946.

27 M. P. Stewart and J. M. Buriak, Exciton-mediated hydrosilylation on photoluminescent nanocrystalline silicon., *J. Am. Chem. Soc.*, 2001, **123**, 7821–7830.

28 J. M. Buriak, Organometallic Chemistry on Silicon and Germanium Surfaces, *Chem. Rev.*, 2002, **102**, 1271–1308, DOI: 10.1021/cr000064s.

29 B. J. Eves, Q.-Y. Sun, G. P. Lopinski and H. Zuilhof, Photochemical Attachment of Organic Monolayers onto H-Terminated Si(111): Radical Chain Propagation Observed via STM Studies, *J. Am. Chem. Soc.*, 2004, **126**, 14318–14319, DOI: 10.1021/ja045777x.

30 M. R. Linford and C. E. D. Chidsey, Alkyl monolayers covalently bonded to silicon surfaces, *J. Am. Chem. Soc.*, 1993, **115**, 12631–12632.

31 M. R. Linford, P. Fenter, P. M. Eisenberger and C. E. D. Chidsey, Alkyl monolayers on silicon prepared from 1-alkenes and hydrogen-terminated silicon, *J. Am. Chem. Soc.*, 1995, **117**, 3145–3155.

32 J. Holm and J. T. Roberts, Thermally Induced Hydrosilylation at Deuterium-Terminated Silicon Nanoparticles: An Investigation of the Radical Chain Propagation Mechanism, *Langmuir*, 2009, **25**, 7050–7056, DOI: 10.1021/la8042236.

33 L. F. Cason and H. G. Brooks, An Interesting Side-Reaction in the Preparation of Triphenylvinylsilane 1a, *J. Am. Chem. Soc.*, 1952, **74**, 4582–4583, DOI: 10.1021/ja01138a039.

34 R. Nagel and H. W. Post, Studies in Silico-Organic Compounds. XXI. Alkyl and Phenyl Derivatives of vinyltrichlorosilane, *J. Org. Chem.*, 1952, **17**, 1379–1381, DOI: 10.1021/jo50010a016.

35 D. Seyferth and D. L. Alleston, The Cleavage of Hexamethyldisiloxane and Hexamethyldigermoxane by Methyllithium: A Convenient Preparation of Lithium Trimethylsilanolate and Lithium Trimethylgermanolate, *Inorg. Chem.*, 1963, **2**, 418–420, DOI: 10.1021/ic50006a048.

36 T. Iimura, S. Onodera, T. Okawa and M. Yoshitake, WO2003064436 A1, 2003.

37 I. M. D. Höhlein, J. Kehrle, T. K. Purkait, J. G. C. Veinot and B. Rieger, Photoluminescent silicon nanocrystals with chlorosilane surfaces - synthesis and reactivity, *Nanoscale*, 2015, **7**, 914–918, DOI: 10.1039/C4NR05888G.

38 T. M. Stefanac, M. A. Brook and R. Stan, Radical Reactivity of Hydrovinylsilanes: Homooligomers, *Macromolecules*, 1996, **29**, 4549–4555, DOI: 10.1021/ma951495t.

39 J. Brandrup, E. H. Immergut and E. A. Grulke, *Polymer handbook*, Wiley, New York, Chichester, 4th edn, 2004.

40 S. Koltzenburg, M. Maskos and O. Nuyken, *Polymere: Synthese*, Eigenschaften und Anwendungen, Springer Spektrum, Berlin, 1st edn, 2014.

41 G. Odian, *Principles of Polymerization*, John Wiley and Sons, New Jersey, 4th edn, 2004.

42 C. Chatgilialoglu, Structural and Chemical Properties of Silyl Radicals, *Chem. Rev.*, 1995, **95**, 1229–1251, DOI: 10.1021/cr00037a005.

4.2.4. Reprint Permissions

Julian

Von: CONTRACTS-COPYRIGHT (shared) <Contracts-Copyright@rsc.org>
Gesendet: Dienstag, 20. Juni 2017 15:47
An: 'Julian'
Betreff: RE: Copyright Permissions

Dear Julian,

Thank you for your email.

The Royal Society of Chemistry (RSC) hereby grants permission for the use of your paper(s) specified below in the printed and microfilm version of your thesis. You may also make available the PDF version of your paper(s) that the RSC sent to the corresponding author(s) of your paper(s) upon publication of the paper(s) in the following ways: in your thesis via any website that your university may have for the deposition of theses, via your university's Intranet or via your own personal website. We are however unable to grant you permission to include the PDF version of the paper(s) on its own in your institutional repository. The Royal Society of Chemistry is a signatory to the STM Guidelines on Permissions (available on request).

Please note that if the material specified below or any part of it appears with credit or acknowledgement to a third party then you must also secure permission from that third party before reproducing that material.

Please ensure that the thesis states the following:

Reproduced by permission of The Royal Society of Chemistry

and include a link to the paper on the Royal Society of Chemistry's website.

Please ensure that your co-authors are aware that you are including the paper in your thesis.

Regards,
Antonella

From: Julian [mailto:julian.kehrle@makro.ch.tum.de]
Sent: 19 June 2017 19:05
To: CONTRACTS-COPYRIGHT (shared) <Contracts-Copyright@rsc.org>
Subject: Copyright Permissions

Dear Ladies and Gentlemen,

We recently published a paper in RSC Nanoscale: J. Kehrle, S. Kaiser, T. K. Purkait, M. Winnacker, T. Helbich, S. I. Vagin, J. G. C. Veinot, B. Rieger, *Nanoscale* **2017** (DOI: 10.1039/C7NR02265D)

Unfortunately I cannot request the copyright permission for a complete print of the manuscript for my cumulative PhD thesis (see below). Thus I would kindly ask you for formal copyright permissions in this particular case.

Thank you in advance!

Sincerely,

Julian Kehrle

1

4.3. Superhydrophobic Silicon Nanocrystal – Silica Aerogel Hybrid Materials: Synthesis, Properties, and Sensing Application

4.3.1. Summary

Silica aerogels are attractive materials with good forecasts due to their unique properties and straightforward sol-gel preparation procedures. The combination of SiNCs with silica aerogels has good prospects in the biomedical field. It also has good scopes in coating materials and unprecedented sensing platforms. Thus, the aim of the investigation is to prepare SiNC/silica aerogel hybrid materials with 3, 5 and 8 nm SiNCs.

Triethoxyvinylsilane (TEVS) was chosen to be the linker between SiNCs and the gels. It was hydrosilylated on the SiNCs' surfaces by radical grafting *via* azobisisobutyronitril (AIBN). The purified TEVS-SiNCs were then intercalated into the aerogels by two approaches. TEVS-SiNCs were on one hand added to the acid catalyzed gelation procedure with the tetraethyl orthosilicate (TEOS) precursor. As ethanol and water were used as solvents, the TEVS-SiNCs were available as agglomerates. On the other hand, SiNCs were easily dispersed in toluene and subsequently added to the aged alcogel after it was subjected to the solvent exchange from ethanol/water to toluene. By this approach, SiNCs were 'washed into' the pores of the gels. After the solvent exchange procedure, remaining silanol groups were reacted with trimethylsilylchloride to achieve the water-repellent properties. X-ray photoelectron spectroscopy (XPS), scanning electron microscopy (SEM), and high-resolution transmission electron measurements (TEM) were used to prove the presence of SiNCs in the final aerogels. The SiNC crystallites with their characteristic lattice fringes could be detected. Nitrogen adsorption measurements and small angle X-ray scattering (SAXS) disclosed that the structure of the aerogels differed depending on the intercalation procedure of SiNCs. If the SiNCs were added to the network during the gelation process, a fractal network structure with many small pores and high surface areas (>1160 m^2g^{-1}) would form. In contrast, the "washed-in" SiNCs were in the pores because they reduced the pore radii and the pore volumes of the aerogels to below 1000 m^2g^{-1}. Although the aerogel networks were exposed to significant changes by the addition of SiNCs, the macroscopic properties remained similar. The different SiNC/silica aerogel composite materials exhibited superhydrophobic properties and emitted size dependent PL at ~700 nm, ~750-800 nm and ~900 nm for intercalated 3, 5 and 8 nm SiNCs, respectively. With these properties, the composite containing 3 nm "washed in" SiNCs were used to extract 3-nitrotoluene (3-NT) from water. Concentration dependent quenching of the SiNC PL was attributed to an accumulation effect of the toxic substance in the aerogel structure.

4.3.2. Bibliographic Data

Superhydrophobic Silicon Nanocrystal – Silica Aerogel Hybrid Materials: Synthesis, Properties, and Sensing Application

Langmuir **2018**.

Julian Kehrle, Tapas K. Purkait, Simon Kaiser, Konstantinos N. Raftopoulos, Malte Winnacker, Theresa Ludwig, Maryam Aghajamali, Marianne Hanzlik, Katia Rodewald, Tobias Helbich, Christine M. Papadakis, Jonathan G. C. Veinot and Bernhard Rieger

M.Sc. J. Kehrle, M.Sc. S. Kaiser, Dr. M. Winnacker, M.Sc. T. Ludwig, M.Sc. T. Helbich, Dipl.Min. K. Rodewald, Prof. Dr. B. Rieger

Catalysis Research Center/WACKER Lehrstuhl für Makromolekulare Chemie, Technische Universität München, Lichtenbergstraße 4, 85748 Garching bei München, Germany
E-mail: rieger@tum.de

Dr. Tapas K. Purkait:

Department of Chemistry, Johns Hopkins University, Baltimore, MD 21218, USA

B.Sc. M. Aghajamali, Prof. Dr. J. G. C. Veinot
Department of Chemistry, University of Alberta, 11227 Saskatchewan Drive, Edmonton, Alberta, T6G 2G2, Canada

E-Mail: jveinot@ualberta.ca

Dr. K. N. Raftopoulos, Prof. Dr. C. M. Papadakis

Physik weicher Materie, Technische Universität München, James-Frank-Str. 1, 85748 Garching bei München, Germany

Dr. M. Hanzlik

Division of Electron Microscopy, Technische Universität München, Lichtenbergstraße 4, 85748 Garching bei München, Germany

Direct Link: DOI 10.1021/acs.langmuir.7b03746

Supporting Information:

https://pubs.acs.org/doi/suppl/10.1021/acs.langmuir.7b03746/suppl_file/la7b03746_si_001.pdf

4.3.3. Reprint of the Original Manuscript

LANGMUIR Article
Cite This: *Langmuir* XXXX, XXX, XXX−XXX pubs.acs.org/Langmuir

Superhydrophobic Silicon Nanocrystal−Silica Aerogel Hybrid Materials: Synthesis, Properties, and Sensing Application

Julian Kehrle,[†] Tapas K. Purkait,[‡] Simon Kaiser,[†] Konstantinos N. Raftopoulos,[§] Malte Winnacker,[†] Theresa Ludwig,[†] Maryam Aghajamali,[∥] Marianne Hanzlik,[⊥] Katia Rodewald,[†] Tobias Helbich,[†] Christine M. Papadakis,[§] Jonathan G. C. Veinot,*[,∥] and Bernhard Rieger*[,†]

[†]Catalysis Research Center/WACKER Lehrstuhl für Makromolekulare Chemie and [⊥]Division of Electron Microscopy, Technische Universität München, Lichtenbergstraße 4, 85748 Garching bei München, Germany

[‡]Department of Chemistry, Johns Hopkins University, Baltimore, Maryland 21218, United States

[§]Physik Weicher Materie, Technische Universität München, James-Frank-Str. 1, 85748 Garching bei München, Germany

[∥]Department of Chemistry, University of Alberta, 11227 Saskatchewan Drive, Edmonton, Alberta T6G 2G2, Canada

Supporting Information

ABSTRACT: Silicon nanocrystals (SiNCs) are abundant and exhibit exquisitely tailorable optoelectronic properties. The incorporation of SiNCs into highly porous and lightweight substrates such as aerogels leads to hybrid materials possessing the attractive features of both materials. This study describes the covalent deposition of SiNCs on and intercalation into silica aerogels, explores the properties, and demonstrates a prototype sensing application of the composite material. SiNCs of different sizes were functionalized with triethoxyvinylsilane (TEVS) via a radical grafting approach and subsequently used for the synthesis of photoluminescent silica hybrids. The resulting SiNC-containing aerogels possess high porosities, SiNC-based size-dependent photoluminescence, transparency, and a superhydrophobic macroscopic surface. The materials were used to examine the photoluminescence response toward low concentrations of 3-nitrotoluene (270 μM), demonstrating their potential as a sensing platform for high-energy materials.

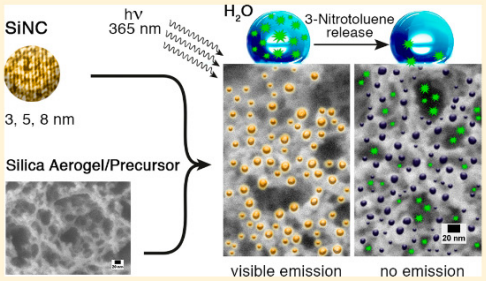

INTRODUCTION

Quantum dots (or semiconductor nanocrystals) of group II−VI and III−V elements (e.g., CdS, CdSe, and ZnS) exhibit bright photoluminescence (PL) arising from quantum confinement.[1−3] Although they provide impressive optoelectronic properties, these direct band gap semiconductors consist of toxic and rare elements.[4,5] By contrast, silicon is purported to be nontoxic, as well as the second most abundant element in the earth's crust; furthermore, silicon-based nanomaterials possess a tailorable optical response.[6,7] The formation of SiNC-based hybrids and composite materials presumably constitutes one of the most important aims in this rather young field of science and engineering, as it holds promise of preserving the properties of silicon nanocrystals (SiNCs) while inducing new features for potential applications; for example, we recently showed quenching of dodecyl-SiNC PL by low concentrations of high-energy organic compounds commonly used in explosives.[8−16]

Silica aerogels are a widely investigated class of materials, showing high porosity, transparency, and insulating properties.[17−20] Silica aerogel formation requires a sol−gel process—the hydrolysis and condensation of a tetraalkoxysilane precursor in acidic or basic conditions—to obtain alcogels.[21] Solvent exchange and appropriate drying procedures are applied to minimize capillary forces and prevent the gel from collapsing.[22,23] When using template-free procedures, the pores within the aerogel are disordered and appear in different size regimes. Although one-step-acid-catalyzed gelation leads to poorly branched gels with a linear micro- and meso-porous structure, alkaline conditions or a two-step acidic hydrolysis/condensation generates gels with enhanced cross-linking, a low microporosity, a broad distribution of larger pores, and a network of silica nanoparticles.[23−26] Silica aerogels provide surface areas of ~1000 m^2/g or higher and, in many cases, appear optically transparent because of their low Rayleigh scattering and low refractive index.[23] Furthermore, superhydrophobic aerogels can be obtained from surface functionalization with trimethylsilylchloride (TMSCl).[26,27] The pore structures and surface properties define the range of aerogel applications.[28] Because of their open pore network, they are

Received: October 29, 2017
Revised: February 15, 2018
Published: March 31, 2018

DOI: 10.1021/acs.langmuir.7b03746
Langmuir XXXX, XXX, XXX−XXX

useful for filtration,[29] as adsorbing media,[18] for waste containment,[23] as catalyst supports,[30] as thermal insulators,[31−33] and so forth.[34]

Of late, we have reported about silica aerogels containing SiNCs bearing various hydrophilic surface functionalities.[35] The resulting hybrids containing physically intercalated SiNCs brought new insights into the interaction of the SiNC surface polarity with silica aerogel structures.[36,37] Hybrids of this type hold promise in applications such as sensing[13] and could be used as energy-transfer materials,[38] evoked from the photothermic response of the SiNCs.[39] To address the requirements of the composite materials (e.g., lightweight, porosity, PL, hydrophobicity, etc.) a fundamental understanding of their formation process and properties is crucial. Herein, we present an essential study of the covalent intercalation of SiNCs of different sizes in superhydrophobic aerogels. We describe their properties and demonstrate how these hybrid materials could be used to detect low (i.e., 270 μM) concentrations of model high-energy materials in aqueous solutions.

RESULTS AND DISCUSSION

Triethoxyvinylsilane-SiNCs as Precursors. Hydride-terminated SiNCs were prepared following a well-established procedure.[40] Briefly, reductive thermolysis of hydrogen silsesquioxane (HSQ) was achieved upon heating to 1100 °C in N_2/H_2 (95%/5% v/v) for 1 h and a composite oxide containing SiNCs ($d \approx 3$ nm) was obtained. Subsequent heating at 1200 or 1300 °C in a flowing argon atmosphere induced SiNC growth to approximate diameters of 5 and 8 nm, respectively.[40] Alcoholic hydrofluoric acid etching was employed to liberate hydride-terminated SiNCs that were extracted into toluene.

In contrast to our previous studies,[35] in which hydrophilic SiNCs were physically mixed with silicon alkoxide precursors to produce hybrid aerogels, the intent of this investigation was to include SiNCs as covalently bonded structural components of the aerogel or to tether them to the surface. The chemical attachment of SiNCs is required to improve cross-linking of the hybrid material and to prevent the SiNCs from being washed-out by solvents or water. In this context, it was necessary to identify and install a surface group exhibiting appropriate reactivity. Vinylsilanes (e.g., triethoxyvinylsilane; TEVS) are attractive for this purpose; they bear hydrolyzable moieties capable of reacting with Si−OH groups, which is crucial to sol−gel chemistry or silica surface chemistry, and they have previously been tethered to SiNC surfaces.[37] The reaction of choice for derivatizing hydride-terminated SiNCs in the present study was radical-initiated surface functionalization, as it affords a well-defined surface coverage (Scheme 1a).[41,42]

Functionalized SiNCs were purified upon multiple solvent (toluene)/antisolvent (methanol) dispersion/precipitation steps. The resulting particles could be readily redispersed in toluene to provide a transparent "solution" that was stable indefinitely under inert atmosphere or a cloudy dispersion in ethanol that was stable for several hours. Both dispersions were used to intercalate the SiNCs into the gels (vide infra; Scheme 1b).

TEVS-functionalized SiNCs (TEVS-SiNCs) were evaluated using a variety of methods. The attenuated total reflectance infrared spectrum (ATR−IR) of hydride-terminated SiNCs was dominated by a distinctive Si−H feature at 2089 cm^{-1} (Figure 1a) that decreased significantly in intensity when SiNCs were modified with TEVS (Figure 1b). Other features in the IR

Scheme 1. (a) Functionalization of SiNCs with TEVS (Et: Ethyl), (b) Approaches Used for the Intercalation of SiNCs into the Alco- and Aerogels [(I) Intercalation of SiNCs in the Network by Addition Prior to Gelation; (II) Wash-In Approach into the Pores after Gelation]

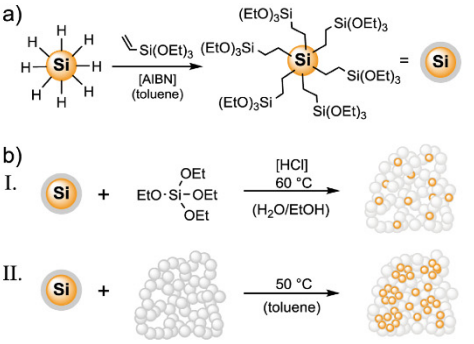

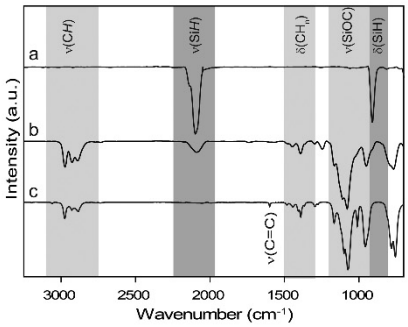

Figure 1. Representative ATR−IR spectra of (a) 3 nm hydride-terminated SiNCs, (b) TEVS-SiNCs, and (c) TEVS.

spectrum of the TEVS-modified SiNCs included symmetric C−H stretching vibrations (2973−2889 cm^{-1}), asymmetric CH_2 and CH_3 bending deriving from the ethylene bridge and the ethyl groups (1446 and 1391 cm^{-1}), and symmetric (1164, 1109, and 1078 cm^{-1}) and asymmetric (767 cm^{-1}) Si−O−C stretching; all spectral features were consistent with successful grafting of TEVS onto SiNC surfaces. The ^{1}H NMR spectrum of TEVS-SiNCs (Figure S1) provided qualitative information regarding organic surface moieties and was consistent with the conclusion that the SiNC surfaces were derivatized. Broad features attributed to ethoxy protons (4.17 and 1.54 ppm) as well as the ethylene bridge (0.41 ppm) between the SiNC and the ethoxy silane were identified. Similar spectral signatures were noted in the ATR−IR and ^{1}H NMR spectra of 5 and 8 nm SiNCs (Figures S1 and S2).

X-ray photoelectron spectroscopy (XPS) measurements of 3, 5, and 8 nm TEVS-SiNCs were performed and provided insights into the chemical nature (i.e., composition and oxidation state) of the nanomaterials. The survey spectrum showed that the SiNCs contained only Si, C, and O at the sensitivity of the XPS method (Figures S3−S5). The Si 2p spectral region of the high-resolution spectrum was dominated by two features—a Si(0) emission at 99.3 eV arising from the

DOI: 10.1021/acs.langmuir.7b03746
Langmuir XXXX, XXX, XXX−XXX

core and a feature assigned to Si(III) at 102.7 eV, which was attributed to surface-tethered triethoxysilyl groups. Smaller suboxide components were also noted.

To evaluate the particle dimensions, a variety of complementary methods were employed. Dynamic light scattering (DLS) measurements performed for toluene suspensions revealed hydrodynamic diameters of 5.6 ± 2.0, 7.8 ± 1.2, and 16.6 ± 3.4 nm (Figure S6). The hydrodynamic diameters suggest a small degree of aggregation of the SiNCs to dimers and oligomers in the solvent. Furthermore, solvated particle dimensions obtained by DLS include a solvation sphere and often overestimate nanoparticle core dimensions determined with other methods. Small-angle X-ray scattering (SAXS) of aggregated TEVS-SiNCs provides mean diameters of 2.9 ± 2.5, 5.2 ± 5.0, and 8.8 ± 3.3 nm for 3, 5, and 8 nm SiNCs, respectively (Supporting Information section 2.2.2). Transmission electron microscopy (TEM) indicated crystalline Si core sizes of 3.2 ± 0.6, 4.2 ± 0.6, and 7.1 ± 1.4 nm with 0.32 nm lattice fringes (Figure 2a–c; Figure S7). Consistent with the

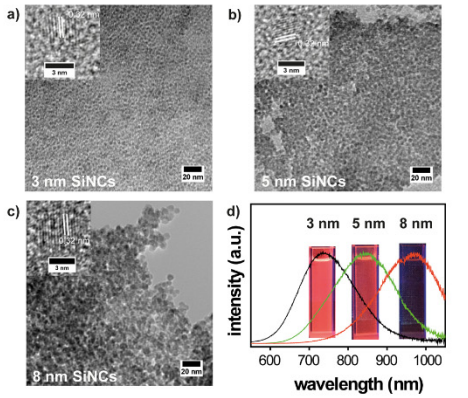

Figure 2. (a–c) TEM with high resolution (HR)-TEM images (inset) and (d) PL emission (in toluene) of 3, 5, and 8 nm TEVS-SiNCs (365 nm excitation).

observed particle sizes, present nanocrystals exhibited a size-dependent PL (i.e., $d \approx 3$, 5, and 8 nm TEVS-SiNCs show maxima at 733, 842, and 986 nm, respectively; Figure 2d).[42]

Preparation of SiNC–Silica Aerogel Hybrid Materials. To obtain functional aerogels, we intercalated SiNCs into alcogels using two approaches: either SiNCs were added by mixing with the ethanol prior to gelation (I, Scheme 1b) or gelation, aging, and solvent exchange to toluene were conducted in the absence of SiNCs, which were then washed in the lyogel (II, Scheme 1b). In all approaches, gelation and aging of lyogels were performed at 60 °C using 31/31/38 (v/v/v) tetraethyl orthosilicate/ethanol/HCl aq (at pH = 3). TEVS-SiNCs were well-suitable for hydrolysis and condensation reactions and were cross-linked by acid-catalyzed protocols (Supporting Information part 2.2). Ripening under acidic conditions in ethanol/water is a slow process involving several equilibrium reactions.[21] Thus, increased temperatures (60 °C) and long reaction times (40 h) were required to obtain the alcogels. After ripening, solvent exchange with toluene was performed and TMSCl was used as the reactant leading to a hydrophobic surface of the lyogel. The hydrophobic properties are required to allow the diffusion of organic molecules into the material pores and shield them from water. Aerogels were finally obtained by supercritical drying, using CO_2 as the solvent. Not surprisingly, the ATR–IR spectrum of the isolated aerogels is dominated by Si–O stretching vibrations at 1065 cm^{-1} and C–H stretching modes at 2962 cm^{-1}, which we confidently attribute to the Si–CH_3 groups (Figure S18a). Thermogravimetric analysis (TGA) measurements of all aerogel samples suggested a low influence of SiNCs on the thermal stabilities of the aerogel system (Figure S16).

Aerogels were prepared using 3, 5, and 8 nm SiNCs and in the absence of SiNCs. As expected, no Si(0) was detected in the Si 2p high-resolution XPS spectrum of the SiNC-free aerogel [Figure 3a(i)]; however, a clear Si(0) feature at 99.3 eV was noted for all other samples with intercalated SiNCs [Figure 3a(ii,iii)]. In all samples, Si(II) and Si(III) features arising from silicon suboxides and the surface TMS groups were observed at 102.7 and 101.8 eV; Si(IV) at 103.6 eV could be assigned to the aerogel network.

To analyze the surface structures, HIM and SEM were performed (Figure 3b,c). HIM showed smooth featureless surfaces for the SiNC-free sample [Figure 3b(i)] and the aerogel containing incorporated 8 nm SiNCs [I; Figure 3b(ii)]; the surface of aerogels in which SiNCs were "washed-in" (II) appeared rough and porous [Figure 3b(iii)]. In SEM images, the SiNC-free aerogel exhibits an open pore network [Figure 3c(i); Figures S19, S22, and S24]. If TEVS-SiNCs were added before gelation (I), the aerogel was similar to the SiNC-free system (Figure 3c(ii); Figures S20, S23, and S25).

Time-resolved DLS measurements during the gelation process including TEVS-SiNCs demonstrate that the progress of gelation was accelerated by the presence of SiNCs, which act as "seeds" (Figure S15; Supporting Information part 2.3.1). Although SEM analysis of samples prepared when SiNCs were added before gelation (I) did not result in major influences on the aerogel structures, washed-in SiNCs (II) had an influence on the pore radii of the aerogel composites [vide infra; Figure 3c(iii); Figure S21]. The SEM images suggested free SiNCs attached to aerogel surfaces (II).

Dark-field (DF)-TEM and HR-TEM were performed to confirm the presence of SiNCs in the aerogels (Figure 4). We found crystalline areas in the DF-TEM of the aerogels containing 8 nm SiNCs (Figure 4a); HR-TEM confirmed lattice fringes of 0.32 nm consistent with the literature value for Si(111).[43] With the decreasing SiNC size, DF- as well as HR-TEM of 5 nm SiNCs on silica aerogel still showed nanocrystallites, although with lower contrasts. A region of 3 nm SiNCs (II) was observed by applying annular dark-field scanning transmission electron microscopy (ADF-STEM) to a xerogel sample obtained by drying under ambient conditions [Figure 4a(iii)]. The HR-TEM of the observed region again demonstrates crystallites with lattice fringes of 0.32 nm,[43] thus evidencing that SiNCs were located on the air-dried gel [Figure 4b(iii)]. Once the SiNCs were added prior to gelation (I), SiNCs were inaccessible to TEM analysis, as they were probably covered by the silica matrix.

Structure and Properties of the Hybrid Materials. To analyze the pore structure of the aerogels, nitrogen adsorption measurements were performed (Figure 5; Figures S27, and S28). All adsorption curves show type-IV isotherms with hysteresis loops assigned to H1 and H2 types.[44] H1 behavior suggests cylinder-like pore channels. However, these are

DOI: 10.1021/acs.langmuir.7b03746
Langmuir XXXX, XXX, XXX–XXX

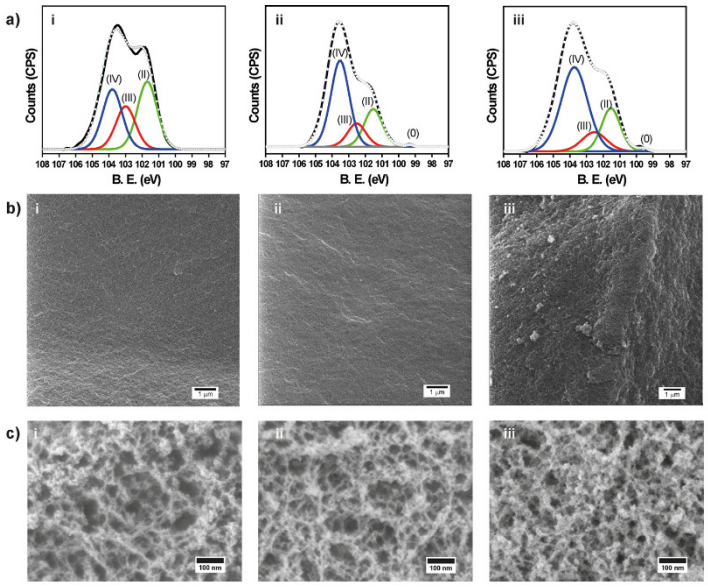

Figure 3. (a) HR-XPS spectra of the Si 2p orbital (fitting results are shown for the silicon spectrum with Si $2p_{3/2}$ signal; Si $2p_{1/2}$ signals have been omitted for clarity) (b) helium-ion microscopy (HIM) and (c) scanning electron microscopy (SEM) images of aerogel surfaces without SiNCs (i), with 8 nm SiNCs added before gelation (ii) and with 8 nm SiNCs washed in the lyogel previous to hydrophobizing and supercritical drying (iii).

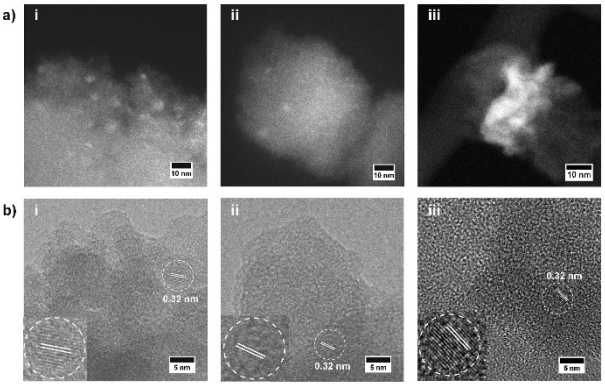

Figure 4. (a) DF-TEM and (b) HR-TEM images (inset: magnification of the silicon lattice fringes) of aerogels containing 8 nm (i) and 5 nm SiNCs (ii). (i,ii) were dried using supercritical CO_2. To obtain the 3 nm SiNCs in structure (iii), a alcogel was air-dried and imaged by ADF-STEM instead. Structures are obtained by the wash-in approach (II).

partially blocked or form cavities, which can be observed from the delay in the desorption toward lower relative pressure (H2). Whenever aerogels were prepared by adding SiNCs before the gelation step (I), the isotherms were similar to the SiNC-free aerogel but the pore blocking seems to be more dominant (Figure 5b). If SiNCs were added by applying the wash-in approach (II), the hysteresis loops generally narrowed suggesting a change toward greater uniformity, structural changes, or the reduction of pore blocking (Figure 5c). This is consistent with particles residing in the aerogel pores.

Using the Barrett–Joyner–Halenda model of the desorption branch, pore volumes and surface areas of the present aerogel samples were determined (Table 1). The reference SiNC-free aerogel exhibited a pore-size distribution from 0 to 25 nm with a mean pore radius of 4.3 nm, a total pore volume of 3.5 cm^3/g, and a total surface area of 1110 m^2/g, which is comparable to literature known aerogels.[20] Aerogels containing 5 and 8 nm SiNCs added before gelation (I) exhibited smaller mesopores than the reference (Table 1, Figures 5d and S29a). The pore volume of the silica aerogel with 3 nm SiNCs added during

DOI: 10.1021/acs.langmuir.7b03746
Langmuir XXXX, XXX, XXX–XXX

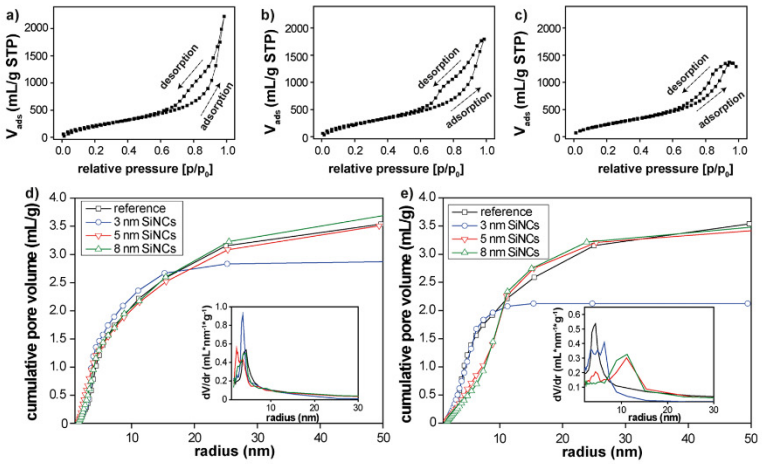

Figure 5. Nitrogen adsorption and desorption isotherms of (a) SiNC-free aerogel, (b) aerogel containing 3 nm SiNCs added prior to gelation (I) and (c) the aerogel containing 3 nm SiNCs washed in after gelation (II). The cumulative pore volumes and the pore-volume distributions (insets) are given for aerogels containing 3, 5, and 8 nm SiNCs in the network structure (d, I) and in the pores (e, II).

Table 1. Summary of Nitrogen Adsorption Analysis [Mean Pore Radii (R^P), Total Pore Volume (V^P), and Specific Surface Areas (A^P)] and SAXS Analysis (Correlation and Contour Lengths) of Reference Aerogel Compared to Aerogels Containing SiNCs Added to Gelation (I) and Washed-In (II)

	SiNC-free reference	3 nm (I)	5 nm (I)	8 nm (I)	3 nm (II)	5 nm (II)	8 nm (II)
R^P (nm)	4.3	3.6	3.6/2.1	3.6/2.1	6.2	11.0/4.2	11.0
V^P (cm^3/g)	3.6	2.9	3.4	3.4	2.1	3.4	3.5
A^P (m^2/g)	1110	1215	1218	1157	998	876	847
correlation length (nm)	9.76 ± 0.05	8.56 ± 0.05	9.47 ± 0.12	9.63 ± 0.12	8.77 ± 0.06	11.60 ± 0.10	10.14 ± 0.06
contour length (nm)	5.31 ± 0.03	3.39 ± 0.03	5.03 ± 0.06	4.48 ± 0.03	5.06 ± 0.03	3.45 ± 0.03	3.75 ± 0.004

gelation (I) was mainly limited to small mesopores with a narrow size distribution of pores with ~20 nm radii. The behavior is similar, if the adsorption branch of the hysteresis is regarded (Figure S29a), albeit for the adsorption branch mesopores with 15 nm of radius are more dominant. Generally, the aerogel surface area increased when smaller SiNCs were used (Table 1; I). Thus, the inclusion of SiNCs into the aerogel network during the gelation process (I) led to an increasing number of smaller pores which contributed to a high surface area, presumably arising from strong cross-linking by SiNCs (Figure S29c). Furthermore, the reduced pore surface of the adsorption branch indicates smaller pores, with delayed nitrogen adsorption (Figure S29e; vide infra).

Larger deviations from the SiNC-free sample are observed for aerogels containing washed-in TEVS-SiNCs (II; Figure 5e). Samples containing 3 nm SiNCs displayed smaller pore volumes (2.1 cm^3/g), larger mean pore radii (6.2 nm) (Figures 5e and S29b inset; Table 1), and no pores above R^P = 15 nm. Aerogels containing 5 and 8 nm SiNCs exhibited a main pore distribution between 6.3 and 15.1 nm (R^P) that we attribute to the shrinkage of bigger pores and blocking of small pores by the SiNCs; this also led to a decrease in the pore volume (Table 1, Figure S29b). The analysis of the adsorption branches again yields lower surface areas in comparison to the desorption branches. This indicates a significant number of small pores albeit for the aerogels with washed-in SiNCs they are not as dominant as in the aerogels containing SiNCs added to gelation, which reside in the network.

To gain better insights into the nanostructure of the synthesized aerogels, SAXS analysis was performed (Supporting Information part 2.3.7). The SAXS curves could be best-fitted with a model describing flexible cylinders.[45] This way, fractal dimensions of about 2.5 were obtained for all aerogels (Table S3).[46] The correlation length, i.e., the mean distance of the fractal structure fragments forming the microstructures was between 8.6 and 9.6 nm for aerogels containing SiNCs in the network, which were added before gelation (I, Table 1; Figure S30). The fractal units consisted of a network of flexible cylinders with an average contour length of 3.4−5.0 nm, which corresponds roughly to the size of one SiNC. Furthermore, Kuhn lengths and cylinder radii given for all samples were assigned to a few oligomerized units for all aerogel samples (Figure S31, Kuhn lengths ≈ 0.2 nm, cylinder radii ≈ 0.4 nm). The reduction in correlation and contour lengths of the aerogels with 3 nm SiNCs added before gelation (Table 1, I) correlates with the decrease in pore volume as observed with nitrogen adsorption measurements (Figure 5). The same effect could also be seen for 5 and 8 nm SiNCs.

Washed-in 3 nm SiNCs after gelation (II) reduced the correlation and the contour lengths of the respective aerogel (Table 1). However, for aerogel containing washed-in 5 and 8 nm SiNCs after gelation (II), higher correlation lengths and significantly reduced contour lengths were analyzed. Because of

DOI: 10.1021/acs.langmuir.7b03746
Langmuir XXXX, XXX, XXX−XXX

smaller sizes, 5 nm SiNCs are presumably drawn deeper into the pores than 8 nm SiNCs, leading to a more compact, but less homogeneous network; this would account for the short contour length. These results correlate with nitrogen adsorption (Figure 5), showing a high penetration of the pores with 3 nm SiNCs, a partial penetration with 5 nm SiNCs, and a low penetration with 8 nm SiNCs.

The optical properties of the present hybrid materials were also investigated. When following approach I, aerogels became cloudy and brittle, presumably because of remaining SiNC-aggregates and cracks in the network. The SiNC-free aerogel as well as those prepared using approach II were more transparent when viewed against a bright background (Figure 6a). This

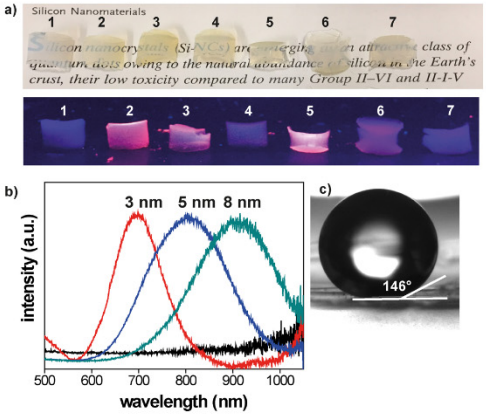

Figure 6. (a) Images of the aerogel−SiNC composites (1, reference; 2−4, aerogels containing washed-in 3, 5, and 8 nm SiNCs obtained by approach II; 5−7, aerogels with directly intercalated 3, 5, and 8 nm SiNCs according to approach I) under ambient (top) and 365 nm UV-light (bottom), (b) PL of aerogel−SiNC composites obtained from the wash-in approach (365 nm excitation wavelength). (c) Image of the drop shape on the aerogel.

presumably results from negligible light scattering because of a low concentration of small silica particles and small SiNCs.[23,42] All SiNC-containing aerogels showed SiNC size-dependent photoluminescence (Figure 6b/Figure S26). The PL spectra of the SiNCs attached to silica aerogels exhibited blue shifts compared with free SiNCs (vide supra) that are reasonably attributed to some oxidation resulting from the processing procedures.[47,48] This effect increased when SiNCs were directly added to the gelation (I, PL^{3nm} = 690 nm; PL^{5nm} = 753 nm; PL^{8nm} = 898 nm) and thus exposed to these conditions for a longer time. Using the wash-in approach (II), HCl was released from the reaction of alcogel OH groups with TMSCl, thus leading to weaker PL shifts (PL^{3nm} = 698 nm; PL^{5nm} = 807 nm; PL^{8nm} = 920 nm). In all cases, the size-dependent PL properties of the SiNC were maintained.[18]

The present aerogels were rendered hydrophobic by bonding TMS moieties to their surfaces. In drop shape analysis (3 μL water), the SiNC-free aerogel shows a static contact angle of 139.0°. Because of a higher density of the hydrophobic silane and lower pore radii when SiNCs were added to the gelation procedures (I; Figure S32), hydrophobicity of the respective aerogels was enhanced and water contact angles of 141.8° (8 nm SiNCs), 146.3° (5 nm SiNCs; Figure 6c), and 148° (3 nm SiNCs) were observed. By contrast, contact angles decreased to 130.4° (8 nm SiNCs), 130.3° (5 nm SiNCs), and 130.5° (3 nm SiNCs) for aerogel−SiNC composite materials with the use of the wash-in approach after gelation (II) (II; Figure S33). This can be attributed to changes in surface roughness [vide supra, Figure 3(iii)] and in the surface energy arising from surface-tethered SiNCs.[49] However, all aerogels exhibited a super-hydrophobic character close to flat surfaces coated with perfluorodecyl-modified SiNCs (168°).[14] From this change in the surface polarity, ready adsorption of organic compounds in the pores was facilitated. Highlighting the ability of the present aerogels to "take up" organic analytes, a representative TGA of a xylene-soaked aerogel (reference) shows a weight loss of 82.1%, whereas negligible weight loss was noted when the aerogel was exposed to water for the same period and then evaluated using TGA (Figure S17).

3-Nitrotoluene Sensing and Accumulation by a Hybrid SiNC−Silica Aerogel. The application of silica aerogels as sensors for nucleotides, oxygen, humidity, and bacteria has been demonstrated earlier.[22,50−52] However, in such examples either concentrated analytes were used or complex devices had to be constructed to obtain a sensing performance. The present hydrophobic SiNC−silica aerogel composites hold potential as simple optically responsive materials in sensors for nitroaromatic species without the requirement of post-treatment. As a proof-of-concept demonstration of this capability, we chose to explore the application of aerogel−SiNC composites obtained from the wash-in approach (II) with 3 nm SiNCs because the nanocrystals were located on the pore surfaces and emitted a bright red PL (698 nm, vide supra).

Because of the unpolar features of the composite, we first performed PL quenching with 3-nitrotoluene (3-NT) solutions in toluene (Figure 7a). We observed quenching of the PL increasing with the 3-NT concentration, which is consistent with the quenching of the PL of dodecyl-SiNCs as shown in the literature.[13] On this basis, we tested the composite material as an adsorbent and sensor for a diluted solution of 3-NT in water (270 μM ≙ 37 mg/L; maximum solubility of 3-NT in water is 0.5 g/L).[53] Thus, a 10 mg piece of the silica aerogel/3 nm SiNC composite was added to the 3-NT/water solution. Because of its low density and hydrophobic character, the silica aerogel floated on of the solution. In this configuration, the quench of the PL intensity occurred to be time-dependent. After 8 h, the PL was quenched to a minimum level by accumulation of 3-NT and no further changes occurred (Figure 7b). The time-resolved study was then followed by the determination of the symmetric and the asymmetric stretching vibrations of 3-NT at 1352 and 1531 cm^{-1} in ATR−IR (Figure 7c; Figure S18b). The outer surface of the composite was dried prior to each measurement to exclude surface impurities indicating that 3-NT had steadily been soaked in the gel. After two hours of exposure to the solution, the silica aerogel/3 nm SiNC composite showed a small nitroaromatic signal which increased with time (Figure 7, gray bar). Thus, we propose that 3-NT was transported into the aerogel composite through the coaction of capillary forces and the adsorption of 3-NT vapor in the composite. The accumulation of the 3-NT in the aerogel initiated the PL quenching, which proceeded uniformly through the hybrid material. To support this proposal, TGA was performed. The silica aerogel−SiNC composite material was measured after 8 h of soaking in aqueous 3-NT (and surface

DOI: 10.1021/acs.langmuir.7b03746
Langmuir XXXX, XXX, XXX−XXX

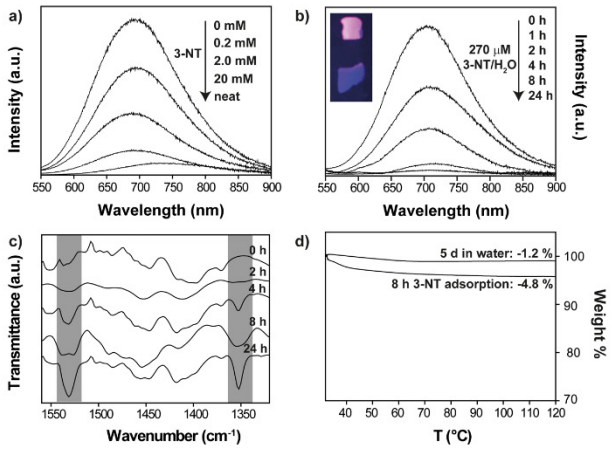

Figure 7. (a) PL measurement (365 nm excitation) of a silica aerogel/3 nm SiNC nanocomposite exposed to various concentrations of 3-NT in toluene. (b) Time-resolved PL quench using 40 mL of a 270 μM solution of 3-NT in water. Accumulation of 3-NT in the aerogel observed by (c) ATR−IR spectroscopy (the highlighted bands at 1352 and 1531 cm^{-1} are the symmetric and asymmetric stretching vibrations of the NO bond) and (d) TGA curves of the SiNC−silica aerogel composite material after 5 d in water and 8 h in a 270 μM solution of 3-NT in water.

drying afterward) and a reference was analyzed after 5 d in water (Figure 7d). Given the hydrophobic nature, the TGA demonstrates that adsorbed 3-NT led to a significantly higher weight loss than that could be achieved by the control sample in pure water. Thus, a significant uptake of the organic analyte in the hybrid material occurred, while water was shielded. 3-NT was also desorbed from the dried aerogel sample by treatment with pentane. Gas chromatography−mass spectrometry analysis of the solution showed the signal of 3-NT (m/z = 137 g/mol) (10.8 min retention time; Figures S34 and S35). After desorption of 3-NT from the aerogel pores, PL returned. This demonstrates the reversibility of the quenching process. Hence, the hybrid material is promising for the adsorption and simultaneous time, or concentration-resolved sensing of certain organic analytes (e.g., nitroaromatics) leading to potential applications in water purification or in the recovery of organic substances from water.

■ CONCLUSIONS

The preparation of SiNC-based composite materials enabled the combination of unique properties and thus is of great importance for potential applications such as sensing or catalysis. In this paper, we present a study contributing to the design of a hybrid material containing SiNCs covalently attached to silica aerogels. Furthermore, the influence of various preparation methods was examined and the potential application of the hybrid materials as a sensor was demonstrated.

Photoluminescent 3, 5, and 8 nm SiNCs obtained from thermal HSQ treatment were modified by TEVS grafting and subsequently linked to silica gels following two approaches: SiNCs were directly added to the gelation procedure or SiNCs were washed-in afterward. Both approaches were followed by supercritical drying.

The addition of SiNCs to the gelation resulted in an intercalation into the silica network and narrowing of the pores by enhanced cross-linking from the nanodomains. By contrast, if SiNCs were washed in the alcogel, crystallites were observed on the gel surfaces indicating that the SiNCs were located on the pore surfaces; an effect on the pore arrangement was demonstrated by nitrogen adsorption and SAXS analysis. Although both approaches—gelation with SiNCs and washing SiNCs into the aerogels—exhibited different structures, size-dependent optical properties of the SiNCs were majorly sustained.

Because of their high water-repellent properties and the bright PL, an aerogel/3 nm SiNC composite material was tested for its capacity of sensing of minimal concentrations of 3-NT in water. SiNC-PL quenching has been found to occur because of a simultaneous accumulation effect of 3-NT in the aerogel, demonstrating the capacity of the hybrid aerogels in sensing applications. If the properties of both materials are combined, the composite materials might play promising roles in many fields of application, such as catalysis, energy conversion, bioanalytics, or in the detection of environmental pollutants. To obtain a useful material for these applications, future research is focusing on the illumination of the molecule adsorption mechanism, the sensitivity of the hybrid materials toward molecules with different polarities, and the impact of SiNC−silica aerogel pore sizes to the sensing efficiencies.

■ ASSOCIATED CONTENT

Supporting Information

The Supporting Information is available free of charge on the ACS Publications website at DOI: 10.1021/acs.langmuir.7b03746.

Experimental procedures, general information supporting analysis data, and explanation on SAXS data (PDF)

■ AUTHOR INFORMATION

Corresponding Authors

*E-mail: jveinot@ualberta.ca (J.G.C.V.).
*E-mail: rieger@tum.de (B.R.).

DOI: 10.1021/acs.langmuir.7b03746
Langmuir XXXX, XXX, XXX−XXX

ORCID
Christine M. Papadakis: 0000-0002-7098-3458
Jonathan G. C. Veinot: 0000-0001-7511-510X
Bernhard Rieger: 0000-0002-0023-884X

Author Contributions

The manuscript was written through contributions of all authors. All authors have given approval to the final version of the manuscript.

Notes

The authors declare no competing financial interest.

■ ACKNOWLEDGMENTS

IRTG 2022/ATUMS (DFG) and NSERC are thanked gratefully for research funding. J.K. thanks TUM Graduate School for financial support. T.L. gratefully acknowledges funding from Clariant AG. T.H. thanks Studienstiftung des deutschen Volkes for the financial support. Dr. Carsten Troll is thanked for support with the technical equipment. Franz Koschany and Ursula Herrmann are acknowledged for performing nitrogen adsorption measurements. The staff of the UofA NanoFab are thanked for their assistance with XPS and HIM analyses. We thank Dr. Kai Cui at National Institute for Nanotechnology (NINT), University of Alberta for HR-TEM analysis. K.N.R. gratefully acknowledges the financial support by the TUM Universitätsstiftung. Jan David Schütz is acknowledged for the design of the TOC graphic. We thank our groups for helpful discussions.

■ ABBREVIATIONS

3-NT, 3-nitrotoluene; DF-TEM, dark field transmission electron microscope; HF, hydrofluoric acid; HR-TEM, high resolution TEM; HSQ, hydrogen silsesquioxane; PL, photoluminescence; SAXS, small angle X-ray scattering; SEM, scanning electron microscopy; SiNC, silicon nanocrystal; STEM, scanning tunneling electron microscopy; TEOS, tetraethyl orthosilicate; TEVS, triethoxyvinylsilane; TGA, thermogravimetric analysis; TMS, trimethylsilyl; XPS, X-ray photoelectron spectroscopy

■ REFERENCES

(1) Yoffe, A. D. Semiconductor quantum dots and related systems: Electronic, optical, luminescence and related properties of low dimensional systems. *Adv. Phys.* **2001**, *50*, 1−208.
(2) Alivisatos, A. P. Semiconductor Clusters, Nanocrystals, and Quantum Dots. *Science* **1996**, *271*, 933−937.
(3) Brus, L. Quantum crystallites and nonlinear optics. *Appl. Phys. A: Solids Surf.* **1991**, *53*, 465−474.
(4) Hardman, R. A Toxicologic Review of Quantum Dots: Toxicity Depends on Physicochemical and Environmental Factors. *Environ. Health Perspect.* **2006**, *114*, 165−172.
(5) Derfus, A. M.; Chan, W. C. W.; Bhatia, S. N. Probing the Cytotoxicity of Semiconductor Quantum Dots. *Nano Lett.* **2004**, *4*, 11−18.
(6) Ding, Z.; Quinn, B. M.; Haram, S. K.; Pell, L. E.; Korgel, B. A.; Bard, A. J. Electrochemistry and Electrogenerated Chemiluminescence from Silicon Nanocrystal Quantum Dots. *Science* **2002**, *296*, 1293−1297.
(7) Erogbogbo, F.; Yong, K.-T.; Roy, I.; Xu, G.; Prasad, P. N.; Swihart, M. T. Biocompatible Luminescent Silicon Quantum Dots for Imaging of Cancer Cells. *ACS Nano* **2008**, *2*, 873−878.
(8) Qian, C.; Sun, W.; Wang, L.; Chen, C.; Liao, K.; Wang, W.; Jia, J.; Hatton, B. D.; Casillas, G.; Kurylowicz, M.; Yip, C. M.; Mastronardi, M. L.; Ozin, G. A. Non-wettable, oxidation-stable, brightly luminescent, perfluorodecyl-capped silicon nanocrystal film. *J. Am. Chem. Soc.* **2014**, *136*, 15849−15852.
(9) Gonzalez, C. M.; Iqbal, M.; Dasog, M.; Piercey, D. G.; Lockwood, R.; Klapötke, T. M.; Veinot, J. G. C. Detection of high-energy compounds using photoluminescent silicon nanocrystal paper based sensors. *Nanoscale* **2014**, *6*, 2608−2612.
(10) Gonzalez, C. M.; Veinot, J. G. C. Silicon nanocrystals for the development of sensing platforms. *J. Mater. Chem. C* **2016**, *4*, 4836−4846.
(11) Nguyen, A.; Gonzalez, C. M.; Sinelnikov, R.; Newman, W.; Sun, S.; Lockwood, R.; Veinot, J. G. C.; Meldrum, A. Detection of nitroaromatics in the solid, solution, and vapor phases using silicon quantum dot sensors. *Nanotechnology* **2016**, *27*, 105501.
(12) Höhlein, I. M. D.; Werz, P. D. L.; Veinot, J. G. C.; Rieger, B. Photoluminescent silicon nanocrystal-polymer hybrid materials via surface initiated reversible addition-fragmentation chain transfer (RAFT) polymerization. *Nanoscale* **2015**, *7*, 7811−7818.
(13) Kehrle, J.; Helbich, T.; Iqbal, M.; Hadidi, L.; Veinot, J. G. C.; Rieger, B. Surface-Initiated Group-Transfer Polymerization − A Catalytic Approach to Stimuli-Responsive Silicon Nanocrystal Hybrid Materials. *MRS Online Proc. Libr.* **2015**, *1770*, 13−18.
(14) Kehrle, J.; Höhlein, I. M. D.; Yang, Z.; Jochem, A.-R.; Helbich, T.; Kraus, T.; Veinot, J. G. C.; Rieger, B. Thermoresponsive and photoluminescent hybrid silicon nanoparticles by surface-initiated group transfer polymerization of diethyl vinylphosphonate. *Angew. Chem., Int. Ed.* **2014**, *53*, 12494−12497.
(15) Hessel, C. M.; Reid, D.; Panthani, M. G.; Rasch, M. R.; Goodfellow, B. W.; Wei, J.; Fujii, H.; Akhavan, V.; Korgel, B. A. Synthesis of Ligand-Stabilized Silicon Nanocrystals with Size-Dependent Photoluminescence Spanning Visible to Near-Infrared Wavelengths. *Chem. Mater.* **2012**, *24*, 393−401.
(16) Dasog, M.; Kehrle, J.; Rieger, B.; Veinot, J. G. C. Silicon Nanocrystals and Silicon-Polymer Hybrids: Synthesis, Surface Engineering, and Applications. *Angew. Chem., Int. Ed.* **2016**, *55*, 2322−2339.
(17) Rubin, M.; Lampert, C. M. Transparent silica aerogels for window insulation. *Sol. Energy Mater.* **1983**, *7*, 393−400.
(18) *Aerogels Handbook*; Aegerter, A. M., Leventis, N., Koebel, M. M., Eds.; Springer New York: NY, 2011.
(19) Hüsing, N.; Schubert, U. Aerogele−luftige materialien: Chemie, struktur und eigenschaften. *Angew. Chem.* **1998**, *110*, 22−47.
(20) Gesser, H. D.; Goswami, P. C. Aerogels and related porous materials. *Chem. Rev.* **1989**, *89*, 765−788.
(21) Brinker, C. J. Hydrolysis and condensation of silicates: Effects on structure. *J. Non-Cryst. Solids* **1988**, *100*, 31−50.
(22) Soleimani Dorcheh, A.; Abbasi, M. H. Silica aerogel; synthesis, properties and characterization. *J. Mater. Process. Technol.* **2008**, *199*, 10−26.
(23) Gurav, J. L.; Jung, I.-K.; Park, H.-H.; Kang, E. S.; Nadargi, D. Y. Silica Aerogel: Synthesis and Applications. *J. Nanomater.* **2010**, *2010*, 1.
(24) Venkateswara Rao, A.; Bhagat, S. D. Synthesis and physical properties of TEOS-based silica aerogels prepared by two step (acid−base) sol−gel process. *Solid State Sci.* **2004**, *6*, 945−952.
(25) Venkateswara Rao, A.; Haranath, D. Effect of methyltrimethoxysilane as a synthesis component on the hydrophobicity and some physical properties of silica aerogels. *Microporous Mesoporous Mater.* **1999**, *30*, 267−273.
(26) Venkateswara Rao, A.; Kulkarni, M. M.; Amalnerkar, D. P.; Seth, T. Superhydrophobic silica aerogels based on methyltrimethoxysilane precursor. *J. Non-Cryst. Solids* **2003**, *330*, 187−195.
(27) Malfait, W. J.; Zhao, S.; Verel, R.; Iswar, S.; Rentsch, D.; Fener, R.; Zhang, Y.; Milow, B.; Koebel, M. M. Surface Chemistry of Hydrophobic Silica Aerogels. *Chem. Mater.* **2015**, *27*, 6737−6745.
(28) Akimov, Y. K. Fields of application of aerogels (review). *Instrum. Exp. Tech.* **2003**, *46*, 287−299.
(29) Cooper, D. W. Theoretical study of a new material for filters: aerogels. *Part. Sci. Technol.* **1989**, *7*, 371.

DOI: 10.1021/acs.langmuir.7b03746
Langmuir XXXX, XXX, XXX−XXX

(30) Schneider, M.; Baiker, A. Aerogels in Catalysis. *Catal. Rev.: Sci. Eng.* **1995**, *37*, 515−556.
(31) Baetens, R.; Jelle, B. P.; Gustavsen, A. Aerogel insulation for building applications: a state-of-the-art review. *Energy Build.* **2011**, *43*, 761−769.
(32) Reim, M.; Körner, W.; Manara, J.; Korder, S.; Arduini-Schuster, M.; Ebert, H.-P.; Fricke, J. Silica aerogel granulate material for thermal insulation and daylighting. *Sol. Energy* **2005**, *79*, 131−139.
(33) Warner, J. H.; Rubinsztein-Dunlop, H.; Tilley, R. D. Surface morphology dependent photoluminescence from colloidal silicon nanocrystals. *J. Phys. Chem. B* **2005**, *109*, 19064−19067.
(34) Schmidt, M.; Schwertfeger, F. Applications for silica aerogel products. *J. Non-Cryst. Solids* **1998**, *225*, 364−368.
(35) Aghajamali, M.; Iqbal, M.; Purkait, T. K.; Hadidi, L.; Sinelnikov, R.; Veinot, J. G. C. Synthesis and Properties of Luminescent Silicon Nanocrystal/Silica Aerogel Hybrid Materials. *Chem. Mater.* **2016**, *28*, 3877−3886.
(36) Höhlein, I. M. D.; Kehrle, J.; Purkait, T. K.; Veinot, J. G. C.; Rieger, B. Photoluminescent silicon nanocrystals with chlorosilane surfaces - synthesis and reactivity. *Nanoscale* **2015**, *7*, 914−918.
(37) Guan, M.; Wang, W.; Henderson, E. J.; Dag, Ö.; Kübel, C.; Chakravadhanula, V. S. K.; Rinck, J.; Moudrakovski, I. L.; Thomson, J.; McDowell, J.; Powell, A. K.; Zhang, H.; Ozin, G. A. Assembling photoluminescent silicon nanocrystals into periodic mesoporous organosilica. *J. Am. Chem. Soc.* **2012**, *134*, 8439−8446.
(38) Regli, S.; Kelly, J. A.; Shukaliak, A. M.; Veinot, J. G. C. Photothermal Response of Photoluminescent Silicon Nanocrystals. *J. Phys. Chem. Lett.* **2012**, *3*, 1793−1797.
(39) Kelly, J. A.; Shukaliak, A. M.; Fleischauer, M. D.; Veinot, J. G. C. Size-Dependent Reactivity in Hydrosilylation of Silicon Nanocrystals. *J. Am. Chem. Soc.* **2011**, *133*, 9564−9571.
(40) Hessel, C. M.; Henderson, E. J.; Veinot, J. G. C. Hydrogen Silsesquioxane: A Molecular Precursor for Nanocrystalline Si−SiO 2 Composites and Freestanding Hydride-Surface-Terminated Silicon Nanoparticles. *Chem. Mater.* **2006**, *18*, 6139−6146.
(41) Kehrle, J.; Kaiser, S.; Purkait, T. K.; Winnacker, M.; Helbich, T.; Vagin, S.; Veinot, J. G. C.; Rieger, B. In-Situ IR-Spectroscopy as Tool for Monitoring the Radical Hydrosilylation Process on Silicon Nanocrystal Surfaces. *Nanoscale* **2017**, *9*, 8489−8495.
(42) Yang, Z.; Gonzalez, C. M.; Purkait, T. K.; Iqbal, M.; Meldrum, A.; Veinot, J. G. C. Radical Initiated Hydrosilylation on Silicon Nanocrystal Surfaces: An Evaluation of Functional Group Tolerance and Mechanistic Study. *Langmuir* **2015**, *31*, 10540−10548.
(43) Dasog, M.; Yang, Z.; Regli, S.; Atkins, T. M.; Faramus, A.; Singh, M. P.; Muthuswamy, E.; Kauzlarich, S. M.; Tilley, R. D.; Veinot, J. G. C. Chemical Insight into the Origin of Red and Blue Photoluminescence Arising from Freestanding Silicon Nanocrystals. *ACS Nano* **2013**, *7*, 2676−2685.
(44) Thommes, M.; Kaneko, K.; Neimark, A. V.; Olivier, J. P.; Rodriguez-Reinoso, F.; Rouquerol, J.; Sing, K. S. W. Physisorption of gases, with special reference to the evaluation of surface area and pore size distribution (IUPAC Technical Report). *Pure Appl. Chem.* **2015**, *87*, 1051−1069.
(45) Kumari, H.; Armitage, S. E.; Kline, S. R.; Damodaran, K. K.; Kennedy, S. R.; Atwood, J. L.; Steed, J. W. Fluorous 'ponytails' lead to strong gelators showing thermally induced structure evolution. *Soft Matter* **2015**, *11*, 8471−8478.
(46) Kline, S. R. Reduction and Analysis of SANS and USANS Data Using IGOR Pro. *J. Appl. Crystallogr.* **2006**, *39*, 895−900.
(47) Pi, X. D.; Liptak, R. W.; Nowak, J. D.; Wells, N. P.; Carter, C. B.; Campbell, S. A.; Kortshagen, U. Air-stable full-visible-spectrum emission from silicon nanocrystals synthesized by an all-gas-phase plasma approach. *Nanotechnology* **2008**, *19*, 245603.
(48) Ledoux, G.; Gong, J.; Huisken, F.; Guillois, O.; Reynaud, C. Photoluminescence of size-separated silicon nanocrystals: confirmation of quantum confinement. *Appl. Phys. Lett.* **2002**, *80*, 4834−4836.
(49) Mammen, L.; Deng, X.; Untch, M.; Vijayshankar, D.; Papadopoulos, P.; Berger, R.; Riccardi, E.; Leroy, F.; Vollmer, D. Effect of Nanoroughness on Highly Hydrophobic and Superhydrophobic Coatings. *Langmuir* **2012**, *28*, 15005−15014.
(50) Wang, C.-T.; Wu, C.-L.; Chen, L.-C.; Huang, Y.-H. Humidity sensors based on silica nanoparticle aerogel thin films. *Sens. Actuators, B* **2005**, *107*, 402−410.
(51) Pajonk, G. M. Some applications of silica aerogels. *Colloid Polym. Sci.* **2003**, *281*, 637−651.
(52) Ayers, M. R.; Hunt, A. J. Molecular oxygen sensors based on photoluminescent silica aerogels. *Aerogels 7: Proceedings of the 7th International Symposium on Aerogels 7th International Symposium on Aerogels*, 1998; Vol. *225*, pp 343−347.
(53) Budavari, S. *The Merck Index*, 11th ed.; Merck & Co.: Rahway, 1989.

DOI: 10.1021/acs.langmuir.7b03746
Langmuir XXXX, XXX, XXX−XXX

4.3.4. Reprint Permissions

ACS Publications
Most Trusted. Most Cited. Most Read.

Title: Superhydrophobic Silicon Nanocrystal–Silica Aerogel Hybrid Materials: Synthesis, Properties, and Sensing Application

Author: Julian Kehrle, Tapas K. Purkait, Simon Kaiser, et al

Publication: Langmuir

Publisher: American Chemical Society

Date: Apr 1, 2018

Copyright © 2018, American Chemical Society

LOGIN

If you're a copyright.com user, you can login to RightsLink using your copyright.com credentials.

Already a RightsLink user or want to learn more?

PERMISSION/LICENSE IS GRANTED FOR YOUR ORDER AT NO CHARGE

This type of permission/license, instead of the standard Terms & Conditions, is sent to you because no fee is being charged for your order. Please note the following:

- Permission is granted for your request in both print and electronic formats, and translations.
- If figures and/or tables were requested, they may be adapted or used in part.
- Please print this page for your records and send a copy of it to your publisher/graduate school.
- Appropriate credit for the requested material should be given as follows: "Reprinted (adapted) with permission from (COMPLETE REFERENCE CITATION). Copyright (YEAR) American Chemical Society." Insert appropriate information in place of the capitalized words.
- One-time permission is granted only for the use specified in your request. No additional uses are granted (such as derivative works or other editions). For any other uses, please submit a new request.

4.4. Silicon Nanocrystals and Silicon-Polymer Hybrids: Synthesis, Surface Engineering, and Applications

4.4.1. Summary

Arising from their low toxicity, the bright photoluminescence (PL) in the visible region and their straightforward synthesis, SiNCs are useful in many applications. However, their uses are often limited due to surface oxidation, quenching of the PL, low dispersibility in organic solvents and aggregation. Therefore, surface engineering is a major objective in this diverse field of science. The presented review article summarizes the synthesis, surface engineering and application of silicon nanocrystals and their hybrid materials. Based on hydride terminated SiNC surfaces, a variety of reaction profiles are of interest.

The tendency for surface oligomerization occurring from thermal grafting, the formation of fluorocarbon surface groups, the efficient borane catalyzed hydrosilylation of alkenes and alkynes and the advantages of diazonium salt and radical initiators in SiNC surface grafting are reviewed. Alternative reactions involving heteroatoms as surface groups (e.g. amines, trioctylphosphine oxide, acetals and lithium organyls) are discussed in detail. Although the generation and utilization of halogen surface groups is comparatively challenging, it is an important contribution to the SiNC science: PL properties depend on the atom (Cl, Br or I), halogen surface groups can simple be substituted and they allow the generation of hypervalent interactions at the Si center with carbonyls and nitriles.

Physical mixtures of SiNCs with polymers often lead to aggregation, oxidation or destabilization of the nanoparticles in the matrix. Good results could be obtained upon using PEDOT:PSS stabilization within micro plasma reactors. Improved stabilities were realized by covalent attached polymers like polystyrene or polysiloxanes. Furthermore, the reversible addition-chain fragment chain transfer (RAFT) and the group-transfer polymerization (GTP) on SiNC surfaces were reviewed as a contribution for functional surface polymers. Thus, SiNCs with specified surface groups could be applied in various applications like sensing of nitroaromatics and dopamine, *in-vitro* and *in-vivo* bioimaging, light emitting diodes with high quantum yields, high stability battery anodes and in catalysis.

4.4.2. Bibliographic Data – Angew. Chem. Int. Ed./Angew. Chem.

Silicon Nanocrystals and Silicon-Polymer Hybrids: Synthesis, Surface Engineering, and Applications

Mita Dasog, Julian Kehrle, Bernhard Rieger, Jonathan G. C. Veinot

Angew. Chem. Int. Ed. ***2016****, 55,* 2322.

Dr. M. Dasog
Division of Chemistry and Chemical Engineering, California Institute of Technology, 1200 East California Boulevard, Pasadena, CA 91125 (USA)

J. Kehrle, Prof. Dr. B. Rieger
WACKER-Lehrstuhl für Makromolekulare Chemie
Technische Universität München, Lichtenbergstraße 4, 85747 Garching (Germany)

Prof. Dr. J. G. C. Veinot
Department of Chemistry, University of Alberta, 11227 Saskatchewan Drive, Edmonton, Alberta T6G 2G2 (Canada)

Direct Link: DOI 10.1002/anie.201506065

Silicium-Nanokristalle und Silicium-Polymer-Hybridmaterialien: Synthese, Oberflächenmodifikation und Anwendungen

Mita Dasog, Julian Kehrle, Bernhard Rieger, Jonathan G. C. Veinot

Angewandte Chemie ***2016****, 128, 2366.*

Dr. M. Dasog
Division of Chemistry and Chemical Engineering, California Institute of Technology, 1200 East California Boulevard, Pasadena, CA 91125 (USA)

J. Kehrle, Prof. Dr. B. Rieger
WACKER-Lehrstuhl für Makromolekulare Chemie
Technische Universität München, Lichtenbergstraße 4, 85747 Garching (Germany)

Prof. Dr. J. G. C. Veinot
Department of Chemistry, University of Alberta, 11227 Saskatchewan Drive, Edmonton, Alberta T6G 2G2 (Canada)

Direct Link: DOI 10.1002/ange.201506065

4.4.3. Reprint of the Original Manuscript

GDCh Reviews Angewandte International Edition Chemie

Silicon Nanocrystals

International Edition: DOI: 10.1002/anie.201506065
German Edition: DOI: 10.1002/ange.201506065

Silicon Nanocrystals and Silicon-Polymer Hybrids: Synthesis, Surface Engineering, and Applications

Mita Dasog, Julian Kehrle, Bernhard Rieger, and Jonathan G. C. Veinot**

Keywords:
hybrid materials · photoluminescence · quantum dots · silicon nanocrystals · surface chemistry

GDCh Reviews Angewandte International Edition Chemie

Silicon nanocrystals (Si-NCs) are emerging as an attractive class of quantum dots owing to the natural abundance of silicon in the Earth's crust, their low toxicity compared to many Group II–VI and III–V based quantum dots, compatibility with the existing semiconductor industry infrastructure, and their unique optoelectronic properties. Despite these favorable qualities, Si-NCs have not received the same attention as Group II–VI and III–V quantum dots, because of their lower emission quantum yields, difficulties associated with synthesizing monodisperse particles, and oxidative instability. Recent advancements indicate the surface chemistry of Si-NCs plays a key role in determining many of their properties. This Review summarizes new reports related to engineering Si-NC surfaces, synthesis of Si-NC/polymer hybrids, and their applications in sensing, diodes, catalysis, and batteries.

From the Contents

1. Introduction

Semiconductor quantum dots have emerged as a new class of luminescent materials whose emission properties can be tuned by changing the nanocrystal size,[1] shape,[2] composition,[3] and dopants.[4] Since their discovery thirty years ago, quantum dots have revolutionized the field of nanotechnology owing to their fascinating optoelectronic properties and their diverse applications have reached across the fields of physical and life sciences, engineering, and medicine. Today, semiconductor quantum dots are on the forefront of many research fields and are being investigated for applications such as solar cells,[5] LEDs,[6] catalysis,[7] bio-imaging,[8] magnetic materials,[9] sensing,[10] bioassays,[11] lasing,[12] and quantum computing,[13] among others. The most well-known quantum dots are composed of Group II–VI, IV–VI, and III–V type semiconductors. Unfortunately, these contain toxic heavy metals, such as cadmium, lead, mercury, and arsenic as well as elements whose reserves are depleting, such as indium and selenium. With increased awareness of the harmful effects of toxic heavy metals, their use in consumer products is becoming increasingly regulated as evidenced by the European Union Directive 2011/65/EU ("Restriction of the use of certain hazardous substances") that limits or bans the use of these elements. Consequently, efforts have been made to establish alternative quantum-dot materials that are nontoxic and abundant.

It is an understatement that we live in a technological world made possible by silicon (Si). While bulk Si has dominated the microelectronics industry for over half a century, it is not photoluminescent at room temperature and has limited optical applications. It was only twenty five years ago with the discovery of porous silicon (*p*-Si) by Canham,[14] that nanostructured Si began being explored and applied for its optical properties.[15] Today, a wide spectrum of methods have been reported for preparing silicon nanocrystals (Si-NCs). The most commonly used methods can be generally classified as reduction of silicon halides,[16] oxidation of metal silicides,[17] thermal disproportionation of silicon-rich oxides,[18] and decomposition of silane or disilane[19] using plasma or heat (See Scheme 1). Other methods such as magnesiothermic reduction,[20] thermal decomposition of silicon precursor in supercritical fluid,[21] and etching[22] or mechanochemical ball milling[23] of bulk silicon to prepare Si-NCs have also been reported. These procedures as well as their advantages and disadvantages were recently reviewed and will not be discussed herein.[24]

Most procedures yield Si-NCs terminated with a hydride, halogen, or oxide surface.[25] Hydride and halogen surfaces are oxidatively unstable and hydride as well as oxide terminated Si-NCs are not readily dispersed in common solvents; hence Si-NCs bearing these surfaces require further modification to passivate their surfaces and render them compatible with solvents. Conventionally, semiconductor quantum dots possess a core–shell structure where the core material is covered with a lattice-matching wide-band-gap material that confines the excitons within the core, isolates them from surface states, and increases the probability of radiative recombination.[26] Unfortunately, known methods for preparing Si-NCs do not offer ready access to similar structures. As a result, Si-NCs are typically functionalized directly with organic ligands. These surface modifications allow for the preparation of nanomaterials with a variety of functionalities and improved properties. Herein we review recent work related to tailoring Si-NC surfaces to manipulate

[*] Dr. M. Dasog
Division of Chemistry and Chemical Engineering
California Institute of Technology
1200 East California Boulevard, Pasadena, CA 91125 (USA)
J. Kehrle, Prof. Dr. B. Rieger
WACKER-Lehrstuhl für Makromolekulare Chemie
Technische Universität München
Lichtenbergstrasse 4, 85747 Garching (Germany)
E-mail: rieger@tum.de
Prof. Dr. J. G. C. Veinot
Department of Chemistry
University of Alberta
11227 Saskatchewan Drive, Edmonton, Alberta T6G 2G2 (Canada)
E-mail: jveinot@ualberta.ca

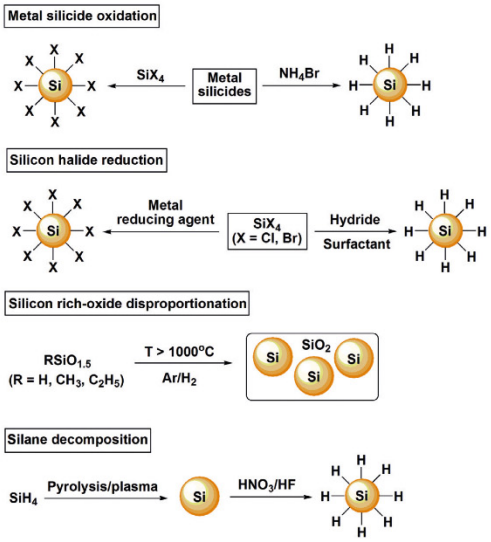

Scheme 1. General methods for preparing Si-NCs.

their dispersability, stability, photoluminescence (PL), quantum yields, and applications.

2. Monolayer Surfaces

Covalent attachment of functional monolayers onto bulk silicon surfaces began with the pioneering work of Linford and Chidsey; in their ground breaking work they investigated reactions of 1-alkenes and 1-alkynes with hydride-terminated Si(111) and Si(100) bulk surfaces.[27] In the ensuing decades, similar methodologies have been extended to porous silicon and freestanding Si-NCs.[28] Correspondingly numerous methods have been established to generate Si–C, Si–O, Si–N,[24,25] and more recently Si–S[29] linkages on NCs. Still, Si–C linked monolayers have long been considered the surface of choice. The following discussion focuses on the recent advances in reactivity of hydride and halogen surfaces on Si-NCs.

2.1. Hydrosilylation Reactions

Hydrosilylation involves the addition of a Si–H bond across multiple C–C bonds and is typically facilitated by exposure to heat,[30] light,[31] radical initiators,[32] transition-metal catalysts,[33] Lewis acids,[34] or plasmons.[35] Thermally initiated hydrosilylation is widely employed; it proceeds independent of particle size and shape, does not require a catalyst that could contaminate the product and compromise target properties, and provides efficient surface coverage. The generally accepted mechanism for this reaction involves the thermally initiated homolytic cleavage of surface Si–H bonds to provide surface silyl radicals that subsequently

Mita Dasog received her Ph.D. in 2014 from the University of Alberta, Canada, where she investigated syntheses and optical properties of silicon based nano- and micromaterials under the supervision of Prof. Jonathan Veinot. She is currently an NSERC postdoctoral fellow at the California Institute of Technology with Prof. Nathan Lewis investigating the interaction of light with semiconductors.

Bernhard Rieger studied chemistry at the Ludwig-Maximilians-Universität München and received his Ph.D. in 1988. After research at the University of Massachusetts at Amherst and in the plastics laboratory of BASF SE, he received his Habilitation in 1995 at the University of Tübingen. In the same year, he became Professor ordinarius at the Department of Materials and Catalysis at the University of Ulm. In 2006, he was appointed professor at Technische Universität München. Since then, he holds the WACKER-Chair of Macromolecular Chemistry and works as director of the Institute of Silicon Chemistry at TUM.

Julian Kehrle studied Chemistry at the Technische Universität München, where he received his Master's degree in 2012. Currently he is working on his Ph.D. thesis at the WACKER Chair of Macromolecular Chemistry under the supervision of Prof. Rieger. He is interested in the synthesis and the preparation of functional silicon-nanocrystal-based hybrid materials. This work is performed in cooperation with the Veinot group under the frame of the IRTG 2022.

Dr. Veinot is a professor in the Chemistry Department at the University of Alberta. His research aims to develop methods for preparing, and investigating advanced nanomaterials (NMs) and optoelectronic polymers. His team established a straightforward, scalable method that affords tailored Si nanocrystals that has become the method of choice in seven international groups. He is a former Chair of the Chemical Society of Canada Materials Chemistry Division, Associate Editor of the Canadian Journal of Chemistry, and Canadian Director of the Alberta/Technical University of Munich International Graduate School for Hybrid Functional materials.

react with terminal carbon–carbon multiple bonds. While a few rare exceptions exist,[36] reactions of this type are typically performed in neat alkene/alkyne and until recently it has long been assumed that they yielded surface-bonded monolayers. In 2014, Yang et al. conclusively demonstrated that typical thermal hydrosilylation conditions induce ligand oligomerization and that the degree of oligomerization increases with oxygen content, reaction temperature, and ligand concentration.[37] The reaction products were analyzed using NALDI (nanostructure assisted laser desorption/ionization) mass spectrometry and oligomers of up to seven repeat units could form when dodecene was employed (Figure 1a). Consistent with these findings, Panthani et al.

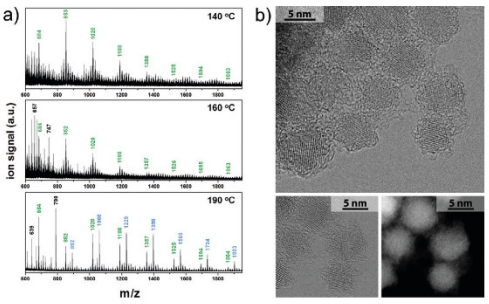

Figure 1. a) NALDI mass spectra of dodecyl-functionalized Si-NCs at the indicated temperatures. b) Bright field (top, bottom left) and dark field (bottom right) STEM images of alkyl-passivated Si-NCs on the edge of a graphene support. Reproduced and adapted with permission from the American Chemical Society.[37,38]

published TEM images of alkyl-stabilized Si-NCs obtained from thermal hydrosilylation. Their images were obtained using graphene supports and show what appear to be ligands around the NC surface (Figure 1b).[38] It is reasonable that ligand oligomerization contributes to the robustness, increased stability, and PL quantum yields[39] of thermally hydrosilylated Si-NC surfaces, however these long electrically insulating alkyl chains also present a potential challenge to the eventual application of Si-NCs in optoelectronic devices.

Qian et al. tethered fluoro-substituted alkenes onto Si-NC surfaces in attempts to enhance the oxidative stability.[40] Perfluorodecyl groups were grafted onto Si-NC surfaces upon heating in a microwave reactor (Scheme 2). The researchers propose this approach is a facile and "green" method for modifying Si-NC surfaces. They also propose an

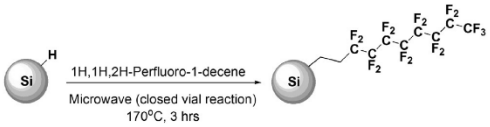

Scheme 2. A summary of the synthesis of perfluorodecyl-functionalized Si-NCs. Adapted with permission from the American Chemical Society.[40]

associated increase in absolute PL quantum yield resulting from the low frequency of carbon–fluorine stretching modes that minimize non-radiative relaxation pathways. In addition they noted enhanced oxidative and PL stability in perfluorodecyl functionalized Si-NCs compared to the dodecyl surface ligand upon exposure to humidity. Similar work from the same group also indicated that introducing heteroatoms (i.e., C–X bonds; X = S or F) into the surface-bonded alkyl or aryl moieties lead to enhanced absolute photoluminescence quantum yields presumably because of the associated lowering of the C–X bond vibration frequency.[41]

While a very small number of exceptions exist,[42] thermal hydrosilylation requires high reaction temperatures, and as a result only high-boiling alkenes and alkynes can be conveniently grafted onto Si-NC surfaces. Photochemically induced hydrosilylation provides a seemingly obvious alternative. However, its utility is limited by size-dependent reactivity, intolerance to chemical functionality, and long reaction times.[43] Other room-temperature hydrosilylation routes make use of transition-metal catalysts, but these additives can compromise Si-NC properties (e.g., PL quenching) and removing the residual catalyst is difficult.[44] Recently, Purkait et al. modified Si-NC surface chemistry at room-temperature via borane-catalyzed hydrosilylation.[45] They functionalized Si-NCs with a variety of terminal alkenes and alkynes (Scheme 3), realizing up to 96% surface coverage.

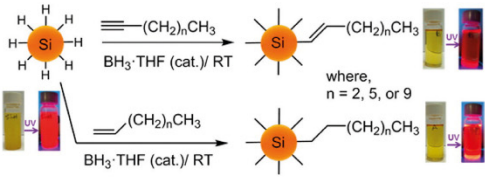

Scheme 3. Borane-catalyzed hydrosilylation of Si-NC surfaces with terminal alkenes and alkynes. Reproduced and adapted with permission from the American Chemical Society.[45]

Höhlein et al. also reported a room-temperature route to Si-NC surface hydrosilylation initiated by diazonium salts (Scheme 4).[46] While diazonium salts have been used to directly graft aryl groups onto silicon surfaces,[47] their use as radical initiators has only been shown for porous silicon.[48] The researchers also investigated the influence of substituents on the efficacy of the reaction and found that those with electron-withdrawing groups provided the highest surface coverage. Diazonium-salt-initiated hydrosilylation was also tolerant of various functional groups and afforded attachment of hydrocarbon alkenes and alkynes, vinyl laurate, methyl methacrylate, ethynyltrimethylsilane, and chlorodimethyl(vinyl)silane. In another study, the same researchers demonstrated that chlorodimethyl(vinyl)silane functionalized Si-NCs could be further modified upon reaction with alcohols, silanols, and organolithium reagents.[49]

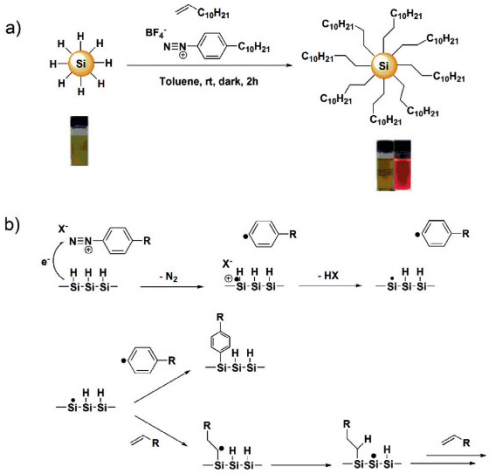

Scheme 4. a) Modification of Si-NCs with alkenes via diazonium-salt-induced hydrosilylation. b) Proposed mechanism for diazonium-salt reactivity with silicon hydride surfaces. Reproduced and adapted with permission from John Wiley and Sons.[46]

2.2. Alternative Reactions on the Silicon Hydride Surface

While hydrosilylation remains the leading approach toward Si-NC surface functionalization, attempts to circumvent its limitations have seen exploration of the reactivity of Si–H surfaces. Some recently reported reactions are summarized in Scheme 5. While hydrosilylation leads to optical properties dominated by band-gap emission, investigations to date suggest that most alternative functionalization pathways yield materials that emit from defect/surface states.

We have shown hydride-terminated Si-NCs react directly with amines to afford Si-N covalent linkages.[50] The surface passivation resulting from this reaction is incomplete and significant oxidation is observed. The incorporation of nitrogen and oxygen moieties onto the surface leads to particle-size-independent surface-species-based blue photoluminescence.[51,52] Hydride terminated Si-NCs also react with CO_2 at high pressures (i.e., 10 bar) and temperatures above 100 °C, yielding an acetal surface that provides blue-green photoluminescence.[53] At longer reaction times the surface acetal groups decompose forming formaldehyde and oxidized particles that precipitate from the reaction mixture. Analogous to molecular silanes, hydride-terminated Si-NCs react with phosphine oxides forming the corresponding tri-substituted phosphine.[53] Under ambient conditions, the reduced phosphines are oxidized to the corresponding phosphine oxide and stabilize oxide-coated Si-NCs in organic solvents. The optical properties of these phosphine-oxide-stabilized oxide-coated Si-NCs are complex; studies indicate band gap and defect states play a role in determining the emission maxima. The relative PL quantum yields obtained for Si-NCs derived from reactions of hydride-terminated Si-NCs with amines, CO_2, and phosphine oxides are higher relative to those obtained for hydrosilylated Si-NCs.[53] However, in contrast to Si-NCs exhibiting band-gap-based PL, those emitting from surface states appeared to photobleach (Figure 2).

Höhlein et al. further demonstrated that hydride-terminated Si-NCs react directly with organolithium reagents via cleavage of surface Si–Si bonds to form Si–Li and Si–R

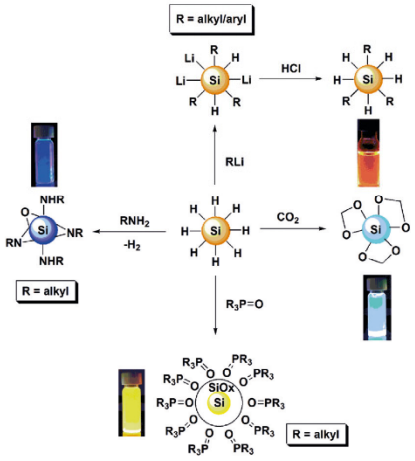

Scheme 5. Reactivity of Si-H terminated Si-NCs with organolithium reagents, carbon dioxide, alkylamines, and alkylphosphine oxides. Reproduced and adapted with permission from John Wiley and Sons and The American Chemical Society.[53,54]

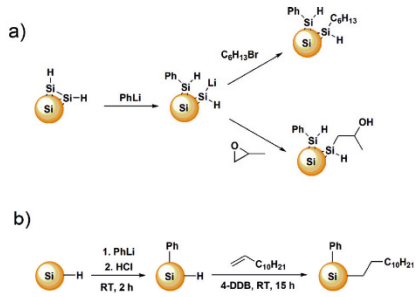

Scheme 6. a) Reaction of Si-NCs with phenyllithium and subsequent reactivity of Si-Li groups and b) reaction of Si-NCs with phenyllithium and subsequent reactivity of Si-H groups yielding mixed-surface Si-NCs. Reproduced and adapted with permission from John Wiley and Sons.[54]

surface species (Scheme 6a).[54] The reaction proceeds at room temperature and the Si–H bonds can be further functionalized to yield mixed monolayers (Scheme 6b).

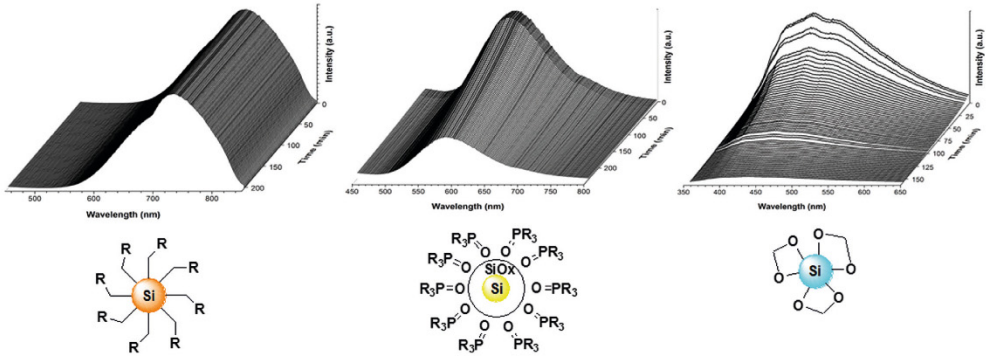

Figure 2. Photostability of Si-NCs stabilized with dodecyl, trioctylphosphine oxide, and acetal functional groups. The Si-NC solutions were continuously illuminated for over 150 min. Reproduced and adapted with permission from The American Chemical Society.[53]

2.3. Halogenated Silicon Surfaces

Most solution-phase methods for preparing chloride- or bromide-terminated Si-NCs never see the halogen-terminated particles isolated; they are typically derivatized in situ. The versatile reactivity of Si–X (X = Cl, Br) surfaces has seen these particles derivatized using numerous approaches including reactions with Grignard and organolithium reagents, amines, alcohols, silanols. This body of work has been reviewed elsewhere.[24,25]

Of particular interest, Wheeler et al. prepared chloride-terminated Si-NCs via decomposition of $SiCl_x$ in the presence of H_2 in a non-thermal plasma reactor and stabilized the Si–bond with hard donor molecules via hypervalent interactions (Figure 3).[55] ATR-FTIR analysis revealed shifts in the

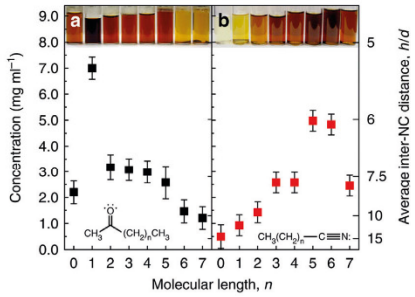

Figure 3. Concentration of chloride terminated Si-NCs as a function of molecular length *n* of the stabilizing group a) *n*-alkanone and b) *n*-alkanenitriles. Reproduced and adapted with permission from Nature publishing group.[55]

stretching modes of carbonyl, nitrile, and Si–Cl bonds consistent with interactions between Si-NC and donor molecules (Figure 4). The stability of the colloidal NC suspensions depended upon the donor strength; interestingly,

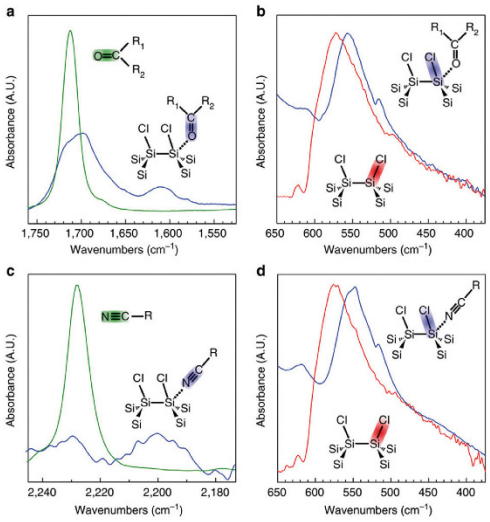

Figure 4. ATR-FTIR spectra depicting hypervalent interactions between ketones and nitriles with chloride-terminated Si-NCs. Reproduced and adapted with permission from Nature publishing group.[55]

the surface-bonded groups were labile—an unprecedented discovery for Si surfaces.

While halogen termination of Si-NCs has been achieved in situ, few reports outlining the deliberate halogenation of Si-NCs have appeared. Chlorination/alkylation on bulk Si-(111) and Si(100) surfaces was first reported by Bansal et al. and gives a well-ordered, chemically passivated surface.[56] Chlorination is achieved by treating atomically flat bulk Si surfaces with PCl_5 at temperatures higher than 90 °C in the presence of benzoyl peroxide. We investigated similar reactivity with hydride-terminated Si-NCs.[57] In the case of the Si-NC system PCl_5 chlorination proceeded at room temperature without a radical initiator (Figure 5a). A complication of this

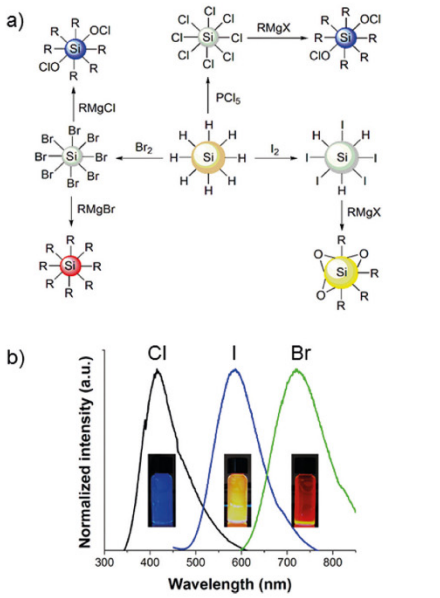

Figure 5. a) Schematic representation of halogenation and alkylation of hydride terminated Si-NCs and b) PL spectra of alkylated Si-NCs derived from halogenated surfaces. Reproduced and adapted with permission from the American Chemical Society.[58]

approach is that PCl_5 etches the Si-NC surface at elevated temperatures and can lead to complete dissolution of the particles.[58] Similarly, bromination can be achieved upon reaction of hydride-terminated Si-NCs with elemental bromine at room temperature. Anisotropic etching of the Si-NCs was also observed for this reaction, albeit faster than that noted for PCl_5. Iodination can be achieved upon reaction of elemental iodine with hydride-terminated Si-NCs, however this procedure does not lead to complete modification. The formation of Si–X (X = Cl, Br and I) was confirmed using Raman and X-ray photoelectron spectroscopy.

Halogen exchange was observed between bromide-terminated Si-NCs and RMgCl reagents. Alkyl-functionalized Si-NCs obtained from chloride, bromide, and iodide surfaces exhibited blue, red, and yellow-orange photoluminescence, respectively (Figure 5b). While the red photoluminescence originated from a transition across the band gap (confirmed through long-lived excited states), the blue and yellow-orange photoluminescence appear to originate from surface defects and had nanosecond lifetimes.

Bell et al. reported room temperature bromination of hydride terminated Si-NCs using N-bromosuccinimide (Scheme 7).[59] NCs functionalized in this way were subsequently modified upon exposure to alcohols to yield red photoluminescent Si-NCs.

Residual chorine-based impurities can influence Si-NC optical properties. Often, blue photoluminescence is reported for particles derived from chloride surfaces. We have demonstrated that oxychloride moieties can induce surface-state-based blue emission that is independent of particle size.[58] In contrast, well-passivated Si-NC alkyl surfaces derived from bromide termination show size-dependent photoluminescence from band-gap emission.

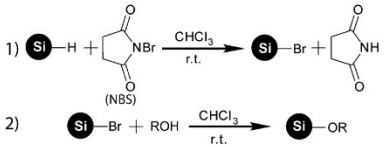

Scheme 7. Bromination of hydride terminated Si-NCs with N-bromosuccinimide and its subsequent alkoxylation. Reproduced and adapted with permission from the Royal Chemical Society.[59]

Recently, numerous groups have explored the chloride surface of Si-NCs as a reactive platform for attaching substituted amines. Li et al. and Wang et al. demonstrated that attaching aryl amines bearing different substituents can influence the Si-NC photoluminescence maximum (Figure 6).[60,61] The origin of this luminescence remains in question, however solvatochromism demonstrated by our group is consistent with the emission arising from a charge-transfer state involving silicon oxynitrides. The PL from aminated surfaces are short-lived with excited-state lifetimes (ca. 5 ns) and exhibit very high quantum yields (ca. 75%).

Zhai et al. used chloride terminated Si-NCs for straightforward attachment of D-mannose and L-alanine to yield luminescent water-soluble particles (Figure 7).[62] This route provides a general method for attaching sugars and amino acids to Si-NCs. Uptake and PL emission of mannose- and alanine-functionalized Si-NCs in MCF-7 cells was also shown.

3. Si-NC/Polymer Hybrid Materials

Hybrids of functional polymers and semiconductor nanocrystals are attractive because the properties of the individual components may be tuned independently. Combining these complementary materials into a hybrid offers new systems that possess the properties of the components, as well as hybrid characteristics arising from the synergistic interactions between the nanomaterial and polymer. A variety of approaches for assembling polymers and quantum dots of binary (e.g., CdSe, InP, PbTe),[63] ternary (e.g., $CuInSe_2$, $CuInS_2$),[64] and quaternary (e.g., $Cu_2ZnSnSe_4$)[65] compound semiconductors have been established. In contrast, Si-NC/polymer hybrids remain in the early stages of development, partly because of limited availability of well-defined Si-NCs.

Physical blending of components provides a straightforward approach toward obtaining hybrids. This approach was employed by Liu et al., who combined hydride terminated Si-NCs with regio-regular poly-3-hexylthiophene (P3HT, a common and useful optoelectronic polymer) and explored the composite in prototype photovoltaic devices.[66] While promising, this procedure was plagued by particle aggregation that lead to non-uniform films and comparatively poor prototype device performance. To improve material homo-

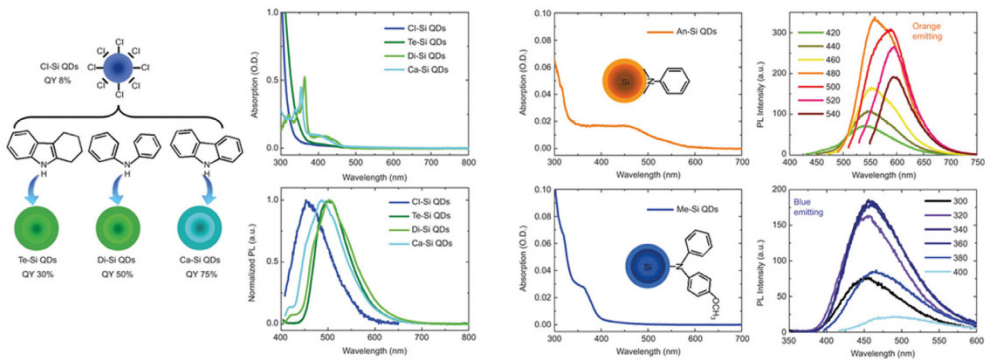

Figure 6. Absorption and emission spectra of Si-NCs functionalized with substituted amines. Reproduced and adapted with permission from the Nature publishing group.[61]

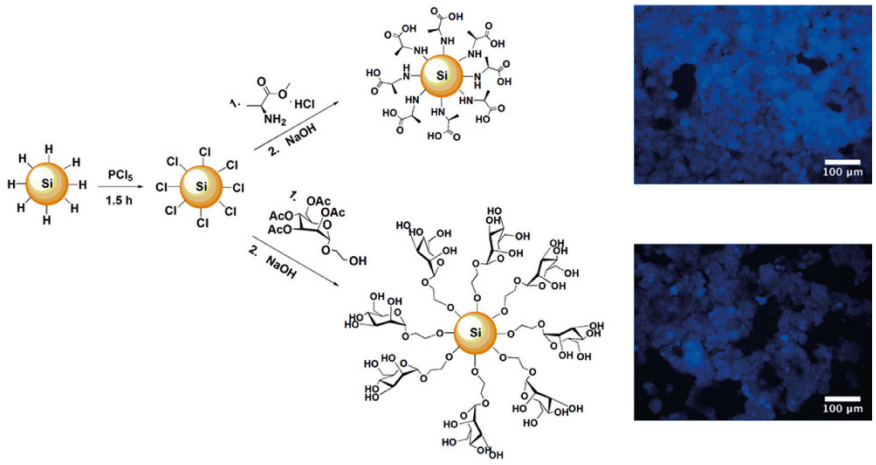

Figure 7. Synthesis of alanine and mannose functionalized Si-NCs and fluorescence images of MCF-7 cells incubated with Si-NCs bearing the corresponding functional groups. Adapted with permission from the Royal Chemical Society.[62]

geneity Mitra et al. employed an atmospheric-pressure microplasma technique to coat Si-NCs with PEDOT:PSS polymer (Figure 8a).[67] This provided a uniform polymer coating on the NCs and improved their stability, solvent dispersability (Figure 8b), and photoluminescence.

Drawing on work related to compound semiconductor quantum dots, Hessel et al. exploited non-covalent interactions; they reported preparation of Si-NC/poly(maleic anhydride) hybrids (Figure 9a).[68] Encapsulating alkyl terminated Si-NCs within this amphiphilic polymer shell made the particles water dispersible and suitable for in vivo biological imaging applications. They also demonstrated that the hybrid was luminescent (Figure 9b), stable over large pH ranges and ionic strengths, large enough to bypass the renal system, and small enough to remain in the circulatory system for extended periods. These properties made these hybrid nanomaterials attractive for biological applications.

While noncovalent interactions are clearly useful in the assembly of nanomaterial/polymer hybrids, these comparatively weak interactions can bring challenges associated with their long-term stability. Forming covalent linkages between the Si-NC and polymers provides one method for improving homogeneity, charge transport, and long-term stability. Yang et al. reported the "one-pot" synthesis of a Si-NC/polystyrene hybrid (Figure 10a) that is chemically resistant, photoluminescent, homogeneous, and solution processable.[69] The hybrid is believed to form by the thermally induced auto-initiated polymerization of styrene. Styrene radicals can abstract hydride from the Si surface leaving behind a silyl radical that reacts with free styrene molecules to yield

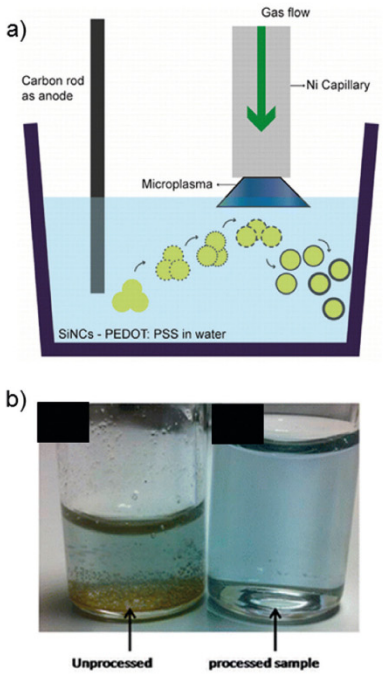

Figure 8. a) Schematic representation of the microplasma apparatus used to coat Si-NCs with PEDOT:PSS and b) photographs of Si-NCs in water-polymer solution before and after microplasma processing. Reproduced and adapted with permission from the American Chemical Society.[67]

polystyrene-functionalized Si-NCs. The researchers fabricated freestanding luminescent films, microfibers, and coated optical fibers using the Si-NC/polystyrene hybrid (Figure 10b–d). Dung et al. showed a similarly prepared Si-NC/polystyrene hybrid was stable to 250 °C and was a useful charge-trapping material in prototype metal-insulator-semiconductor devices and thin-film field-effect transistors.[70] Choi et al. synthesized Si-NC/polystyrene hybrids with varying proportions of the NC and polymer components.[71] The refractive index of spin-coated films increased with the Si-NC concentration.

While simple hydrocarbon-based polymers (i.e., polystyrene) can be attached to the Si-NC surfaces using straightforward hydrosilylation, alternative grafting methods are required to access other functional polymers. Our group recently established a multistep surface-initiated group-transfer polymerization (SI-GTP) procedure for modifying Si-NCs. Polydiethylvinylphosphonate (PDEVP) embedded Si-NCs were synthesized as outlined in Scheme 8.[72] Initially the surfaces of hydride-terminated Si-NCs were modified with ethyleneglycol dimethacrylate (EGDM) using photoinduced hydrosilylation. This new surface served as an anchor for the catalyst (i.e., $Cp_2YCH_2Si(CH_3)_3$; Cp = cyclopentadienyl) that readily polymerizes diethylvinylphosphonate to yield Si-NCs embedded within PDEVP. The resulting material is soluble in water and luminescent (Figure 11a). Importantly, the lower critical solution temperature (LCST) characteristic of the PDEVP was retained in the new hybrid (Figure 11b,c).

Sato et al. reported the synthesis of luminescent, flexible, extendible, and transparent Si-NC/silicone polymer hybrids.[73] Silicone elastomer was directly bonded to the Si-NC surface via siloxane linkages. The luminescent properties of the hybrids were altered by changing the Si-NC size (Figure 12a). This hybrid was molded to form a variety of shapes (Figure 12b) and was photostable under a variety of conditions (e.g., pH, solvent polarity, and mechanical stress).

Höhlein et al. reported an alternative method for interfacing polymers with Si-NCs. They demonstrated surface-initiated reversible addition-fragmentation chain transfer (RAFT) polymerization on Si-NC surfaces with styrene, methyl methacrylate, hexyl acrylate, *N*-isopropylacrylamide, and 4-vinylbenzyl chloride to yield luminescent NC/polymer hybrids.[74] Initially hydride terminated Si-NCs were function-

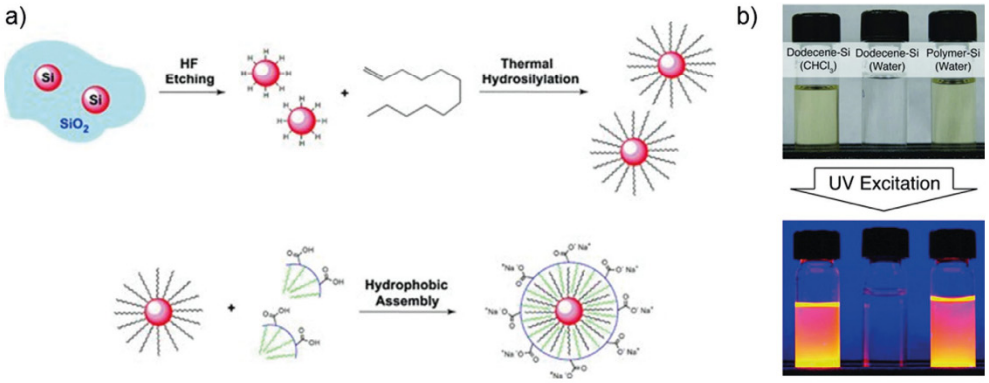

Figure 9. a) Preparation of a Si-NC/poly(maleic anhydride)-based hybrid. b) Photographs of vials containing Si-NC solutions under ambient light and when illuminated by UV (350 nm) light. Reproduced and adapted with permission from John Wiley and Sons.[68]

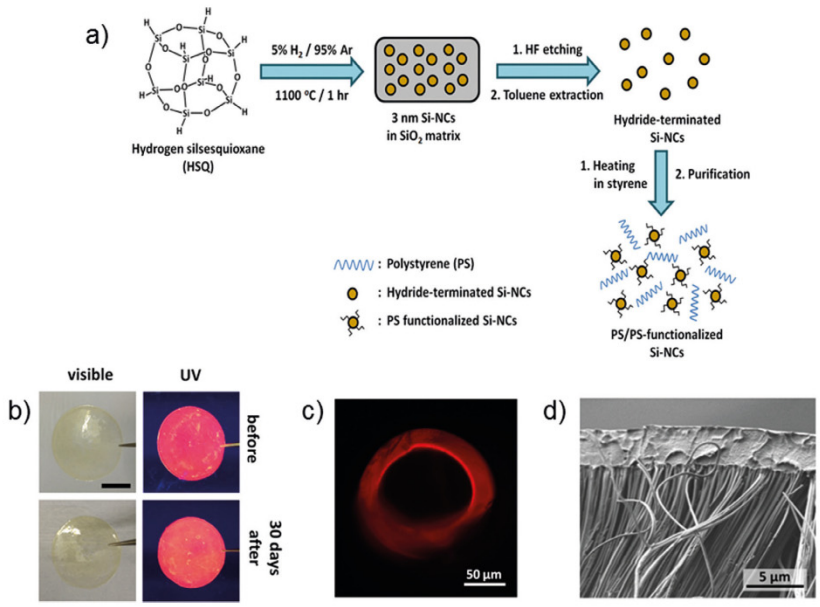

Figure 10. a) Synthesis of Si-NC/polystyrene hybrid; b) chemical stability of free-standing Si-NC/polystyrene thin film in saturated NaOH solution; c) PL image of optical fiber coated with Si-NC/polystyrene and d) SEM image of Si-NC/polystyrene microfibers after removal of the porous alumina template. Reproduced and adapted with permission from John Wiley and Sons.[69]

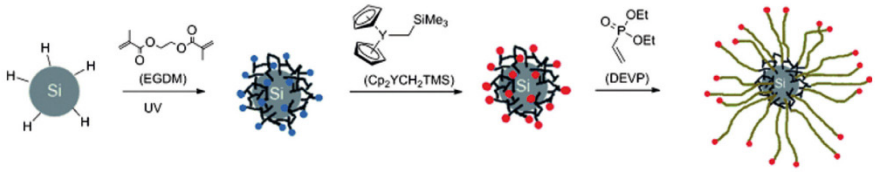

Scheme 8. Synthesis of PDEVP-functionalized Si-NCs. Reproduced and adapted with permission from John Wiley and Sons.[72]

alized with chloro(vinyl)dimethylsilane, which was further modified with 6-hydroxylhexyl 3-(methylthio)-2-phenyl-3-thioxopropanoate (HMT). Polymerization was performed upon addition of a monomer and ethyl-3-(methylthio)-2-phenyl-3-thioxopropanoate (EMPT) mixture to the Si-NC/HMT system (Scheme 9). The process exploited living polymerization and yielded particles with narrow size distributions. The polymer grafted Si-NCs showed higher stability in KOH solution compared to equivalent alkyl functionalized nanoparticles.

4. Applications

Si-NCs have garnered much interest as potential competitors and replacements for conventional Group II–VI and III–V quantum dots. Si-NCs also offer the added advantage of being compatible with common electronics platforms and have low toxicity.[75] Hence, they are attractive materials for electronics and biological applications. Recently, Reviews related to the prototype investigations of Si-NCs in biological, magnetic resonance imaging, and photovoltaic applications have appeared and these topics will not be discussed herein.[24,76–79] Si-NCs have also been investigated as active materials in battery electrodes, sensors, and diodes, as well as catalysts. The following Section provides a perspective on these uses of Si-NCs.

PL-based sensors are attractive because of their high sensitivity, rapid response, portability, limited infrastructure requirements, and low cost.[80] Quantum dots are preferred luminophores because of their stable, tunable emission properties. Cd-based quantum dots were demonstrated as PL sensors to detect nitroaromatic explosives.[81] Our group developed disposable, paper-based sensors using dodecyl-functionalized Si-NCs to detect a series of nitroaromatic, nitroamine, and nitrate ester containing explosives.[82] The

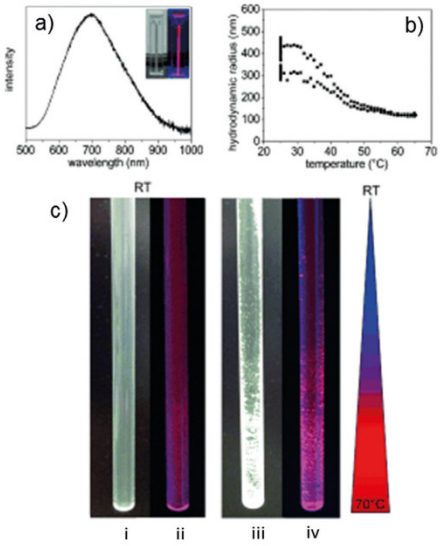

Figure 11. a) PL spectrum of PDEVP grafted Si-NCs at $\lambda_{ex} = 365$ nm (inset: PDEVP/Si-NC solutions under ambient light and UV illumination); b) dynamic light scattering (DLS) measurement of the LCST effect of PDEVP grafted Si-NCs in water and c) dispersion of PDEVP grafted Si-NCs in water at room temperature (i–ii) and after heating the bottom part of the tube to 70 °C for several hours (iii–iv). Reproduced and adapted with permission from John Wiley and Sons.[72]

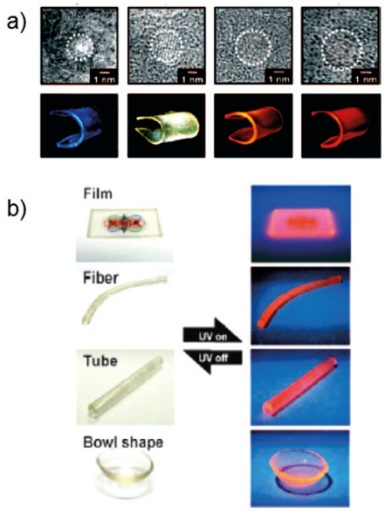

Figure 12. a) TEM micrographs and photographs of Si-NC/silicone elastomer hybrid material emitting different colors under UV illumination and b) images of Si-NC/silicone elastomer drawn into various shapes, viewed under ambient and UV light. Reproduced and adapted with permission from John Wiley and Sons.[73]

paper-based sensor was prepared by dip-coating filter paper in a concentrated toluene solution of Si-NCs. Quenching of the PL of the resulting NC impregnated paper sensors upon exposure to solutions of mononitrotoluene (MNT), dinitrotoluene (DNT), trinitrotoluene (TNT), 1,3,5-trinitroperhy-

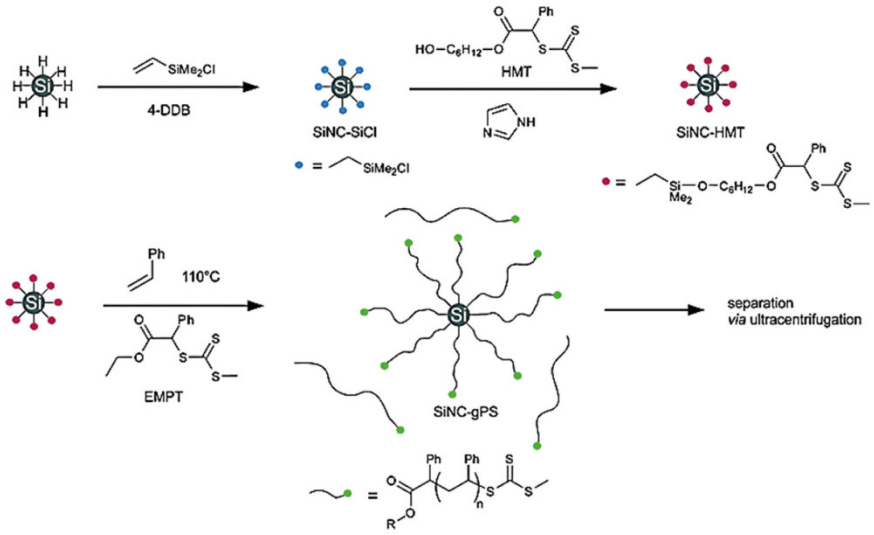

Scheme 9. Surface-initiated RAFT polymerization to yield polystyrene-functionalized Si-NCs. Reproduced and adapted with permission from the Royal Chemical Society.[74]

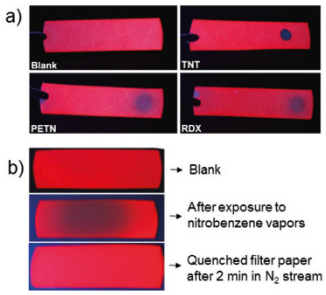

Figure 13. a) Photographs of paper-based sensors under UV illumination upon exposure to the explosives indicated. b) Reversible quenching of Si-NC PL in presence of nitrobenzene vapors. Reproduced and adapted with permission from the Royal Chemical Society.[82]

dro-1,3,5-triazine (RDX), and pentaerythritol tetranitrate (PETN) could be detected visually (Figure 13a). The PL was also quenched upon exposure to solid nitroaromatic residues or nitroaromatic vapors. The quenching was reversible for volatile compounds (Figure 13b). Investigations indicate the quenching of PL arises from electron transfer from the Si-NC to the π^* orbitals of the nitro-containing compounds. These paper-based sensors allowed detection of nitroaromatics at nanogram levels in the solid and vapor phases.

Ban et al. prepared water-dispersible amino-capped Si-NCs as PL probes for the detection of TNT in aqueous media.[83] In the absence of conclusive evidence, they proposed that TNT formed a complex with surface amine groups through strong donor/acceptor interactions and that the resulting TNT/amine complex quenched the Si-NC PL via Förster resonance energy transfer (FRET; Scheme 10). They

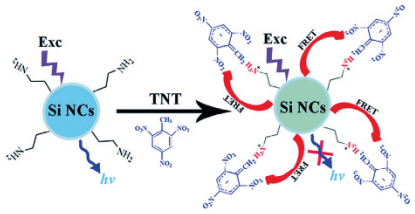

Scheme 10. Schematic representation of luminescence quenching by TNT of amine capped Si-NCs via the FRET mechanism. Reproduced and adapted with permission from the Royal Chemical Society.[83]

further proposed that the quenching efficiencies depended on the binding affinities of nitro-analytes on the Si-NC surface and the electron-accepting ability of the nitro-containing compounds. Similarly, Zhang et al. showed selective dopamine detection using luminescent Si-NCs in aqueous medium at very low concentrations of the analyte dopamine (ca. nM).[84] They also showed that other common molecules in a living system did not interfere with dopamine making the method selective (Figure 14).

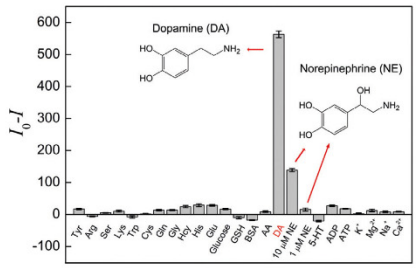

Figure 14. Fluorescence responses of Si-NCs in the presence of various analytes. Reproduced and adapted with permission from the American Chemical Society.[84]

Properties such as tunable luminescence and straightforward fabrication, among others, make quantum dots attractive emissive materials for light-emitting diode (LED) applications. Generally, the quantum dots are placed between layers of organic polymers that serve as charge-transport media. Hybrid nanocrystal–organic LEDs of this type have been fabricated using Si-NCs. A typical device structure is shown in Figure 15.

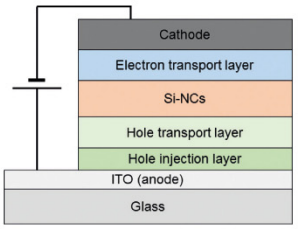

Figure 15. Typical device architecture of a hybrid Si-NC organic LED.

Cheng et al. reported infrared electroluminescence at 868 nm from a hybrid Si-NC/organic LED with an external quantum efficiency of 0.6%.[85] The Si-NCs were prepared by decomposition of silane gas using non-thermal plasma and were functionalized with dodecyl groups. The researchers observed a direct correlation between emissive-layer (i.e. the Si-NC layer) thickness and external quantum efficiencies of the device. The same research group later reported hybrid NC/organic LEDs consisting of 3 and 5 nm dodecyl functionalized Si-NCs that showed external quantum efficiencies up to 8.6%.[86] They attributed the increase in the efficiencies to an increase in the energy gap of hole- and electron-transport layers that provided better confinement of both charge carriers and excitons in the NC emissive layer.

Similarly, Maier-Flaig et al. reported red/orange electroluminescence from hybrid Si-NC/organic LEDs consisting of allylbenzene-functionalized Si-NCs up to maximum external quantum efficiencies of 1.1%; they propose that Si-NC size polydispersity leads to rapid degradation of the LEDs causing short circuits.[87] They also observed inhomogeneous emissions across the device that were reasonably attributed to

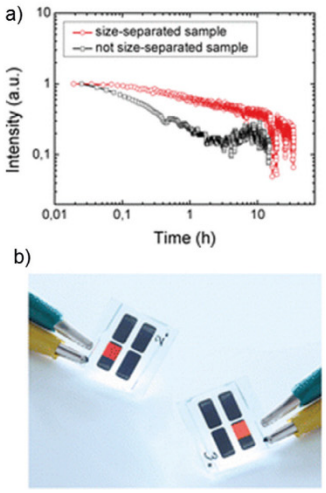

Figure 16. a) Electroluminescence intensity of polydisperse and size-separated Si-NCs over time at a constant current of 1.6 mA cm $^{-2}$ and b) photographs of hybrid Si-NC/organic LEDs showing red and orange electroluminescence. Reproduced and adapted with permission from the American Chemical Society.[87]

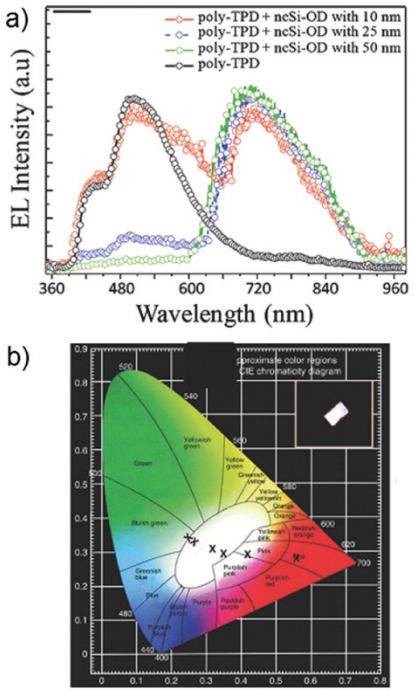

Figure 17. a) Electroluminescence spectra with and without the Si-NCs at various thicknesses and b) CIE diagram showing the chromaticity coordinates of various devices (inset: Photograph of a white LED). Reproduced and adapted with permission from John Wiley and Sons.[88]

impurities and defects arising from particles of various sizes. Upon purification of Si-NCs using size-selective precipitation, the researchers fabricated brighter, more stable (Figure 16a) and homogeneously emissive devices (Figure 16b).

Ghosh et al. reported white-light emission from hybrid Si-NC/organic LEDs by combining emission from Si-NCs and a luminescent polymer in the device active layer.[88] The researchers combined the red emission from octadecyl functionalized Si-NCs and blue-green emission from poly-TPD to yield white light (Figure 17) with external quantum efficiencies ranging from 0.033–0.36%.

Lin et al. recently demonstrated the fabrication of Si-NC-based photodiodes.[89] Thin films of allyl disulfide functionalized Si-NCs showed enhanced conductivity compared to alkyl-functionalized particles. They proposed the lone-pair electrons on the disulfide structural unit facilitated the charge transport process. Photodiodes were fabricated from the Si-NC ink by spin coating on ITO glass. An electron-blocking layer (PEDOT:PSS) was added between the ITO and Si-NC layers to improve the charge separation in the device (Figure 18a). The device showed UV responsivity (Figure 18b) with a peak photoresponse of 0.02 AW^{-1}, thus making it applicable for UV detection.

The same research group also showed that Si nanoparticles can aid in hydrogen generation from water in the absence of any external stimulants (e.g., light, heat, or electricity). Si nanoparticles (ca. 10 nm) generated hydrogen gas at an accelerated rate by splitting water:[90] the rate was found to be 1000 times faster than bulk Si, 150 times that of 100 nm Si particles, and six times faster than metal formulations, thus making it a potential material for hydrogen generation. Peng et al. showed that Si-NCs prepared via the high-energy ball milling process can be used to catalyze the reduction of carbon dioxide.[91] Under illumination, Si-NCs with no surface groups photochemically reduced CO_2 to formaldehyde. However, no reduction products were observed with alkyl-passivated Si-NCs. El-Demellawi et al. demonstrated that Si-NCs can catalyze the dehydrogenation of secondary alcohols to yield ketones and hydrogen.[92] The reactions proceeded at room temperature, without energy input. These observations are of great practical importance because these solvents are routinely used to store and process Si-NCs. Our group demonstrated, that chloride-terminated Si-NCs can catalyze the polymerization of hexylthiophene Grignard reagents to form P3HT (Figure 19).[93] Chloride termination was achieved by reacting hydride terminated Si-NCs with PCl_5 (Figure 5). Polymerization was achieved at room temperature by addition of the Grignard reagent to the chloride-terminated Si-NCs and is believed to proceed similar to Lewis acid mediated polymerization reactions.

Nanostructured Si has gained a lot of attention as a high-capacity anode material for Li-ion batteries. Si exhibits a low working potential and high theoretical charge capacity (4200 mAh g^{-1}), but suffers from structural damage during

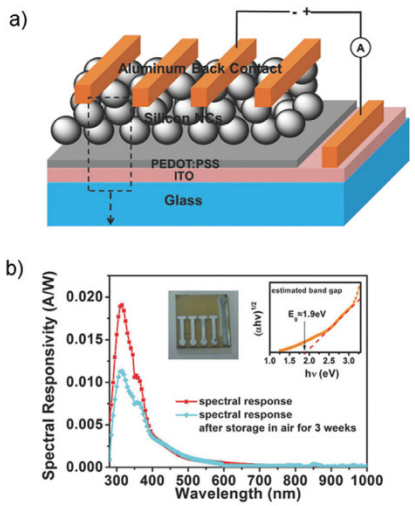

Figure 18. a) Device architecture of a Si-NC based photodiode and b) spectral responsivity of the device to illumination. (Inset: photograph of the Si-NC photodiode and band gap estimation using the Tauc method). Reproduced and adapted with permission from John Wiley and Sons.[89]

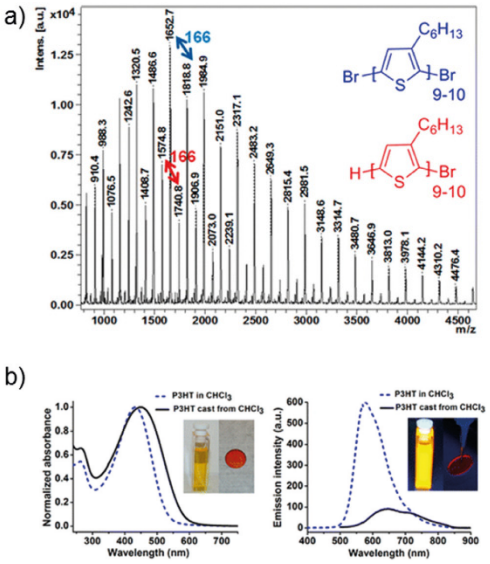

Figure 19. a) MALDI-TOF mass spectrum of P3HT obtained in the presence of chloride terminated Si-NCs and b) UV/Vis absorption (left) and emission (right) spectra of P3HT. Inset: P3HT in chloroform and as a solid film under ambient light (left) and UV illumination (right). Reproduced and adapted with permission from the American Chemical Society.[93]

cycling due to large volume changes (up to 400 %).[94] Si-NCs decrease degradation issues because of their increased surface to volume ratio. Kim et al. demonstrated that battery performance is significantly influenced by Si-NC size.[95] They prepared 5, 10, and 20 nm Si-NCs by reduction of $SiCl_4$ in the presence of different surfactants. While smaller Si-NCs exhibited higher charge capacity (ca. 3000 $mAh\,g^{-1}$ over 40 cycles) compared to larger particles (20 nm), they suffered from lower Coulombic efficiency and capacity retention. However, this obstacle was addressed by encapsulating the smaller Si-NCs within a carbon shell. The researchers concluded that the critical Si-NC size for an efficient battery anode-material was 10 nm. Si nanomaterials have been combined with carbon composites to create hybrids that can overcome common Si-based shortcomings, such as structural degradation, electrical isolation, and formation of an unstable interface.[96] Among the carbon materials employed, graphene is attractive because it can improve carrier transport and mitigates volume changes associated with Li ion uptake.[97] Recently, Ko et al. reported a hybrid material consisting of 5–10 nm amorphous Si nanoparticles and graphene for Li-ion batteries.[98] The material exhibited exquisite elastic properties during the volume change, a capacity of up to 2858 $mAh\,g^{-1}$, 92.5 % Coulombic efficiency, and good cycling stability. Wang et al. prepared a Si-NC/carbon nanotube hybrid upon decomposition of silane gas on vertically aligned carbon nanotubes (Scheme 11).[99] These structures exhibited a highly reversible capacity of 2000 $mAh\,g^{-1}$ over 25 cycles.

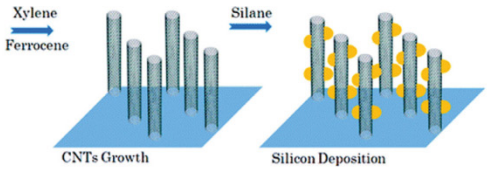

Scheme 11. Schematic of the formation of Si-NC/carbon nanotube hybrids for Li-ion battery application. Reproduced and adapted with permission from the American Chemical Society.[99]

Liu et al. designed a "yolk–shell" type of Li-ion anode material by introducing a void space between the Si nanoparticle and carbon layer.[100] The void space compensates for expansion of the Si particle without the disruption of the carbon shell or the interface. Such structures showed capacity up to 2833 $mAh\,g^{-1}$, high cycle life (ca. 1000), and Coulombic efficiencies of 99.8 %. Other reports on Si nanomaterials based Li-ion battery anodes have been reviewed and are not detailed here.[101]

5. Conclusions and Outlook

In this Review, we have outlined recent important developments related to Si-NC surface chemistry and their

influence on stability, solubility, mechanical, and optoelectronic properties. While hydrosilylation has long been the "go to" reaction for derivatizing Si-NC surfaces, new insights, such as surface-initiated oligomerization, slower reactivity of photochemical hydrosilylation, and borane-catalyzed hydrosilylation, have recently been demonstrated. In addition, new reactivity has emerged for Si hydride and Si halogen surfaces that enable the attachment of ligands with versatile functional groups and enable reactions at lower temperatures. Si-NC/polymer hybrid materials have also been prepared that show synergistic properties, the processable polymers allows the materials to be formed into various morphologies. Polymerization is carried out on the Si-NC surface using radical initiators, RAFT, or surface-initiated group-transfer polymerization methods. Incorporation of polymers onto Si-NC surfaces further expands the field of accessible functional materials. Tunable surface chemistry enables Si-NCs and the hybrids to be further employed in diodes, sensors, catalysis, bioimaging, and photovoltaics, among others.

Readily available, sustainable, and non-toxic, Si-NCs are amenable to commercial-scale applications. While not as well-known as their compound semiconductor counterparts, Si-NCs offer a host of exciting opportunities for both pure and applied research. While proof-of-concept devices highlighting this promise have been fabricated, significant technical advances are required before these materials can be commercialized. Many questions remain unaddressed, including: How to achieve completely oxide free Si-NC surfaces with smaller ligands? How can LED external quantum efficiencies be increased in Si-NC-based devices? What specific emitting species and electronic transitions lead to surface-defect-based emissions? Silicon may be the "grand-old semiconductor", however, it is a relative newcomer to the field of quantum dots and it offers numerous new opportunities to researchers in many fields.

Abbreviations

ATR-FTIR	attenuated total reflectance Fourier transfer infrared spectroscopy
a.u.	arbitrary units
CIE	International Commission on Illumination (Commission Internationale de l'Éclairage)
DNT	dinitrotoluene
ITO	indium tin oxide
LED	light-emitting diode
MALDI	Matrix assisted laserdesorption/ionization
MNT	mononitrotoluene
NALDI	nanostructure assisted laser desorption/ionization
NC	nanocrystal
P3HT	poly-3-hexyl thiophene
PEDOT:PSS	poly(3,4-ethylenedioxythiophene)-poly(styrenesulfonate)
PETN	Pentaerythritol tetranitrate
PL	photoluminescence
Poly-TPD	Poly(4-butylphenyl diphenylamine)
p-Si	porous silicon
PV	photovoltaic
RAFT	reversible addition fragment transfer polymerization
RDX	1,3,5-Trinitroperhydro-1,3,5-triazine
SI-GTP	surface-initiated group-transfer polymerization
Si	silicon
TNT	trinitrotoluene

Acknowledgements

We are grateful to National Engineering Research Council of Canada (NSERC Discovery Grant and CREATE programs) for continued generous support, Canada Foundation for Innovation (CFI), Alberta Science and Research Investment Program (ASRIP), Alberta Innovates Technology Futures (AITF), iCiNano (iCORE Centre for Interdisciplinary Nanoscience) WACKER Chemie AG, Deutsche Forschungsgemeinschaft (DFG), and IRTG 2022 (ATUMS). We thank Jan David Schütz for designing the frontispiece art. M.D. thanks NSERC, Killam Trusts, and AITF for fellowships. J.K. thanks TUM Graduate School for financial support. J.V. acknowledges Richard Siemens for taking the biography photograph. Finally we would like to thank Veinot and Rieger group members for useful discussions.

How to cite: *Angew. Chem. Int. Ed.* **2016**, *55*, 2322–2339
Angew. Chem. **2016**, *128*, 2366–2384

[1] a) A. P. Alivisatos, *Science* **1996**, *271*, 933–937; b) I. Moreels, K. Lambert, D. Smeets, D. De Muynck, T. Nollet, J. C. Martins, F. Vanhaecke, A. Vantomme, C. Delerue, G. Allan, Z. Hens, *ACS Nano* **2009**, *3*, 3023–3030; c) S. Neeleshwar, C. L. Chen, C. B. Tsai, Y. Y. Chen, C. C. Chen, S. G. Shyu, M. S. Seehra, *Phys. Rev. B* **2005**, *71*, 201307.

[2] a) A. M. Smith, S. Nie, *Acc. Chem. Res.* **2010**, *43*, 190–200; b) W. E. Buhro, V. L. Colvin, *Nat. Mater.* **2003**, *2*, 138–139; c) T. R. Gordon, T. Paik, D. R. Klein, G. V. Naik, H. Caglayan, A. Boltasseva, C. B. Murray, *Nano Lett.* **2013**, *13*, 2857–2863; d) M. A. El-Sayed, *Acc. Chem. Res.* **2004**, *37*, 326–333.

[3] a) M. D. Regulacio, M. Y. Han, *Acc. Chem. Res.* **2010**, *43*, 621–630; b) R. E. Bailey, S. Nie, *J. Am. Chem. Soc.* **2003**, *125*, 7100–7106; c) D. Pan, D. Weng, X. Wang, Q. Xiao, W. Chen, C. Xu, Z. Yang, Y. Lu, *Chem. Commun.* **2009**, 4221–4223.

[4] a) N. S. Karan, D. D. Sarma, R. M. Kadam, N. Pradhan, *J. Phys. Chem. Lett.* **2010**, *1*, 2863–2866; b) J. D. Bryan, D. R. Gamelin, *Prog. Inorg. Chem.* **2005**, *54*, 47–126; c) S. Sarkar, N. S. Karan, N. Pradhan, *Angew. Chem. Int. Ed.* **2011**, *50*, 6065–6069; *Angew. Chem.* **2011**, *123*, 6189–6193; d) P. V. Radovanovic, N. S. Norberg, K. E. McNally, D. R. Gamelin, *J. Am. Chem. Soc.* **2002**, *124*, 15192–15193; e) C. M. Tyrakowski, P. T. Snee, *Phys. Chem. Chem. Phys.* **2014**, *16*, 837–855.

[5] a) C. M. Chuang, P. R. Brown, V. Bulović, M. G. Bawendi, *Nat. Mater.* **2014**, *13*, 796–801; b) I. J. Kramer, J. C. Minor, G. Moreno-Bautista, L. Rollny, P. Kanjanaboos, D. Kopilovic, S. M. Thon, G. H. Carey, K. W. Chou, D. Zhitomirsky, A. Amassian, E. H. Sargent, *Adv. Mater.* **2015**, *27*, 116–121; c) P. V. Kamat, *J. Phys. Chem. C* **2008**, *112*, 18737–18753; d) G. H. Carey, A. L. Abdelhady, Z. Ning, S. M. Thon, O. M. Bakr, E. H. Sargent, *Chem. Rev.* **2015**, DOI: 10.1021/acs.chemrev.5b00063.

[6] a) L. Qian, Y. Zheng, J. Xue, P. H. Holloway, *Nat. Photonics* **2011**, *5*, 543–548; b) Y. L. Kong, I. A. Tamargo, H. Kim, B. N.

Johnson, M. K. Gupta, T. Koh, H. Chin, D. A. Steingart, B. P. Rand, M. C. McAlpine, *Nano Lett.* **2014**, *14*, 7017 – 7023; c) E. Jang, S. Jun, H. Jang, J. Lim, B. Kim, Y. Kim, *Adv. Mater.* **2010**, *22*, 3076 – 3080; d) J. M. Caruge, J. E. Halpert, V. Wood, V. Bulović, M. G. Bawendi, *Nat. Photonics* **2008**, *2*, 247 – 250; e) V. Wood, V. Bulović, *Nano Rev.* **2010**, *1*; f) S. Coe, W. Woo, M. G. Bawendi, V. Bulović, *Nature* **2002**, *420*, 800 – 803.

[7] a) J. Shen, Y. Zhu, C. Li, *Chem. Commun.* **2012**, *48*, 3686 – 3699; b) D. Mosconi, D. Mazzier, S. Silvestrini, A. Privitera, C. Marega, L. Franco, A. Moretto, *ACS Nano* **2015**, *9*, 4156 – 4164; c) T. J. Macdonald, T. Nann, *Nanomaterials* **2011**, *1*, 79 – 88.

[8] a) J. Li, J. Zhu, *Analyst* **2013**, *138*, 2506 – 2515; b) B. A. Kairdolf, A. M. Smith, T. H. Stokes, M. D. Wang, A. N. Young, S. Nie, *Annu. Rev. Anal. Chem.* **2013**, *6*, 143 – 162; c) Y. Wang, R. Hu, G. Lin, I. Roy, K. Yong, *ACS Appl. Mater. Interfaces* **2013**, *5*, 2786 – 2799; d) P. Zrazhevskiy, M. Sena, X. Gao, *Chem. Soc. Rev.* **2010**, *39*, 4326 – 4354; e) P. Wu, X. Yan, *Chem. Soc. Rev.* **2013**, *42*, 5489 – 5521; f) S. Jin, Y. Hu, Z. Gu, L. Liu, H. Wu, *J. Nanomater.* **2011**, 834139.

[9] a) D. A. Schwartz, N. S. Norberg, Q. P. Nguyen, J. M. Parker, D. R. Gamelin, *J. Am. Chem. Soc.* **2003**, *125*, 13205 – 13218; b) K. D. Mahajan, Q. Fan, J. Dorcéna, G. Ruan, J. O. Winter, *Biotechnol. J.* **2013**, *8*, 1424 – 1434; c) K. M. Hanif, R. W. Meulenberg, G. F. Strouse, *J. Am. Chem. Soc.* **2002**, *124*, 11495 – 11502; d) P. Wojnar, J. Suffczynski, K. Kowalik, A. Golnik, G. Karczewski, J. Kossut, *Phys. Rev. B* **2007**, *75*, 155301.

[10] a) Z. Yue, F. Lisdat, W. J. Parak, S. G. Hickey, L. Tu, N. Sabir, D. Dorfs, N. C. Bigall, *ACS Appl. Mater. Interfaces* **2013**, *5*, 2800 – 2814; b) C. Y. Zhang, H. C. Yeh, M. T. Kuroki, T. H. Wang, *Nat. Mater.* **2005**, *4*, 826 – 831; c) R. Freeman, I. Willner, *Chem. Soc. Rev.* **2012**, *41*, 4067 – 4085; d) S. Silvi, A. Credi, *Chem. Soc. Rev.* **2015**, *44*, 4275 – 4289; e) T. Jin, A. Sasaki, M. Kinjo, J. Miyazaki, *Chem. Commun.* **2010**, *46*, 2408 – 2410.

[11] a) A. R. Clapp, I. L. Medintz, J. M. Mauro, B. R. Fisher, M. G. Bawendi, H. Mattoussi, *J. Am. Chem. Soc.* **2004**, *126*, 301 – 310; b) Y. Wu, S. K. Campos, G. P. Lopez, M. A. Ozbun, L. A. Sklar, T. Buranda, *Anal. Biochem.* **2007**, *364*, 180 – 192; c) X. Gao, S. Nie, *Anal. Chem.* **2004**, *76*, 2406 – 2410; d) J. L. West, N. J. Halas, *Annu. Rev. Biomed. Eng.* **2003**, *5*, 285 – 292; e) T. Liu, B. Liu, H. Zhang, Y. Wang, *J. Fluoresc.* **2005**, *15*, 729 – 733.

[12] a) N. N. Ledentsov, *Semicond. Sci. Technol.* **2011**, *26*, 014001; b) D. L. Huffaker, G. Park, Z. Zou, O. B. Shchekin, D. G. Deppe, *Appl. Phys. Lett.* **1998**, *73*, 2564 – 2566; c) V. I. Klimov, A. A. Mikhailovsky, S. Xu, A. Malko, J. A. Hollingsworth, C. A. Leatherdale, H. J. Eisler, M. G. Bawendi, *Science* **2000**, *290*, 314 – 317; d) H. J. Eisler, V. C. Sundar, M. G. Bawendi, M. Walsh, H. I. Smith, V. Klimov, *Appl. Phys. Lett.* **2002**, *80*, 4614 – 4616.

[13] a) T. Géza, C. S. Lent, *Phys. Rev. A* **2001**, *63*, 052315; b) Y. S. Weinstein, C. S. Hellberg, J. Levy, *Phys. Rev. A* **2005**, *72*, 020304; c) J. M. Elzerman, R. Hanson, L. H. W. van Beveren, B. Witkamp, L. M. K. Vandersypen, L. P. Kouwenhoven, *Nature* **2004**, *430*, 431 – 435.

[14] a) A. G. Cullis, L. T. Canham, *Nature* **1991**, *353*, 335 – 338; b) A. G. Cullis, L. T. Canham, P. D. J. Calcott, *J. Appl. Phys.* **1997**, *82*, 909 – 965.

[15] a) P. C. Searson, J. M. Macauly, S. M. Prokes, *J. Electrochem. Soc.* **1992**, *139*, 3373 – 3377; b) J. P. Proot, C. Delerue, G. Allan, *Appl. Phys. Lett.* **1992**, *61*, 1948 – 1950; c) J. H. Park, L. Gu, G. von Maltzahn, E. Ruoslahti, S. N. Bhatia, M. J. Sailor, *Nat. Mater.* **2009**, *8*, 331 – 336; d) M. P. Stewart, J. M. Buriak, *Adv. Mater.* **2000**, *12*, 859 – 869; e) F. Cunin, T. A. Schmedake, J. R. Link, Y. Y. Li, J. Koh, S. N. Bhatia, M. J. Sailor, *Nat. Mater.* **2002**, *1*, 39 – 41.

[16] a) R. K. Baldwin, K. A. Pettigrew, E. Ratai, M. P. Augustine, S. M. Kauzlarich, *Chem. Commun.* **2002**, 1822 – 1823; b) M. Sletnes, J. Maria, T. Grande, M. Lindgren, M. A. Einarsud, *Dalton Trans.* **2014**, *43*, 2127 – 2133; c) J. H. Warner, A. Hashino, K. Yamamoto, R. D. Tilley, *Angew. Chem. Int. Ed.* **2005**, *44*, 4550 – 4554; *Angew. Chem.* **2005**, *117*, 4626 – 4630; d) A. Shiohara, S. Prabakar, A. Faramus, C. Y. Hsu, P. S. Lai, P. T. Northcote, R. D. Tilley, *Nanoscale* **2011**, *3*, 3364 – 3370; e) A. Shiohara, S. Hanada, S. Prabakar, K. Fujioka, T. H. Lim, K. Yamamoto, P. T. Northcote, R. D. Tilley, *J. Am. Chem. Soc.* **2010**, *132*, 248 – 253.

[17] a) C. S. Yang, R. A. Bley, S. M. Kauzlarich, H. W. H. Lee, G. R. Delgado, *J. Am. Chem. Soc.* **1999**, *121*, 5191 – 5195; b) T. M. Atkins, M. C. Cassidy, M. Lee, S. Ganguly, C. M. Marcus, S. M. Kauzlarich, *ACS Nano* **2013**, *7*, 1609 – 1617; c) B. M. Nolan, T. Henneberger, M. Waibel, T. F. Fässler, S. M. Kauzlarich, *Inorg. Chem.* **2015**, *54*, 396 – 401; d) K. A. Pettigrew, Q. Liu, P. P. Power, S. M. Kauzlarich, *Chem. Mater.* **2003**, *15*, 4005 – 4011; e) T. M. Atkins, A. Thibert, D. S. Larsen, S. Dey, N. D. Browning, S. M. Kauzlarich, *J. Am. Chem. Soc.* **2011**, *133*, 20664 – 20667.

[18] a) C. M. Hessel, E. J. Henderson, J. G. C. Veinot, *Chem. Mater.* **2006**, *18*, 6139 – 6146; b) E. J. Henderson, J. A. Kelly, J. G. C. Veinot, *Chem. Mater.* **2009**, *21*, 5426 – 5434; c) M. Dasog, C. Rachinsky, J. G. C. Veinot, *J. Mater. Chem.* **2011**, *21*, 12422 – 12427; d) C. M. Hessel, D. Reid, M. G. Panthani, M. R. Rasch, B. W. Goodfellow, J. Wei, H. Fujii, V. Akhavan, B. A. Korgel, *Chem. Mater.* **2012**, *24*, 393 – 401; e) M. L. Mastronardi, F. Hennrich, E. J. Henderson, F. Maier-Flaig, C. Blum, J. Reichenbach, U. Lemmer, C. Kübel, D. Wang, M. M. Kappes, G. A. Ozin, *J. Am. Chem. Soc.* **2011**, *133*, 11928 – 11931.

[19] a) L. Mangolini, E. Thimsen, U. Kortshagen, *Nano Lett.* **2005**, *5*, 655 – 659; b) X. D. Pi, R. W. Liptak, J. D. Nowak, N. P. Wells, C. B. Carter, S. A. Campbell, U. Kortshagen, *Nanotechnology* **2008**, *19*, 245603; c) X. Li, Y. He, M. T. Swihart, *Langmuir* **2004**, *20*, 4720 – 4727; d) F. Huisken, G. Ledoux, O. Guillois, C. Reynaud, *Adv. Mater.* **2002**, *14*, 1861 – 1865; e) X. Li, Y. He, S. S. Talukdar, M. T. Swihart, *Langmuir* **2003**, *19*, 8490 – 8496.

[20] M. Dasog, Z. Yang, J. G. C. Veinot, *CrystEngComm* **2012**, *14*, 7576 – 7578.

[21] J. D. Holmes, K. J. Ziegler, R. C. Doty, L. E. Pell, K. P. Johnston, B. A. Korgel, *J. Am. Chem. Soc.* **2001**, *123*, 3743 – 3748.

[22] a) J. Choi, N. S. Wang, V. Reipa, *Langmuir* **2007**, *23*, 3388 – 3394; b) J. Hwang, Y. Jeong, K. H. Lee, Y. Seo, J. Kim, J. W. Hong, E. Kamaloo, T. A. Camesano, J. Choi, *Ind. Eng. Chem. Res.* **2015**, *54*, 5982 – 5989.

[23] a) A. S. Heintz, M. J. Fink, B. S. Mitchell, *Adv. Mater.* **2007**, *19*, 3984 – 3988; b) A. S. Chaudhary, D. A. Sheppard, M. Paskevicius, M. Saunders, C. E. Buckley, *RSC Adv.* **2014**, *4*, 21979 – 21983.

[24] X. Cheng, S. B. Lowe, P. J. Reece, J. J. Gooding, *Chem. Soc. Rev.* **2014**, *43*, 2680 – 2700.

[25] J. G. C. Veinot, *Chem. Commun.* **2006**, 4160 – 4168.

[26] a) H. Zhu, N. Song, T. Lian, *J. Am. Chem. Soc.* **2010**, *132*, 15038 – 15045; b) K. Gong, J. E. Martin, L. E. Shea-Rohwer, P. Lu, D. F. Kelley, *J. Phys. Chem. C* **2015**, *119*, 2231 – 2238; c) S. Kim, B. Fisher, H. J. Eisler, M. Bawendi, *J. Am. Chem. Soc.* **2003**, *125*, 11466 – 11467.

[27] M. R. Linford, P. Fenter, P. M. Eisenberg, C. E. D. Chidsey, *J. Am. Chem. Soc.* **1995**, *117*, 3145 – 3155.

[28] a) J. M. Buriak, *Chem. Rev.* **2002**, *102*, 1271 – 1308; b) S. Ciampi, J. B. Harper, J. J. Gooding, *Chem. Soc. Rev.* **2010**, *39*, 2158 – 2183; c) F. Tian, A. V. Teplyakov, *Langmuir* **2013**, *29*, 13 – 28.

[29] Y. Yu, C. E. Rowland, R. D. Schaller, B. A. Korgel, *Langmuir* **2015**, *31*, 6886 – 6893.

[30] a) R. Boukherroub, S. Morin, F. Bensebaa, D. D. M. Wayner, *Langmuir* **1999**, *15*, 3831 – 3835; b) J. E. Bateman, R. D. Eagling, D. R. Worrall, B. R. Horrocks, A. Houlton, *Angew.*

Chem. Int. Ed. **1998**, *37*, 2683 – 2685; *Angew. Chem.* **1998**, *110*, 2829 – 2831.

[31] a) V. I. Boiadjiev, G. M. Brown, L. A. Pinnaduwage, G. Goretzki, P. V. Bonnesen, T. Thundat, *Langmuir* **2005**, *21*, 1139 – 1142; b) L. A. Huck, J. M. Buriak, *Langmuir* **2012**, *28*, 16285 – 16295; c) R. L. Cicero, M. R. Linford, C. E. D. Chidsey, *Langmuir* **2000**, *16*, 5688 – 5695; d) F. Hua, M. T. Swihart, E. Ruckenstein, *Langmuir* **2005**, *21*, 6054 – 6062; e) Z. Yang, G. B. De Los Reyes, L. V. Titova, I. Sychugov, M. Dasog, J. Linnros, F. A. Hegmann, J. G. C. Veinot, *ACS Photonics* **2015**, *2*, 595 – 605.

[32] J. M. Schmeltzer, L. A. Porter, M. P. Stewart, J. M. Buriak, *Langmuir* **2002**, *18*, 2971 – 2974.

[33] a) A. B. Sieval, R. Linke, H. Zuilhof, E. J. R. Sudhölter, *Adv. Mater.* **2000**, *12*, 1457 – 1460; b) R. D. Tilley, J. H. Warner, K. Yamamoto, I. Matsui, H. Fujimori, *Chem. Commun.* **2005**, 1833 – 1835; c) R. D. Tilley, K. Yamamoto, *Adv. Mater.* **2006**, *18*, 2053 – 2056.

[34] a) J. M. Buriak, M. P. Stewart, T. W. Geders, M. J. Allen, H. C. Choi, J. Smith, D. Raftery, L. T. Canham, *J. Am. Chem. Soc.* **1999**, *121*, 11491 – 11502; b) J. M. Buriak, M. J. Allen, *J. Am. Chem. Soc.* **1998**, *120*, 1339 – 1340; c) L. J. Webb, N. S. Lewis, *J. Phys. Chem. B* **2003**, *107*, 5404 – 5412.

[35] a) H. Sugimura, S. Mo, K. Yamashiro, T. Ichii, K. Murase, *J. Phys. Chem. C* **2013**, *117*, 2480 – 2485; b) F. Liu, E. J. Luber, L. A. Huck, B. C. Olsen, J. M. Buriak, *ACS Nano* **2015**, *9*, 2184 – 2193.

[36] a) S. L. Weeks, B. Macco, M. C. M. van de Sanden, S. Agarwal, *Langmuir* **2012**, *28*, 17295 – 17301; b) B. N. Jariwala, O. S. Dewey, P. Stradins, C. V. Ciobanu, S. Agarwal, *ACS Appl. Mater. Interfaces* **2011**, *3*, 3033 – 3041.

[37] Z. Yang, M. Iqbal, A. R. Dobbie, J. G. C. Veinot, *J. Am. Chem. Soc.* **2013**, *135*, 17595 – 17601.

[38] M. G. Panthani, C. M. Hessel, D. Reid, G. Casillas, M. José-Yacamán, B. A. Korgel, *J. Phys. Chem. C* **2012**, *116*, 22463 – 22468.

[39] F. Sangghaleh, I. Sychugov, Z. Yang, J. G. C. Veinot, J. Linnros, *ACS Nano* **2015**, *9*, 7097 – 7104.

[40] C. Qian, W. Sun, L. Wang, C. Chen, K. Liao, W. Wang, J. Jia, B. D. Hatton, G. Casillas, M. Kurylowicz, C. M. Yip, M. L. Mastronardi, G. A. Ozin, *J. Am. Chem. Soc.* **2014**, *136*, 15849 – 15852.

[41] J. Rinck, D. Schray, C. Kübel, A. K. Powell, G. A. Ozin, *Small* **2015**, *11*, 335 – 340.

[42] M. Woods, S. Carlsson, Q. Hong, S. N. Patole, L. H. Lie, A. Houlton, B. R. Horrocks, *J. Phys. Chem. B* **2005**, *109*, 24035 – 24045.

[43] a) J. A. Kelly, A. M. Shukaliak, M. D. Fleischauer, J. G. C. Veinot, *J. Am. Chem. Soc.* **2011**, *133*, 9564 – 9571; b) J. A. Kelly, J. G. C. Veinot, *ACS Nano* **2010**, *4*, 4645 – 4656; c) Z. Yang, G. B. De Los Reyes, L. V. Titova, I. Sychugov, M. Dasog, J. Linnros, F. A. Hegmann, J. G. C. Veinot, *ACS Photonics* **2015**, *2*, 595 – 605.

[44] a) S. Li, I. N. Germanenko, M. S. El-Shall, *J. Phys. Chem. B* **1998**, *102*, 7319 – 7322; b) D. Andsager, J. Hilliard, J. M. Hetrick, L. H. Abuhassan, M. Plisch, M. H. Nayfeh, *J. Appl. Phys.* **1993**, *74*, 4783 – 4785.

[45] T. K. Purkait, M. Iqbal, M. H. Wahl, K. Gottschling, C. M. Gonzales, M. A. Islam, J. G. C. Veinot, *J. Am. Chem. Soc.* **2014**, *136*, 17914 – 17917.

[46] I. M. D. Höhlein, J. Kehrle, T. Helbich, Z. Yang, J. G. C. Veinot, B. Rieger, *Chem. Eur. J.* **2014**, *20*, 4212 – 4216.

[47] J. Pinson, F. Podvorica, *Chem. Soc. Rev.* **2005**, *34*, 429 – 439.

[48] D. Wang, J. M. Buriak, *Langmuir* **2006**, *22*, 6214 – 6221.

[49] I. M. D. Höhlein, J. Kehrle, T. K. Purkait, J. G. C. Veinot, B. Rieger, *Nanoscale* **2015**, *7*, 914 – 918.

[50] a) M. Dasog, Z. Yang, S. Regli, T. M. Atkins, A. Faramus, M. P. Singh, E. Muthuswamy, S. M. Kauzlarich, R. D. Tilley, J. G. C. Veinot, *ACS Nano* **2013**, *7*, 2676 – 2685; b) M. Dasog, J. G. C. Veinot, *Phys. Status Solidi B* **2014**, *251*, 2216 – 2220.

[51] O. Wolf, M. Dasog, Z. Yang, I. Balberg, J. G. C. Veinot, O. Millo, *Nano Lett.* **2013**, *13*, 2516 – 2521.

[52] J. Fuzell, A. Thibert, T. M. Atkins, M. Dasog, E. Busby, J. G. C. Veinot, S. M. Kauzlarich, D. S. Larsen, *J. Phys. Chem. Lett.* **2013**, *4*, 3806 – 3812.

[53] M. Dasog, G. B. De Los Reyes, L. V. Titova, F. A. Hegmann, J. G. C. Veinot, *ACS Nano* **2014**, *8*, 9636 – 9648.

[54] I. M. D. Höhlein, A. Angi, R. Sinclnikov, J. G. C. Veinot, B. Rieger, *Chem. Eur. J.* **2015**, *21*, 2755 – 2758.

[55] L. M. Wheeler, N. R. Neale, T. Chen, U. R. Kortshagen, *Nat. Commun.* **2013**, *4*, 2197.

[56] A. Bansal, X. Li, I. Lauermann, N. S. Lewis, S. I. Yi, W. H. Weinberg, *J. Am. Chem. Soc.* **1996**, *118*, 7225 – 7226.

[57] M. Dasog, J. G. C. Veinot, *Phys. Status Solidi A* **2012**, *209*, 1844 – 1846.

[58] M. Dasog, K. Bader, J. G. C. Veinot, *Chem. Mater.* **2015**, *27*, 1153 – 1156.

[59] J. P. Bell, J. E. Cloud, J. Cheng, C. Ngo, S. Kodambaka, A. Sellinger, S. K. R. Williams, Y. Yang, *RSC Adv.* **2014**, *4*, 51105 – 51110.

[60] Q. Li, Y. He, J. Chang, L. Wang, H. Chen, Y. W. Tan, H. Wang, Z. Shao, *J. Am. Chem. Soc.* **2013**, *135*, 14924 – 14927.

[61] L. Wang, Q. Li, H. Y. Wang, J. C. Huang, R. Zhang, Q. D. Chen, H. L. Xu, W. Han, Z. Z. Shao, H. B. Sun, *Light Sci. Appl.* **2015**, *4*, e245.

[62] Y. Zhai, M. Dasog, R. B. Snitynsky, T. K. Purkait, M. Aghajamali, A. H. Hahn, C. B. Sturdy, T. L. Lowary, J. G. C. Veinot, *J. Mater. Chem. B* **2014**, *2*, 8427 – 8433.

[63] a) W. Shi, H. Zeng, Y. Sahoo, T. Y. Ohulchanskyy, Y. Ding, Z. L. Wang, M. Swihart, P. N. Prasad, *Nano Lett.* **2006**, *6*, 875 – 881; b) J. Liu, T. Tanaka, K. Sivula, A. P. Alivisatos, J. M. J. Fréchet, *J. Am. Chem. Soc.* **2004**, *126*, 6550 – 6551; c) X. Huang, J. Li, *J. Am. Chem. Soc.* **2007**, *129*, 3157 – 3162; d) J. M. Tsay, M. Pflughoefft, L. A. Bentolila, S. Weiss, *J. Am. Chem. Soc.* **2004**, *126*, 1926 – 1927.

[64] a) A. Guchhait, A. J. Pal, *ACS Appl. Mater. Interfaces* **2013**, *5*, 4181 – 4189; b) G. Zhu, C. Bao, Y. Liu, X. Shen, C. Xi, Z. Xu, Z. Ji, *Nanoscale* **2014**, *6*, 11147 – 11156; c) P. Reiss, E. Couderc, J. D. Girolamo, A. Pron, *Nanoscale* **2011**, *3*, 446 – 489; d) W. Yao, S. H. Yu, X. Y. Huang, J. Jiang, L. Q. Zhao, L. Pan, J. Li, *Adv. Mater.* **2005**, *17*, 2799 – 2802.

[65] a) P. Chawla, S. Singh, S. N. Sharma, *Beilstein J. Nanotechnol.* **2014**, *5*, 1235 – 1244; b) J. J. Wang, J. S. Hu, Y. G. Guo, L. J. Wan, *NPG Asia Mater.* **2012**, *4*, e2.

[66] C. Y. Liu, Z. C. Holman, U. R. Kortshagen, *Nano Lett.* **2009**, *9*, 449 – 452.

[67] S. Mitra, S. Cook, V. Švrček, R. A. Blackey, W. Zhou, J. Kovač, U. Cvelbar, D. Mariotti, *J. Phys. Chem. C* **2013**, *117*, 23198 – 23207.

[68] C. M. Hessel, M. R. Rasch, J. L. Hueso, B. W. Goodfellow, V. A. Akhavan, P. Puvanakrishnan, J. W. Tunnel, B. A. Korgel, *Small* **2010**, *6*, 2026 – 2034.

[69] Z. Yang, M. Dasog, A. R. Dobbie, R. Lockwood, Y. Zhi, A. Meldrum, J. G. C. Veinot, *Adv. Funct. Mater.* **2014**, *24*, 1345 – 1353.

[70] M. X. Dung, J. K. Choi, H. D. Jeong, *ACS Appl. Mater. Interfaces* **2013**, *5*, 2400 – 2409.

[71] J. K. Choi, M. X. Dung, H. D. Jeong, *Mater. Chem. Phys.* **2014**, *148*, 463 – 472.

[72] J. Kehrle, I. M. D. Höhlein, Z. Yang, A. R. Jochem, T. Helbich, T. Kraus, J. G. C. Veinot, B. Rieger, *Angew. Chem. Int. Ed.* **2014**, *53*, 12494 – 12497; *Angew. Chem.* **2014**, *126*, 12702 – 12705.

[73] K. Sato, N. Fukata, K. Hirakuri, M. Murakami, T. Shimizu, Y. Yamauchi, *Chem. Asian J.* **2010**, *5*, 50 – 55.
[74] I. M. D. Höhlein, P. D. L. Werz, J. G. C. Veinot, B. Rieger, *Nanoscale* **2015**, *7*, 7811 – 7818.
[75] N. H. Alsharif, C. E. Berger, S. S. Varanasi, Y. Chao, B. R. Horrocks, H. K. Datta, *Small* **2008**, *5*, 221 – 228.
[76] B. F. P. McVey, R. D. Tilley, *Acc. Chem. Res.* **2014**, *47*, 3045 – 3051.
[77] Z. Li, Q. Sun, Y. Zhu, B. Tan, Z. P. Xu, S. X. Dou, *J. Mater. Chem. B* **2014**, *2*, 2793 – 2818.
[78] F. Peng, Y. Su, Y. Zhong, C. Fan, S. T. Lee, Y. He, *Acc. Chem. Res.* **2014**, *47*, 612 – 623.
[79] M. Schnabel, C. Weiss, P. Löper, P. R. Wilshaw, S. Janz, *Phys. Status Solidi A* **2015**, *212*, 1649 – 1661.
[80] L. Basabe-Desmonts, D. N. Reinhoudt, M. Crego-Calama, *Chem. Soc. Rev.* **2007**, *36*, 993 – 1017.
[81] a) K. Zhang, H. Zhou, Q. Mei, S. Wang, G. Guan, R. Liu, J. Zhang, Z. Zhang, *J. Am. Chem. Soc.* **2011**, *133*, 8424 – 8427; b) R. Freeman, T. Finder, L. Bahshi, R. Gill, I. Willner, *Adv. Mater.* **2012**, *24*, 6416 – 6421.
[82] C. M. Gonzalez, M. Iqbal, M. Dasog, D. G. Piercey, R. Lockwood, T. M. Klapötke, J. G. C. Veinot, *Nanoscale* **2014**, *6*, 2608 – 2612.
[83] R. Ban, F. Zheng, J. Zhang, *Anal. Methods* **2015**, *7*, 1732 – 1737.
[84] X. Zhang, X. Chen, S. Kai, H. Y. Wang, J. Yang, F. G. Wu, Z. Chen, *Anal. Chem.* **2015**, *87*, 3360 – 3365.
[85] K. Y. Cheng, R. Anthony, U. R. Kortshagen, R. J. Holmes, *Nano Lett.* **2010**, *10*, 1154 – 1157.
[86] K. Y. Cheng, R. Anthony, U. R. Kortshagen, R. J. Holmes, *Nano Lett.* **2011**, *11*, 1952 – 1956.
[87] F. Maier-Flaig, J. Rinck, M. Stephan, T. Bocksrocker, M. Bruns, C. Kübel, A. K. Powell, G. A. Ozin, U. Lemmer, *Nano Lett.* **2013**, *13*, 475 – 480.
[88] B. Ghosh, Y. Masuda, Y. Wakayama, Y. Imanaka, J. Inoue, K. Hashi, K. Deguchi, H. Yamada, Y. Sakka, S. Ohki, T. Shimizu, N. Shirahata, *Adv. Funct. Mater.* **2014**, *24*, 7151 – 7160.
[89] T. Lin, X. Liu, B. Zhou, Z. Zhan, A. N. Cartwright, M. T. Swihart, *Adv. Funct. Mater.* **2014**, *24*, 6016 – 6022.
[90] F. Erogbogbo, T. Lin, P. M. Tucciarone, K. M. LaJoie, L. Lai, G. D. Patki, P. N. Prasad, M. T. Swihart, *Nano Lett.* **2013**, *13*, 451 – 456.
[91] F. Peng, J. Wang, G. Ge, T. He, L. Cao, Y. He, H. Ma, S. Sun, *Mater. Lett.* **2013**, *92*, 65 – 67.
[92] J. K. El-Demellawi, C. R. Holt, E. Abou-Hamad, Z. A. Al-Talla, Y. Saih, S. Chaieb, *ACS Appl. Mater. Interfaces* **2015**, *7*, 13794 – 13800.
[93] M. A. Islam, T. K. Purkait, J. G. C. Veinot, *J. Am. Chem. Soc.* **2014**, *136*, 15130 – 15133.
[94] J. Chen, *Materials* **2013**, *6*, 156 – 183.
[95] H. Kim, M. Seo, M. H. Park, J. Cho, *Angew. Chem. Int. Ed.* **2010**, *49*, 2146 – 2149; *Angew. Chem.* **2010**, *122*, 2192 – 2195.
[96] a) P. Zuo, G. Yin, Y. Ma, *Electrochim. Acta* **2007**, *52*, 4878 – 4883; b) Y. Xu, Y. Zhu, C. Wang, *J. Mater. Chem. A* **2014**, *2*, 9751 – 9757; c) J. Wu, X. Qin, H. Zhang, Y. B. He, B. Li, L. Ke, W. Lv, H. Du, Q. H. Yang, F. Kang, *Carbon* **2015**, *84*, 434 – 443.
[97] a) I. H. Son, J. H. Park, S. Kwon, S. Park, M. H. Rümmeli, A. Bachmatiuk, H. J. Song, J. Ku, J. W. Choi, J. Choi, S. G. Doo, H. Chang, *Nat. Commun.* **2015**, *6*, 7393; b) F. Maroni, R. Raccichini, A. Birrozzi, G. Carbonari, R. Tossici, F. Croce, R. Marassi, F. Nobili, *J. Power Sources* **2014**, *269*, 873 – 882; c) J. K. Lee, K. B. Smith, C. M. Hayner, H. H. Kung, *Chem. Commun.* **2010**, *46*, 2025 – 2027; d) M. Zhou, X. Li, B. Wang, Y. Zhang, J. Ning, Z. Xiao, X. Zhang, Y. Chang, L. Zhi, *Nano Lett.* **2015**, *15*, 6222 – 6228.
[98] M. Ko, S. Chae, S. Jeong, P. Oh, J. Cho, *ACS Nano* **2014**, *8*, 8591 – 8599.
[99] W. Wang, P. N. Kumta, *ACS Nano* **2010**, *4*, 2233 – 2241.
[100] N. Liu, H. Wu, M. T. McDowell, Y. Yao, C. Wang, Y. Cui, *Nano Lett.* **2012**, *12*, 3315 – 3321.
[101] a) B. Liang, Y. Liu, Y. Xu, *J. Power Sources* **2014**, *267*, 469 – 490; b) D. Ma, Z. Cao, A. Hu, *Nano Micro Lett.* **2014**, *6*, 347 – 358; c) X. Su, Q. Wu, J. Li, X. Xiao, A. Lott, W. Lu, B. W. Sheldon, J. Wu, *Adv. Energy Mater.* **2014**, *4*, 1 – 23; d) M. R. Zamfir, H. T. Nguyen, E. Moyen, Y. H. Lee, D. Pribat, *J. Mater. Chem. A* **2013**, *1*, 9566 – 9586; e) J. R. Szczech, S. Jin, *Energy Environ. Sci.* **2011**, *4*, 56 – 72; f) H. Kim, E. J. Lee, Y. K. Sun, *Mater. Today* **2014**, *17*, 285 – 297.

Received: July 2, 2015
Revised: September 18, 2015
Published online: November 26, 2015

4.4.4. Reprint Permission – Angew. Chem. Int. Ed.

JOHN WILEY AND SONS LICENSE
TERMS AND CONDITIONS

Jun 19, 2017

This Agreement between Julian Kehrle ("You") and John Wiley and Sons ("John Wiley and Sons") consists of your license details and the terms and conditions provided by John Wiley and Sons and Copyright Clearance Center.

License Number	4132630839543
License date	Jun 19, 2017
Licensed Content Publisher	John Wiley and Sons
Licensed Content Publication	Angewandte Chemie International Edition
Licensed Content Title	Silicon Nanocrystals and Silicon-Polymer Hybrids: Synthesis, Surface Engineering, and Applications
Licensed Content Author	Mita Dasog,Julian Kehrle,Bernhard Rieger,Jonathan G. C. Veinot
Licensed Content Date	Nov 26, 2015
Licensed Content Pages	18
Type of use	Dissertation/Thesis
Requestor type	Author of this Wiley article
Format	Print and electronic
Portion	Full article
Will you be translating?	No
Title of your thesis / dissertation	Surface Hydrosilylation: The Key to Silicon Nanocrystal Hybrid and Composite Materials
Expected completion date	Aug 2017
Expected size (number of pages)	190
Requestor Location	Julian Kehrle Lichtenbergstraße 4 Garching, 85748 Germany Attn: Julian Kehrle
Publisher Tax ID	EU826007151
Billing Type	Invoice
Billing Address	Julian Kehrle Lichtenbergstraße 4 Garching, Germany 85748 Attn: Julian Kehrle
Total	0.00 EUR
Terms and Conditions	

TERMS AND CONDITIONS

This copyrighted material is owned by or exclusively licensed to John Wiley & Sons, Inc. or one of its group companies (each a"Wiley Company") or handled on behalf of a society with

5. Conclusion and Outlook

Silicon Nanocrystal based hybrid materials gain increasing interests in applications, such as drug delivery, sensing, catalysis or energy conversion. As “the” first step in the preparation of hybrid materials, the understanding of surface grafting has a high priority in this rather young field of science. Hence, the aim of this thesis is to study surface processes and to synthesize promising materials for various applications.

A hybrid material consisted of silicon nanocrystals (SiNCs) and poly(diethyl vinylphosphonate) (PDEVP) was prepared, which combined the features of both materials – the photoluminescence of the SiNCs and the lower critical solution temperature effect of the PDEVP. The water-soluble hybrid material could be precipitated from water through heating. The stable SiNCs’ photoluminescence (PL) could be used to analyze the residence of the material. This is a result of the preparation pathway, which integrated the SiNCs in a partially hydrophobic poly(ethylene glycol dimethacrylate) (PEGDM) network, which was surrounded by the water-soluble polymer. In a further study the ideal catalyst and monomer concentrations were verified and the surface grafting of methyl methacrylate, dimethyl vinylphosphonate and diisopropyl vinylphosphonates from ethylene glycol dimethacrylate decorated SiNC surfaces was shown. Improvement of the present materials can be promising for simultaneous and target oriented drug delivery for example in inflammations, which generally come along with enhanced temperatures in infected body cells.

After these investigations, the attention was turned towards the understanding of the azobisisobutyronitrile initiated hydrosilylation of olefins on hydride terminated surfaces. The studies were performed using the *in-situ* infrared spectroscopy (IR) technique. Vinylsilanes were used as model compounds for the evaluation of steric impacts. *In-situ* IR in combination with time resolved UV-VIS measurements clearly demonstrated that SiNC agglomerates break up during grafting. The whole grafting process was strictly dependent on the concentration of radicals (e.g. initiator concentration or decomposition temperature); with low radical concentrations chain processes were observed. Solution oligomerization plays an important role for the initiation of the hydride terminated SiNC surfaces. Additionally, the process was sensitive towards steric changes of the monomer. In contrast, no effect was observed if the monomer concentration was varied. These studies are fundamental in understanding this cheap and functional group tolerant SiNC hydrosilylation approach.

In the third part of this thesis, SiNCs were covalently interconnected with silica aerogels through triethoxyvinylsilane surface groups. Two approaches for the intercalation of SiNCs were performed. If SiNCs were directly added to the alcogel formation, SiNCs were located in the silica network and induced a stronger crosslinking. In contrast, if SiNCs were washed in the alcogel after the gelation process, they were located in the pores. In all cases, the alcogels were reacted with trimethylsilyl chloride before supercritical drying resulting in superhydrophobic properties. In addition, the superhydrophobic materials had very high porosities, surface areas of ~ 1000 m^2/g and SiNC size dependent photoluminescence. The materials could be used for

the accumulation of 3-nitrotoluene from a low concentrated solution in water, with simultaneous elimination of the photoluminescence. This behavior indicates promising material properties for the disposal or recovery of organic molecules (e.g. pollutants).

6. Addendum: Oxasilacycles Leading to UV-Curable Polymers: Synthesis and Application

6.1. Introduction and State of the Art

The use of UV coatings bears an enormous potential in saving energy, compared to thermally cured coatings. Well known photocuring systems are based on radical reactions, arising from the photosensitive activation of benzophenone and its derivatives or on UV curable epoxy lacquers.[297,298] Photoacid generators can be applied as alternatives to the well-established procedures. From the excitation with UV light, they generate Brønstedt acids, which can be exploited for the hydrolysis of Si-O-R bonds. In the present systems, Si-O-R bonds are the binding structure in oxasilacycles. The demonstrated molecules give new chances for the crosslinking of polymers without the release of volatile organic compounds (VOC; Scheme 39).

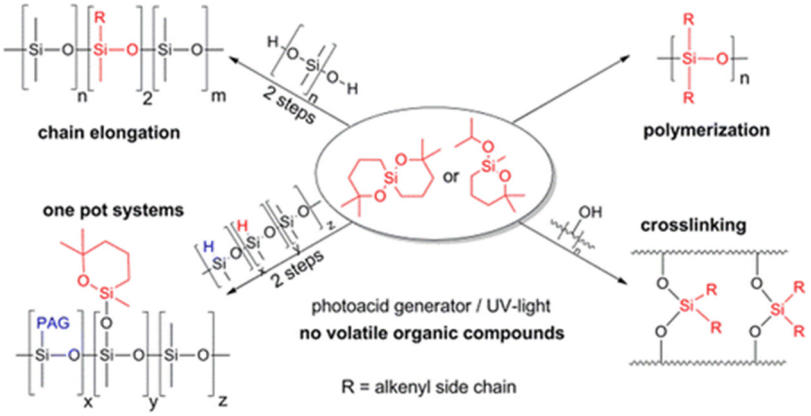

Scheme 39. Overview of applications of oxasilacycles in polymer chemistry.[299] Reproduced and adapted with permission from reference 300. Copyright 2014 American Chemical Society.

Hydrosilylation with *tris*(pentafluorophenyl borane)

A crucial step in the preparation of oxasilacycles is the hydrosilylation with *tris*(pentafluorophenyl borane) (BCF). It acts as a mild and homogeneous hydrosilylation catalyst, which allows the reaction of aryl- and alkyl substituted olefins with highly substituted silanes.[206] Thus, BCF is the best catalyst for the preparation of oxasilacycles. Gevorgyan *et al.* elucidated the mechanism of BCF hydrosilylation reactions (Scheme 40). The formation of the *ate*-complex in the first equilibrium reaction is crucial for the process. The subsequent nucleophilic attack of the olefin at the silicon cation is the rate determining step of the reaction leading to the formation of a 1-trialkylsilyl-2-alkylium ion. Fast proton transfer leads to the regeneration of the Lewis acid.

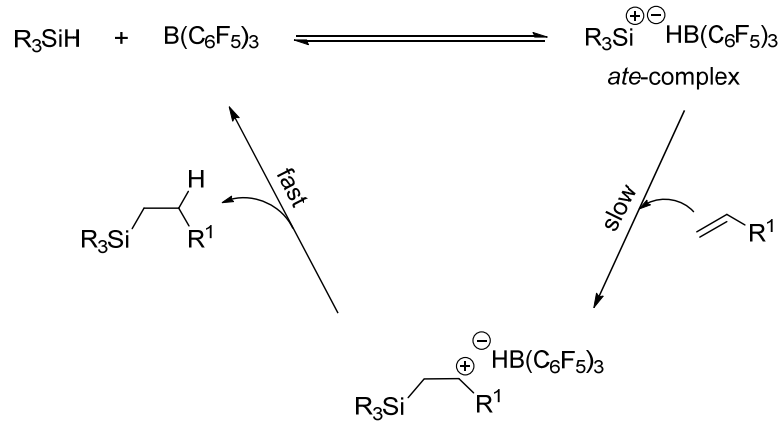

Scheme 40. BCF catalyzed hydrosilylation reaction according to Gevorgyan et al.[206]

Shchepin *et al.* published, that besides the bimolecular reactions, BCF is well suitable for the intramolecular hydrosilylation.[300] By a variation of the molecule sizes of the terminal olefins, they could selectively synthesize *endo*-5 and *endo*-6 membered rings, which are the binding motives of oxasilacycles. However, several side reactions need to be excluded during intramolecular hydrosilylations. Alkylhydroxysilanes react with alkylhydrosilanes to (poly)siloxanes in the presence of BCF.[206,301] Furthermore, metathesis reactions can occur or trace water can coordinate to the boron center reducing the rate of the hydrosilylation reaction.[302]

Synthesis and reactions of polysiloxanes

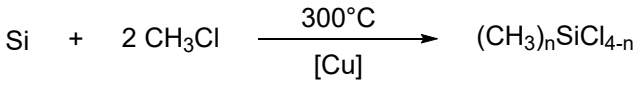

Scheme 41. Preparation of methylchlorosilanes.[303]

In the synthesis of oxasilacycles, the linear precursor for the intramolecular hydrosilylation reaction is obtained by the condensation of the reactive α-hydroxy-ω-alkenes with a chlorosilane ($Cl_nH_mSiR_{(4-n-m)}$). Such silanes are prepared in the *Müller-Rochow* process (Scheme 41).[303,304] In the process silicon is reacted with methyl chloride in the presence of a copper catalyst and other metals (e.g., Ca, Mg, Zn), the so-called promoters. Mainly dimethyl dichlorosilane is yielded from this reaction, but also other methylchlorosilanes are gained in lower quantities. Methyl chloride can be prepared from the reaction of methanol with hydrogen chloride. Phenylchlorosilanes are obtained from a comparable reaction of silicon with phenyl chloride, albeit at elevated temperatures. The addition of hydrogen chloride to the reaction forms hydrosilanes. In any case rectification/distillation is used to separate the fractions and to obtain the purified silanes.[303,304]

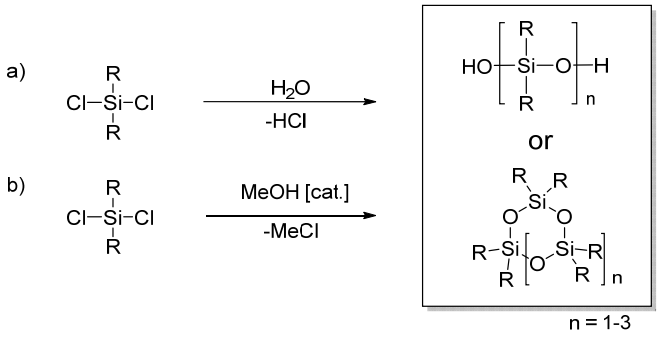

Scheme 42. Preparation of oligomeric and cyclic siloxanes from dialkyldichlorosilanes: a) hydrolysis, b) methanolysis.

Most of the chlorosilanes are used for the generation of polysiloxanes. However, the linear polysiloxanes are prepared in two stages. Hydrolysis-condensation or methanolysis-condensation of dialkyldichlorosilanes are applied for the preparation of cyclic precursors or oligomer species (Scheme 42). If water is used, hydroxy terminated, linear and cyclic polysiloxanes are formed in 20 - 80 % yield (Scheme 42 a). [303,304] If the reaction is performed under very diluted conditions, mainly cyclic products are obtained; eight membered rings (D4) are formed as main and six- (D3) or ten membered rings (D5) as side products. In contrast, the removal of hydrochloric acid from the equilibrium enhances the formation of linear oligomers. The formed hydrochloric acid can be reused in the preparation of methyl chloride.

Methanolysis and condensation (Scheme 42 b) is very important in the technical preparation of polydimethylsiloxanes, as the formed methyl chloride can be easily reused in the *Müller-Rochow* reaction. Diluted methanol is used as well in the WACKER- as in the BAYER process.[303,304] However, both approaches differ in the process parameters. In the WACKER process, dimethyl dichlorosilane and methanol react in reverse flow at 100 °C in a packed reactor. This procedure mostly forms linear oligomers with terminal OH-groups. In the BAYER process, the reaction runs in a column in presence of zinc chloride, which results in cyclic polysiloxanes (mainly D4).

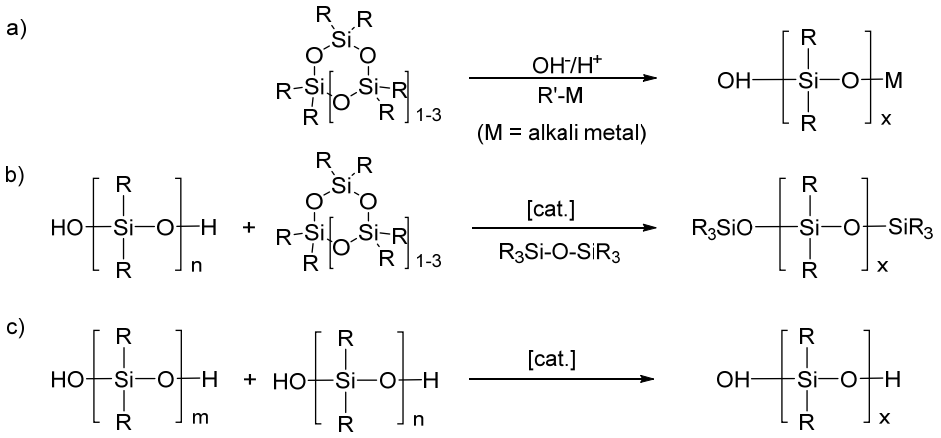

Scheme 43. Procedures for the preparation of high molecular polydimethylsiloxanes from oligomer and cyclic precursors: a) ring opening polymerization, b) equilibrium reaction, c) polycondensation.[303,305]

Various procedures are known to further polymerize the linear and cyclic oligomers (Scheme 43). Some methods allow an intercalation of phenyl-, vinyl- or hydride terminated monomers or oligomers into the chain.[303,304]

One important approach for the synthesis of polydimethylsiloxanes is the anionic ring opening polymerization (ROP) of D3, D4 and D5 cycles.[306] As polymerization initiators, nucleophilic bases, such as alkaline silanolates, or alkaline organyls are used.[307] In the technical ROP process, potassium hydroxide is often used for D4 cycles and lithium hydroxide for D3 cycles.[304] Another promising approach for the ROP of cyclic siloxanes is the use of cationic starters, such as Lewis or Brønstedt acids. Examples are sulfuric acid, sulfonic acids or triphenylmethyl *tris*(pentafluorophenyl borane), which are used in combination with other substances (e.g. silyltrifluoromethane sulfonates).[308] In addition to the ROP approach, polydimethylsiloxanes could be synthesized by an acid- or base induced equilibrium polymerization, in which both, linear and cyclic oligomers, were used as "monomers" (Scheme 43 b).[304,305] Linear and hydroxyl terminated polysiloxanes could furthermore be polymerized by the application of $PNCl_2$. In an equilibrium reaction very high molecular weight polysiloxanes and distal OH functional groups were obtained (Scheme 43 c).[303,304]

Linear polydimethylsiloxanes are used in several applications (e.g., oils, lubricants, etc.). In other uses like in packaging or sealing, chemical crosslinking of silicones *via* functional groups is required. Crosslinking of polydimethylsiloxanes can be realized by a radical pathway via vinylsiloxygroups, through hydrosilylation, or by hydrolysis and condensation.[304]

In the radical process, mainly aryl- or dialkyl peroxides are applied. They decompose at elevated temperatures and form radicals.[304] The radicals react with the present vinyl groups and form propyl or butyl bridges. Crosslinking by hydrosilylation requires free Si-H groups and free vinyl groups, as well as a Pt catalyst (*vide supra*). The reaction requires the exclusion of air. The hydrolysis and condensation reaction involves hydrolysable/functional side or terminal groups (e.g., Cl, alkoxy or acetoxy) and in most cases toxic tin catalysts are applied.[304] Often low molecular crosslinkers are required to adjust the properties of the final polymers. If crosslinking occurs at room temperature, acetoxy functionalized polydimethylsiloxanes are used.

Although the crosslinked polysiloxanes possess good properties, their manufacturing has several drawbacks: Catalysts like Pt and Sn are often toxic and dangerous to health; furthermore, they can be expensive. Water cured polysiloxanes cleave volatile organic molecules (e.g., alcohols, acetic acid, hydrochloric acid), which can elicit health problems. Thus, the crosslinking of polysiloxanes with VOC free and catalyst free systems became a research target. Crosslinking *via* photo catalysis has already been described for several applications.[309]

Photo acid generators:

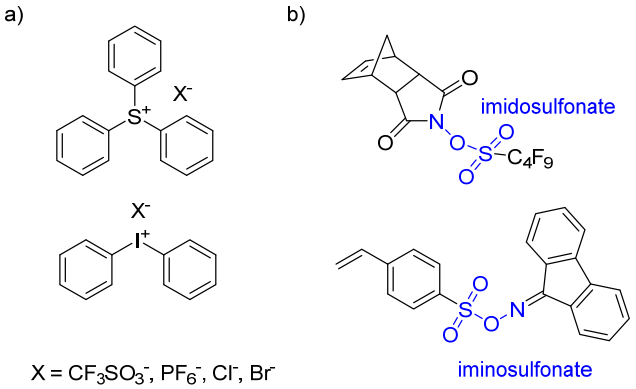

Figure 28. Different photoacid generators: a) ionic,[310,311] b) non-ionic.[312,313]

One strategy for photo crosslinking uses photoacid generators (PAG), also known as photoactive *Brønstedt* acids (Figure 28). Mainly triphenyl sulfonium or diphenyl iodonium triflates or hexafluorophosphates are used as ionic PAGS (Figure 28 a),[310,311] and imido- as well iminosulfonates are established as non-ionic or covalent PAGs (Figure 28 b).[312,313] Protons are generated upon irradiation with UV light.[310–314]

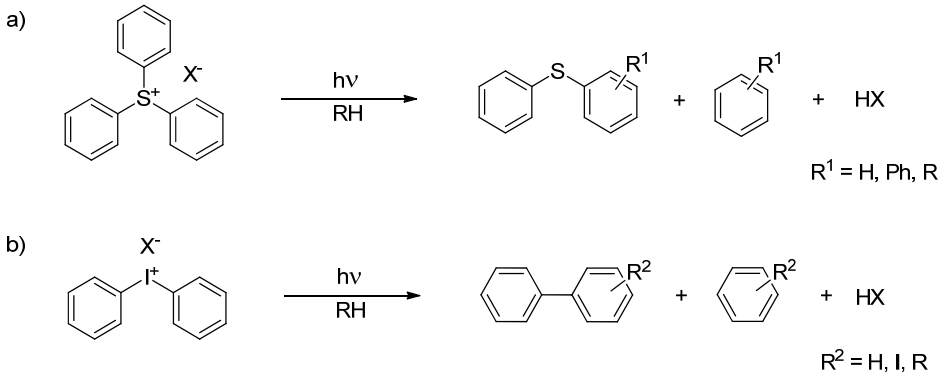

Scheme 44. Decomposition pathways of triphenylsulfonium (a) and diphenyliodonium (b) PAGS.[310,311]

Dektar and Hacker irradiated triphenylsulfonium- and diphenyliodonium salts to determine their reaction pathways (Scheme 44).[310,311] The scientists obtained several aromatic species and a Brønstedt acid (HX), which have formed through the abstraction of a proton by the respective anion.[310,311] Thus, the authors could propose a decomposition mechanism (Scheme 45): Homolytic or heterolytic cleavage of the Ph-S or Ph-I bond occurs during excitation of the PAGs with UV light. Following the heterolytic pathway, diphenyl sulfide or phenyl iodide are formed as side products. Additionally, phenyl cations form, which react with the solvent and induce the release of a proton. Homolytic cleavage of the PAG (through a singlet or a triplet state) results in the formation of phenyl radicals and either diphenyl sulfide or iodbenzene radicals. The radicals recombine and elicit the release of a proton. Although diphenyl iodonium salts preferably decompose through the homolytic and triphenylsulfonium salts decompose through the heterolytic pathway, other factors like the used solvents, the surrounding atmosphere and the addition of photosensitizers play important roles. *[310,311,315]*

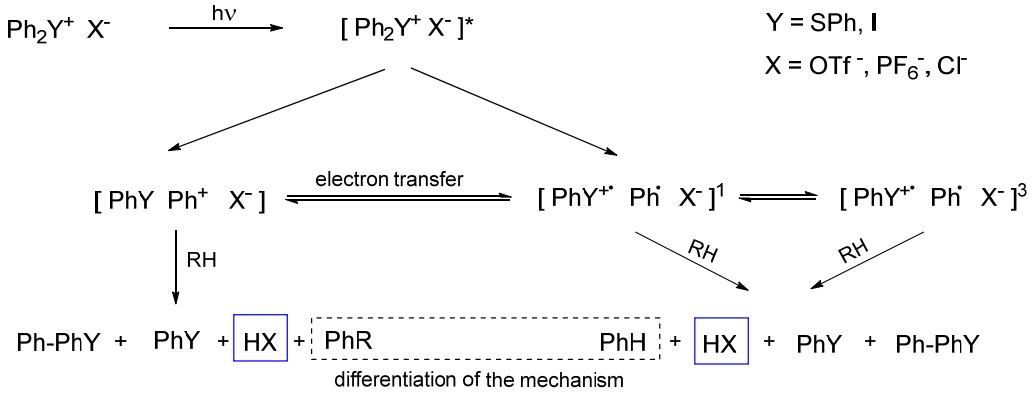

Scheme 45. Photon initiated decomposition mechanism of diphenyliodonium (Y = I) and triphenylsulfonium salts (Y = S-Ph).[310,311]

Although ionic PAGS usually decompose faster and have improved quantum yields, in some reactions, they cause inhomogeneity and diffusion effects as well as proton exchange reactions, which reduced the rates of the target reactions.[312,313,316–319] Often, the excitation of the PAGs was hindered by the reaction mixture. For this reason photosensitizers were added to improve the reactivities[313,320] and non-ionic PAGs are often used. These molecules could be attached to molecules and polymers by a variety of reactions.[321]

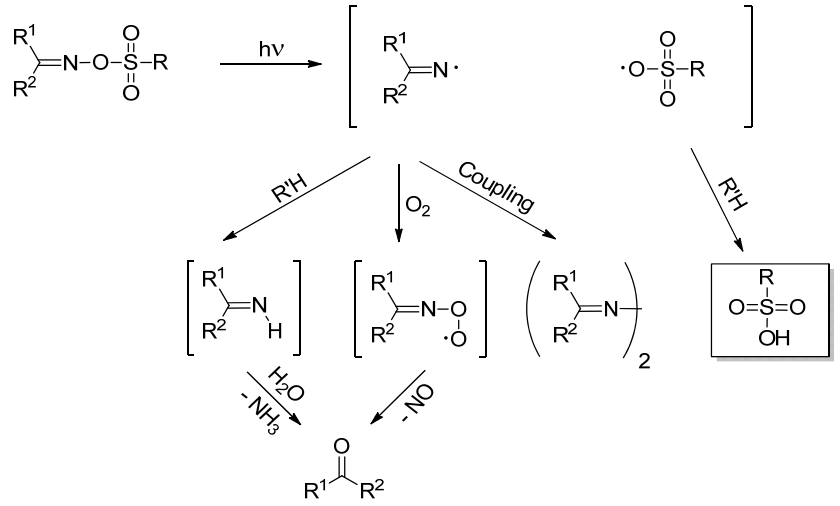

Scheme 46. Decomposition pathways of non-ionic PAGs (e.g. iminosulfonates).[298,312,313,316–318,322,323]

Imino- or imidosulfonate based PAGs decompose homolytically upon excitation with UV light (Scheme 46). The sulfonic acid forms by the reaction of the sulfonate radical with a hydrogen atom from the surrounding. The imino- or imido units form ketones with oxygen or water and dimerize under inert gas.[298,312,313,316–318,322,323]

6.2. Aim of the Study

VOCs are often used in or released during the preparation of silicon based polymers. Polymerization and curing processes often require catalysts, which can cause risk to human

health and the environment. Hence, the development of VOC and heavy metal free reactants and crosslinkers is a hot topic in polymer research. In this context, the aim of this study was the development of novel molecular structures for the crosslinking of different types of polymers. As such oxasilacycles should be synthesized, which were expected to selectively perform a ring opening reaction in the presence of acids and water. The molecules were homopolymerized and were used for the crosslinking of polymers bearing OH moieties. To control the reactivity, special attention should be paid to the use of photo acid generators.

6.3. Summary

Oxasilacycles are promising molecules for the emission free crosslinking of a variety of polymers. The oxasilacycles 2,2,8,8-tetramethyl-1,7-dioxa-6-silaspiro[5.5]undecane, 2-isopropoxy-2,6,6-trimethyl-1,2-oxasilinane and 2,2,6,6-tetramethyl-1,2-oxasilinane were synthesized in two or three step procedures: First condensation of 2-methylpent-4-en-2-ol with a chlorohydrosilane was performed in the presence of methyl imidazole previous to the intramolecular BCF catalyzed hydrosilylation of the terminal olefin with the free Si-H group. For the preparation of 2-isopropoxy-2,6,6-trimethyl-1,2-oxasilinane an additional condensation step of the remaining Si-Cl group with isopropanol was required.

To monitor the reactivity of oxasilacycles with a photoacid generator (triphenylsulfonium triflate - TST, diphenyliodonium hexafluorophosphate - DHP, diphenyliodonium triflate - DIT) irradiation (200 – 300 nm), *in-situ* IR studies were conducted. To do so, the ring opening rates of the model system 2,2,6,6-tetramethyl-1,2-oxasilinane were monitored by tracking the intensity of the C-O band at 845 cm^{-1}. The rates decreased in the row: DHP > TST > DIT. 3 mol % of DHP (of the oxasilacycle amount) was obtained to be most efficient concentration; increasing PAG concentrations did not increase the ring opening rates. Similar reactivity was observed when 2,2,8,8-tetramethyl-1,7-dioxa-6-silaspiro[5.5]undecane was used, but oligomers or polymers were obtained instead of dimers.

Based on the kinetic studies, the molecules were prototyped in chain elongation or crosslinking of different polymers. First, poly(styrene-co-hydroxyethyl methacrylate) (M_w = 140.000 g/mol) was crosslinked by addition of 10 wt% of 2,2,8,8-tetramethyl-1,7-dioxa-6-silaspiro[5.5]undecane and TST within 2 h. The crosslinked polymer contained a significant amount of Si, was not soluble in any solvents and became thermally more stable than its non-crosslinked counterpart.
In a second approach 2-isopropoxy-2,6,6-trimethyl-1,2-oxasilinane was attached to HO-terminated polydimethylsiloxane *via* hydrolysis of the isopropoxysilyl group and subsequent condensation. In the second step photopolymerization of the telechelic polymer was performed using TST. The obtained polymer had a molecular weight of about 210.000 g/mol and a polydispersity of 1.2. Although the demonstrated telechelic structure showed unprecedented reactivity, the reaction had to be performed in solution, as PAG had to be solved prior to the reaction. Hence, the direct connection of a non-ionic PAG, namely N-hydroxy-5-norbornene-2,3-dicarboximide perfluoro-1-butanesulfonate (HNDPB) to ((15%−18% methylhydrosiloxane)−dimethylsiloxane copolymer) (PDMS-H) by hydrosilylation with a Pt catalyst was performed in the first stage. In the second step, the reaction of the Si-H groups with water formed Si-OH moieties, which could be readily connected with 2-isopropoxy-2,6,6-trimethyl-1,2-oxasilinane *via* condensation. The polymer was afterwards crosslinked by UV irradiation and had a gel-content (solid content after refluxing in THF) of 71 %.

6.4. Bibliographic Data

Oxasilacycles Leading to UV-Curable Polymers: Synthesis and Application

Christian A. Anger[†], Julian Kehrle[†], Konrad Hindelang[†], Jonathan G. C. Veinot[‡], Jürgen Stohrer[§], and Bernhard Rieger[†]

Macromolecules ***2014****, 47, 8497.*

[†] Institut für Siliciumchemie, Technische Universität München, Lichtenbergstraße 4, Garching bei München 85747, Germany

[‡] Department of Chemistry, University of Alberta, Edmonton, Alberta T6G 2G2, Canada

[§] Consortium für elektrochemische Industrie, Wacker Chemie AG, Zielstattstraße 20, 81379 München, Germany

Direct Link: DOI 10.1021/ma501857a

Supporting Information:

http://pubs.acs.org/doi/suppl/10.1021/ma501857a/suppl_file/ma501857a_si_001.pdf

6.5. Reprint of the Original Manuscript

Macromolecules

Article

pubs.acs.org/Macromolecules

Oxasilacycles Leading to UV-Curable Polymers: Synthesis and Application

Christian A. Anger,[†] Julian Kehrle,[†] Konrad Hindelang,[†] Jonathan G. C. Veinot,[‡] Jürgen Stohrer,[§] and Bernhard Rieger*[,†]

[†]Institut für Siliciumchemie, Technische Universität München, Lichtenbergstraße 4, Garching bei München 85747, Germany

[‡]Department of Chemistry, University of Alberta, Edmonton, Alberta T6G 2G2, Canada

[§]Consortium für elektrochemische Industrie, Wacker Chemie AG, Zielstattstraße 20, 81379 München, Germany

Supporting Information

ABSTRACT: Many applications of polymeric materials desire and in certain instances require various functions in one family of polymeric architectures. In this work, synthetic routes and methods to obtain novel oxasilacycles and their use in polymer chemistry as both monomer and cross-linking agents are presented. Photoacid generators are used for the acid-catalyzed ring-opening polymerization of the synthesized oxasilacycles allowing photoinitiated and controlled polymerizations. The polymerization behavior and influence of different photoacids as well as the influence of catalyst loading are examined using *in situ* IR spectroscopy. The synthesized cyclic structures offer a broad variety in polymer chemistry. Oxasilaspirocycles can either homopolymerize or function as a cross-linking reactant in organic polymers. A polystyrene−hydroxyethyl methacrylate copolymer is cross-linked via polycondensation reactions of the oxasilaspirocycle. An isopropoxy-substituted oxasilamonocycle is synthesized for the modification of hydroxyl-terminated polydimethylsiloxanes for photoacid-initiated polymerizable telechelic structures. Additionally, the synthesis of multifunctional oligomers containing the photoacid generator unit and the cross-linking agent leads to highly cross-linked polydimethylsiloxane-based structures. In this system it is possible to predefine the gel content as well as the viscosity of the cross-linked polydimethylsiloxane after irradiation by the ratio of oxasilacycle to polydimethylsiloxane.

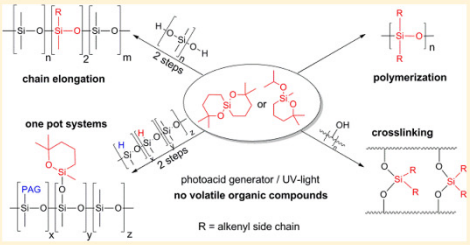

INTRODUCTION

Rational design of polysiloxane-based materials offers the possibility of combining numerous properties, including low temperature flexibility, high thermal stability, biocompatibility, hydrophobicity, and resistance to oxidation into one versatile system.[1] In this regard, the preparation of novel monomers for the synthesis of polysiloxanes is of particular interest.[2] Oxasilacycles are promising candidates for the formation of new materials as well as their application as cross-linking agents for polysiloxanes and organic polymers.[3] A common approach for preparing oxasilacycles is intramolecular hydrosilylation using Karstedt's (i.e., $Pt_2(dvs)_3)_3$) or Speier's catalyst (i.e., H_2PtCl_6 in isopropanol).[4] These metal-mediated procedures afford high catalyst turnover numbers; however, the endo/exoselectivity can be poor.[4b,5] Metalloid catalysts (e.g., trispentafluorophenylborane) offer an alternative hydrosilylation route for obtaining oxasilacycles that provides improved synthetic selectivity.[6,7] As a result, metalloid-mediated reactions are preferable for the preparation of new monomers and cross-linking agents.

The most widely recognized example of oxasilacycle ring-opening polymerization is the reaction of hexamethylcyclotrisiloxane (D3) catalyzed by triflic acid.[8] Many studies have also investigated the polymerization and equilibration of octamethylcyclotetrasiloxane (D4).[9] Most cationic polymerizations of D4 are catalyzed by strong protic (e.g., concentrated sulfuric acid and trifluoromethanesulfonic acid) or by Lewis acids.[10]

Yet another route toward polymerizing oxasilacycles is exploiting photoacid generators (PAG). These reactions provide the added benefit of light induced initiation and short polymerization times. Photoacids such as diphenyliodonium hexafluorophosphate (DHP), triphenylsulfonium triflate (TST), and diphenyliodonium triflate (DIT) have been widely employed in photoinitiated polymerizations, cross-linking of polymers and oligomers, and transformation of functional groups on polymer chains.[11] Photoacids are also utilized in the photoinitiated cationic polymerization of epoxy monomers and vinyl ethers.[11a] In this contribution we elaborate upon a convenient method for preparing oxasilacycles of controlled structure developed in our laboratory and discuss a detailed study

Received: September 8, 2014
Revised: November 6, 2014
Published: November 26, 2014

dx.doi.org/10.1021/ma501857a | Macromolecules 2014, 47, 8497−8505

of their ring-opening reactivity in the presence of a variety of PAGs.

For oxasilacycles to be useful, a precisely defined structural moiety must be introduced. This defined structure facilitates reactivity under appropriate UV-initiated polymerization conditions as well as selective cleavage of carbon−oxygen bonds. A tertiary alkoxy functional group bonded to the silicon atom is a well-known binding motif used to induce this desired reactivity and is appropriate for photoacid generator catalyzed conditions (Figure 1a).[12] In addition, a well-defined ring structure offers the

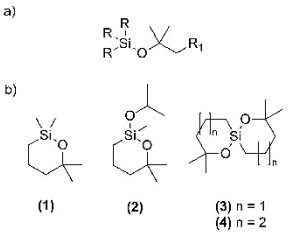

Figure 1. (a) Tertiary binding moieties as useful binding motif for cross-linking reactions R, R^1 = organic groups. (b) Oxasilacycle architectures with the binding motif described in (a).

benefit of an additional degree of control in subsequent polymerization reactions and eliminates known challenges associated with production of volatile organic byproducts like isobutene. In this regard, we turned our attention to syntheses, kinetic investigations, and applications of oxasilacycles (Figure 1b) which offer straightforward polymerization and cross-linking as well as a synthetic approach to preparing tailored polysiloxanes.[12] In general, we planned to investigate 2,2,6,6-tetramethyl-1,2-oxasilinane (**1**) as model substrate for kinetic studies and intended to develop 2-isopropoxy-2,6,6-trimethyl-1,2-oxasilinane (**2**), 2,2,8,8-tetramethyl-1,7-dioxa-6-silaspiro[5.5]undecane (**3**), and 2,2,9,9-tetramethyl-1,8-dioxa-7-silaspiro[6.6]tridecane (**4**) as efficient substrates for the use in polymer and polysiloxane chemistry.

RESULTS AND DISCUSSION

Synthesis of the Oxasilacycles. To obtain the oxasilacycles **1** and **2**, first, a nucleophilic substitution at chlorosilane derivatives by tertiary alcohols (**5**) was performed to give the corresponding alkoxysilane (Scheme 1a). In order to obtain oxasilacycle **2** with two differing hydrolyzable groups, the chlorosilane derivative was substituted with isopropanol.

Applying a thiol catalyst, Cai and Roberts were able to receive derivatives of **1** in an intramolecular hydrosilylation reaction before.[13] However, the used catalyst preferably provides the 5-exo species. Additionally for Pt^0 catalysts the selectivity of the intramolecular hydrosilylation is low.[4b,5] Therefore, we used trispentafluorophenylborane ($B(C_6F_5)_3$)-catalyzed intramolecular hydrosilylation to obtain the target oxasilacycles.

1 could be obtained in 61% yield after hydrosilylation. Although dimers are expected as final reaction products, investigations of the reactivity of **1** toward PAGs under UV irradiation provide valuable insight into the photoacid-catalyzed ring-opening process. However, **1** is not suitable for the buildup of polymeric structures or cross-linking reactions. Thus, we worked on the preparation of multifunctional oxasilacycles. One

Scheme 1. Synthetic Routes for 2,2,6,6-Tetramethyl-1,2-oxasilinane (1) and 2-Isopropoxy-2,6,6-trimethyl-1,2-oxasilinane (2)[a]

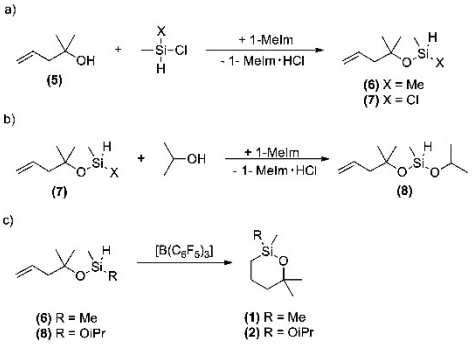

[a](a) Addition of 2-methylpent-4-en-2-ol (**5**) to dimethylchlorosilane or methyldichlorosilane to obtain dimethyl((2-methylpent-4-en-2-yl)oxy)silane (**6**) or chloro(methyl)((2-methylpent-4-en-2-yl)oxy)-silane (**7**) using 1-methylimidazole (1-MeIm) as base. (b) Addition of isopropanol to **7** to obtain isopropoxy(methyl)((2-methylpent-4-en-2-yl)oxy)silane (**8**). (c) Hydrosilylation of **6** or **8** yields in 2,2,6,6-tetramethyl-1,2-oxasilinane (**1**) or 2-isopropoxy-2,6,6-trimethyl-1,2-oxasilinane (**2**).

approach was the synthesis of 2-isopropoxy-2,6,6-trimethyl-1,2-oxasilinane (**2**) featured with two Si−O bonding motifs differing in reactivities (Scheme 1). The three-step synthesis affords the desired product in 76% yield after hydrosilylation. To build up polymeric structures and to cross-link organic polymers bearing OH groups, **3** and **4** offer valuable silanol groups after hydrolysis under acidic conditions. The synthetical procedure to obtain **3** and **4** is similar to the formation of **1** and has been described earlier by our group (Scheme S1).[3,12]

1 and **3** offer valuable stability against moisture and short-term stability toward water. Therefore, these compounds are readily suitable for polymer applications under acidic conditions. While the Si−O−C bond in the cyclic structure of **4** has been found to stay stable for several days, the isopropoxy moiety was cleaved easily. Therefore, this molecule could be used for direct binding to polysiloxanes with silanole groups. **4** straightly tends to hydrolyze and polymerize under ambient conditions. PAG-induced polymerization is too fast to monitor the reaction kinetics by *in situ* Fourier-transfer infrared spectroscopy (FT-IR). Therefore, no further investigations regarding **4** were excecuted.

PAG-Initiated Reactions of Oxasilacycles. To investigate the reaction of oxasilacycles and optimize the polycondensation

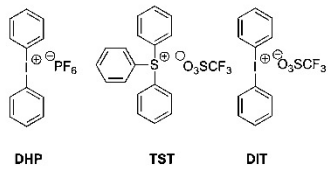

Figure 2. Photoacid generators (PAGs) used for time-resolved ring-opening studies of **1** and **3**.

reaction conditions, *in situ* FT-IR studies monitoring the disappearance of the C−O bond (i.e., **1** at 845 cm^{-1} and **3** at 998 cm^{-1}) were performed for a series of PAGs, i.e., diphenyliodonium hexafluorophosphate (DHP), triphenylsulfonium triflate (TST), and diphenyliodonium triflate (DIT). For simplicity, all kinetic investigations were performed with **1** (Scheme 2) and **3** (Scheme 3). **1** has been synthesized as model

Scheme 2. Proposed Mechanism for the Ring-Opening Reaction of 1

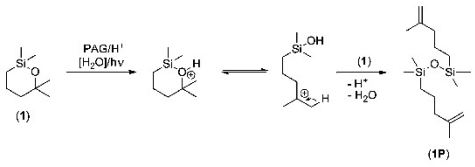

Scheme 3. Photoacid Generator (PAG) Induced Reactions with 3[12]

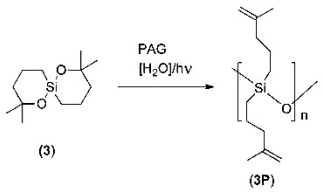

compound for oxasilacycles with one reactive group after ring-opening. One silanol group mainly allowed the formation of dimeric product (**1P**), which could be confirmed by gas chromatography coupled with mass spectroscopy (GC-MS). **2** is an interesting molecule for the attachment to polymeric O−H groups. Since **2** has two leaving groups with different reactivities, the kinetics of **1** were used as basis for the reactivity of the cyclic Si−O−C bond.

Additionally, the reactivity of **3** was monitored to estimate the behavior of an oxasilaspirocycle bearing two equivalent Si−O−C moieties. This molecule has been shown as efficient cross-linker in micellation and polymer chemistry.[3,12] Further potential applications, like chain elongation of OH-terminated polysiloxanes, cross-linking of organic polymers, and a polysiloxane bearing PAG and oxasilacycle groups, are provided within this article. Therefore, kinetic investigations are of high interest.

To identify the most appropriate PAG for initiating the desired reactions of the present oxasilacycles, photoinduced reactions were performed at a PAG concentration of 3 mol % and irradiation at 200−300 nm (note: λ_{max} = TST, 235 nm; DIT, 230 nm; DHP, 230 nm) and monitored using *in situ* FTIR (998 cm^{-1}). The ring-opening reactions of **1** and **3** proceed fastest with DHP, followed by DIT and finally TST (Figure 3A). This trend is due to the relative strengths of the acids produced by the PAG. Upon irradiation TST and DIT generate sulfonic acid (pK_a = −5.21) and DHP yields hexafluorophosphoric acid (pK_a = −10). Furthermore, DHP exhibits a better solubility in dichloromethane, making it more accessible for the reaction. Therefore, we chose DHP as the PAG of choice for the investigation of the concentration dependencies.

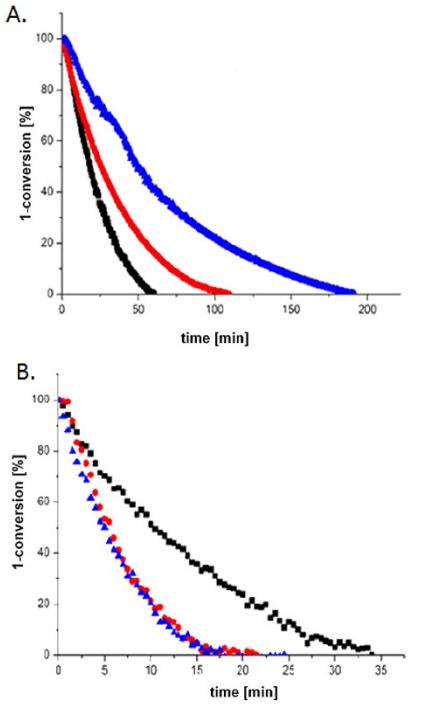

Figure 3. (A) *In situ* IR absorption of the C−O bond of **3** (998 cm^{-1}) catalyzed by PAG (DHP (3 mol %; black squares), TST (3 mol %; red cycles), and DIT (3 mol %; blue triangle)) upon irradiation with 200−300 nm light. (B) *In situ* IR monitoring of the DHP concentration dependence of the reaction of **1** ((3 mol % (blue triangle), 4.5 mol % (red circles), 6 mol % (black square); C−O band at 845 cm^{-1}) upon 200−300 nm irradiation.

The optimal DHP concentration for reactions with **1** and **3** was determined by a kinetic study using time-resolved *in situ* FTIR (Figure 3B). As expected from bond dissociation energies (i.e., C−O = 340 kJ/mol; Si−O = 444 kJ/mol),[14] selective cleavage of the C−O bond was observed as evidenced by the decrease of the IR absorption at 845 cm^{-1} (**1**), while the intensity of the Si−O band did not change.

The time required for C−O bond cleavage to reach completion was found to depend upon PAG concentration (i.e., 3 mol % DHP, 25 min; 4.5 mol %; DHP, 22 min; 6 mol % DHP, 35 min). With a DHP concentration of 6 mol % longer reaction times were required, contrary to the expected linear dependence of reaction rate on catalyst concentration of a first-order kinetic process. The observed reaction rate dependence arises from a limitation in the condensation reaction because bond formation rates are similar to that of the bond cleavage (Figures S1−S3). In this context, the decrease of reaction rate with higher catalyst concentrations must arise from a bottleneck in PAG activation. The present observations are analogous to those reported for photoinduced living graft polymerizations,[15] and a so-called "inner filter effect" likely plays an important role. This effect occurs because high concentrations of absorbing

molecules impact (i.e., lower) the intensity of the excitation light throughout the reaction mixture. As a result, only a small percentage of the irradiation actually reaches the photoacid generator leading to longer reaction times.[16]

Because photoreactions of **1** are limited to the formation of dimer **1P**, we now turn our discussion to the photoinduced PAG catalyzed polymerization of **3**. These homopolymerizations are expected to yield alkenyl side chain substituted polysiloxanes. Polymerization of **3** is conveniently followed by *in situ* FTIR upon monitoring the C−O bond absorption at 998 cm^{-1}. The influence of PAG concentration on reaction rate is shown in Figure S4. The polymerization reaction is slow compared to the analogous dimerization of **1** to **1P**. This difference in reactivity arises because the oxasilaspirocycle polymerization requires cleavage of two C−O bonds—in this context the catalyst loading per functional group is effectively halved. A catalytic amount of water must be added to the polymerization reaction to induce initiation. Presumably, water facilitates formation of hydrogen-bonded water complexes which contribute to proton transfer from the nucleophile to the oxasilaspirocycle ring.[17] The reaction speed increases substantially upon raising the catalyst concentration from 3 to 4.5 mol %. Consistent with "inner filter effect" noted above for **1**, further increasing the PAG concentration to 6 mol % leads to a limitation in the activation of the PAG, and the reaction speed decreases.

Although DHP was found to be the most efficient PAG for C−O bond cleavage and Si−O−Si bond formation, we chose TST for polymer cross-linking and chain elongation experiments since the reaction times are not remarkably slower, and in earlier studies we found higher degrees of polymerization using TST.[12]

Cross-Linking of Organic Polymers. To extend the utility of the present oxasilacycles in polymer chemistry, we explored **3** as a potential cross-linking additive in organic polymers preventing any byproducts such as volatile organic compounds. A easy accessible copolymer from the radical polymerization of 1 equiv of styrene and 20 equiv of 2-(hydroxyethyl) methacrylate (HEMA) initiated by 0.3 mol % dibenzoyl peroxide (BPO) was prepared (Scheme S2). After precipitation from ethanol and freeze-drying, the copolymer showed a M_w of 140 000 g/mol (PDI = 2.7) (GPC, DSC: Figures S33 and S34). Following isolation, the styrene−HEMA copolymer was cross-linked by addition of 10 wt % (0.26 mmol) **3** in acetone and 10 mol % (relative to **3**) of TST followed by irradiation at 200−300 nm for 2 h (Scheme 4). The resulting precipitate was isolated by filtration and dried in a vacuum. Consistent with cross-linking, the resulting product is insoluble in common organic solvents such as tetrahydrofuran, acetone, and trichlorobenzene.

The influence of the photocatalyzed cross-linking was evaluated using differential scanning calorimetry (DSC). Evaluation of the non-cross-linked polymer showed an exothermic process at 160 °C during the first heating cycle (Figure S34) that is readily attributed to polymer etherification. In contrast, DSC evaluation of the siloxane cross-linked copolymer inidicates that it is more thermally stable than its non-cross-linked counterpart (Figure S36), and the thermally induced esterification no longer occurs. Further evidence of covalent cross-linking (resulting from reaction with **3**) was obtained by Soxhlet extraction of the cross-linked polymer in THF. Even after extend extraction times up to 4 h no soluble fraction was obtained, resulting in a gel content of 100%. To further confirm the incorporation of the siloxane species into the polymer, energy dispersive X-ray analysis (EDX) was performed,

Scheme 4. Cross-Linking of Styrene-*co*-HEMA with 3

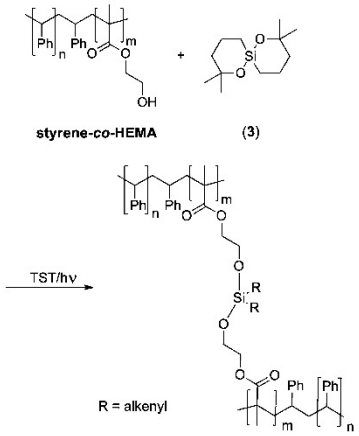

and it showed silicon was uniformly distributed throughout the sample (Figure S38).

Oxasilacycles and Their Application in Polydimethylsiloxane Chemistry. The present oxasilacycles also offer the opportunity to prepare unique telechelic polymers. These polymers are generally used for chain extension and network formation.[18] The formation of UV-curable telechelic structures via end-group functionalization with radical polymerizable groups has been described.[19]

Here, we demonstrate the capping of hydroxyl-terminated polydimethylsiloxane (HO-PDMS) with **2** to afford novel telechelic structures (Scheme 5). This reaction occurs readily

Scheme 5. Synthetic Route for the Telechelic Polydimethylsiloxane and Photoinduced Chain Elongation Using TST[a]

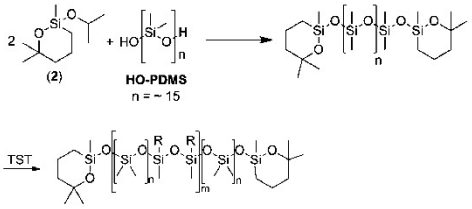

[a]R = alkenyl group; n = repeating units from HO-PDMS; m = repeating units after polymerization with **2**.

even at room temperature. It is important to remove any isopropanol byproduct to shift the equilibrium in favor of the target telechelic structure. MALDI-TOF analysis showed quantitative conversion of **2** and HO-PDMS to the telechelic structure (Figure S41). This could further be confirmed by ^{1}H NMR spectroscopy, where the signals of the cyclic moieties of **2** could be obtained, while there was no evidence of characteristic signals from the isopropoxy moiety (Figure S39).

Polymerization of the oxasilacycle functionalized PDMS was achieved upon irradiation of a solution of the telechelic structure

Scheme 6. Synthetic Route To Obtain Bifunctional Silicone Polymers[a]

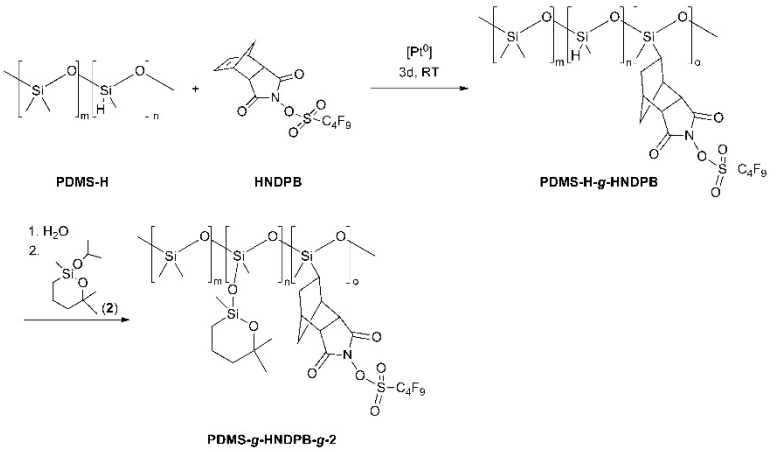

[a]First step: Pt^0-catalyzed hydrosilylation of *N*-hydroxy-5-norbornene-2,3-dicarboximide perfluoro-1-butanesulfonate. Second step: condensation reaction of compound **2**.

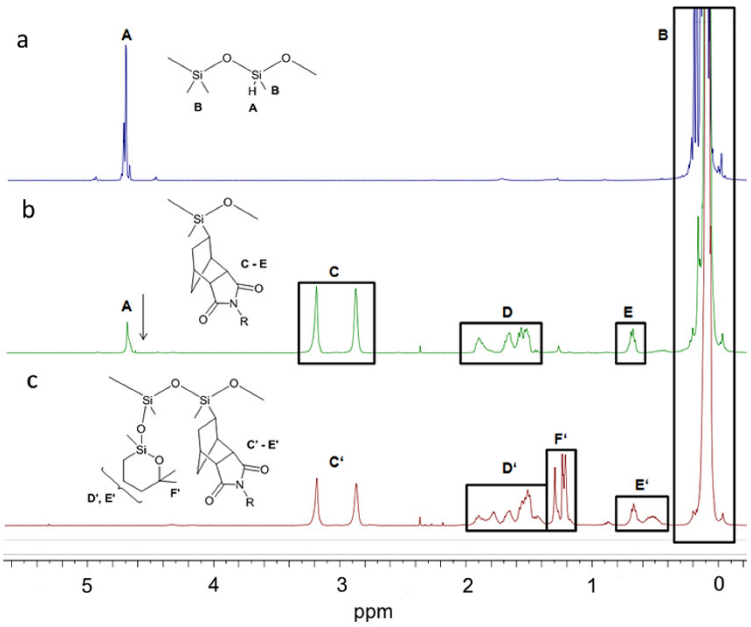

Figure 4. ^{1}H NMR spectra: (a) PDMS-H; (b) PDMS-H-*g*-HNDPB; (c) PDMS-*g*-HNDPB-*g*-**2**.

and TST in dichloromethane for 2 h with UV light (200−300 nm). The resulting substituted polysiloxane structure is shown in Scheme 6. The molecular weight (M_w) of the resulting polysiloxane is 210 000 g/mol with a PDI of 1.2 determined via GPC relative to polystyrene standards.

Having demonstrated the chain extension of HO-PDMS via PAG-catalyzed ring-opening of oxasilacycles, we aimed at cross-linkable polymers, bearing pendant PAG and oxasilacycle functionalities. The goal of this aspect of our study was to prepare an oligomer with homogeneously distributed function-

alities that allows effective UV-initiated cross-linking. It is envisioned that such bifunctional polymers could be used for the photoinduced formation of thin films and coatings without addition of other compounds. Furthermore, these oligomers are expected to offer substantial improvements in ease of handling because reactions are only initiated upon light exposure.

In this context, we prepared a PDMS oligomer functionalized with *N*-hydroxy-5-norbornene-2,3-dicarboximide perfluoro-1-butanesulfonate (HNDPB) photoacid generator moieties and the photopolymerizable oxasilacycle **2** as summarized in Scheme 6. Hydrogen-substituted polydimethylsiloxane was used ((15%−18% methylhydrosiloxane)−dimethylsiloxane copolymer) (PDMS-H) as a backbone and starting material. Karstedt's catalyst (0.4 mol %) mediated hydrosilylation was employed to graft the HNDPB onto the PDMS-H backbone (Scheme 6). The hydrosilylation reaction is readily followed using ^{1}H NMR spectroscopy by monitoring the decrease of hydride signal at 4.68 ppm of PDMS-H (Figure 3) and the removal of PAG double bond (6.20 ppm, Figure S45).

To achieve a condensation reaction between PDMS-H-*g*-HNDPB and **2**, a stoichiometric amount of water (relative to the residual hydride content) was added. This water is necessary for the Pt-catalyzed conversion of the residual hydride functionalities to hydroxyl groups and the hydrolysis of the isopropoxy group of **2**, thus yielding PDMS-*g*-HNDPB-*g*-**2**.[20] Conveniently, during this procedure the Karstedt's catalyst decomposes to colloidal Pt(0) which is removed via Celite filtration. Different grafted PAG:**2** ratios were investigated (i.e., 1:9, 5:5, and 7.5:2.5). In all cases, no residual hydride moieties on PDMS backbone are detected at the sensitivity of NMR spectroscopy.

Upon irradiation the bifunctional polymers cross-linked (rendering them insoluble). The gel content of the cross-linked product was determined upon refluxing in THF and directly correlates with the amount of cross-linker and photoacid generator in the bifunctional oligomer/prepolymer (i.e., PAG:-cross-linker, gel content weight; 1:9, 71%; 5:5, 43%; 7.5:2.5, 32%). These data indicate the lowest concentration of PAG (i.e., the highest concentration of **2**) yields the highest gel content. Higher concentrations of **2** in the polymer lead to a slower reaction rate due to the corresponding low concentration of PAG; however, this structure leads to more cross-linking and thus a higher amount of insoluble polysiloxane. Over the defined ratio of HNDPB to **2**, a broad range of metal, and VOC-free silicones might find their way of application in the field of photocurable polymers.

■ CONCLUSIONS AND OUTLOOK

Since the past century, polymers are an important class of materials with high impact to applications in daily life. Especially cross-linking and chain elongation of polymers have improved material properties and processability significantly. However, such modifications often lead to the release of volatile organic compounds (VOCs) and therefore provide health and environmental risks. Therefore, our main goal was the development of oxasilacycles as useful molecules for polymer altering without the described disadvantages. We presented a detailed investigation of the synthesis and photoreactivity of a new family of oxasilacycles and applied these versatile molecules in polymer chemistry. Synthetic approaches were developed to synthesize the monofunctional molecule 2,2,6,6-tetramethyl-1,2-oxasilinane (**1**) and bifunctional oxasilacycles, like 2-isopropoxy-2,6,6-trimethyl-1,2-oxasilinane (**2**), 2,2,8,8-tetramethyl-1,7-dioxa-6-silaspiro[5.5]undecane (**3**), and 2,2,9,9-tetramethyl-1,8-dioxa-7-silaspiro[6.6]tridecane (**4**). To obtain these molecules, the main step was trispentafluorophenylborane-catalyzed intramolecular hydrosilylation.

In situ IR spectroscopic studies of the ring-opening reactions of compounds **1** and **3** showed higher catalytic activities of diphenyliodonium hexafluorophosphate compared to triphenylsulfonium triflate and diphenyliodonium triflate. This can be explained by a better solubility of diphenyliodonium hexafluorophosphate in dichloromethane. Diphenyliodonium hexafluorphosphate showed a limitation of the ring-opening speed in the case of **1** and **3** by a catalyst loading of 6 mol % and higher. This limitation relates to the full absorption of light in the solution resulting in a limitation of the acid generation ("inner filter effect").

The use of compounds **2** and **3** in the synthesis of polymers free of volatile organic compounds were investigated. Irradiation of a copolymer of hydroxyethyl(methyl acrylate) and styrene using triphenylsulfonium triflate as PAG and **3** lead to a covalently cross-linked polymer, with better thermal stability than non-cross-linked copolymer.

2 has been used for the synthesis of telechelic structures bearing oxasilacycles as end groups in quantitative yield which have been chain extended to linear polydimethylsiloxanes with a remarkable higher molecular mass by means of photoacids. Oxasilacycle **2** has also been used for the synthesis of a multifunctional polymer bearing pendant oxasilacycles as cross-linker and *N*-hydroxy-5-norbornene-2,3-dicarboximide perfluoro-1-butanesulfonate as photoacid generator grafted on the oligosiloxane chain. Via the ratio of the photoacid generator to **2** the amount of cross-linking points and speed could be tailored. The irradiation of the multifunctional oligomer showed that the gel content directly correlates to the amount of cross-linker in the bifunctional oligomer. For the ratios of PAG to **2**—1/9, 5/5, and 7.5/2.5—a gel content (residue weight) of 71%, 43%, and 32% has been obtained, respectively.

■ EXPERIMENTAL SECTION

All chemicals were purchased from commercial sources and were used as received. Diethyl ether, dichloromethane, and pentane were dried and purified directly before their usage by a solvent purification system (MBRAUN SPS-800). All syntheses were performed under inert and dry conditions. 1-Methylimidazole was dried by distillation over sodium and stored over molecular sieve (3 Å). Infrared spectra were recorded on a ReactIR 45m of Mettler-Toledo, and the UV irradiation was executed with a MAX-302 of ASAHI SPECTRA. Nuclear magnetic resonance spectra were recorded on a Bruker Avance 500 UltraShield (500 MHz) and an Avance 300 (300 MHz). They were recorded in ppm, and the solvent was used as an internal standard ($CDCl_3$) at 7.24 ppm for ^{1}H and at 77.0 ppm for ^{13}C. The coupling constants *J* are given in hertz, and the multiplicities were abbreviated as follows: s = singlet, d = duplet, m = multiplet. Mass spectra were recorded on a Thermo Scientific DFS (electron impact, EI, 70 eV). MALDI-ToF MS measurements were performed on a Bruker Ultraflex ToF/ToF mass spectrometer with an acetone/cinnamic acid matrix. Differential scanning calorimetry was performed on a TA Instruments DSC Q 2000 with a heating rate of 10 K/min. The molecular weights were determined with a Varian PL-GPC-50 at 35 °C with the eluent THF (1 mL/min). EDX spectra were obtained using a SwiftED-TM EDX unit (Oxford Instruments) attached to a Hitachi TM-1000 tabletop microscope. 2-Methylpent-4-en-2-ol (**5**) and tris(pentafluorophenyl)borane were prepared according to literature methods.[21]

Dimethyl((2-methylpent-4-en-2-yl)oxy)silane (6). In a Schlenk two-necked flask with dropping funnel and reflux condenser 14.2 g (150 mmol, 1 equiv) of dimethylchlorosilane was dissolved in 500 mL of diethyl ether (cooled in an ice bath) at 0 °C. The dropping funnel was charged with 15.00 g (150 mmol, 1 equiv) of 2-methylpent-4-en-2-ol (**5**)

and 12.3 g (150 mmol, 1 equiv) of 1-methylimidazole. The contents were added dropwise over 30 min. The reaction mixture was allowed to warm to room temperature and stirred for a further 6 h. The resulting methylimidazole hydrochloride was removed by filtration through a Schlenk frit, and the solvent was removed under reduced pressure (200 mbar). After distillation in vacuum (50 mbar, 30 °C), 13.3 g of the liquid product was obtained (84 mmol, 56%). ^{1}H NMR (500 MHz, $CDCl_3$, 296 K): δ [ppm]: 5.90−5.79 (m, 1H), 5.09−4.99 (m, 2H), 4.79−4.71 (m, 1H), 2.24 (d, J = 7.3 Hz, 2H), 1.23 (s, 6H), 0.18 (d, J = 2.9 Hz, 6H) ^{13}C NMR (126 MHz, $CDCl_3$, 300 K): δ [ppm] = 135.2 (s), 117.3 (s), 74.1 (s), 48.9 (s), 29.2 (s), 0.9 (s). ^{29}Si NMR (99 MHz, $CDCl_3$) [ppm]: −7.7. HRMS ($C_8H_{18}OSi$): calcd: 158.1127; found: 157.1038.

2,2,6,6-Tetramethyl-1,2-oxasilinane (1). 743 mg (1.45 mmol, 2.5 mol %) of $B(C_6F_5)_3$ was added to a solution of 9.21 g (58.2 mmol) of dimethyl((2-methylpent-4-en-2-yl)oxy)silane (**6**) in 200 mL of methylene chloride (DCM) and was stirred for 20 h. The solvent was afterward removed under reduced pressure (150 mbar), and the product was purified by condensation in a vacuum. 5.66 g of 2,2,6,6-tetramethyl-1-oxa-2-silacyclohexane (35.7 mmol, 61%) was obtained as a colorless liquid. ^{1}H NMR (500 MHz, $CDCl_3$) δ [ppm]: 1.84−1.77 (m, 2H), 1.51−1.48 (m, 2H), 1.23 (s, 6H), 0.61−0.55 (t, ^3J = 0.4 Hz, 2H), 0.12 (s, 6H). ^{13}C NMR (126 MHz, $CDCl_3$) δ [ppm]: 73.5 (s), 41.1 (s), 30.8 (s), 17.9 (s), 12.8 (s), 1.5 (s). ^{29}Si NMR (99 MHz, $CDCl_3$) δ [ppm]: 10.47. MS (EI), m/z (%): 143.14 (95) [$(M - CH_3)^+$]. HRMS ($C_8H_{18}OSi$): calcd: 158.1127; found: 158.1121.

Chloro(methyl)((2-methylpent-4-en-2-yl)oxy)silane (7). In a three-necked Schlenk flask with dropping funnel and reflux condenser, 8.63 g (75 mmol, 1.5 equiv) of methyldichlorosilane was dissolved in 500 mL of dry pentane. Under rapid stirring at −20 °C a mixture of 5.01 g (50 mmol, 1 equiv) of 2-methylpent-4-en-2-ol (**5**) and 4.11 g (50 mmol, 1 equiv) of 1-methylimidazole were dropped in the beforehand prepared solution within 45 min and stirred for 1 h. The suspension was allowed to warm to room temperature, and the resulting methyl imidazole hydrochloride was then filtrated with a Schlenk frit. The solvent was removed under reduced pressure (200 mbar). After fractionated condensation in a vacuum (12 mbar, 60 °C oil bath temperature) 4.02 g (22.5 mmol, 45%) of chloro(methyl)((2-methylpent-4-en-2-yl)oxy)silane was obtained as a colorless liquid. ^{1}H NMR (300 MHz, $CDCl_3$) δ [ppm]: 5.92−5.76 (m, 1H), 5.30 (q, J = 1.9 Hz, 1H), 5.12−5.01 (m, 2H), 2.30 (d, J = 7.4 Hz, 2H), 1.33 (s, 6H), 0.51 (d, J = 2.0 Hz, 3H). ^{13}C NMR (126 MHz, $CDCl_3$) δ [ppm]: 134.4, 118.0, 77.2, 48.6, 29.2, 28.9, 3.0. ^{29}Si NMR (99 MHz, $CDCl_3$) δ [ppm]: −15.0.

Isopropoxy(methyl)((2-methylpent-4-en-2-yl)oxy)silane (8). In three-necked Schlenk flask with dropping funnel and reflux condenser 4.13 g (23.1 mmol, 1 equiv) of chloro(methyl)((2-methylpent-4-en-2-yl)oxy)silane (**7**) was dissolved in 300 mL of dry pentane. Afterward, a mixture of 1.52 g (18.5 mmol, 0.8 equiv) of 1-methylimidazole and 1.39 g (23.1 mmol, 1 equiv) of isopropanol was dropped at 0 °C under rapid stirring to the beforehand prepared solution. The solution was kept at this temperature for another 30 min, and the resulting methylimidazole hydrochloride was then filtrated with a Schlenk frit and the solvent was removed under reduced pressure (200 mbar). After fractionated condensation in a vacuum 1.17 g (5.78 mmol, 43%) of isopropoxy-(methyl)((2-methylpent-4-en-2-yl)oxy)silane was obtained as a colorless liquid. ^{1}H NMR (300 MHz, $CDCl_3$, 300 K) δ [ppm]: 5.95−5.78 (m, 1H), 5.00 (s, 1H), 4.84−4.59 (m, 1H), 4.16 (dt, J = 12.2, 6.1 Hz, 1H), 2.27 (d, J = 7.3 Hz, 1H), 1.28 (s, 3H), 1.20 (d, J = 6.1 Hz, 2H), 0.18 (d, J = 1.8 Hz, 1H). ^{13}C NMR (126 MHz, $CDCl_3$) δ [ppm]: 135.1, 117.4, 74.7, 65.7, 5.2, 29.5, 29.4, 25.66, −0.3. ^{29}Si NMR (99 MHz, $CDCl_3$) δ [ppm]: −27.6. HRMS m/z ($C_{10}H_{22}O_2Si$): calcd: 202.1389; found: 202.1335 [M^+].

2-Isopropoxy-2,6,6-trimethyl-1,2-oxasilinane (2). In a Schlenk flask 1.17 g (5.78 mmol) of isopropoxy(methyl)((2-methylpent-4-en-2-yl)oxy)silane (**8**) was dissolved in 150 mL of dichloromethane. 40 mg (0.08 mmol, 1.4 mol %) of $B(C_6F_5)_3$ was added, and the reaction mixture was stirred at room temperature for 12 h. Afterward, the solvent was reduced under vacuum, and 0.9 g (4.44 mmol, 76%) of 2-isopropoxy-2,6,6-trimethyl-1,2-oxasilinane was purified via fractioned condensation. ^{1}H NMR (300 MHz, $CDCl_3$) δ [ppm]: 4.24−4.07 (m, 1H), 1.84−1.71 (m, 2H), 1.54−1.47 (m, 2H), 1.29 (s, 3H), 1.23 (s, 3H), 1.17 (t, J = 6.1 Hz, 6H), 0.74−0.62 (m, 1H), 0.54−0.42 (m, 1H), 0.11 (s, 3H). ^{13}C NMR (75 MHz, $CDCl_3$) δ [ppm]: 74.3, 64.6, 41.1, 31.5, 30.2, 25.8, 17.8, 11.6, −1.1. ^{29}Si NMR (60 MHz, $CDCl_3$) δ [ppm]: −11.5. MS (EI), m/z (%): 187.2 (100) [$M - CH_3)^+$], 160.1 (15), 159.1 (24), 145.1 (28), 143.1 (13) [$(M - OCH(CH_3)_2)^+$], 117.1 (23). HRMS ($C_{12}H_{24}O_2{}^{28}Si$): calcd: 202.1389; found: 202.1381.

Irradiations. *Variation of Photoacid Generator via in Situ IR Spectroscopy.* 1 mL of 2,2,8,8-tetramethyl-1,7-dioxa-6-silaspiro[5.5]-undecane (1.05 g, 4.59 mmol; **3**) was dissolved in 3 mL of DCM. This solution was measured via *in situ* IR spectroscopy until the signal was constant. 3 mol % (0.14 mmol) of the photoacid generator dissolved in 1 mL of DCM and 1.24 mg of water (1.5 mol %) were added to the solution. The ratios of PAG in the different measurements are listed in Table S1. After the IR signal was constant, the UV irradiation in the range of 200−300 nm was started.

Variation of the Amount DHP. 1 mL of 2,2,8,8-tetramethyl-1,7-dioxa-6-silaspiro[5.5]undecane (1.049 g, 4.59 mmol, **3**) or 0.727 g (4.59 mmol) of 2,2,6,6-tetramethyl-1-oxa-2-silacyclohexane (**1**) was dissolved in 3 mL of DCM. This solution was measured via *in situ* IR spectrometry until the signal was constant. The amount of diphenyliodonium hexafluorophosphate dissolved in 1 mL of DCM and 1.24 mg of water (1.5 mol %) in the case of 2,2,8,8-tetramethyl-1,7-dioxa-6-silaspiro[5.5]-undecane was added (amount of PAG in the measurements: Table S2). After the IR signal was constant, the UV irradiation (200−300 nm) was started. The dimerization product of 2,2,6,6-tetramethyl-1-oxa-2-silacyclohexane (**1**) was characterized by GC-MS. MS (EI), m/z (%): 298.17 (24) [M^+], 283.17, (100) [$(M - CH_3)^+$], 270.17 (25), 255,14 (16), 243.15 (25).

Cross-Linking of the Organic Polymer. *Synthesis of Polystyrene−poly(2-(hydroxyethyl) methacrylate) Copolymer.* 7.19 mmol (936 mg, 1 equiv) of 2-hydroxyethyl methacrylate, 144 mmol (15 g, 20 equiv) of styrene, and 106 mg (0.44 mmol) of dibenzoylperoxide were degassed via three freeze−thaw−pump cycles and afterward stirred for 4 h at 80 °C. The viscous polymer was precipitated in 400 mL of ethanol at 0 °C and freeze-dried in benzene after filtration. M_w = 141 000 g/mol (PDI: 2.71).

Irradiation. 600 mg of polystyrene−poly(2-(hydroxyethyl) methacrylate) copolymer, 60 mg (0.26 mmol, 10 wt %) of 2,2,8,8-tetramethyl-1,7-dioxa-6-silaspiro[5.5]undecane (**3**), and 10.83 mg (0.026 mmol) of TST were dissolved in 150 mL of acetone and irradiated for 2 h (200−300 nm) under rapid stirring. The precipitated cross-linked polymer was filtered off and afterward dried for several hours under in a vacuum. For the EDX measurements the cured polymer was extracted for 4 h by Soxhlet extraction in THF and dried for several hours.

Telechelic Structure. In a baked out Schlenk flask 210 mg of 2-isopropoxy-2,6,6-trimethyl-1,2-oxasilinane (1.04 mmol; **2**) and 294 mg of hydroxyl-terminated polydimethyiloxane (0.26 mmol) were dissolved in 10 mL of benzene and stirred for 24 h. Afterward, the solution was dried for several hours in a vacuum. The telechelic structure was obtained in a quantitative yield. The reaction process can be followed by ^{1}H NMR spectroscopy via the cleavage of the isopropoxy group. ^{1}H NMR (500 MHz,C_6D_6, 300 K) δ [ppm]: 1.84−1.78 (m, 2H), 1.73−1.68 (m, 2H), 1.36−1.34 (s, 6H), 1.26−1.25 (s, 6H), 0.79−0.68 (m, 4H), 0.59−0.44 (m, 4H), 0.34−0.18 (m, 96H). ^{13}C-DEPT135-NMR (126 MHz, C_6D_6, 300 K) δ [ppm]: 128.06, 40.93, 31.73, 29.55, 17.85, 12.97, 1.15, 0.86, 0.22. ^{29}Si NMR (99 MHz C_6D_6, 300 K) δ [ppm]: −19.30, −19.49, −19.57, −21.40, −21.78, −21.84, −21.95.

PDMS-H-*g*-HNDPB. To a stirred solution of 0.4 mol % (according to the olefin content of *N*-hydroxy-5-norbornene-2,3-dicarboximide perfluoro-1-butanesulfonate) Karstedt's catalyst (2% Pt in xylene) in 15 mL of toluene, HNDPB and PDMS-H were added. The mixture was stirred for 3 days at room temperature. The residual solution was used without further purification. The educts were converted quantitatively to PDMS-H-*g*-HNDPB (ratio: Table S3). ^{13}C NMR (126 MHz, $CDCl_3$) δ [ppm]: 168.7, 168.3, 48.8, 45.6, 40.7, 40.5, 39.8, 26.2, 24.7, 24.6, 0.9−2.0. ^{19}F NMR (471 MHz, $CDCl_3$) δ [ppm]: −80.7, −106.8, −120.4, −125.9 ppm. ^{1}H NMR (12.5% HNDPB) (500 MHz, $CDCl_3$) δ [ppm]: 4.68 (s, 0.13 H), 3.18 (s, 2H), 2.86 (s, 2H), 1.95−1.74 (m, 1H), 173−

1.62 (m, 1H), 1.62−1.45 (m, 2H), 0.76−0.61 (m, 1H), 0.33 − −0.16 (m, 39H). ^{1}H NMR (8.3% PAG) (500 MHz, $CDCl_3$) δ [ppm]: 4.68 (s, 0.7 H), 3.18 (s, 2H), 2.86 (s, 2H), 1.95−1.74 (m, 1H), 173−1.62 (m, 1H), 1.62−1.45 (m, 2H), 0.76−0.61 (m, 1H), 0.33 − −0.16 (m, 62H). ^{1}H NMR (1.7% HNDPB) (500 MHz, $CDCl_3$) δ [ppm]: 4.68 (s, 7.8 H), 3.18 (s, 2H), 2.86 (s, 2H), 1.95−1.74 (m, 1H), 173−1.62 (m, 1H), 1.62−1.45 (m, 2H), 0.76−0.61 (m, 1H), 0.33−0.16 (m, 326H).

PDMS-*g*-HNDPB-*g*-2. The solution of PDMS-H-*g*-HNDPB was stirred for 1 h with a stoichiometric amount of water at RT. After 1 h, 2-isopropoxy-2,6,6-trimethyl-1,2-oxasilinane (**2**) was added (exact ratios: Table S4). Stirring was continued for 3 days at room temperature. In order to separate the Pt residue, the solution was filtrated over Celite. The solvent was removed in a vacuum. The product was gained in a quantitative yield. ^{13}C NMR (126 MHz, $CDCl_3$) δ [ppm]: 168.8, 168.4, 74.3, 48.0, 45.6, 41.1, 40.6, 39.7, 32.0, 29.3, 26.2, 24.7, 17.70, 12.9, 12.8, 1.9, 1.2, 1.0, 0.9, −1.6. ^{19}F NMR (471 MHz, $CDCl_3$) δ [ppm]: −80.6, −106.6, −120.3, −125.8 ppm. ^{29}Si NMR (99 MHz, $CDCl_3$) δ [ppm]: 8.8, 8.7, 7.6, 7.4, 7.3, 7.2, −18.5, −18.7, −18.9, −19.0, −20.4, −20.7, −20.8, −20.9, −21.20, −21.3, −21.5, −21.8, −21.9, −22.0, −22.1, −22.4, −26.7, −26.9, −27.2, −67.5. ^{1}H NMR (15% **4**) (500 MHz, $CDCl_3$): δ = 4.76−4.64 (m, 11H), 3.19 (s, 2H), 2.89 (s, 2H), 1.93−1.39 (m, 118H), 1.40−1.12 (m, 201H), 0.99−0.42 (m, 66H), 0.29−0.09 (m, 1216H). ^{1}H NMR (8.3% **4**) (500 MHz, $CDCl_3$) δ [ppm]: 3.17 (s, 2H), 2.86 (s, 2H), 1.99−1.36 (m, 8H), 1.36−1.11 (m, 6H), 0.95−0.37 (m, 3H), 0.25−0.1 (m, 65H). ^{1}H NMR (4.2% **4**) (500 MHz, $CDCl_3$) δ [ppm]: 3.17 (s, 2H), 2.86 (s, 2H), 1.97−1.34 (m, 6.4H), 1.30−1.15 (m, 3.5H), 0.93−0.44 (m, 3H), 0.24−0.06 (m, 43.9H).

Irradiation and Gel Content Determination of PDMS-*g*-HNDPB-*g*-2. 70.0 mg of the used PDMS-*g*-HNDPB-*g*-**2** was solved in 3 mL of DCM. A catalytic amount of water was added. The solution was given into a Petri dish, and the solvent was evaporated at 50 °C. Afterward, the film was irradiated for 3 h under UV light (200−300 nm). After 1 day the gel content was determined. Therefore, 50.0 mg of the sample was given in 4 mL of THF. The mixture was refluxed for 2 h at an oil bath temperature of 90 °C and filtrated afterward. The solvent was removed in a vacuum, and the soluble residues dried for several hours before their mass was determined (Table S5, formula S1).

■ ASSOCIATED CONTENT

Supporting Information

Syntheses of **3** and **4**, masses of TST, DHP, and DIT in the *in situ* IR studies and results (Figures S1−S4); composition and experimental procedure to obtain multifunctional polymer and for the irradiation, gel content calculation, NMR spectra of the compounds observed in the synthesis route of **1**−**4**, scheme for the synthesis of the HEMA−styrene copolymer and analysis (GPC, DSC measurements, EDX), ^{1}H NMR spectra and MALDI of the telechelic structure, NMR data, MALDI, and UV−vis of the bifunctional polymer. This material is available free of charge via the Internet at http://pubs.acs.org.

■ AUTHOR INFORMATION

Corresponding Author

*E-mail rieger@tum.de (B.R.).

Author Contributions

C.A.A. and J.K. have contributed equally.

Notes

The authors declare no competing financial interest.

■ ACKNOWLEDGMENTS

The financial support from "Wacker Chemie AG" is gratefully acknowledged. We thank Dr. T. Halbach for valuable discussions regarding synthetic strategies. Dr. C. Troll, Dr. S. Vagin, and Dr. C. Anderson are thanked for their help with the preparation of the manuscript and valuable discussions.

■ ABBREVIATIONS

1, 2,2,6,6-tetramethyl-1,2-oxasilinane; 1MeIm, 1-methylimidazole; **1P**, dimer of **1**; **2**, 2-isopropoxy-2,6,6-trimethyl-1,2-oxasilinane; **3**, 2,2,8,8-tetramethyl-1,7-dioxa-6-silaspiro[5.5]-undecane; **3P**, polymer of **2**; **3**, 2,2,9,9-tetramethyl-1,8-dioxa-7-silaspiro[6.6]tridecane; **4**, 2,2,9,9-tetramethyl-1,8-dioxa-7-silaspiro[6.6]tridecane; **5**, 2-methylpent-4-en-2-ol; **6**, dimethyl-((2-methylpent-4-en-2-yl)oxy)silane; **7**, chloro(methyl)((2-methylpent-4-en-2-yl)oxy)silane; **8**, isopropoxy(methyl)((2-methylpent-4-en-2-yl)oxy)silane; BPO, dibenzoyl peroxide; DHP, diphenyliodonium hexafluorophosphate; DIT, diphenyliodonium triflate; DSC, differential scanning calorimetry; EDX, energy dispersive X-ray analysis; GPC, gel permeation chromatography; FTIR, Fourier-transfer infrared spectroscopy; *g*, grafted; HEMA, hydroxyethyl methacrylate; HNDPB, *N*-hydroxy-5-norbornene-2,3-dicarboximide perfluoro-1-butanesulfonate; HO-PDMS, hydroxyl-terminated polydimethylsiloxane; MALDI-TOF, matrix-assisted laser desorption/ionization time-of-flight; M_w, molecular weight; PAG, photoacid generator; PDI, polydispersity index; PDMS, polydimethylsiloxanes.

■ REFERENCES

(1) Kern, W. Book Review: Chemie und Technologie der Silicone (Chemistry and Technology of Silicones). By W. Noll. *Angew. Chem., Int. Ed. Engl.* **1971**, *10* (5), 360−360.

(2) Ganachaud, F., Boileau, S., Boury, B., Eds.; *Silicon Based Polymers*; Springer: Berlin, 2008.

(3) Anger, C.; Deubel, F.; Salzinger, S.; Stohrer, J.; Halbach, T.; Jordan, R.; Veinot, J. G. C.; Rieger, B. Organic−Inorganic Hybrid Nanoparticles via Photoinduced Micellation and Siloxane Core Cross-Linking of Stimuli-Responsive Copolymers. *ACS Macro Lett.* **2013**, *2* (2), 121−124.

(4) (a) Li, F.; Roush, W. R. Stereoselective Synthesis of syn,syn- and syn,anti-1,3,5-Triols via Intramolecular Hydrosilylation of Substituted Pent-3-en-1,5-diols. *Org. Lett.* **2009**, *11* (13), 2932−2935. (b) Stein, J.; Lewis, L. N.; Gao, Y.; Scott, R. A. In Situ Determination of the Active Catalyst in Hydrosilylation Reactions Using Highly Reactive Pt(0) Catalyst Precursors. *J. Am. Chem. Soc.* **1999**, *121* (15), 3693−3703.

(5) Lewis, L. N.; Sy, K. G.; Bryant, G. L.; Donahue, P. E. Platinum-Catalyzed Hydrosilylation of Alkynes. *Organometallics* **1991**, *10* (10), 3750−3759.

(6) (a) Rubin, M.; Schwier, T.; Gevorgyan, V. Highly Efficient $B(C_6F_5)_3$-Catalyzed Hydrosilylation of Olefins. *J. Org. Chem.* **2002**, *67* (6), 1936−1940. (b) Rubin, M.; Gevorgyan, V. $B(C_6F_5)_3$-Catalyzed Allylation of Secondary Benzyl Acetates with Allylsilanes. *Org. Lett.* **2001**, *3* (17), 2705−2707.

(7) Shchepin, R.; Xu, C.; Dussault, P. $B(C_6F_5)_3$-Promoted Tandem Silylation and Intramolecular Hydrosilylation: Diastereoselective Synthesis of Oxasilinanes and Oxasilepanes. *Org. Lett.* **2010**, *12* (21), 4772−4775.

(8) Qayouh, H.; Lahcini, M.; Six, J.-L.; Kricheldorf, H. R. Polymerizations of Hexamethylcyclosiloxane Catalyzed by Metal Sulfonate/Acid Chloride Combinations. *J. Appl. Polym. Sci.* **2012**, *124* (5), 4114−4120.

(9) (a) Scott, D. W. Equilibria between Linear and Cyclic Polymers in Methylpolysiloxanes. *J. Am. Chem. Soc.* **1946**, *68* (11), 2294−2298. (b) Patnode, W.; Wilcock, D. F. Methylpolysiloxanes1. *J. Am. Chem. Soc.* **1946**, *68* (3), 358−363. (c) Lebrun, J.-J.; Sauvet, G.; Sigwalt, P. Polymerization of Octamethylcyclotetrasiloxane Initiated by a Super-acid. *Makromol. Chem., Rapid Commun.* **1982**, *3* (11), 757−763. (d) Toskas, G.; Besztercey, G.; Moreau, M.; Masure, M.; Sigwalt, P. Cationic Polymerization of Hexamethylcyclotrisiloxane by Trifluoromethanesulfonic Acid and Its Derivatives. 2. Reaction Involving Activated Trifluoromethylsulfonates. *Macromol. Chem. Phys.* **1995**, *196* (9), 2715−2735.

(10) Wang, Q.; Zhang, H.; Prakash, G. K. S.; Hogen-Esch, T. E.; Olah, G. A. Cationic Ring-Opening Polymerization of Cyclosiloxanes Initiated

by Electron-Deficient Organosilicon Reagents. *Macromolecules* **1996**, *29* (21), 6691−6694.
(11) (a) Shirai, M.; Tsunooka, M. Photoacid and Photobase Generators: Chemistry and Applications to Polymeric Materials. *Prog. Polym. Sci.* **1996**, *21* (1), 1−45. (b) Shirai, M.; Tsunooka, M. Photoacid and Photobase Generators: Prospects and Their Use in the Development of Polymeric Photosensitive Systems. *Bull. Chem. Soc. Jpn.* **1998**, *71* (11), 2483−2507.
(12) Anger, C. A.; Hindelang, K.; Helbich, T.; Halbach, T.; Stohrer, J.; Rieger, B. Photoinduced Polysiloxane Architectures from Spirosiloxane Precursors via Intramolecular Hydrosilylation. *ACS Macro Lett.* **2012**, *1* (10), 1204−1207.
(13) Cai, Y. R.; Brian, P. Intramolecular Radical-Chain Hydrosilylation Catalysed by Thiols: Cyclisation of Alkenyloxysilanes. *J. Chem. Soc., Perkin Trans. 1* **1998**, 467−474.
(14) Riedel, E. *Anorganische Chemie*; de Gruyter: New York, 1999.
(15) Ma, H.; Davis, R. H.; Bowman, C. N.; Novel, A. Sequential Photoinduced Living Graft Polymerization. *Macromolecules* **1999**, 33 (2), 331−335.
(16) Lakowicz, J. R. *Principles of Fluorescence Spectroscopy*, 3rd ed.; Springer Science + Business Media: Berlin, 2006.
(17) Cypryk, M.; Apeloig, Y. Mechanism of the Acid-Catalyzed Si−O Bond Cleavage in Siloxanes and Siloxanols. A Theoretical Study. *Organometallics* **2002**, *21* (11), 2165−2175.
(18) Goodman, I. *Telechelic Polymers: Synthesis and Applications*; Goethals, E. J., Ed.; CRC Press Inc.: Boca Raton, FL, 1989; ISBN 0-8493-6764-6. *Br. Polym. J.* **1990**, 22 (3), 261−261.
(19) Mazurek, M.; Leir, C. M.; Galkiewicz, R. K. Telechelic Siloxanes with Hydrogen-Bonded Polymerizable End-Groups. II. IR Studies of End-Groups Interactions—Model Amides and Ureas. *J. Appl. Polym. Sci.* **2010**, *117* (2), 982−995.
(20) Kennedy, J. P. K P. Oxidation with Water in the Presence of a Platinum Catalyst. US 7071277 B2, 2001.
(21) (a) August, R.; McEwen, I.; Taylor, R. The Mechanism of Thermal Eliminations. Part 22. Rate Data for Pyrolysis of Primary, Secondary, and Tertiary β-Hydroxyalkenes, β-Hydroxy Esters, and β-Hydroxy Ketones. The Dependence of Transition-State Structure for Six-Centre Eliminations upon Compound Type. *J. Chem. Soc., Perkin Trans. 2* **1987**, 1683−1689. (b) Chernega, A. N.; Graham, A. J.; Green, M. L. H.; Haggitt, J.; Lloyd, J.; Mehnert, C. P.; Metzler, N.; Souter, J. Synthesis of Fluorophenyl Derivatives of Iron, Molybdenum and Tungsten via $B(C_6F_5)_3$ and Unusual Carbon-Fluorine Bond Reactions. *J. Chem. Soc., Dalton Trans.* **1997**, 2293−2304.

6.6. Reprint Permissions

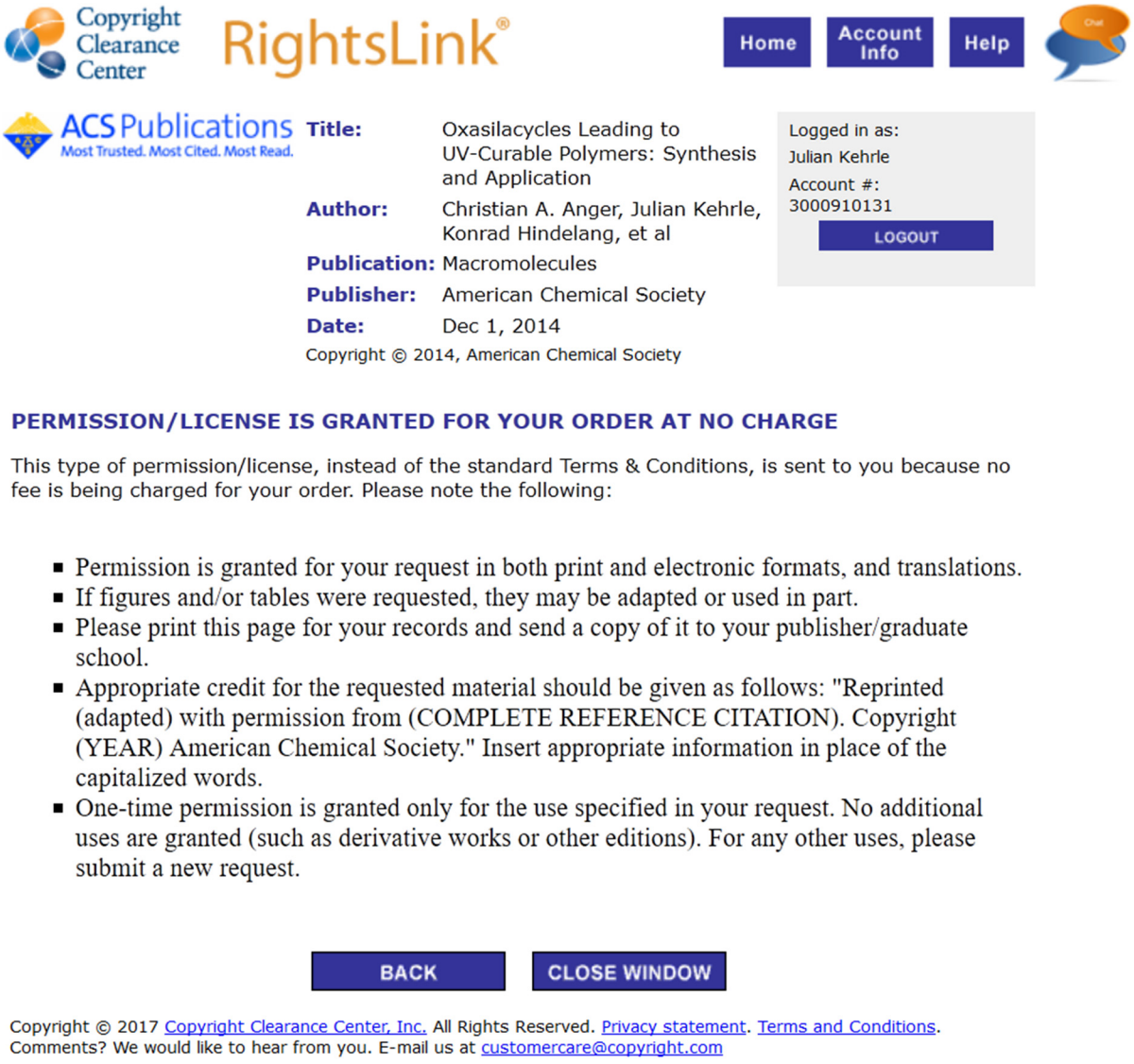

Copyright Clearance Center RightsLink®

Home | Account Info | Help

ACS Publications
Most Trusted. Most Cited. Most Read.

Title: Oxasilacycles Leading to UV-Curable Polymers: Synthesis and Application
Author: Christian A. Anger, Julian Kehrle, Konrad Hindelang, et al
Publication: Macromolecules
Publisher: American Chemical Society
Date: Dec 1, 2014
Copyright © 2014, American Chemical Society

Logged in as:
Julian Kehrle
Account #:
3000910131
LOGOUT

PERMISSION/LICENSE IS GRANTED FOR YOUR ORDER AT NO CHARGE

This type of permission/license, instead of the standard Terms & Conditions, is sent to you because no fee is being charged for your order. Please note the following:

- Permission is granted for your request in both print and electronic formats, and translations.
- If figures and/or tables were requested, they may be adapted or used in part.
- Please print this page for your records and send a copy of it to your publisher/graduate school.
- Appropriate credit for the requested material should be given as follows: "Reprinted (adapted) with permission from (COMPLETE REFERENCE CITATION). Copyright (YEAR) American Chemical Society." Insert appropriate information in place of the capitalized words.
- One-time permission is granted only for the use specified in your request. No additional uses are granted (such as derivative works or other editions). For any other uses, please submit a new request.

BACK | CLOSE WINDOW

Copyright © 2017 Copyright Clearance Center, Inc. All Rights Reserved. Privacy statement. Terms and Conditions.
Comments? We would like to hear from you. E-mail us at customercare@copyright.com

7. List of Publications

J. Kehrle, T. K. Purkait, S. Kaiser, K. N. Raftopoulos, M. Winnacker, T. Ludwig, M. Aghajamali, M. Hanzlik, K. Rodewald, T. Helbich, C. M. Papadakis, J. G. C. Veinot, B. Rieger, *Langmuir* **2018**, *34*, 4888.

J. Kehrle, S. Kaiser, T. K. Purkait, M. Winnacker, T. Helbich, S. Vagin, J. G. C. Veinot, B. Rieger, *Nanoscale* **2017**, *9*, 8489.

M. Dasog, J. Kehrle, B. Rieger, J. G. C. Veinot, *Angewandte Chemie* **2016**, *128*, 2366.

M. Dasog, J. Kehrle, B. Rieger, J. G. C. Veinot, *Angew. Chem. Int. Ed.* **2016**, *55*, 2322.

T. Helbich, A. Lyuleeva, I. M. D. Höhlein, P. Marx, L. M. Scherf, J. Kehrle, T. F. Fässler, P. Lugli, B. Rieger, *Chem. Eur. J.* **2016**, *22*, 6194.

J. Kehrle, T. Helbich, M. Iqbal, L. Hadidi, J. G. Veinot, B. Rieger, *MRS Proc.* **2015**, *1770*.

I. M. D. Höhlein, J. Kehrle, T. K. Purkait, J. G. C. Veinot, B. Rieger, *Nanoscale* **2015**, *7*, 914.

J. Kehrle, I. M. D. Höhlein, Z. Yang, A.-R. Jochem, T. Helbich, T. Kraus, J. G. C. Veinot, B. Rieger, *Angew. Chem. Int. Ed.* **2014**, *53*, 12494.

I. M. D. Höhlein, J. Kehrle, T. Helbich, Z. Yang, J. G. C. Veinot, B. Rieger, *Chem. Eur. J.* **2014**, *20*, 4212.

C. A. Anger, J. Kehrle, K. Hindelang, J. G. C. Veinot, J. Stohrer, B. Rieger, *Macromolecules* **2014**, *47*, 8497.

8. List of Figures, Schemes and Tables

8.1. Figures

8.2. Schemes

8.3. Table

9. Literature

[1] Richard P. Feynman, *There is Plenty of Room at the Bottom*, Pasadena, **1959**.

[2] a) G. Binnig, H. Rohrer, *Scanning tunneling microscope*, **1982**, Google Patents, can be found under http://www.google.com/patents/US4343993; b) J. Li, Y. Song, *High Density Data Storage: Principle, Technology, and Materials* **2009**, 193.

[3] M. G. Panthani, C. M. Hessel, D. Reid, G. Casillas, M. José-Yacamán, B. A. Korgel, *J. Phys. Chem. C* **2012**, *116*, 22463.

[4] I. I. Slowing, J. L. Vivero-Escoto, C.-W. Wu, V. S.-Y. Lin, *Adv. Drug Deliv. Rev.* **2008**, *60*, 1278.

[5] J. Sun, L. Gao, Q. Zhang, *J. Am. Ceram. Soc.* **2003**, *86*, 1677.

[6] a) R. Narayanan, M. A. El-Sayed, *Nano Lett.* **2004**, *4*, 1343; b) M.-C. Daniel, D. Astruc, *Chem. Rev.* **2004**, *104*, 293.

[7] S. Ossicini, M. Amato, R. Guerra, M. Palummo, O. Pulci, *Nanoscale Res. Lett.* **2010**, *5*, 1637.

[8] H. Haug, S. W. Koch, *Quantum theory of the optical and electronic properties of semiconductors*, World Scientific, **2004**.

[9] Nozik, A. J., Beard, M. C., Luther, J. M., M. Law, Ellingson, R. J., Johnson, J. C., *Chem. Rev.* **2010**, *110*, 6873.

[10] X. Gao, Y. Cui, R. M. Levenson, Chung, Leland W K, S. Nie, *Nat Biotech* **2004**, *22*, 969.

[11] Z. Yue, F. Lisdat, W. J. Parak, S. G. Hickey, L. Tu, N. Sabir, D. Dorfs, N. C. Bigall, *ACS Appl. Mater. Interfaces* **2013**, *5*, 2800.

[12] A. M. Derfus, W. C. W. Chan, S. N. Bhatia, *Nano Lett.* **2004**, *4*, 11.

[13] J. Liu, F. Erogbogbo, K.-T. Yong, L. Ye, J. Liu, R. Hu, H. Chen, Y. Hu, Y. Yang, J. Yang, I. Roy, N. A. Karker, M. T. Swihart, P. N. Prasad, *ACS Nano* **2013**, *7*, 7303.

[14] L. Brus, *J. Phys. Chem.* **1994**, *98*, 3575.

[15] K. A. Littau, P. J. Szajowski, A. J. Muller, A. R. Kortan, L. E. Brus, *J. Phys. Chem.* **1993**, *97*, 1224.

[16] J. G. C. Veinot, *Chem. Commun.* **2006**, 4160.

[17] Z. Zhou, L. Brus, R. Friesner, *Nano Lett.* **2003**, *3*, 163.

[18] M. Dasog, J. Kehrle, B. Rieger, J. G. C. Veinot, *Angew. Chem. Int. Ed.* **2016**, *55*, 2322.

[19] A. F. Holleman, N. Wiberg, *Lehrbuch der Anorganischen Chemie*, Walter de Gruyter & Co., Berlin, **2007**.

[20] "Mineral Commodity Summaries", can be found under http://minerals.usgs.gov/minerals/pubs/commodity/silicon/mcs-2012-simet.pdf, **2012**.

[21] J. M. Buriak, *Chem. Rev.* **2002**, *102*, 1271.

[22] La Zazzera, J. F. Evans, M. Deruelle, M. Tirrell, C. R. Kessel, P. McKeown, *J. Electrochem. Soc.* **1997**, *144*, 2184.

[23] M. R. Linford, C. E. D. Chidsey, *J. Am. Chem. Soc.* **1993**, *115*, 12631.

[24] M. R. Linford, P. Fenter, P. M. Eisenberger, C. E. D. Chidsey, *J. Am. Chem. Soc.* **1995**, *117*, 3145.

[25] De Villeneuve, C Henry, J. Pinson, M. C. Bernard, P. Allongue, *J. Phys. Chem. B* **1997**, *101*, 2415.

[26] a) M. M. Sung, G. J. Kluth, O. W. Yauw, R. Maboudian, *Langmuir* **1997**, *13*, 6164; b) A. B. Sieval, A. L. Demirel, J. W.M. Nissink, Linford, Van der Maas, JH, W. H. de Jeu, H. Zuilhof, E. J.R. Sudhölter, *Langmuir* **1998**, *14*, 1759; c) J. Terry, M. R. Linford, C. Wigren, R. Cao, P. Pianetta, C. E. D. Chidsey, *Appl. Phys. Lett.* **1997**, *71*, 1056; d) J. Terry, M. R. Linford, C. Wigren, R. Cao, P. Pianetta, C. E. D. Chidsey, *J. Appl. Phys.* **1999**, *85*, 213; e) F. Ozanam, C. Vieillard, M. Warntjes, T. Dubois, M. Pauly, J.-N. Chazalviel, *Can. J. Chem. Eng.* **1998**, *76*, 1020; f) A. Fidélis, F. Ozanam, J.-N. Chazalviel, *Surf. Sci.* **2000**, *444*, L7-L10.

[27] R. L. Cicero, M. R. Linford, C. E. D. Chidsey, *Langmuir* **2000**, *16*, 5688.

[28] A. Bansal, X. Li, I. Lauermann, N. S. Lewis, S. I. Yi, W. H. Weinberg, *J. Am. Chem. Soc.* **1996**, *118*, 7225.

[29] a) T. Okubo, H. Tsuchiya, M. Sadakata, T. Yasuda, K. Tanaka, *Appl. Surf. Sci.* **2001**, *171*, 252; b) J. He, S. N. Patitsas, K. F. Preston, R. A. Wolkow, D. D.M. Wayner, *Chem. Phys. Lett.* **1998**, *286*, 508; c) X.-Y. Zhu, V. Boiadjiev, J. A. Mulder, R. P. Hsung, R. C. Major, *Langmuir* **2000**, *16*, 6766; d) H. Luo, C. E. D. Chidsey, Y. Chabal (Eds.) *Infrared spectroscopy of covalently bonded species on silicon surfaces: Deuterium, chlorine, and cobalt tetracarbonyl*, Cambridge Univ Press, **1997**.

[30] X. Zhao, Wei, C. M., L. Yang, Chou, M. Y., *Phys. Rev. Lett.* **2004**, *92*, 236805.

[31] C. M. Gonzalez, M. Iqbal, M. Dasog, D. G. Piercey, R. Lockwood, T. M. Klapötke, Veinot, Jonathan G C, *Nanoscale* **2014**, *6*, 2608.

[32] R. Ban, F. Zheng, J. Zhang, *Anal. Methods* **2015**, *7*, 1732.

[33] X. Zhang, X. Chen, S. Kai, H.-Y. Wang, J. Yang, F.-G. Wu, Z. Chen, *Anal. Chem.* **2015**, *87*, 3360.

[34] a) Y. Cui, Q. Wei, H. Park, C. M. Lieber, *Science* **2001**, *293*, 1289; b) Z. Li, Y. Chen, X. Li, T. I. Kamins, K. Nauka, R. S. Williams, *Nano Lett.* **2004**, *4*, 245; c) X. T. Zhou, J. Q. Hu, C. P. Li, D. D.D. Ma, C. S. Lee, S. T. Lee, *Chem. Phys. Lett.* **2003**, *369*, 220.

[35] F. Erogbogbo, K.-T. Yong, I. Roy, R. Hu, W.-C. Law, W. Zhao, H. Ding, F. Wu, R. Kumar, M. T. Swihart, P. N. Prasad, *ACS Nano* **2010**, *5*, 413.

[36] Y. Zhai, M. Dasog, R. B. Snitynsky, T. K. Purkait, M. Aghajamali, A. H. Hahn, C. B. Sturdy, T. L. Lowary, J. G. C. Veinot, *J. Mater. Chem. B* **2014**, *2*, 8427.

[37] R. D. Tilley, K. Yamamoto, *Adv. Mater.* **2006**, *18*, 2053.

[38] A. Shiohara, S. Hanada, S. Prabakar, K. Fujioka, T. H. Lim, K. Yamamoto, P. T. Northcote, R. D. Tilley, *J. Am. Chem. Soc.* **2010**, *132*, 248.

[39] M. Rosso-Vasic, E. Spruijt, Z. Popović, K. Overgaag, B. van Lagen, B. Grandidier, D. Vanmaekelbergh, D. Domínguez-Gutiérrez, L. de Cola, H. Zuilhof, *J. Mater. Chem.* **2009**, *19*, 5926.

[40] J.-H. Park, L. Gu, G. von Maltzahn, E. Ruoslahti, S. N. Bhatia, M. J. Sailor, *Nature Mater.* **2009**, *8*, 331.

[41] F. Erogbogbo, K.-T. Yong, I. Roy, G. Xu, P. N. Prasad, M. T. Swihart, *ACS Nano* **2008**, *2*, 873.

[42] F. Erogbogbo, T. Lin, P. M. Tucciarone, K. M. LaJoie, L. Lai, G. D. Patki, P. N. Prasad, M. T. Swihart, *Nano Lett.* **2013**, *13*, 451.

[43] M. A. Islam, T. K. Purkait, Veinot, Jonathan G C, *J. Am. Chem. Soc.* **2014**, *136*, 15130.

[44] C.-Y. Liu, Z. C. Holman, U. R. Kortshagen, *Nano Lett.* **2008**, *9*, 449.

[45] M. Schnabel, C. Weiss, P. Löper, P. R. Wilshaw, S. Janz, *Phys. Status Solidi A* **2015**, *212*, 1649.

[46] a) N. Koshida, N. Matsumoto, *Mater. Sci. Eng., R* **2003**, *40*, 169; b) H. Rong, A. Liu, R. Jones, O. Cohen, D. Hak, R. Nicolaescu, A. Fang, M. Paniccia, *Nature* **2005**, *433*, 292; c) X. Duan, Y. Huang, R. Agarwal, C. M. Lieber, *Nature* **2003**, *421*, 241.

[47] F. Maier-Flaig, J. Rinck, M. Stephan, T. Bocksrocker, M. Bruns, C. Kübel, A. K. Powell, G. A. Ozin, U. Lemmer, *Nano Lett.* **2013**, *13*, 475.

[48] B. Ghosh, Y. Masuda, Y. Wakayama, Y. Imanaka, J.-i. Inoue, K. Hashi, K. Deguchi, H. Yamada, Y. Sakka, S. Ohki, *Adv. Funct. Mater.* **2014**, *24*, 7151.

[49] a) Y. Cui, Z. Zhong, D. Wang, W. U. Wang, C. M. Lieber, *Nano Lett.* **2003**, *3*, 149; b) X. Duan, C. Niu, V. Sahi, J. Chen, J. W. Parce, S. Empedocles, J. L. Goldman, *Nature* **2003**, *425*, 274; c) Z. C. Holman, C.-Y. Liu, U. R. Kortshagen, *Nano Lett.* **2010**, *10*, 2661.

[50] a) M. Yoshio, H. Wang, K. Fukuda, T. Umeno, N. Dimov, Z. Ogumi, *J. Electrochem. Soc.* **2002**, *149*, A1598-A1603; b) J. O. Besenhard, J. Yang, M. Winter, *J. Power Sources* **1997**, *68*, 87; c) S.-L. Chou, J.-Z. Wang, M. Choucair, H.-K. Liu, J. A. Stride, S.-X. Dou, *Electrochem. Commun.* **2010**, *12*, 303; d) C. K. Chan, H. Peng, G. Liu, K. McIlwrath, X. F. Zhang, R. A. Huggins, Y. Cui, *Nature Nanotechnol.* **2008**, *3*, 31; e) M.-H. Park, M. G. Kim, J. Joo, K. Kim, J. Kim, S. Ahn, Y. Cui, J. Cho, *Nano Lett.* **2009**, *9*, 3844; f) H. Kim, M. Seo, M.-H. Park, J. Cho, *Angew. Chem. Int. Ed.* **2010**, *49*, 2146.

[51] J. K. Lee, K. B. Smith, C. M. Hayner, H. H. Kung, *Chem. Commun.* **2010**, *46*, 2025.

[52] I. H. Son, J. H. Park, S. Kwon, S. Park, M. H. Rümmeli, A. Bachmatiuk, H. J. Song, J. Ku, J. W. Choi, J.-m. Choi, *Nat. Commun.* **2015**, *6*.

[53] M. Ko, S. Chae, S. Jeong, P. Oh, J. Cho, *ACS Nano* **2014**, *8*, 8591.

[54] A. Xing, J. Zhang, Z. Bao, Y. Mei, A. S. Gordin, K. H. Sandhage, *Chem. Commun.* **2013**, *49*, 6743.

[55] H. Okamoto, Y. Sugiyama, H. Nakano, *Chem. Eur. J.* **2011**, *17*, 9864.

[56] X. Cheng, S. B. Lowe, P. J. Reece, J. J. Gooding, *Chem. Soc. Rev.* **2014**, *43*, 2680.

[57] X. Lu, K. J. Anderson, P. Boudjouk, B. A. Korgel, *Chem. Mater.* **2015**, *27*, 6053.

[58] T. Helbich, A. Lyuleeva, I. M. D. Höhlein, P. Marx, L. M. Scherf, J. Kehrle, T. F. Fässler, P. Lugli, B. Rieger, *Chem. Eur. J.* **2016**, *22*, 6194.

[59] G. Bomchil, A. Halimaoui, R. Herino, *Microelectron. Eng.* **1988**, *8*, 293.

[60] M. T. Kelly, J. K. M. Chun, A. B. Bocarsly, *Appl. Phys. Lett.* **1994**, *64*, 1693.

[61] O. K. Andersen, T. Frello, E. Veje, *J. Appl. Phys.* **1995**, *78*, 6189.

[62] Cullis, A. G., L. T. Canham, P. D.J. Calcott, *J. Appl. Phys.* **1997**, *82*, 909.

[63] L. T. Canham (Ed.) *Properties of porous silicon*, Institution of Electrical Engineers, **1997**.

[64] L. T. Canham, *Appl. Phys. Lett.* **1990**, *57*, 1046.

[65] a) Cullis, A. G., L. T. Canham, *Nature* **1991**, *353*, 335; b) M. J. Sailor, E. J. Lee, *Adv. Mater.* **1997**, *9*, 783.

[66] a) A. Halimaoui, C. Oules, G. Bomchil, A. Bsiesy, F. Gaspard, R. Herino, M. Ligeon, F. Muller, *Appl. Phys. Lett.* **1991**, *59*, 304; b) P. McCord, S.-L. Yau, A. J. Bard, *Center for Academic Publications Japan* **1982**, *12*, 479; c) M. P. Stewart, J. M. Buriak, *Adv. Mater.*

2000, *12*, 859; d) F. Namavar, H. P. Maruska, N. M. Kalkhoran, *Appl. Phys. Lett.* **1992**, *60*, 2514.

[67] Z. Bao, M. R. Weatherspoon, S. Shian, Y. Cai, P. D. Graham, S. M. Allan, G. Ahmad, M. B. Dickerson, B. C. Church, Z. Kang, H. W. Abernathy III, C. J. Summers, M. Liu, K. H. Sandhage, *Nature* **2007**, *446*, 172.

[68] K. Chen, Z. Bao, J. Shen, G. Wu, B. Zhou, K. H. Sandhage, *J. Mater. Chem.* **2012**, *22*, 16196.

[69] J. Ahn, H. S. Kim, J. Pyo, J.-K. Lee, W. C. Yoo, *Chem. Mater.* **2016**, *28*, 1526.

[70] M. Waitzinger, M. S. Elsaesser, Berger, Raphael J. F., J. Akbarzadeh, H. Peterlik, N. Hüsing, *Monatsh. Chem.* **2015**, *147*, 269.

[71] S. Maher, M. Alsawat, T. Kumeria, D. Fathalla, G. Fetih, A. Santos, F. Habib, D. Losic, *Adv. Funct. Mater.* **2015**, *25*, 5107.

[72] Z. Xia, S. C. Davis, A. A. Eftekhar, A. S. Gordin, M. Askari, Q. Li, F. Ghasemi, K. H. Sandhage, A. Adibi, *Adv. Opt. Mater.* **2014**, *2*, 235.

[73] a) W.-S. Kim, Y. Hwa, J.-H. Shin, M. Yang, H.-J. Sohn, S.-H. Hong, *Nanoscale* **2014**, *6*, 4297; b) Z. Lu, J. Zhu, D. Sim, W. Zhou, W. Shi, H. H. Hng, Q. Yan, *Chem. Mater.* **2011**, *23*, 5293.

[74] a) B. Lalmi, H. Oughaddou, H. Enriquez, A. Kara, S. Vizzini, B. Ealet, B. Aufray, *Appl. Phys. Lett.* **2010**, *97*, 223109; b) U. Kim, I. Kim, Y. Park, K.-Y. Lee, S.-Y. Yim, J.-G. Park, H.-G. Ahn, S.-H. Park, H.-J. Choi, *ACS Nano* **2011**, *5*, 2176.

[75] J. Böhm, O. Hassel, *Z. anorg. allg. Chem.* **1927**, *160*, 152.

[76] S. Yamanaka, H. Matsu-ura, M. Ishikawa, *Mater. Res. Bull.* **1996**, *31*, 307.

[77] Y. Sugiyama, H. Okamoto, T. Mitsuoka, T. Morikawa, K. Nakanishi, T. Ohta, H. Nakano, *J. Am. Chem. Soc.* **2010**, *132*, 5946.

[78] P. Vogt, P. de Padova, C. Quaresima, J. Avila, E. Frantzeskakis, M. C. Asensio, A. Resta, B. Ealet, G. Le Lay, *Phys. Rev. Lett.* **2012**, *108*, 155501.

[79] O. D. Restrepo, R. Mishra, J. E. Goldberger, W. Windl, *J. Appl. Phys.* **2014**, *115*, 33711.

[80] a) Y. Kumai, H. Kadoura, E. Sudo, M. Iwaki, H. Okamoto, Y. Sugiyama, H. Nakano, *J. Mater. Chem.* **2011**, *21*, 11941; b) Y. Kumai, H. Nakano, *Jpn. J. Appl. Phys.* **2015**, *54*, 35201; c) Y. Kumai, S. Shirai, E. Sudo, J. Seki, H. Okamoto, Y. Sugiyama, H. Nakano, *J. Power Sources* **2011**, *196*, 1503.

[81] Y. Liu, H. Shu, P. Liang, D. Cao, X. Chen, W. Lu, *J. Appl. Phys.* **2013**, *114*, 94308.

[82] U. Kim, I. Kim, Y. Park, K.-Y. Lee, S.-Y. Yim, J.-G. Park, H.-G. Ahn, S.-H. Park, H.-J. Choi, *ACS Nano* **2011**, *5*, 2176.

[83] F. Li, R. Lu, Q. Yao, E. Kan, Y. Liu, H. Wu, Y. Yuan, C. Xiao, K. Deng, *J. Phys. Chem. C* **2013**, *117*, 13283.

[84] a) T. H. Osborn, A. A. Farajian, O. V. Pupysheva, R. S. Aga, Lew Yan Voon, L. C., *Chem. Phys. Lett.* **2011**, *511*, 101; b) F.-b. Zheng, C.-w. Zhang, *Nanoscale Res. Lett.* **2012**, *7*, 1.

[85] a) N. Gao, W. T. Zheng, Q. Jiang, *Phys. Chem. Chem. Phys.* **2012**, *14*, 257; b) Y. Ding, Y. Wang, *Appl. Phys. Lett.* **2012**, *100*, 83102.

[86] H. Okamoto, Y. Sugiyama, K. Nakanishi, T. Ohta, T. Mitsuoka, H. Nakano, *Chem. Mater.* **2015**, *27*, 1292.

[87] H. Nakano, M. Nakano, K. Nakanishi, D. Tanaka, Y. Sugiyama, T. Ikuno, H. Okamoto, T. Ohta, *J. Am. Chem. Soc.* **2012**, *134*, 5452.

[88] T. Helbich, A. Lyuleeva, T. Ludwig, L. M. Scherf, T. F. Fässler, P. Lugli, B. Rieger, *Adv. Funct. Mater.* **2016**, *26*, 6848.

[89] V. Schmidt, J. V. Wittemann, S. Senz, U. Gösele, *Adv. Mater.* **2009**, *21*, 2681.

[90] A. T. Heitsch, C. M. Hessel, V. A. Akhavan, B. A. Korgel, *Nano Lett.* **2009**, *9*, 3042.

[91] B. K. Teo, X. H. Sun, *Chem. Rev.* **2007**, *107*, 1454.

[92] a) R. S. Wagner, W. C. Ellis, *Appl. Phys. Lett.* **1964**, *4*, 89; b) Y. Cui, L. J. Lauhon, M. S. Gudiksen, J. Wang, C. M. Lieber, *Appl. Phys. Lett.* **2001**, *78*, 2214.

[93] P. R. Bandaru, P. Pichanusakorn, *Semicond. Sci. Technol.* **2010**, *25*, 24003.

[94] W. I. Park, G. Zheng, X. Jiang, B. Tian, C. M. Lieber, *Nano Lett.* **2008**, *8*, 3004.

[95] J. L. Lensch-Falk, E. R. Hemesath, D. E. Perea, L. J. Lauhon, *J. Mater. Chem.* **2009**, *19*, 849.

[96] a) A. M. Morales, C. M. Lieber, *Science* **1998**, *279*, 208; b) D. P. Yu, C. S. Lee, I. Bello, X. S. Sun, Y. H. Tang, G. W. Zhou, Z. G. Bai, Z. Zhang, S. Q. Feng, *Solid State Commun.* **1998**, *105*, 403; c) Y. F. Zhang, Y. H. Tang, N. Wang, D. P. Yu, C. S. Lee, I. Bello, S. T. Lee, *Appl. Phys. Lett.* **1998**, *72*, 1835.

[97] a) N. Wang, Y. H. Tang, Y. F. Zhang, C. S. Lee, S. T. Lee, *Phys. Rev. B: Condens. Matter* **1998**, *58*, R16024; b) N. Wang, Y. H. Tang, Y. F. Zhang, C. S. Lee, I. Bello, S. T. Lee, *Chem. Phys. Lett.* **1999**, *299*, 237; c) R.-Q. Zhang, Y. Lifshitz, S.-T. Lee, *Adv. Mater.* **2003**, *15*, 635; d) M. Shao, L. Cheng, M. Zhang, Ma, Dorthy Duo Duo, J. A. Zapien, S.-T. Lee, X. Zhang, *Appl. Phys. Lett.* **2009**, *95*, 143110.

[98] a) L. Schubert, P. Werner, N. D. Zakharov, G. Gerth, F. M. Kolb, L. Long, U. Gösele, T. Y. Tan, *Appl. Phys. Lett.* **2004**, *84*, 4968; b) B. Fuhrmann, H. S. Leipner, H.-R. Höche, L. Schubert, P. Werner, U. Gösele, *Nano Lett.* **2005**, *5*, 2524.

[99] J. D. Holmes, K. P. Johnston, R. C. Doty, B. A. Korgel, *Science* **2000**, *287*, 1471.

[100] a) T. Hanrath, B. A. Korgel, *Adv. Mater.* **2003**, *15*, 437; b) H.-Y. Tuan, A. Ghezelbash, B. A. Korgel, *Chem. Mater.* **2008**, *20*, 2306; c) F. Wang, A. Dong, J. Sun, R. Tang, H. Yu, W. E. Buhro, *Inorg. Chem.* **2006**, *45*, 7511.

[101] X. Lu, T. Hanrath, K. P. Johnston, B. A. Korgel, *Nano Lett.* **2003**, *3*, 93.

[102] H.-Y. Tuan, D. C. Lee, T. Hanrath, B. A. Korgel, *Nano Lett.* **2005**, *5*, 681.

[103] C. M. Hessel, A. T. Heitsch, B. A. Korgel, *Nano Lett.* **2010**, *10*, 176.

[104] X. Lu, C. M. Hessel, Y. Yu, T. D. Bogart, B. A. Korgel, *Nano Lett.* **2013**, *13*, 3101.

[105] B. K. Teo, C. P. Li, X. H. Sun, N. B. Wong, S. T. Lee, *Inorg. Chem.* **2003**, *42*, 6723.

[106] a) X. Yang, J. Ni, *Phys. Rev. B: Condens. Matter* **2005**, *72*, 195426; b) G. G. Guzmán-Verri, Voon, LC Lew Yan, *Phys. Rev. B: Condens. Matter* **2007**, *76*, 75131; c) E. Durgun, S. Tongay, S. Ciraci, *Phys. Rev. B: Condens. Matter* **2005**, *72*, 75420; d) S. B. Fagan, R. J. Baierle, R. Mota, da Silva, Antonio JR, A. Fazzio, *Phys. Rev. B: Condens. Matter* **2000**, *61*, 9994; e) G. Seifert, T. Köhler, H. M. Urbassek, E. Hernandez, T. Frauenheim, *Phys. Rev. B: Condens. Matter* **2001**, *63*, 193409; f) G. Seifert, T. Frauenheim, T. Köhler, H. M. Urbassek, *Phys. Status Solidi B* **2001**, *225*, 393; g) M. e. Zhang, Y. H. Kan, Q. J. Zang, Z. M. Su, R. S. Wang, *Chem. Phys. Lett.* **2003**, *379*, 81; h) J. Bai, X. C. Zeng, H. Tanaka, J. Y. Zeng, *Proc. Natl. Acad. Sci. U S A* **2004**, *101*, 2664; i) R. Q. Zhang, S. T. Lee, C.-K. Law, W.-K. Li, B. K. Teo, *Chem. Phys. Lett.* **2002**, *364*, 251; j) R. Q. Zhang, H.-L. Lee, W.-K. Li, B. K. Teo, *J. Phys. Chem. B* **2005**, *109*, 8605.

[107] a) Y.-W. Chen, Y.-H. Tang, L.-Z. Pei, C. Guo, *Adv. Mater.* **2005**, *17*, 564; b) Y. H. Tang, L. Z. Pei, Y. W. Chen, C. Guo, *Phys. Rev. Lett.* **2005**, *95*, 116102.

[108] a) M. de Crescenzi, P. Castrucci, M. Scarselli, M. Diociaiuti, P. S. Chaudhari, C. Balasubramanian, T. M. Bhave, S. V. Bhoraskar, *Appl. Phys. Lett.* **2005**, *86*, 231901; b) P. Castrucci, M. Scarselli, M. de Crescenzi, M. Diociaiuti, P. S. Chaudhari, C. Balasubramanian, T. M. Bhave, S. V. Bhoraskar, *Thin Solid Films* **2006**, *508*, 226.

[109] a) J. Sha, J. Niu, X. Ma, J. Xu, X. Zhang, Q. Yang, D. Yang, *Adv. Mater.* **2002**, *14*, 1219; b) S. Y. Jeong, J. Y. Kim, H. D. Yang, B. N. Yoon, S.-H. Choi, H. K. Kang, C. W. Yang, Y. H. Lee, *Adv. Mater.* **2003**, *15*, 1172; c) M. Zhou, R. Li, J. Zhou, X. Guo, B. Liu, Z. Zhang, E. Xie, *J. Appl. Phys.* **2009**, *106*, 124315; d) M. B. Ishai, F. Patolsky, *J. Am. Chem. Soc.* **2009**, *131*, 3679; e) J. Hu, Y. Bando, Z. Liu, J. Zhan, D. Golberg, T. Sekiguchi, *Angew. Chem. Int. Ed.* **2004**, *43*, 63; f) C. Mu, Q. Zhao, D. Xu, Q. Zhuang, Y. Shao, *J. Phys. Chem. B* **2007**, *111*, 1491.

[110] N. H. Alsharif, C. E. M. Berger, S. S. Varanasi, Y. Chao, B. R. Horrocks, H. K. Datta, *Small* **2009**, *5*, 221.

[111] Z. Ding, *Science* **2002**, *296*, 1293.

[112] J. Heitmann, *Dissertation*, Martin-Luther-Universität, Halle-Wittenberg, **2003**.

[113] J. I. Pankove, *Optical processes in semiconductors*, Courier Corporation, **2012**.

[114] G. Eranna, *Crystal Growth and Evaluation of Silicon for VLSI and ULSI*, CRC Press, Boca Raton, FL, **2015**.

[115] A. Angı, R. Sinelnikov, A. Meldrum, J. G. C. Veinot, I. Balberg, D. Azulay, O. Millo, B. Rieger, *Nanoscale* **2016**, *8*, 7849.

[116] A. D. Yoffe, *Adv. Phys.* **2001**, *50*, 1.

[117] J. A. Kelly, A. M. Shukaliak, M. D. Fleischauer, J. G. C. Veinot, *J. Am. Chem. Soc.* **2011**, *133*, 9564.

[118] C. M. Hessel, D. Reid, M. G. Panthani, M. R. Rasch, B. W. Goodfellow, J. Wei, H. Fujii, V. Akhavan, B. A. Korgel, *Chem. Mater.* **2012**, *24*, 393.

[119] F. Hua, M. T. Swihart, E. Ruckenstein, *Langmuir* **2005**, *21*, 6054.

[120] P. V. Avramov, D. G. Fedorov, P. B. Sorokin, Chernozatonskii, *Los Alamos Natl. Lab., Prepr. Arch., Condens. Matter* **1**, *2007*.

[121] G. A. Ozin, A. Arsenault, L. Cademartiri, *Nanochemistry*. *A Chemical Approach to Nanomaterials*, The Royal Society of Chemistry, **2008**.

[122] G. Belomoin, E. Rogozhina, J. Therrien, P. V. Braun, L. Abuhassan, M. H. Nayfeh, L. Wagner, L. Mitas, *Phys. Rev. B: Condens. Matter* **2002**, *65*, 193406.

[123] F. A. Reboredo, G. Galli, *J. Phys. Chem. B* **2005**, *109*, 1072.

[124] M. Dasog, De los Reyes, Glenda B, L. V. Titova, F. A. Hegmann, Veinot, Jonathan G C, *ACS Nano* **2014**, *8*, 9636.

[125] a) G. Belomoin, J. Therrien, A. Smith, S. Rao, R. Twesten, S. Chaieb, M. H. Nayfeh, L. Wagner, L. Mitas, *Appl. Phys. Lett.* **2002**, *80*, 841; b) M. H. Nayfeh, O. Akcakir, G. Belomoin, N. Barry, J. Therrien, E. Gratton, *Appl. Phys. Lett.* **2000**, *77*, 4086; c) M. H. Nayfeh, N. Barry, J. Therrien, O. Akcakir, E. Gratton, G. Belomoin, *Appl. Phys. Lett.* **2001**, *78*, 1131; d) R. A. Bley, S. M. Kauzlarich, J. E. Davis, H. W. H. Lee, *Chem. Mater.* **1996**, *8*, 1881.

[126] J. R. Heath, *Science* **1992**, *258*, 1131.

[127] N. A. Dhas, C. P. Raj, A. Gedanken, *Chem. Mater.* **1998**, *10*, 3278.

[128] R. K. Baldwin, J. Zou, K. A. Pettigrew, G. J. Yeagle, R. D. Britt, S. M. Kauzlarich, *Chem. Commun.* **2006**, 658.

[129] A. E. Finholt, A. C. Bond Jr, H. I. Schlesinger, *J. Am. Chem. Soc.* **1947**, *69*, 1199.

[130] J. P. Wilcoxon, G. A. Samara, *Appl. Phys. Lett.* **1999**, *74*, 3164.

[131] J. H. Warner, H. Rubinsztein-Dunlop, R. D. Tilley, *J. Phys. Chem. B* **2005**, *109*, 19064.

[132] J. H. Warner, A. Hoshino, K. Yamamoto, R. Tilley, *Angew. Chem.* **2005**, *117*, 4626.

[133] R. D. Tilley, J. H. Warner, K. Yamamoto, I. Matsui, H. Fujimori, *Chem. Commun.* **2005**, 1833.

[134] R. K. Baldwin, K. A. Pettigrew, J. C. Garno, P. P. Power, G.-y. Liu, S. M. Kauzlarich, *J. Am. Chem. Soc.* **2002**, *124*, 1150.

[135] R. K. Baldwin, K. A. Pettigrew, E. Ratai, M. P. Augustine, S. M. Kauzlarich, *Chem. Commun.* **2002**, 1822.

[136] J. Zou, R. K. Baldwin, K. A. Pettigrew, S. M. Kauzlarich, *Nano Lett.* **2004**, *4*, 1181.

[137] R. K. Baldwin, K. A. Pettigrew, J. C. Garno, P. P. Power, G.-y. Liu, S. M. Kauzlarich, *J. Am. Chem. Soc.* **2002**, *124*, 1150.

[138] R. A. Bley, S. M. Kauzlarich, *J. Am. Chem. Soc.* **1996**, *118*, 12461.

[139] D. Mayeri, B. L. Phillips, M. P. Augustine, S. M. Kauzlarich, *Chem. Mater.* **2001**, *13*, 765.

[140] C.-S. Yang, R. A. Bley, S. M. Kauzlarich, H. W. H. Lee, G. R. Delgado, *J. Am. Chem. Soc.* **1999**, *121*, 5191.

[141] Q. Liu, S. M. Kauzlarich, *Mater. Sci. Eng., B* **2002**, *96*, 72.

[142] K. A. Pettigrew, Q. Liu, P. P. Power, S. M. Kauzlarich, *Chem. Mater.* **2003**, *15*, 4005.

[143] a) S. Lee, W. J. Cho, C. S. Chin, I. K. Han, W. J. Choi, Y. J. Park, J. D. Song, J. I. Lee, *Jpn. J. Appl. Phys.* **2004**, *43*, L784; b) S. Lee, W. J. Cho, I. K. Han, W. J. Choi, J. I. Lee, *Phys. Status Solidi B* **2004**, *241*, 2767.

[144] B. D. Rowsell, J. G. C. Veinot, *Nanotechnology* **2005**, *16*, 732.

[145] J. D. Holmes, K. J. Ziegler, R. C. Doty, L. E. Pell, K. P. Johnston, B. A. Korgel, *J. Am. Chem. Soc.* **2001**, *123*, 3743.

[146] D. S. English, L. E. Pell, Z. Yu, P. F. Barbara, B. A. Korgel, *Nano Lett.* **2002**, *2*, 681.

[147] D. C. Lee, T. Hanrath, B. A. Korgel, *Angew. Chem. Int. Ed.* **2005**, *44*, 3573.

[148] T. Murthy, N. Miyamoto, M. Shimbo, J. Nishizawa, *J. Cryst. Growth* **1976**, *33*, 1.

[149] W. L. Wilson, P. F. Szajowski, Le Brus, *Science-New York Then Washington* **1993**, *262*, 1242.

[150] W. R. Cannon, S. C. Danforth, J. S. Haggerty, R. A. Marra, *J. Am. Ceram. Soc.* **1982**, *65*, 330.

[151] W. R. Cannon, S. C. Danforth, J. H. Flint, J. S. Haggerty, R. A. Marra, *J. Am. Ceram. Soc.* **1982**, *65*, 324.

[152] a) E. Borsella, S. Botti, M. Cremona, S. Martelli, R. M. Montereali, A. Nesterenko, *J. Matter. Sci. Lett.* **1997**, *16*, 221; b) S. Botti, R. Coppola, F. Gourbilleau, R. Rizk, *J. Appl. Phys.* **2000**, *88*, 3396.

[153] a) F. Huisken, B. Kohn, V. Paillard, *Appl. Phys. Lett.* **1999**, *74*, 3776; b) G. Ledoux, J. Gong, F. Huisken, *Appl. Phys. Lett.* **2001**, *79*, 4028; c) G. Ledoux, J. Gong, F. Huisken, O. Guillois, C. Reynaud, *Appl. Phys. Lett.* **2002**, *80*, 4834; d) L. B. Ma, T. Schmidt, O. Guillois, F. Huisken, *Appl. Phys. Lett.* **2009**, *95*, 13115; e) K. Potrick, T. Schmidt, S. Bublitz, C. Mühlig, W. Paa, F. Huisken, *Appl. Phys. Lett.* **2011**, *98*, 83111.

[154] a) F. Hua, F. Erogbogbo, M. T. Swihart, E. Ruckenstein, *Langmuir* **2006**, *22*, 4363; b) X. Li, Y. He, S. S. Talukdar, M. T. Swihart, *Langmuir* **2003**, *19*, 8490.

[155] X. Li, Y. He, M. T. Swihart, *Langmuir* **2004**, *20*, 4720.

[156] U. Kortshagen, *J. Phys. D-Appl. Phys* **2009**, *42*, 113001.

[157] D. Jurbergs, E. Rogojina, L. Mangolini, U. Kortshagen, *Appl. Phys. Lett.* **2006**, *88*, 3116.

[158] a) L. Mangolini, U. Kortshagen, *Adv. Mater.* **2007**, *19*, 2513; b) L. Mangolini, E. Thimsen, U. Kortshagen, *Nano Lett.* **2005**, *5*, 655; c) M. Otobe, T. Kanai, T. Ifuku, H. Yajima, S. Oda, *J. Non-Cryst. Solids.* **1996**, *198*, 875; d) A. Bapat, M. Gatti, Y.-P. Ding, S. A. Campbell, U. Kortshagen, *J. Phys. D-Appl. Phys* **2007**, *40*, 2247; e) L. Mangolini, D. Jurbergs, E. Rogojina, U. Kortshagen, *J. Lumin.* **2006**, *121*, 327.

[159] J. Knipping, H. Wiggers, B. Rellinghaus, P. Roth, D. Konjhodzic, C. Meier, *J. Nanosci. Nanotechno.* **2004**, *4*, 1039.

[160] R. M. Sankaran, D. Holunga, R. C. Flagan, K. P. Giapis, *Nano letters* **2005**, *5*, 537.

[161] C. M. Hessel, E. J. Henderson, J. G. C. Veinot, *Chem. Mater.* **2006**, *18*, 6139.

[162] C. M. Hessel, E. J. Henderson, J. G. C. Veinot, *J. Phys. Chem. C* **2007**, *111*, 6956.

[163] a) D. Nesheva, C. Raptis, A. Perakis, I. Bineva, Z. Aneva, Z. Levi, S. Alexandrova, H. Hofmeister, *J. Appl. Phys.* **2002**, *92*, 4678; b) B. Garrido, C. Garcia, S.-Y. Seo, P. Pellegrino, D. Navarro-Urrios, N. Daldosso, L. Pavesi, F. Gourbilleau, R. Rizk, *Phys. Rev. B: Condens. Matter* **2007**, *76*, 245308; c) S.-M. Liu, S. Sato, K. Kimura, *Langmuir* **2005**, *21*, 6324.

[164] S.-M. Liu, Y. Yang, S. Sato, K. Kimura, *Chem. Mater.* **2006**, *18*, 637.

[165] E. J. Henderson, J. A. Kelly, J. G. C. Veinot, *Chem. Mater.* **2009**, *21*, 5426.

[166] Z. Yang, A. R. Dobbie, K. Cui, J. G. C. Veinot, *J. Am. Chem. Soc.* **2012**, *134*, 13958.

[167] J. K. Kang, C. B. Musgrave, *J. Chem. Phys.* **2002**, *116*.

[168] G. W. Trucks, K. Raghavachari, G. S. Higashi, Y. J. Chabal, *Phys. Rev. Lett.* **1990**, *65*, 504.

[169] a) L. Pauling, *J. Am. Chem. Soc.* **1932**, *54*, 3570; b) S. Gronert, R. Glaser, A. Streitwieser, *J. Am. Chem. Soc.* **1989**, *111*, 3111.

[170] S. Niesar, W. Fabian, N. Petermann, D. Herrmann, E. Riedle, H. Wiggers, M. S. Brandt, M. Stutzmann, *Green* **2011**, *1*.

[171] R. N. Pereira, S. Niesar, W. B. You, A. F. da Cunha, N. Erhard, A. R. Stegner, H. Wiggers, M.-G. Willinger, M. Stutzmann, M. S. Brandt, *J. Phys. Chem. C* **2011**, *115*, 20120.

[172] a) P. V. Kamat, *J. Phys. Chem. C* **2008**, *112*, 18737; b) C.-W. Jiang, M. A. Green, *J. Appl. Phys.* **2006**, *99*, 114902; c) E.-C. Cho, S. Park, X. Hao, D. Song, G. Conibeer, S.-C. Park, M. A. Green, *Nanotechnology* **2008**, *19*, 245201.

[173] H. Kim, M. Seo, M.-H. Park, J. Cho, *Angew. Chem.* **2010**, *122*, 2192.

[174] Y. Xu, Y. Zhu, C. Wang, *J. Mater. Chem. A* **2014**, *2*, 9751.

[175] W. Wang, P. N. Kumta, *ACS Nano* **2010**, *4*, 2233.

[176] K.-Y. Cheng, R. Anthony, U. R. Kortshagen, R. J. Holmes, *Nano Lett.* **2010**, *10*, 1154.

[177] K.-Y. Cheng, R. Anthony, U. R. Kortshagen, R. J. Holmes, *Nano Lett.* **2011**, *11*, 1952.

[178] T. Lin, X. Liu, B. Zhou, Z. Zhan, A. N. Cartwright, M. T. Swihart, *Adv. Funct. Mater.* **2014**, *24*, 6016.

[179] M. Dasog, Z. Yang, S. Regli, T. M. Atkins, A. Faramus, M. P. Singh, E. Muthuswamy, S. M. Kauzlarich, R. D. Tilley, J. G. C. Veinot, *ACS Nano* **2013**, *7*, 2676.

[180] B. Marciniec, *Hydrosilylation: a comprehensive review on recent advances*, Springer Science & Business Media, **2009**.

[181] a) J. M. Buriak, *Chem. Commun.* **1999**, 1051; b) M. P. Stewart, J. M. Buriak, *Angew. Chem. Int. Ed.* **1998**, *37*, 3257.

[182] A. B. Sieval, R. Linke, H. Zuilhof, E. Sudhölter, JR, *Adv. Mater.* **2000**, *12*, 1457.

[183] J. F. Harrod, A. J. Chalk, *J. Am. Chem. Soc.* **1964**, *86*, 1776.

[184] S. Sakaki, N. Mizoe, M. Sugimoto, *Organometallics* **1998**, *17*, 2510.

[185] L. Ruizendaal, S. P. Pujari, V. Gevaerts, J. M. J. Paulusse, H. Zuilhof, *Chem. Asian J.* **2011**, *6*, 2776.

[186] J. R. Siekierzycka, M. Rosso-Vasic, H. Zuilhof, A. M. Brouwer, *J. Phys. Chem. C* **2011**, *115*, 20888.

[187] a) D. Andsager, J. Hilliard, J. M. Hetrick, L. H. AbuHassan, M. Plisch, M. H. Nayfeh, *J. Appl. Phys.* **1993**, *74*, 4783; b) S. Li, I. N. Germanenko, M. S. El-Shall, *J. Phys. Chem. B* **1998**, *102*, 7319.

[188] Y. Yu, C. M. Hessel, T. D. Bogart, M. G. Panthani, M. R. Rasch, B. A. Korgel, *Langmuir* **2013**, *29*, 1533.

[189] J. M. Buriak, M. J. Allen, *J. Am. Chem. Soc.* **1998**, *120*, 1339.

[190] a) B. N. Jariwala, O. S. Dewey, P. Stradins, C. V. Ciobanu, S. Agarwal, *ACS Appl. Mater. Interfaces* **2011**, *3*, 3033; b) S. L. Weeks, B. Macco, M. C.M. van de Sanden, S. Agarwal, *Langmuir* **2012**, *28*, 17295; c) J. A. Kelly, E. J. Henderson, J. G. C. Veinot, *Chem. Commun.* **2010**, *46*, 8704.

[191] a) F. Effenberger, G. Götz, B. Bidlingmaier, M. Wezstein, *Angew. Chem. Int. Ed.* **1998**, *37*, 2462; b) R. Boukherroub, S. Morin, F. Bensebaa, D. D.M. Wayner, *Langmuir* **1999**, *15*, 3831.

[192] Z. Yang, M. Iqbal, A. R. Dobbie, J. G. C. Veinot, *J. Am. Chem. Soc.* **2013**, *135*, 17595.

[193] F. Sangghaleh, I. Sychugov, Z. Yang, J. G. C. Veinot, J. Linnros, *ACS Nano* **2015**, *9*, 7097.

[194] C. Qian, W. Sun, L. Wang, C. Chen, K. Liao, W. Wang, J. Jia, B. D. Hatton, G. Casillas, M. Kurylowicz, *J. Am. Chem. Soc.* **2014**, *136*, 15849.

[195] J. Rinck, D. Schray, C. Kübel, A. K. Powell, G. A. Ozin, *Small* **2015**, *11*, 335.

[196] M. Woods, S. Carlsson, Q. Hong, S. N. Patole, L. H. Lie, A. Houlton, B. R. Horrocks, *J. Phys. Chem. B* **2005**, *109*, 24035.

[197] M. Guan, W. Wang, E. J. Henderson, O. Dag, C. Kübel, V. S. K. Chakravadhanula, J. Rinck, I. L. Moudrakovski, J. Thomson, J. McDowell, A. K. Powell, H. Zhang, G. A. Ozin, *J. Am. Chem. Soc.* **2012**, *134*, 8439.

[198] Y. Kanai, A. Selloni, *J. Am. Chem. Soc.* **2006**, *128*, 3892.

[199] F. A. Reboredo, E. Schwegler, G. Galli, *J. Am. Chem. Soc.* **2003**, *125*, 15243.

[200] M. P. Stewart, J. M. Buriak, *J. Am. Chem. Soc.* **2001**, *123*, 7821.

[201] J. A. Kelly, J. G. C. Veinot, *ACS Nano* **2010**, *4*, 4645.

[202] Z. Yang, G. B. de los Reyes, L. V. Titova, I. Sychugov, M. Dasog, J. Linnros, F. A. Hegmann, J. G. C. Veinot, *Acs Photonics* **2015**, *2*, 595.

[203] M. H. Mobarok, T. K. Purkait, M. A. Islam, M. Miskolzie, J. G. C. Veinot, *Angew. Chem.* **2016**, 6073.

[204] T. K. Purkait, M. Iqbal, M. H. Wahl, K. Gottschling, C. M. Gonzalez, M. A. Islam, Veinot, Jonathan G C, *J. Am. Chem. Soc.* **2014**, *136*, 17914.

[205] T. K. Purkait, M. Iqbal, M. A. Islam, M. H. Mobarok, C. M. Gonzalez, L. Hadidi, J. G. C. Veinot, *J. Am. Chem. Soc.* **2016**, *138*, 7114.

[206] M. Rubin, T. Schwier, V. Gevorgyan, *J. Org. Chem.* **2002**, *67*, 1936.

[207] a) J. M. Buriak, M. P. Stewart, T. W. Geders, M. J. Allen, H. C. Choi, J. Smith, D. Raftery, L. T. Canham, *J. Am. Chem. Soc.* **1999**, *121*, 11491; b) M. Mewald, M. Oestreich, *Chem. Eur. J.* **2012**, *18*, 14079; c) K. Oertle, H. Wetter, *Tetrahedron Lett.* **1985**, *26*, 5511; d) N. Asao, T. Sudo, Y. Yamamoto, *J. Org. Chem.* **1996**, *61*, 7654.

[208] I. M. D. Höhlein, J. Kehrle, T. Helbich, Z. Yang, J. G. C. Veinot, B. Rieger, *Chem. Eur. J.* **2014**, *20*, 4212.

[209] Z. Yang, C. M. Gonzalez, T. K. Purkait, M. Iqbal, A. Meldrum, Veinot, Jonathan G C, *Langmuir* **2015**, *31*, 10540.

[210] J. Brandrup, E. H. Immergut, E. A. Grulke, *Polymer handbook*, Wiley-Interscience, New York, **1999**.

[211] I. M. D. Höhlein, J. Kehrle, T. K. Purkait, J. G. C. Veinot, B. Rieger, *Nanoscale* **2015**, *7*, 914.

[212] I. M. D. Höhlein, Werz, Patrick D. L., J. G. C. Veinot, B. Rieger, *Nanoscale* **2015**, *7*, 7811.

[213] M. V. Wolkin, J. Jorne, P. M. Fauchet, G. Allan, C. Delerue, *Physical review letters* **1999**, *82*, 197.

[214] L. M. Wheeler, N. R. Neale, T. Chen, U. R. Kortshagen, *Nat. Commun.* **2013**, *4*.

[215] M. Dasog, K. Bader, J. G. C. Veinot, *Chem. Mater.* **2015**, *27*, 1153.

[216] M. Dasog, J. G. C. Veinot, *Phys. Status Solidi A* **2012**, *209*, 1844.

[217] J. P. Bell, J. E. Cloud, J. Cheng, C. Ngo, S. Kodambaka, A. Sellinger, S. K. R. Williams, Y. Yang, *RSC Adv.* **2014**, *4*, 51105.

[218] L. Wang, Q. Li, H.-Y. Wang, J.-C. Huang, R. Zhang, Q.-D. Chen, H.-L. Xu, W. Han, Z.-Z. Shao, H.-B. Sun, *Light-Sci. Appl* **2015**, *4*, e245.

[219] Q. Li, Y. He, J. Chang, L. Wang, H. Chen, Y.-W. Tan, H. Wang, Z. Shao, *J. Am. Chem. Soc.* **2013**, *135*, 14924.

[220] G. B. de los Reyes, M. Dasog, M. Na, L. V. Titova, J. G. C. Veinot, F. A. Hegmann, *Phys. Chem. Chem. Phys.* **2015**, *17*, 30125.

[221] M. Dasog, J. G. C. Veinot, *Phys. Status Solidi B* **2014**, *251*, 2216.

[222] M. Dasog, S. Kraus, R. Sinelnikov, J. G.C. Veinot, B. Rieger, *Chem. Commun.* **2017**, *53*, 3114.

[223] W. Sun, C. Qian, Le He, K. K. Ghuman, A. P. Y. Wong, J. Jia, A. A. Jelle, P. G. O'Brien, L. M. Reyes, T. E. Wood, *Nat. Commun.* **2016**, *7*.

[224] I. M. D. Höhlein, A. Angı, R. Sinelnikov, J. G. C. Veinot, B. Rieger, *Chem. Eur. J.* **2015**, *21*, 2755.

[225] C. M. Hessel, M. R. Rasch, J. L. Hueso, B. W. Goodfellow, V. A. Akhavan, P. Puvanakrishnan, J. W. Tunnel, B. A. Korgel, *Small* **2010**, *6*, 2026.

[226] S. Mitra, S. Cook, V. Švrček, R. A. Blackley, W. Zhou, J. Kovač, U. Cvelbar, D. Mariotti, *J. Phys. Chem. C* **2013**, *117*, 23198.

[227] X. Cheng, S. B. Lowe, S. Ciampi, A. Magenau, K. Gaus, P. J. Reece, J. J. Gooding, *Langmuir* **2014**, *30*, 5209.

[228] Z. Yang, M. Dasog, A. R. Dobbie, R. Lockwood, Y. Zhi, A. Meldrum, J. G. C. Veinot, *Adv. Funct. Mater.* **2014**, *24*, 1345.

[229] a) K. S. Khuong, W. H. Jones, W. A. Pryor, K. N. Houk, *J. Am. Chem. Soc.* **2005**, *127*, 1265; b) S. Koltzenburg, M. Maskos, O. Nuyken, *Polymere: Synthese, Eigenschaften und Anwendungen*, Springer Spektrum, Berlin, **2014**.

[230] M. X. Dung, J.-K. Choi, H.-D. Jeong, *ACS Appl. Mater. Interfaces* **2013**, *5*, 2400.

[231] J.-K. Choi, M. X. Dung, H.-D. Jeong, *Mater. Chem. Phys.* **2014**, *148*, 463.

[232] K. Sato, N. Fukata, K. Hirakuri, M. Murakami, T. Shimizu, Y. Yamauchi, *Chem. Asian J.* **2010**, *5*, 50.

[233] M. A. Islam, T. K. Purkait, M. H. Mobarok, I. Hoehlein, R. Sinelnikov, M. Iqbal, D. Azulay, I. Balberg, O. Millo, B. Rieger, *Angew. Chem. Int. Ed.* **2016**, *55*, 7393.

[234] M. Aghajamali, M. Iqbal, T. K. Purkait, L. Hadidi, R. Sinelnikov, J. G. C. Veinot, *Chem. Mater.* **2016**.

[235] J. Chen, *Materials* **2013**, *6*, 156.

[236] a) P. Zuo, G. Yin, Y. Ma, *Electrochim. acta* **2007**, *52*, 4878; b) J. Wu, X. Qin, H. Zhang, Y.-B. He, B. Li, L. Ke, W. Lv, H. Du, Q.-H. Yang, F. Kang, *Carbon* **2015**, *84*, 434.

[237] a) F. Maroni, R. Raccichini, A. Birrozzi, G. Carbonari, R. Tossici, F. Croce, R. Marassi, F. Nobili, *J. Power Sources* **2014**, *269*, 873; b) M. Zhou, X. Li, B. Wang, Y. Zhang, J. Ning, Z. Xiao, X. Zhang, Y. Chang, L. Zhi, *Nano Lett.* **2015**, *15*, 6222.

[238] N. Liu, H. Wu, M. T. McDowell, Y. Yao, C. Wang, Y. Cui, *Nano Lett.* **2012**, *12*, 3315.

[239] S. Niesar, R. Dietmueller, H. Nesswetter, H. Wiggers, M. Stutzmann, *Phys. Status Solidi A* **2009**, *206*, 2775.

[240] R. Dietmueller, A. R. Stegner, R. Lechner, S. Niesar, R. N. Pereira, M. S. Brandt, A. Ebbers, M. Trocha, H. Wiggers, M. Stutzmann, *Appl. Phys. Lett.* **2009**, *94*, 83.

[241] a) S. Niesar, A. R. Stegner, R. N. Pereira, M. Hoeb, H. Wiggers, M. S. Brandt, M. Stutzmann, *Appl. Phys. Lett.* **2010**, *96*, 193112; b) S. Niesar, R. N. Pereira, A. R. Stegner, N. Erhard, M. Hoeb, A. Baumer, H. Wiggers, M. S. Brandt, M. Stutzmann, *Adv. Funct. Mater.* **2012**, *22*, 1190.

[242] J. K. El-Demellawi, C. R. Holt, E. Abou-Hamad, Z. A. Al-Talla, Y. Saih, S. Chaieb, *ACS Appl. Mater. Interfaces* **2015**, *7*, 13794.

[243] F. Peng, J. Wang, G. Ge, T. He, L. Cao, Y. He, H. Ma, S. Sun, *Mater. Lett.* **2013**, *92*, 65.

[244] F. Erogbogbo, C.-W. Chang, J. L. May, L. Liu, R. Kumar, W.-C. Law, H. Ding, K. T. Yong, I. Roy, M. Sheshadri, *Nanoscale* **2012**, *4*, 5483.

[245] F. Erogbogbo, C.-W. Chang, J. May, P. N. Prasad, M. T. Swihart, *Nanoscale* **2012**, *4*, 5163.

[246] C. Tu, X. Ma, P. Pantazis, S. M. Kauzlarich, A. Y. Louie, *J. Am. Chem. Soc.* **2010**, *132*, 2016.

[247] F. Erogbogbo, C.-A. Tien, C.-W. Chang, K.-T. Yong, W.-C. Law, H. Ding, I. Roy, M. T. Swihart, P. N. Prasad, *Bioconjugate Chem.* **2011**, *22*, 1081.

[248] K.-T. Yong, W.-C. Law, R. Hu, L. Ye, L. Liu, M. T. Swihart, P. N. Prasad, *Chem. Soc. Rev.* **2013**, *42*, 1236.

[249] Y. Zhong, F. Peng, F. Bao, S. Wang, X. Ji, L. Yang, Y. Su, S.-T. Lee, Y. He, *J. Am. Chem. Soc.* **2013**, *135*, 8350.

[250] C. M. Gonzalez, J. G. C. Veinot, *J. Mater. Chem. C* **2016**, *4*, 4836.

[251] S. Silvi, A. Credi, *Chem. Soc. Rev.* **2015**, *44*, 4275.

[252] M. Amelia, S. Impellizzeri, S. Monaco, I. Yildiz, S. Silvi, F. M. Raymo, A. Credi, *ChemPhysChem* **2011**, *12*, 2280.

[253] R. Freeman, J. Girsh, I. Willner, *ACS Appl. Mater. Interfaces* **2013**, *5*, 2815.

[254] Y. Lou, Y. Zhao, J. Chen, J.-J. Zhu, *J. Mater. Chem. C* **2014**, *2*, 595.

[255] a) I. N. Germanenko, S. Li, M. S. El-Shall, *J. Phys. Chem. B* **2001**, *105*, 59; b) W. C. Trogler, M. J. Sailor, *Chem. Eur. J.* **2000**, *6*, 2205.

[256] A. Nguyen, C. M. Gonzalez, R. Sinelnikov, W. Newman, S. Sun, R. Lockwood, J. G. C. Veinot, A. Meldrum, *Nanotechnology* **2016**, *27*, 105501.

[257] a) J. Zhang, S.-H. Yu, *Nanoscale* **2014**, *6*, 4096; b) G. Shtenberg, N. Massad-Ivanir, E. Segal, *Analyst* **2015**, *140*, 4507.

[258] a) Y. Yi, J. Deng, Y. Zhang, H. Li, S. Yao, *Chem. Commun.* **2013**, *49*, 612; b) Q. Chen, M. Liu, J. Zhao, X. Peng, X. Chen, N. Mi, B. Yin, H. Li, Y. Zhang, S. Yao, *Chem. Commun.* **2014**, *50*, 6771.

[259] Z. H. Zhang, R. Lockwood, J.G.C. Veinot, A. Meldrum, *Sens. Actuators, B* **2013**, *181*, 523.

[260] J. Lin, Q. Wang, *RSC Adv.* **2015**, *5*, 27458.

[261] Y. Yi, G. Zhu, C. Liu, Y. Huang, Y. Zhang, H. Li, J. Zhao, S. Yao, *Anal. Chem.* **2013**, *85*, 11464.

[262] Plastics Europe, "Facts about Plastics", can be found under http://www.plasticseurope.org/, **2017**.

[263] B. S. Soller, N. Zhang, B. Rieger, *Macromol. Chem. Phys.* **2014**, *215*, 1946.

[264] S. Salzinger, B. Rieger, *Macromol. Rapid Commun.* **2012**, *33*, 1327.

[265] S. Collins, D. G. Ward, *J. Am. Chem. Soc.* **1992**, *114*, 5460.

[266] H. Yasuda, H. Yamamoto, K. Yokota, S. Miyake, A. Nakamura, *J. Am. Chem. Soc.* **1992**, *114*, 4908.

[267] W. R. Mariott, E. Y.-X. Chen, *Macromolecules* **2005**, *38*, 6822.

[268] S. Salzinger, U. B. Seemann, A. Plikhta, B. Rieger, *Macromolecules* **2011**, *44*, 5920.

[269] N. Zhang, S. Salzinger, B. S. Soller, B. Rieger, *J. Am. Chem. Soc.* **2013**, *135*, 8810.

[270] P. T. Altenbuchner, B. S. Soller, S. Kissling, T. Bachmann, A. Kronast, S. I. Vagin, B. Rieger, *Macromolecules* **2014**, *47*, 7742.

[271] a) J. R. Ebdon, D. Price, B. J. Hunt, P. Joseph, F. Gao, G. J. Milnes, L. K. Cunliffe, *Polym. Degrad. Stab.* **2000**, *69*, 267; b) D. Price, K. Pyrah, T. R. Hull, G. J. Milnes, J. R. Ebdon, B. J. Hunt, P. Joseph, *Polym. Degrad. Stab.* **2002**, *77*, 227; c) D. Price, K. Pyrah, T. R. Hull, G. J. Milnes, J. R. Ebdon, B. J. Hunt, P. Joseph, C. S. Konkel, *Polym. Degrad. Stab.* **2001**, *74*, 441; d) T. Bock, H. Möhwald, R. Mülhaupt, *Macromol. Chem. Phys.* **2007**, *208*, 1324; e) B. Bingöl, *dissertation*, Johannes Gutenberg-Universität, Mainz, **2007**; f) H. Steininger, M. Schuster, K. D. Kreuer, A. Kaltbeitzel, B. Bingöl, W. H. Meyer, S. Schauff, G. Brunklaus, J. Maier, H. W. Spiess, *Phys. Chem. Chem. Phys.* **2007**, *9*, 1764; g) J. Parvole, P. Jannasch, *Macromolecules* **2008**, *41*, 3893; h) D. Markova, A. Kumar, M. Klapper, K. Müllen, *Polymer* **2009**, *50*, 3411; i) R. Perrin, M. Elomaa, P. Jannasch, *Macromolecules* **2009**, *42*, 5146; j) T. Wagner, A. Manhart, N. Deniz, A. Kaltbeitzel, M. Wagner, G. Brunklaus, W. H. Meyer, *Macromol. Chem. Phys.* **2009**, *210*, 1903; k) D. Lanzinger, S. Salzinger, B. S. Soller, B. Rieger, *Ind. Eng. Chem. Res.* **2015**, *54*, 1703; l) M. Ingratta, M. Elomaa, P. Jannasch, *Polym. Chem.* **2010**, *1*, 739; m) V. Atanasov, J. Kerres,

Macromolecules **2011**, *44*, 6416; n) Y. E. Greish, P. W. Brown, *Biomaterials* **2001**, *22*, 807; o) J. Ellis, A. D. Wilson, *Dent. Matter.* **1992**, *8*, 79; p) R. A. Gemeinhart, C. M. Bare, R. T. Haasch, E. J. Gemeinhart, *J. Biomed. Mater. Res.* **2006**, *78*, 433; q) J.-H. Seo, R. Matsuno, M. Takai, K. Ishihara, *Biomaterials* **2009**, *30*, 5330; r) T. Goda, R. Matsuno, T. Konno, M. Takai, K. Ishihara, *J. Biomed. Mater. Res.* **2009**, *89*, 184; s) L. Macarie, G. Ilia, *Prog. Polym. Sci.* **2010**, *35*, 1078; t) R. Georgieva, R. Tsevi, K. Kossev, R. Kusheva, M. Balgjiska, R. Petrova, V. Tenchova, I. Gitsov, K. Troev, *J. Med. Chem.* **2002**, *45*, 5797; u) S. Monge, B. Canniccioni, A. Graillot, J.-J. Robin, *Biomacromolecules* **2011**, *12*, 1973.

[272] U. B. Seemann, J. E. Dengler, B. Rieger, *Angew. Chem. Int. Ed.* **2010**, *49*, 3489.

[273] S. Salzinger, B. S. Soller, A. Plikhta, U. B. Seemann, E. Herdtweck, B. Rieger, *J. Am. Chem. Soc.* **2013**, *135*, 13030.

[274] B. S. Soller, S. Salzinger, C. Jandl, A. Pöthig, B. Rieger, *Organometallics* **2015**, *34*, 2703.

[275] a) S. Aoshima, S. Kanaoka in *Adv. Polym. Sci.*, Springer Berlin Heidelberg, **2008**, pp. 169–208; b) I. C. Sanchez, M. T. Stone, *Polymer Blends* **2000**, *1*, 15.

[276] N. Zhang, S. Salzinger, B. Rieger, *Macromolecules* **2012**, *45*, 9751.

[277] N. Zhang, S. Salzinger, F. Deubel, R. Jordan, B. Rieger, *J. Am. Chem. Soc.* **2012**, *134*, 7333.

[278] N. Zhang, S. Salzinger, F. Deubel, B. Rieger, WO 2013/072309, **2012**.

[279] S. S. Kistler, *Nature* **1931**, *127*, 741.

[280] a) Gesser, H. D., Goswami, P. C., *Chem. Rev.* **1989**, *89*, 765; b) W. J. Malfait, S. Zhao, R. Verel, S. Iswar, D. Rentsch, R. Fener, Y. Zhang, B. Milow, M. M. Koebel, *Chem. Mater.* **2015**, *27*, 6737; c) D. W. Cooper, *Part. Sci. Technol.* **1989**, *7*, 371.

[281] J. L. Gurav, I.-K. Jung, H.-H. Park, E. S. Kang, D. Y. Nadargi, *J. Nanomater.* **2010**, *2010*, 11.

[282] N. Hüsing, U. Schubert, *Angew. Chem.* **1998**, *110*, 22.

[283] L. L. Hench, J. K. West, *Chem. Rev.* **1990**, *90*, 33.

[284] A. M. Aegerter, N. Leventis, M. M. Koebel (Eds.) *Aerogels Handbook*, Springer New York, New York, NY, **2011**.

[285] A. Soleimani Dorcheh, M. H. Abbasi, *J. Matter. Process. Tech.* **2008**, *199*, 10.

[286] H. E. Bergna, American Chemical Society. Division of Colloid and Surface Chemistry., American Chemical Society. Meeting, *Colloid chemistry of silica*, **1994**.

[287] Am Buckley, M. Greenblatt, *J. Chem. Educ.* **1994**, *71*, 599.

[288] C. J. Brinker, *Glasses and Glass Ceramics from Gels* **1988**, *100*, 31.

[289] a) A. Venkateswara Rao, D. Haranath, *Microporous Mesoporous Mater.* **1999**, *30*, 267; b) A. Venkateswara Rao, S. D. Bhagat, *Solid State Sci.* **2004**, *6*, 945; c) A. Venkateswara Rao, M. M. Kulkarni, D. P. Amalnerkar, T. Seth, *J. Non-Cryst. Solids.* **2003**, *330*, 187.

[290] E. R. Pohl, F. D. Osterholtz in *Molecular Characterization of Composite Interfaces*, Springer, **1985**, p. 157.

[291] R. K. Iler, *The chemistry of silica*, **1979**, Wiley, New York.

[292] R. T. Morrison, R. N. Boyd, *Organic chemistry. Allyn and Bacon Inc., Boston* **1966**.

[293] C. J. Brinker, G. W. Scherer, *Sol-gel science*. *The physics and chemistry of sol-gel processing*, Academic press, **2013**.

[294] "Supercritical Drying", can be found under www.aerogel.org, **2017**.

[295] J. Kehrle, S. Kaiser, T. K. Purkait, M. Winnacker, T. Helbich, S. Vagin, J. G. C. Veinot, B. Rieger, *Nanoscale* **2017**, *9*, 8489.

[296] J. Kehrle, I. M. D. Höhlein, Z. Yang, A.-R. Jochem, T. Helbich, T. Kraus, J. G. C. Veinot, B. Rieger, *Angew. Chem. Int. Ed.* **2014**, *53*, 12494.

[297] R. Schwalm, *UV coatings*. *Basics, recent developments and new applications*, Elsevier, **2006**.

[298] M. Shirai, S. Wakinaka, H. Ishida, M. Tsunooka, M. Tanaka, *J. Polym. Sci. Pol. Lett.* **1986**, *24*, 119.

[299] C. A. Anger, J. Kehrle, K. Hindelang, J. G. C. Veinot, J. Stohrer, B. Rieger, *Macromolecules* **2014**, *47*, 8497.

[300] R. Shchepin, C. Xu, P. Dussault, *Org. Lett.* **2010**, *12*, 4772.

[301] M. A. Brook, J. B. Grande, F. Ganachaud in *Silicon Polymers*, Springer, **2010**, p. 161.

[302] E. Pouget, E. Holgado-Garcia, I. V. Vasilenko, S. V. Kostjuk, J. M. Campagne, F. Ganachaud, *Macromol. Rapid Commun.* **2009**, *30*, 1128.

[303] R. Schliebs, J. Ackermann, *Chem. unserer Zeit* **1987**, *21*, 121.

[304] J. Ackermann, V. Damrath, *Chem. unserer Zeit* **1989**, *23*, 86.

[305] S. W. Kantor, W. T. Grubb, R. C. Osthoff, *J. Am. Chem. Soc.* **1954**, *76*, 5190.

[306] W. Patnode, D. F. Wilcock, *J. Am. Chem. Soc.* **1946**, *68*, 358.

[307] Q. Wang, H. Zhang, G. S. Prakash, T. E. Hogen-Esch, G. A. Olah, *Macromolecules* **1996**, *29*, 6691.

[308] a) J.-J. Lebrun, G. Sauvet, P. Sigwalt, *Macromol. Rapid Commun.* **1982**, *3*, 757; b) G. Toskas, G. Besztercey, M. Moreau, M. Masure, P. Sigwalt, *Macromol. Chem. Phys.* **1995**, *196*, 2715.

[309] a) S. Ritter, F. Sieglhuber, EP2151467 B1, **2011**; b) P.D.C.D. Ball, J.D.C.D. Cremer, V.D.C.D. Stanjek, R.D.C.D. Weidner, DE102006013416 A1, **2007**; c) S. Herrwerth, P. Cavaleiro, J. Esselborn, S. Oestreich, US20050287300 A1, **2005**; d) X. Coqueret, A. Hajaiej, A. Lablache-Combier, C. Loucheux, R. Mercier, L. Pouliquen, L. Randrianarisoa-Ramanantsoa, *Pure and Appl. Chem.* **1990**, *62*, 1603; e) B. Boutevin, L. Abdellah, M. N. Dinia, *Eur. Polym. J.* **1995**, *31*, 1127.

[310] J. L. Dektar, N. P. Hacker, *J. Org. Chem.* **1990**, *55*, 639.

[311] J. L. Dektar, N. P. Hacker, *J. Am. Chem. Soc.* **1990**, *112*, 6004.

[312] M. Shirai, M. Tsunooka, *Prog. Polym. Sci.* **1996**, *21*, 1.

[313] M. Shirai, M. Tsunooka, *Bull. Chem. Soc. Jpn.* **1998**, *71*, 2483.

[314] A. Burawoy, A. R. Thompson, *J. Chem. Soc.* **1956**, 4314.

[315] P. F. A. Buijsen, N. P. Hacker, *Tetrahedron Lett.* **1993**, *34*, 1557.

[316] M. Shirai, M. Tsunooka, M. Tanaka, K. Nishijima, K. Ishikawa, *J. Polym. Sci. A Polym. Chem.* **1989**, *27*, 325.

[317] M. Shirai, N. Katsuta, M. Tsunooka, M. Tanaka, K. Nishijima, *Macromol. Chem. Phys.* **1989**, *190*, 2099.

[318] M. Shirai, M. Hayashi, M. Tsunooka, *Macromolecules* **1992**, *25*, 195.

[319] C. Iwashima, G. Imai, H. Okamura, M. Tsunooka, M. Shirai, *J. Photopolym. Sci. Tech.* **2003**, *16*, 91.

[320] a) D. L. VanderHart, V. M. Prabhu, E. K. Lin, *Chem. Mater.* **2004**, *16*, 3074; b) C.-T. Lee, M. Wang, K. E. Gonsalves, W. Yueh, J. M. Roberts, T. R. Younkin, C. L. Henderson (Eds.) *Effect of PAG and matrix structure on PAG acid generation behavior under UV and high-energy radiation exposure*, International Society for Optics and Photonics, **2008**; c) C. D. Higgins, C. R. Szmanda, A. Antohe, G. Denbeaux, J. Georger, R. L. Brainard, *Jpn. J. Appl. Phys.* **2011**, *50*, 36504; d) J.-K. Lee, M. Chatzichristidi, A. A. Zakhidov, H. S. Hwang, E. L. Schwartz, J. Sha, P. G. Taylor, H. H. Fong, J. A. DeFranco, E. Murotani, *J. Mater. Chem.* **2009**, *19*, 2986.

[321] T. Oyama, T. Yamashita, T. Suzuki, K. Ebitani, M. Hoshino, T. Iijima, M. Tomoi, *React. Funct. Polym.* **2001**, *49*, 99.

[322] M. Shirai, N. Nogi, M. Tsunooka, *React. Funct. Polym.* **1998**, *37*, 147.

[323] M. Shirai, T. Masuda, H. Ishida, M. Tsunooka, M. Tanaka, *Eur. Polym. J.* **1985**, *21*, 781.

10. Statutory Declaration (ger.: *Eidesstattliche Erklärung*)

Ich erkläre an Eides statt, dass ich die bei der Fakultät für Chemie der Technischen Universität München zur Promotionsprüfung vorgelegte Arbeit mit dem Titel

Surface Hydrosilylation: The Key to Silicon Nanocrystal Hybrid and Composite Materials

am **WACKER Lehrstuhl für Makromolekulare Chemie**
unter der Anleitung und Betreuung durch **Prof. Dr. Dr. h.c. Bernhard Rieger**
ohne sonstige Hilfsmittel erstellt und bei der Abfassung nur die gemäß § 6 Ab. 6 und 7 Satz 2 angebotenen Hilfsmittel benutzt habe.

- Ich habe keine Organisation eingeschaltet, die gegen Entgelt Betreuer(innen) für die Anfertigung von Dissertationen sucht, oder die mir obliegende Pflichten hinsichtlich der Prüfungsleistungen für mich ganz oder teilweise erledigt.
- Ich habe die Dissertation in dieser oder ähnlicher Form in keinem anderen Prüfungsverfahren als Prüfungsleistung vorgelegt.
- Die vollständige Dissertation wurde in der Universitätsbibliothek der TUM veröffentlicht. Die Fakultät für Chemie hat der Veröffentlichung zugestimmt.
- Ich habe den angestrebten Doktorgrad noch nicht erworben und bin nicht in einem früheren Promotionsverfahren für den angestrebten Doktor endgültig gescheitert.

Die öffentlich zugängliche Promotionsordnung der TUM ist mir bekannt, insbesondere habe ich die Bedeutung von § 28 (Nichtigkeit der Promotion) und § 29 (Entzug des Doktorgrades) zur Kenntnis genommen. Ich bin mir der Konsequenz einer falschen Eidesstattlichen Erklärung bewusst.

Mit der Aufnahme der personenbezogenen Daten in die Alumni-Datei bei der TUM bin ich einverstanden.

Günzburg, den

Julian Kehrle